CROSSTALK BETWEEN CADMIUM, AND COPPER AND IRON HOMEOSTASIS IN *ARABIDOPSIS THALIANA*

A Dissertation

Presented to the Faculty of the Graduate School

of Cornell University

In Partial Fulfillment of the Requirements for the Degree of

Doctor of Philosophy

by

Sheena Ramos Gayomba

August 2014

CROSSTALK BETWEEN CADMIUM, AND COPPER AND IRON HOMEOSTASIS IN *ARABIDOPSIS THALIANA*

Sheena Ramos Gayomba, Ph. D.

Cornell University 2014

Copper and iron are essential minerals for plant growth, and human health and nutrition. Cadmium, on the other hand, is a highly toxic element that competes with essential elements for uptake and partitioning, and poses a threat to crop productivity and human health. While substantial progress has been made towards understanding how plants maintain homeostasis of copper and iron, how it is achieved in an environment that also contains cadmium is still poorly understood. Two separate studies have identified cross-talk between cadmium toxicity and copper and iron homeostasis in *Arabidopsis thaliana*. With respect to the effect of cadmium on copper homeostasis, we show that cadmium mimics transcriptional copper deficiency responses that result in increased copper uptake and likely intracellular copper reallocation in *A. thaliana*. These effects of cadmium are attributed to a transcription factor, SPL7, and its downstream targets, copper transporters COPT1, COPT2, and COPT6; and Cu/Zn superoxide dismutases, CSD1 and CSD2. With respect to the effect of cadmium on iron homeostasis, we found that cadmium increased expression of an oligopeptide transporter, OPT3. Studies of the biological relevance of this phenomenon revealed that OPT3 is a phloem-specific iron transporter that loads iron into the phloem, controls iron redistribution from mature to developing tissues and seeds, and is involved in systemic iron signaling. We also found that OPT3-dependent systemic iron signaling is important for controlling cadmium partitioning: loss of OPT3 function leads to increased accumulation of cadmium while decreasing accumulation of iron in seeds of *A.*

thaliana. Together, these data suggest that manipulation of the components of essential mineral element homeostasis provide promising avenues for targeted biofortification strategies directed at increasing mineral nutrient density while preventing the entry of toxic elements such as cadmium into edible portions of crops.

BIOGRAPHICAL SKETCH

Sheena Ramos Gayomba was born on October 23, 1986 to two hardworking parents, Arsenia and Alfredo Gayomba. She earned her undergraduate degree in Biochemistry from Rider University in May 2009 and entered Cornell University that year. She earned her Master of Science degree in Crop Science from Cornell University in 2011 and her Doctor of Philosophy degree in Crop Science in 2014. Sheena was a member of the Department of Crop and Soil Sciences graduate student association, a teaching assistant for several courses, a mentor to undergraduate teaching assistants, and a research mentor to several members of the Vatamaniuk Lab.

ACKNOWLEDGMENTS

I would like to give a very big thank you to my family and friends who helped to keep my spirits up these past five years.

To Mom and Dad, for unending love and support, for listening to me when I wanted to quit and cheering me on when I wanted to continue.

To my brothers Ian and Garth, for keeping me company my entire life.

To my advisor, Olena Vatamaniuk, for encouragement and keeping high standards during my graduate career.

To my lab members: Sungjin Kim who shared the ups and downs in graduate life, Jiapei Yan for conversations about science and TA work, Hail Jung who was a second mentor to me, Anuj Sharma for patience and kindness, and to the rest of the lab members who have provided friendship.

Lastly, I would like to thank my committee members, Leon Kochian and Maria Harrison, for guidance.

TABLE OF CONTENTS

LIST OF FIGURES

LIST OF TABLES

CHAPTER I

Preface

Abstract

Copper (Cu) and iron (Fe) are transition elements that are essential for plant growth and development. The ability of Cu and Fe to change redox states ($Cu^{2+} \rightarrow Cu^{+}$ and $Fe^{3+} \rightarrow Fe^{2+}$) allows these metals to participate in redox reactions. Consequently, Cu and Fe are important cofactors in a variety of enzymes participating in electron transfer reactions. However, free Cu and Fe ions are also toxic in excess due to their ability to create reactive oxygen species (ROS) through the Fenton's reaction and thus, homeostasis of these elements is tightly regulated. Despite increasing knowledge of the uptake, translocation, and distribution of essential metals in plants, little is known about how these mechanisms are affected by non-essential and potentially toxic metals such as cadmium (Cd). Cd is a highly toxic element that competes with Fe and other essential elements for uptake into roots and partitioning in plant tissues, thus posing a threat to crop productivity and human health. In the cell, Cd deactivates proteins by binding to thiol groups in structural and catalytic sites, displaces endogenous metal cofactors from their cellular binding sites, and indirectly promotes oxidative stress. Although the hazardous nature of Cd is well known, Cd emission into the environment including agricultural soils continues due to the use of phosphate fertilizers, sewage sludge, and atmospheric deposition from industrial processes. This dissertation presents results of studies on the interaction between Cd and Cu homeostasis, and between Cd and Fe homeostasis in *A. thaliana*.

Overview of copper homeostasis

Copper (Cu) is an essential micronutrient for all organisms because it acts as a cofactor for

enzymes participating in important biological processes such as respiration, photosynthesis and scavenging of oxidative stress (Burkhead et al*.,* 2009, Merchant 2010, Ravet and Pilon 2013). In addition to these functions, plants also employ Cu for the perception of ethylene, nitrogen metabolism, molybdenum cofactor synthesis, cell wall remodeling, response to pathogens, flowering and seed set (Burkhead et al*.,* 2009, Marschner 1995, Mendel and Kruse 2012, Ravet and Pilon 2013, Shorrocks and Alloway 1988). Among visible symptoms of Cu deficiency are stunted growth, distortion of young leaves, and chlorosis/necrosis starting at the apical meristem and extending down the leaf margins, compromised fertilization and seed set (Marschner 1995, Shorrocks and Alloway 1988). This remarkable array of physiological functions of Cu is attributed to its ability to change its oxidation state ($Cu^{2+} \rightarrow Cu^{+}$). However, that same property imposes toxicity when free Cu ions accumulate in cells in excess because of their ability to promote oxidative stress (Valko et al*.,* 2005). Therefore, to prevent deficiency while avoiding toxicity, plants tightly regulate Cu uptake from the soils and root-to-shoot partitioning to maintain the proper concentration of Cu in plant tissues.

Copper mobilization at the root surface and uptake into epidermal root cells

Copper (II) is the dominant form of Cu in soils where it is strongly associated with organic matter as well as Fe and aluminum (Al) oxides (Flemming and Trevors 1989) and must be reduced to Cu(I) for plant uptake. Based on studies in *A. thaliana*, it is proposed that dicots and non-grass monocots employ membrane-bound ferric chelate reductases from the **F**erric **R**eduction **O**xidase (FRO) family, which in addition to reducing Fe(III) to Fe(II) prior uptake in response to Fe deficiency (Connelly et al., 2003), are also involved in Cu(II) to Cu(I) reduction upon Cu deficiency (Burkhead et al., 2009). Consistent with this suggestion, transcript

abundance of *AtFRO3, AtFRO4*, and *AtFRO5* is increased in roots of Cu-deficient *A. thaliana*, and function of AtFRO4 and AtFRO5 is required for the increase in root-surface localized Cu(II) to Cu(I) reduction (Bernal et al., 2012, Mukherjee et al., 2006), Cu(I) enters the cytosol of root epidermal cells *via* plasma membrane localized transporters of the CTR/COPT **C**opper **Tr**ansporter/**Cop**per **T**ransporter family of Cu transporters (Garcia-Molina et al., 2011, Garcia-Molina et al., 2013, Gayomba et al., 2013, Jung et al., 2012, Kampfenkel et al., 1995, Klaumann et al., 2011, Perea-García et al., 2013, Sancenón et al., 2004, Sancenón et al., 2003, Yuan et al., 2010, Yuan et al., 2011). The number of CTR/COPT genes varies among higher plants, with six in *Arabidopsis thaliana* (COPT1 to 6) (Puig et al., 2007, Sancenón et al., 2003), seven in *Oryza sativa* (Yuan et al., 2010; Yuan et al., 2011), and five in *Brachypodium distachyon* (BdCOPT1-5) (Chapter 4 and Jung et al., 2014). The major transport pathways identified in *A. thaliana* are summarized in Figure 1, and discussed herein, with an exception for the Cu-NA phloem transporter discovered in *O. sativa*.

The founding members of the CTR/COPT family, Ctr1p, Ctr2p, and Ctr3p, were first identified in the yeast, *Saccharomyces cerevisiae* (Dancis et al., 1994a, Dancis et al., 1994b, Knight et al., 1996, Peña et al., 2000, Rees et al., 2004). The characterized CTR/COPT proteins localize to different cellular membranes that specify their contribution to Cu homeostasis: *S. cerevisiae* Ctr2p is located on the vacuolar membrane and releases Cu into the cytosol during Cu deficiency (Rees et al., 2004), while high-affinity plasma membrane-localized Ctr1p and Ctr3p are functionally redundant and mediate Cu uptake from extracellular media (Dancis et al., 1994b, Peña et al., 2000).

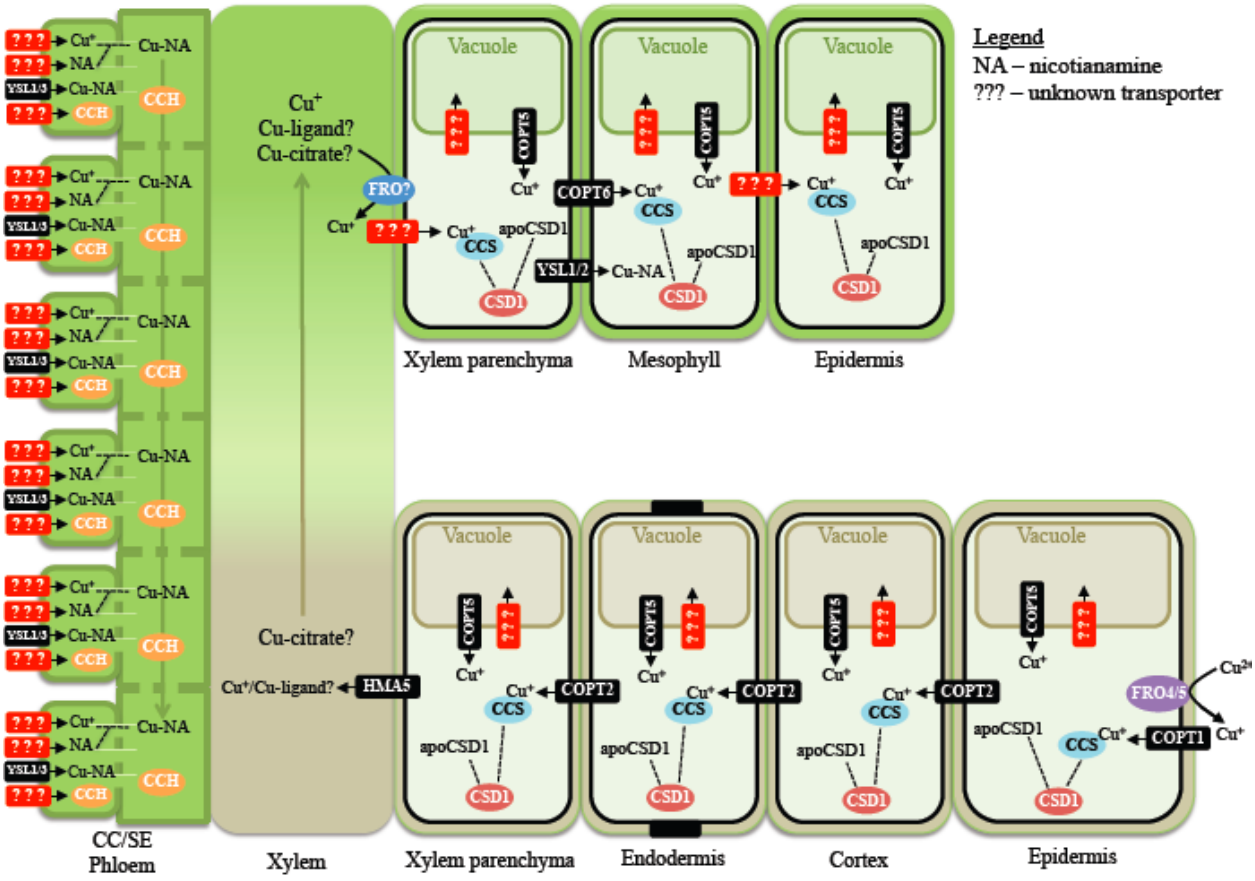

Figure 1. Overview of copper transport in *A. thaliana*. Cu exists as Cu(II) chelates and must be reduced to Cu(I) by FRO3, FRO4, and FRO5 at the plasma membrane of epidermal root cells (Bernal et al., 2012, Mukherjee et al., 2006). Next, the Cu(I) is transported into the cytosol of epidermal cells by COPT1 at the root tip (Sancenón et al., 2004), COPT2 in the main root (Gayomba et al., 2013, Perea-García et al., 2013), and by COPT2 and COPT6 in lateral roots (Chapter 2 and 3, Jung et al., 2012, Gayomba et al., 2013, Perea-García et al., 2013). In the cytosol, Cu(I) is bound to a Cu chaperone, CCS, which delivers Cu to apoCSD1 to create the functional Cu/Zn SOD, CSD1 (Chu et al., 2005). Also present in the vasculature, COPT2 and COPT6 can function to transport Cu throughout the root (Jung et al., 2012, Gayomba et al., 2013, Perea-García et al., 2013). The HMA5 protein effluxes Cu into xylem vessels (Andrés-Colás et al., 2006), where it forms complexes with citrate or an unknown ligand before transport to aboveground tissues in the xylem via the transpiration stream. Cu-ligands must be reduced by an unknown member of the FRO family before uptake into the cytosol of shoot xylem parenchyma cells. As in the root, Cu(I) is delivered to apoCSD1 by the Cu chaperone, CCS, in the cytosol (Chu et al., 2005). COPT6 may mediate Cu(I) distribution into photosynthetic tissue (mesophyll cells) (Jung et al., 2012). In the phloem, free Cu ions may be loaded into companion cells (CC) by an unidentified transporter or as Cu-NA by an orthologue of YSL1/3 (Waters et al., 2006). In addition to, or alternatively to forming complexes with NA, Cu could bind to a copper chaperone, CCH, which has been found in phloem exudates (Mira et al., 2001).

Earlier studies showed that the Cu deficiency phenotype of the *S. cerevisiae ctr1ctr3* double mutant, which cannot grow on non-fermentable media unless supplied by exogenous Cu, was rescued by heterologous expression of *A. thaliana COPT1*, indicating that COPT1 mediates Cu influx (Sancenón et al., 2003). Studies indicate that the major entry pathway of Cu into *A. thaliana* occurs through plasma membrane-localized COPT1 (Andrés-Colás et al., 2010), which is expressed at the root tip (Sancenón et al., 2004). *A. thaliana* plants transformed with an antisense construct targeting *COPT1* mRNA revealed that COPT1 is necessary for root elongation and is also involved in pollen development (Sancenón et al., 2004).

A close relative of COPT1, COPT2, is also a plasma membrane Cu transporter in *A. thaliana* (characterized in Chapter 3, Gayomba et al., 2013, Perea-García et al., 2013). In roots, *COPT2* is expressed in the epidermis, cortex, vascular tissues, lateral roots and root hairs (Gayomba et al. 2013, Perea-García et al., 2013); and in aboveground tissue, *COPT2* is found in the shoot vasculature, the apical meristem, pollen (Gayomba et al., 2013; Perea-García et al., 2013) and the funiculus of mature seeds (Gayomba et al., 2013). The *copt2-1* and *copt2-1.1* alleles, which were identified by Gayomba et al., 2013 and Perea-García et al., 2013, respectively, show no phenotype under Cu deficiency (Gayomba et al., 2013, Perea-García et al., 2013), but the *copt2-1.1* mutant was shown to be resistant to both Cu- and Fe-deficient growth conditions (Perea-García et al., 2013). Nevertheless, COPT2 could function redundantly with another CTR/COPT transporter or with another protein to mediate movement of Cu throughout the root. The intracellular COPT5 protein localizes to the vacuole and pre-vacuolar compartments, and is expressed predominantly in the root during the early seedling stage, and is later expressed in vasculature of leaves, siliques, and flowers (Garcia-Molina et al., 2011, Klaumann et al., 2011). The physiological function of COPT5 is in Cu release into the cytosol, which is especially

needed during Cu-deficiency. Vacuoles purified from rosette leaves of plants expressing the *copt5-1*, *copt5-2*, and *copt5-3* mutant alleles contained more Cu compared to vacuoles isolated from wild-type plants (Klaumann et al., 2011). The loss of the ability to release Cu in the *copt5* mutant results in decreased photosynthetic efficiency (Garcia-Molina et al., 2011) and uneven distribution of Cu among major organs, with *copt5* mutants have more Cu in roots and rosettes, but less Cu in seeds and siliques (Klaumann et al., 2011).

Long-distance copper transport

Radial transport of Cu in root tissues is assumed to occur through the plasmodesmata to the xylem parenchyma, where Cu is mostly likely loaded into xylem vessels via a Cu-transporting P_{1B}-type ATPase, **H**eavy **M**etal **A**TPase 5, HMA5 (Andrés-Colás et al., 2006). Additionally, based on the expression of YSL2 in xylem parenchyma cells and its ability to transport Cu in yeast, YSL2 has been proposed to function in lateral Cu movement in the vasculature (DiDonato et al., 2004). Our recent data suggest that plasma membrane-localized COPT6, which is expressed mainly in the vascular tissues of leaves, might function in Cu distribution in photosynthetic tissues (Chapter 2, and Jung et al., 2012). Data from Garcia-Molina et al. (2013) revealed that the *copt6-2* mutant displays increased Cu content in whole rosettes, but decreased Cu in seeds, pointing to a possible role of COPT6 in phloem-based delivery of Cu from sources to sinks. Consistent with this suggestion, *COPT6* is also expressed in the central replum and funiculus of siliques, seed embryos, and in reproductive organs (Jung et al., 2012, Garcia-Molina et al., 2013). Other studies showed that COPT6 interacts with itself and COPT1 (Jung et al., 2012), suggesting that the COPT family members may interact with each other to form heteromeric protein complexes, as was found in *O. sativa* (Yuan et al., 2010, Yuan et al., 2011).

The physiological relevance of the interaction between *A. thaliana* COPT members has yet to be determined, as AtCOPTs function as homomers to fully complement the *S. cerevisiae ctr1ctr2ctr3* triple mutant (Kampfenkel et al., 1995, Sancenón et al., 2003, Sancenón et al., 2004, Garcia-Molina et al., 2013, Jung et al., 2012, Gayomba et al., 2013, Perea-García et al., 2013), whereas OsCOPTs, except for OsCOPT7, confer high-affinity Cu uptake only when expressed with another OsCOPT family member (Yuan et al., 2010, Yuan et al., 2011).

Copper transport in phloem tissue of senescing leaves is carried out by the **C**opper **Ch**aperone protein, CCH (Mira et al., 2001). However, *cch1* T-DNA mutants show no observable phenotype (Himelblau and Amasino 2001), indicating that this mechanism is not the dominant form of phloem-based delivery of Cu, at least during senescence. In phloem vessels of *O. sativa*, the plasma membrane-localized transporter from the **Y**ellow **S**tripe Transporter-**L**ike family (YSL), OsYSL16, transports Cu as a Cu-nicotianamine (NA) complex (Zheng et al., 2012). *OsYSL16* is expressed in the mature root zone and the leaf blade at the vegetative stage and its expression occurs in all tissues during the reproductive stage, predominantly in leaf blades, flag leaf blades, and in the nodes (Zheng et al., 2012). Cell-type specificity of this expression revealed that *OsYSL16* is found in the phloem and compared to wild-type plants, *ysl16* mutant plants accumulated more Cu in older leaves compared to younger leaves and also had low Cu content in seeds, suggesting a defect in remobilization of Cu from sources to sinks (Zheng et al., 2012). Accordingly, the *ysl16* mutant has higher expression of *OsCOPT1*, *OsCOPT5*, and lower expression of the xylem metal efflux transporter, *HMA9* (Zheng et al., 2012). Although NA levels were slightly higher in *ysl16* plants, foliar application of $^{65}CuCl_2$ or ^{65}Cu-NA revealed that wild-type plants were able to mobilize ^{65}Cu-NA to younger leaves, while remobilization of ^{65}Cu-NA to younger leaves in *ysl16* plants was severely reduced (Zheng et al.,

2012). Interestingly, both wild-type and *ysl16* plants showed little to no mobilization of $^{65}CuCl_2$, suggesting that Cu-NA complexes are the predominant form of Cu in phloem tissue (Zheng et al., 2012). In *A. thaliana*, YSL1 and YLS3 contribute to phloem-based delivery of Cu to seeds (Waters et al., 2006), but the cell-type specificity for *YSL1* and *YSL3* is still not clear. Waters et al. (2006) found that *YSL1* and *YSL3* expression was ubiquitous in vascular cells, while Le Jean et al. (2005) reported that *YSL1* was expressed in xylem parenchyma. Nevertheless, studies in *ysl1ysl3* double mutants indicate that these transporters are important for Cu-NA loading into seeds.

Transcriptional networks controlling copper homeostasis.

Plants have evolved sophisticated mechanisms for maintaining Cu homeostasis to prevent deficiency while avoiding toxicity. This regulation includes transcriptional control of genes encoding proteins that are involved in Cu uptake, trafficking, tissue partitioning and reallocation among Cu requiring enzymes. However, our knowledge of the transcription factors (TFs) involved in Cu homeostasis and the hierarchy of their regulatory pathways in higher plants is limited. Thus far, *A. thaliana* **S**QUAMOSA **P**romoter Binding Protein–**L**ike 7, SPL7, is the only TF that has been shown to play a role in Cu homeostasis in higher plants (Bernal et al., 2012, Yamasaki et al., 2009). Transcriptome analyses revealed that SPL7 is required for the expression of genes encoding several small RNAs, Cu chaperones, Fe chelate reductases (FRO4 and 5) that are involved in Cu(II) to Cu(I) reduction, and several Cu transporters including COPT1, COPT2, the **Z**RT-like **I**RT-like **P**rotein 2, ZIP2, YSL2, and COPT6 (Bernal et al., 2012, Gayomba et al., 2013, Jung et al., 2012). As a result of the important role of SPL7 in Cu homeostasis, the *spl7* knockdown mutants accumulate less Cu and develop slower unless extra Cu is added to the

growth medium (Yamasaki et al., 2009, Bernal et al., 2012, Gayomba et al., 2013).

In addition to stimulating uptake, SPL7 also aids in cellular Cu re-distribution to prioritize the function of Cu-containing proteins during Cu deficiency through the so-called "Cu economy" and "metal-switch" model. In this model SPL7 activates microRNA *miRNA398*, which then degrades expression of genes encoding two major Cu-containing proteins, Cu/Zn superoxide dismutases (SODs), CSD1 and CSD2, which are located in the cytosol and plastid, respectively (Yamasaki et al., 2007, Yamasaki et al., 2009). As *CSD1* and *CSD2* transcripts and activities decrease to release Cu to other Cu requiring functions, their superoxide scavenging activities are replaced by an increase in expression and activity of an Fe-containing SOD, FSD1 (Abdel-Ghany and Pilon 2008, Cohu et al., 2009, Cohu and Pilon 2007, Yamasaki et al., 2007).

SPL7 was also recently shown to directly interact with KIN17 (for **kin**ship to RecA proteins which are involved in DNA repair [Angulo et al., 1991]) in bi-molecular fluorescence studies (Garcia-Molina et al., 2014b). In mammalian cells, KIN17 binds to bent DNA and participates in DNA replication, cell growth cycle regulation, and the preservation of DNA integrity during stress (Masson et al., 2003, Miccoli et al., 2005, Tissier et al., 1995). In plants, KIN17 mediates plant development and tolerance to UV radiation (Garcia-Molina et al., 2014a). The *kin17-1 A. thaliana* mutant has lower expression levels of *COPT2*, *COPT6*, *FSD1*, and *CCH* and direct interaction of KIN17 and SPL7 was detected in the nucleus (Garcia-Molina et al., 2014b). Garcia-Molina et al. (2014b) also observed that *kin17spl7* double mutant plants had enhanced Cu-dependent phenotypes including an early arrest of the main shoot and loss of apical dominance resulting in altered flower structure, reduced silique production and reduced pollen production and viability, and these phenotypes were rescued by Cu addition.

Conclusion

Although our understanding of Cu homeostasis in plants has benefited heavily from research conducted over past few years, it is evident that there are gaps to be filled in terms of our understanding of Cu transport into the phloem and out of the xylem, Cu sequestration, and transcriptional regulation by plant Cu status. Based on studies of Fe homeostasis described below, it seems unlikely that SPL7 is the only transcription factor responsible for Cu regulation in plants, providing an exciting avenue of future research direction. The work described in this dissertation contributes to our current understanding of CTR/COPT function in *A. thaliana*, and their importance in maintaining Cu homeostasis under Cd stress. Additionally, we have provided the first characterization of CTR/COPT members in *B. distachyon.* These chapters have been published as follows:

Jung, H., Gayomba, S. R., Rutzke, M. A., Craft, E., Kochian, L. V. and Vatamaniuk, O. K. (2012) COPT6 is a plasma membrane transporter that functions in copper homeostasis in *Arabidopsis* and is a novel target of SQUAMOSA Promoter-binding Protein-like 7. *J Biol Chem*, **287**, 33252-33267.

Gayomba, S. R., Jung, H., Yan, J., Danku, J., Rutzke, M. A., Bernal, M., Krämer, U., Kochian, L. V., Salt, D. E. and Vatamaniuk, O. K. (2013) The CTR/COPT-dependent copper uptake and SPL7-dependent copper deficiency responses are required for basal cadmium tolerance in *A. thaliana*. *Metallomics*, **5**, 1262-1275.

Jung, H., Gayomba, S. R., Yan, J. and Vatamaniuk, O. K. (2014) *Brachypodium distachyon* as a model system for studies of copper transport in cereal crops. *Front Plant Sci*, **5**, 236.

Overview of iron homeostasis

Iron (Fe), like Cu, is an essential micronutrient that acts as a cofactor of enzymes involved in respiration, photosynthesis, scavenging of oxidative stress due to its ability to change oxidation state from Fe^{3+} to Fe^{2+}. In addition to these functions, plants also require Fe for molybdenum (Mo) metabolism, chlorophyll biosynthesis, flowering and seed set (Bittner 2014, Burkhead et al*.,* 2009, Marschner 1995, Mendel and Kruse 2012, Ravet and Pilon 2013, Shorrocks and Alloway 1988). Fe deficiency manifests as reduced growth, chlorosis of young leaves, low fertilization and seed set (Marschner 1995, Shorrocks and Alloway 1988). However, because excess Fe ions can participate in Fenton reactions to promote oxidative stress (Ravet and Pilon 2013), mechanisms responsible for Fe uptake and distribution within the plant are under tight control.

Iron mobilization at the root surface and uptake into epidermal root cells of dicotyledonous species

Iron (Fe) bioavailability in aerobic soils with neutral to basic pH is below the limits required to sustain plant growth and development because insoluble forms of Fe (III) prevail under these conditions. Consequently, alkaline soils occupying approximately 30% of the world's arable lands are considered Fe-limiting for plant growth (Marschner 1995). To increase Fe bioavailability, *A. thaliana* and other dicotyledonous and non-graminaceous monocotyledonous plants use a ferric reduction-based reductive strategy also known as Strategy I (Figure 2) (Conte and Walker 2011, Hindt and Guerinot 2012, Marschner and Romheld 1994). In brief, this strategy includes the acidification of the rhizosphere by the root plasma membrane H^+-ATPase which increases the solubility of Fe(III) (Santi and Schmidt 2009) and the reduction of Fe(III)

chelates to soluble Fe(II) by the root plasma membrane ferric chelate reductase, FRO2 (Robinson et al., 1999). The solubilized Fe(II) enters the apoplastic space where it constitutes up to 75% of the total Fe of the root (Bienfait et al., 1985). The passive radial diffusion of Fe into the root towards the vasculature in the stele is restricted by the Casparian strip of the endodermis. Thus Fe has to enter the root symplast at the endodermis and then moves via plasmodesmata towards the conductive tissues of the stele. Although Fe can be remobilized from the apoplast in any cell type of the roots, the expression pattern of Fe(II) transporters suggests that the majority of Fe(II) uptake into the symplast occurs in the root epidermal cells and is achieved by the plasma membrane localized high-affinity Fe(II) transporter **I**ron **R**egulated **T**ransporter 1, or IRT1, the founding member of the ZIP transporter family (Eide et al., 1996; Vert et al., 2002). The FRO2/IRT1 system constitutes the major pathway for Fe entry into root epidermal cells. The FRO2-like Fe(III) reduction reactions are considered to be rate limiting because overexpression of this enzyme in different plant species increases their survival under Fe limited conditions (Connolly et al., 2002, Ishimaru et al., 2007, Vasconcelos et al., 2008). *IRT1,* on the other hand, is an essential gene, because *irt1* mutants are seedling-lethal unless the medium is supplied with large amounts of exogenous Fe (Henriques et al., 2002, Varotto et al., 2002, Vert et al., 2002).

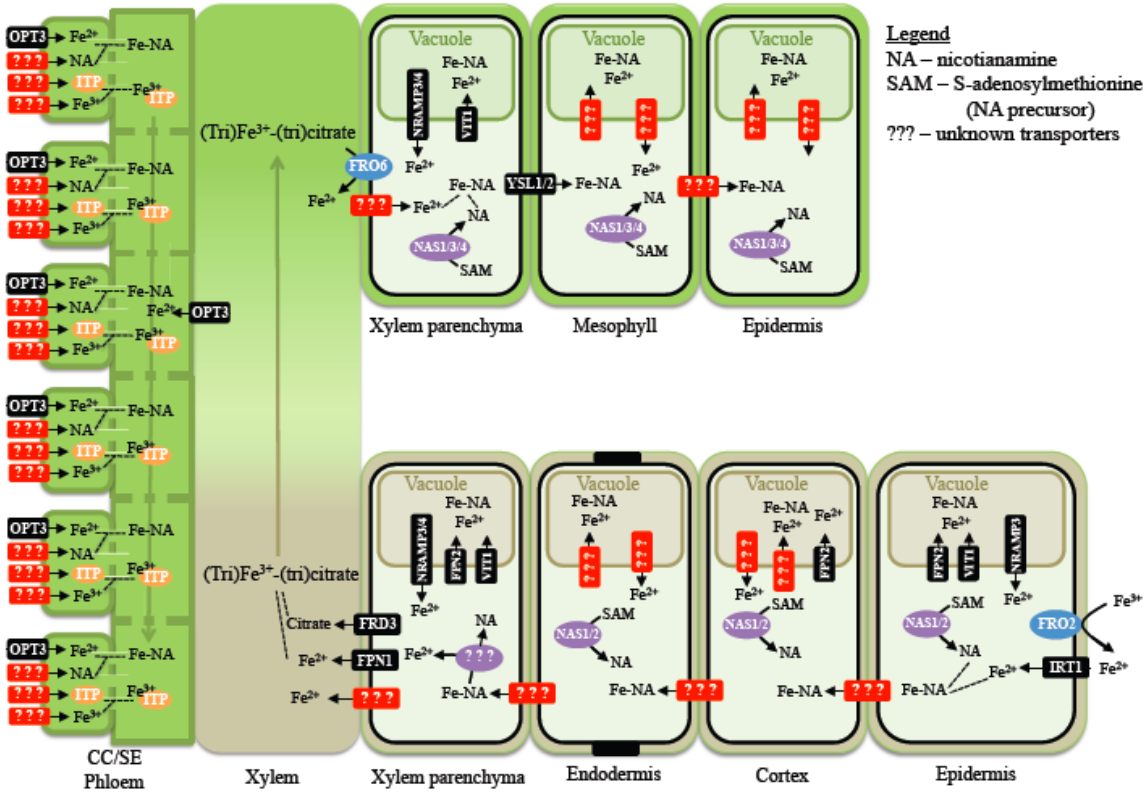

Figure 2. Overview of iron transport in *A. thaliana*. Root ferric chelate reduction reduces Fe(III) chelates to Fe(II) at the root surface, and the Fe^{2+} ions are then transported into the cytosol of root epidermal cells by IRT1 (Eide et al., 1996, Vert et al., 2002). Fe-NA chelates prevail in the cytosol (Rellán-Álvarez et al., 2008), where NA in roots is produced by the enzymes, NAS1 and NAS2 (Klatte et al., 2009). Fe-NA can move throughout the root towards the xylem vessels via an unknown transporter, or through the plasmodesmata. FRD3 transports citrate into the apoplastic space (Green and Rogers, 2004; Durrett et al., 2007), while the FPN1 transporter moves Fe into the root cell vacuole (Morrissey et al., 2009). In the xylem, Fe forms a complex with citrate to form (tri)Fe^{3+}-(tri)citrate (Rellán-Álvarez et al., 2008). In shoot tissue, this chelate complex is reduced through the action of FRO6 (Feng et al., 2006), and Fe enters the xylem parenchyma cells through an unknown transporter. YSL1 and YSL2 mediate transport of Fe-NA to photosynthetic cells (mesophyll cells) (Chu et al., 2010, Le Jean et al., 2005, Waters et al., 2006). In the phloem, Fe(II) ions are loaded into companion cells (CC) by OPT3 (Zhai et al., 2014, Chapter 5), while NA is loaded separately by an unknown transporter. In phloem sap, Fe-NA chelates are the dominant form of Fe (Rellán-Álvarez et al., 2008). Additionally, an **i**ron **t**ransporting **p**rotein (ITP) has been found in phloem exudates (Kruger et al., 2002), suggesting that Fe is transported bound to ITP in the phloem as well. In the root epidermal and xylem parenchyma cells, as well as in shoot xylem parenchyma cells, the Fe concentration in the cytosol is controlled through the action of Fe release or import from the vacuole. The Mn/Fe exporter, NRAMP3, is found in root epidermal cells (Thomine et al., 2003), while both NRAMP3 and NRAMP4 are in root and shoot xylem parenchyma cells (Thomine et al., 2003; Lanquar et al., 2005). *VIT1* and *FPN2*, which mediate Fe import into the vacuole are expressed in the plant vasculature (Kim et al., 2006, Morrissey et al., 2009).

A second "auxiliary" Fe uptake strategy involves the root exudation of phenolic and flavin compounds into the rhizosphere under Fe deficiency to facilitate utilization of apoplastic Fe reserves (Bienfait et al., 1985, Jin et al., 2007, Rodríguez-Celma et al., 2013). The molecular identity of transporter(s) involved in phenolic and flavin secretion or the regulation of the synthesis of these compounds is not well understood in nongraminaceous plants. Recent studies in grasses have shown that the protocatechuic acid effluxer **P**henolics **E**fflux **Z**ero **1**, PEZ1, is required for the mobilization of Fe in the stele of rice (Ishimaru et al., 2011) suggesting that its counterpart in nongraminaceous plants might contribute to Fe uptake as well.

Long-distance iron transport

After initial uptake from the soil into root epidermal cells, Fe moves symplastically towards the vasculature and is effluxed from xylem parenchyma cells into the xylem vessels where it is chelated with citrate and undergoes long-distance transport to the shoot as a tri-Fe(III) tri-citrate complex (Durrett et al., 2007, Larbi et al., 2010, Rellán-Álvarez et al., 2010). Another strong Fe ligand is the non-proteinogenic amino acid, nicotianamine (NA, for review see [Curie et al., 2009]). Fe-citrate and Fe-NA complexes undergo ligand exchange reactions at pH 5.5 and 7.5 such that at the more neutral pH of the cytosol and the phloem sap, the Fe-NA complex might prevail; in contrast the tri-Fe(III) tri-citrate complex is the prevailing form of Fe in the more acidic xylem sap and, likely, in the vacuole (Rellan-Alvarez et al., 2008).

The molecular machinery contributing to the root-to-shoot partitioning of Fe and its redistribution between source and sink tissues, and events involved in shoot-to-root communication of Fe status of the shoot are poorly understood. The key identified players in *A. thaliana* are the **M**ultidrug **a**nd **T**oxin **E**fflux family (MATE) member, **F**erric **R**eductase

Defective 3, FRD3, one of two members of the **I**ron **Reg**ulated/**F**erro**p**orti**n** family, IREG1/FPN1, and members of two distinct clades of the Oligopeptide Transporter family, the YSL proteins and the **O**ligo**p**eptide **T**ransporters (OPTs), for which the family was named (Curie et al., 2009, DiDonato et al., 2004, Durrett et al., 2007, Green and Rogers 2004, Lubkowitz 2011, Morrissey et al., 2009, Rogers and Guerinot 2002, Schaaf et al., 2006, Schaaf et al., 2005). FRD3 is located in the root pericycle (Green and Rogers 2004) and transports citrate from xylem parenchyma cells into xylem vessels (Durrett et al., 2007), acting in concert with IREG1/FPN1, which is proposed to mediate Fe efflux into xylem vessels (Morrissey et al., 2009). Citrate release into the apoplast *via* FRD3 plays an important role in partitioning of Fe between apoplast and symplast of cells surrounding xylem vessels in roots and leaf mesophyll cells (Roschzttardtz et al., 2011); and the lack of proper long distance Fe transport in xylem vessels results in shoot chlorosis and deregulated Fe signaling in the *frd3* mutant (discussed below). A mutation in *IREG1/FPN1*, however, does not prevent Fe accumulation in the root vasculature (Roschzttardtz et al., 2011), suggesting that another Fe transporter operates redundantly with IREG1/FPN. Like *frd3* mutants, *fpn1* mutant plants develop shoot chlorosis when grown in Fe-deficient media (Morrissey et al., 2009). However, *fpn1* mutant plants have normal functioning of IRT1 and FRO2, indicating that Fe signaling is not altered with the loss of IREG1/FPN1 (Morrissey et al., 2009). Transporters contributing to the reabsorption of Fe from the apoplast of xylem vessels into the symplast of leaf xylem parenchyma and surrounding mesophyll cells of leaves have not yet been identified, but members of the YSL family in *A. thaliana* might be involved in this process. Based on the expression of YSL2 in xylem parenchyma cells and its involvement in Fe homeostasis in *A. thaliana*, YSL2 has been proposed to function in lateral Fe movement in the vasculature (DiDonato et al., 2004, Schaaf et al., 2005).

Even less is known about the transporters involved in Fe partitioning between source tissues, such as mature leaves, and sink tissues, such as young leaves and seeds. Based on the tissue expression studies and phenotypes of the single *ysl1* and the double *ysl1ysl3* mutant plants, it has been suggested that YSL1 and YSL3 play a redundant role in the delivery of Fe-NA and other transition metals such as Cu and zinc (Zn) into seeds of *A. thaliana* (Chu et al., 2010, Le Jean et al., 2005, Waters et al., 2006). The close relative of the YSLs, a member of the OPT family, OPT3 have been shown to play a role in the delivery of Fe into seeds (Stacey et al., 2002, Stacey et al., 2008). Based on the ability of OPTs to transport peptides in heterologous systems (for review see Lubkowitz 2011), OPT3 has been suggested to transport Fe chelated with a peptide-based ligand or Fe-NA complexes, however the physiological substrate of OPT3 was unknown until the research findings presented in Chapter 5 were obtained. The role of OPT3 in Fe signaling (discussed below) is further explored in this dissertation in Chapter 5.

Transcriptional networks controlling iron homeostasis

Given the dual essential and toxic natures of Fe, plants have developed strategies to tightly regulate Fe homeostasis to prevent deficiency while avoiding toxicity. As evident from the results of a number of transcriptomic and proteomic studies, plants achieve this homeostasis by fine-tuning the expression, posttranslational modification and the turn-over of proteins that are involved in various aspects of Fe homeostasis and that collectively have been termed the "ferrome" (Buckhout et al*.,* 2009, Colangelo and Guerinot 2004, Garcia et al*.,* 2010, Long et al*.,* 2010, Schmidt and Buckhout 2011, Schuler et al*.,* 2011, Shin et al*.,* 2013, Sivitz et al*.,* 2011, Thimm et al*.,* 2001, Yang et al*.,* 2010). Comparison of datasets from various microarrays studies revealed that the ferrome of *A. thaliana* consists of at least 92 genes that are robustly

differentially expressed in response to Fe deficiency in *A. thaliana* (Schmidt and Buckhout 2011). These genes can be organized into two main regulatory networks controlled by two members of the **b**asic **h**elix–**l**oop–**h**elix (bHLH) family of TFs, FIT and POPEYE. Based on the mode of regulation and function of the downstream targets, FIT is the most upstream factor in Fe-deficiency signaling that directly regulates the expression of genes involved in root iron uptake, while POPEYE regulates expression of genes that are mainly involved in long-distance Fe transport.

The FIT network

The first transcription factor that regulates Fe-deficiency responses in the root was identified in tomato and designated FER1, and its *A. thaliana* ortholog is named **F**ER-Like **I**ron Deficiency Induced **T**ranscription Factor 1/**F**ER-Like **R**egulator of Iron **U**ptake, FIT/FRU (bHLH029) (Bauer et al., 2007, Bauer et al., 2004, Jakoby et al., 2004, Ling et al., 2002). FER1 and FIT belong to the bHLH family of transcription factors and share higher sequence similarity with each other (Heim et al., 2003). Both genes are expressed primarily in root epidermal cells and are transcriptionally induced under Fe deficient conditions. *FER1* and *FIT* loss-of-function mutants exhibit lethal leaf chlorosis and cannot mobilize Fe (Colangelo and Guerinot, 2004, Jakoby et al., 2004, Ling et al., 2002). FER1 is essential for induction of ferric reductase and iron transporter genes in tomato (Bauer et al., 2007, Bauer et al., 2004, Bereczky et al., 2003, Li et al., 2004, Ling et al., 2002). FIT is essential for the transcriptional upregulation of *FRO2* and *IRT1*, and posttranscriptional control of IRT1 as well (Colangelo and Guerinot, 2004, Jakoby et al., 2004).

While the expression of *FIT* is increased under Fe deficiency (Colangelo and Guerinot, 2004, Sivitz et al., 2011), its protein undergoes *26S* proteasome degradation under the same conditions

(Sivitz et al., 2011). To reconcile these simultaneous, yet opposite, responses Sivitz et al. (2011) proposed that constant turnover of the FIT protein produces a high ratio of "fresh" to "exhausted" activators, where "fresh" FIT binds *IRT1* and *FRO2*. After binding to the promoter of *IRT1*/*FRO2*, FIT function is "exhausted" and is consequently degraded. In this way, constant cycling of degraded and newly produced FIT protein allow for sustained or amplified expression of *IRT1* and *FRO2*.

Alternatively, Hindt and Guerinot (2012) suggest that quick degradation of FIT allows tighter control over Fe homeostasis. In this mechanism, FIT is already degraded as soon as Fe sufficiency is reached, and the corresponding decrease in *IRT1* slows down uptake of excess Fe. In accordance with the latter suggestion, it is possible that the binding of FIT to the promoter of its targets stabilizes the protein and prevents proteasome-mediated degradation, whereas the unbound FIT is rapidly degraded to prevent unspecific binding and sporadic interference with gene expression.

Although FIT is essential for activation of the Fe deficiency responses, transgenic *A. thaliana* plants overexpressing *FIT* does result in increased *FRO2* and *IRT1* expression, nor were there any detectable changes in Fe content in tissues, suggesting that FIT may form heterooligomers with other bHLH family members (Colangelo and Guerinot 2004, Yuan et al., 2005). However, data from Sivitz et al. 2011 suggests that it is possible that FIT is degraded in transgenic plants overexpressing *FIT*. Subsequent studies using yeast-two-hybrid and bi-molecular complementation assays revealed that FIT physically interacts with four *A. thaliana* bHLH transcription factors, bHLH38, bHLH39, all part of a 1b subgroup of the bHLH family (Wang et al., 2013, Wu et al., 2012, Yuan et al., 2008). Furthermore, overexpression of FIT with either bHLH38 or bHLH39 in plants resulted in constitutive expression of *FRO2* and *IRT1*, suggesting

that the transcription of *FRO2* and *IRT1* is directly regulated by a FIT/bHLH38 or FIT/bHLH39 complex (Yuan et al., 2008).

Microarray analysis using the *fit1-1* mutant and transgenic plants co-expressing FIT/bHLH38 or FIT/bHLH39 showed that, in addition to *FRO2* and *IRT1*, FIT/bHLH38 or FIT/bHLH39 regulate expression of genes encoding the Cd/Zn transporting P-type ATPase HMA3, **N**icotian**a**mine **S**ynthase enzymes, NAS1 and NAS2, as well as the vacuolar-localized transporters IREG2/FPN2, IRT2, and MTP3, which are involved in the sequestration of heavy metals in the vacuole in the root (Colangelo and Guerinot 2004, Wu et al., 2012). Given the broad substrate specificity of IRT1, which in addition to Fe also facilitates uptake of other transition metals, including Cd (Eide et al., 1996, Rogers et al., 2000, Vert et al., 2002), these transport systems act in concert with IRT1/FRO2 to maintain the adequate Fe supply of the plant, while keeping Cd in the root to prevent the damage of photosynthetic apparatus.

Recently, Wang et al. (2013) showed that FIT also interacts with bHLH100 and bHLH101. Furthermore, co-expression of either *bHLH100* or *bHLH101* with *FIT* in yeast cells activated the *GUS* expression driven by promoters of *FRO2* and *IRT1,* and plants co-expressing *FIT* together with *bHLH101* showed constitutive expression of *FRO2* and *IRT1* in roots, and accumulated more iron in shoots. These findings show that *bHLH100* or *bHLH101* function redundantly with bHLH38 and bHLH39 in regulating the iron-deficiency responses and uptake in *A. thaliana*. Interestingly, *bHLH38*, *bHLH39*, *bHLH100* and *bHLH101* expression does not depend on FIT and all four bHLHs are transcriptionally induced under Fe deficiency in both roots and shoots, in contrast to *FIT, IRT1* and *FRO2,* which have root-specific expression (Wang et al., 2007). This finding raises the question of the existence of not yet identified regulator(s) controlling Fe-deficiency responses of *bHLH38*, *bHLH39*, *bHLH100* and *bHLH101*in roots and shoots.

Additionally, co-overexpression of a master regulator of Fe homeostasis, FIT, with its binding partners, bHLH38 or bHLH39, in *A. thaliana* enhances Cd tolerance by increasing Cd sequestration in roots and improving Fe homeostasis of shoots (Wu et al., 2012). Hence, it is plausible that the identification of components that are involved in crosstalk between Cd toxicity and Fe homeostasis might facilitate devising approaches for the biofortification of staple foods with essential elements like Fe while omitting Cd.

The POPEYE network

A second regulatory system is controlled by another member of the bHLH family, bHLH049 that was designated **P**OPE**YE** (PYE) (Long et al., 2010). In contrast to *FIT*, *PYE* is transcriptionally upregulated in response to Fe deficiency not only in roots but also in shoots of *A. thaliana* and is suggested to play a role in maintaining Fe homeostasis in both Fe replete and deficient conditions (Long et al., 2010, Rodríguez-Celma et al., 2013). Within the root, *PYE* is transcriptionally upregulated in response to Fe limitation in the pericycle, yet the PYE protein moves to adjacent cells, as evident from the ubiquitous localization pattern of PYE-GFP. Thus, PYE may coordinate Fe homeostasis in multiple cell types (Long et al., 2010). Where and how PYE is distributed in the shoot, has not been determined.

The *pye-1* mutation leads to the following morphological responses of *A. thaliana* roots to Fe deficiency: the decreased growth of the primary root, inhibited emergence of root hairs and swelling of cells within the elongation zone of lateral roots. With regards to the effect of PYE on root architecture, it is noteworthy that a direct target of PYE is a MADS-box transcription regulator, ANR1, which regulates lateral root development of *A. thaliana* in response to nitrogen availability (Zhang and Forde, 1998a; Zhang and Forde, 1998b). Therefore, misregulated *ANR1*

expression may affect lateral root development of the *pye-1* mutant. Other targets of PYE include *NAS4* and *FRO3*, suggesting that, in addition to Fe homeostasis, PYE contributes to Cu homeostasis as well. Like other members of the bHLH family, PYE interacts with a protein called **B**RU**T**U**S** (BTS), a putative E3 ubiquitin ligase that in addition to possessing a **R**eally **I**nteresting **N**ew **G**ene (RING) Zn-finger domain, also possesses a putative Fe-binding haemerythrin domain. Since *bts-1* plants are more tolerant to Fe deficiency, this protein is suggested to act as a negative regulator of the Fe deficiency response (Long et al., 2010). Subsequent studies described below identified BTS as an Fe sensor (Long et al., 2010).

The iron sensor

Central to studies in Fe homeostasis is the search for the Fe sensor. Studies of *O. sativa* have shown that a central regulator of Fe deficiency response, the TF **I**ron **D**eficiency-Responsive **E**lement Binding **F**actor 1, OsIDEF1, is also capable of binding Fe through its histidine-asparagine repeats and proline-rich domains, suggesting that it may act as an Fe sensor in rice (Kobayashi et al., 2012). However, these domains also bind to Cu, Ni and Zn with no specificity for Fe over the other metals. The authors propose that OsIDEF1 may detect the ratio of Fe to other metals to sense the progression of Fe deficiency. For example, the ratio of Fe to other metals would be high under Fe sufficient conditions, and would change during Fe deficiency due to decreases in cellular Fe. As Fe may be replaced by other metals, the strength and/or specificity of OsIDEF1 towards its targets may change.

A recent discovery by Kobayashi et al. (2013) characterized two nuclear-localized **H**aemerythrin Motif-Containing **R**ING- And **Z**n-Finger proteins in *O. sativa*, OsHRZ1 and OsHRZ2, as Fe-binding sensors downstream of OsIDEF1. Metal binding assays using full-length

and truncated OsHRZ1 and OsHRZ2 proteins indicate that Fe and Zn competitively and specifically bind to the haemerythrin domain, while ubiquitination assays indicate that OsHRZ1 and OsHRZ2 also function as E3 ligases through the RING and Zn-finger domains found at the C-terminal site (Kobayashi et al., 2013). RNAi knock-down of OsHRZ1 and OsHRZ2, and T-DNA insertions into the OsHRZ1 and OsHRZ2 genes resulted in increased tolerance to Fe deficiency in hydroponics or calcareous soil, suggesting that both are negative regulators of Fe deficiency response (Kobayashi et al., 2013). Consistent with this suggestion, microarray analysis of RNAi knock-down plants revealed that Fe-uptake and utilization genes are upregulated in Fe-sufficient OsHRZ2-RNAi plants, while this response was present, but weaker in OsHRZ1-RNAi plants (Kobayashi et al., 2013).

OsHRZ1 and OsHRZ2 do not have redundant functions, as characterized by the generally weaker tolerance of OsHRZ1-RNAi knockdown plants to calcareous soil, and low seed set by *hrz1* T-DNA insertion mutants (Kobayashi et al., 2013). In contrast, OsHRZ2-RNAi plants are more tolerant to calcareous soil and *hrz2* plants have higher seed production (Kobayashi et al., 2013).

Interestingly, detection of OsHRZ1- and OsHRZ2-GFP tagged proteins show little GFP-mediated fluorescence in Fe sufficient roots and low fluorescence in Fe deficient roots, indicating that OsHRZ1- and OsHRZ2-GFP are degraded in Fe-sufficient root tissues, where the expression of these genes are highest in the stele (Kobayashi et al., 2013). Like FIT, the degradation of OsHRZ1 and OsHRZ2 is mediated by the *26S* proteasome, although degradation of OsHRZ1 and OsHRZ2 is unaffected by Fe status of the plant (Kobayashi et al., 2013).

The closest homolog of OsHRZ1 and OsHRZ2 in *A. thaliana* is BTS, which also possesses the haemerythrin domain (Kobayashi et al., 2013). Further, the haemerythrin domain of BTS

binds Fe and upon binding Fe BTS possesses ubiquitination activity (Kobayashi et al., 2013). Based on close homology to OsHRZ1 and OsHRZ2, and its Fe binding capacity, BTS is proposed to function as Fe sensor in *A. thaliana.* Whether other Fe sensor(s) exist in plants is unknown.

Iron remobilization from the vacuole

Studies of vacuolar Fe transporters highlight the importance of Fe mobilization from storage pools during early germination. **V**acuolar **I**ron **T**ransporter 1, VIT1, is expressed in the vasculature of seedlings and developing seeds (Kim et al., 2006, Zhang et al., 2012) and although *vit1-1* mutants have comparable leaf levels of essential metals compared to wild-type plants at the vegetative/late reproductive stage, *vit1-1* mutants are unable to grow on soil with pH levels of 7.9; where Fe would be unavailable. Fe remobilization from storage pools in the embryo and seeds are crucial to establishment during early germination, but *vit1-1* plants are unable to properly store Fe in seeds and embryos (Kim et al., 2006, Roschzttardtz et al. 2009), resulting in reduced fitness of seedlings on Fe deficient soil. However, *vit1-1* seedlings are able to grow on soil with available Fe (pH 5.6) (Kim et al., 2006) suggesting that uptake mechanisms are still intact in this mutant.

Other vacuolar transporters include members of the **N**atural **R**esistance-**A**ssociated **M**acrophage **P**rotein (NRAMP) family, NRAMP3 and NRAMP4. These two transporters are expressed in the vasculature of roots and shoots, and expression is induced by Fe deficiency (Thomine et al., 2003, Lanquar et al., 2005). *NRAMP3* and *NRAMP4* are expressed during the first two days after germination, before the activation of *IRT1* (Lanquar et al., 2005), suggesting that remobilization of Fe from the vacuole, is crucial during the early germination stage.

Overlapping functions between of *NRAMP3* and *NRAMP4* is demonstrated by the lack of phenotype in the *nramp3-1* and *nramp4-1* single mutants, while *nramp3nramp4* double mutants show transient de-greening during the early germination stage and seedlings are unable to grow on calcareous soil (Lanquar et al., 2005). Overall, Fe loading into the seed cell vacuole by VIT1 and Fe release from the vacuole by NRAMP3 and NRAMP4 highlight the importance of the storage function of the vacuole in Fe homeostasis.

Improper iron localization affects iron status signaling

Given the essential, yet potentially toxic, nature of Fe, expression of *FRO2* and *IRT1* is under tight local and long-distance control. Interestingly, Fe itself plays a signaling role and is regarded as a positive regulator of local signaling (Vert et al., 2003) and analysis of mutants indicate that improper Fe localization affects Fe signaling (Table 1).

Table 1. Mutants with altered iron localization, expression of iron acquisition genes, and iron content in tissues.

Gene	Function	Localization /Expression	Alterations in Fe acquisition genes	Fe content in tissues	Treatments that rescue mutant phenotype
FRD3	Citrate efflux	Plasma membrane/ Root pericycle	Constitutive expression of *FRO2* and *IRT1*	High Fe accumulation in apoplast and vasculature, but less Fe in cytosol	Grafting *frd3* shoots onto Wt roots Citrate addition to growth media
IREG1/ FPN1	Fe influx	Vacuolar membrane/ Root epidermis and cortex	Delayed *IRT1* expression in response to Fe deficiency	Higher Fe in roots	
NAS1 NAS2 NAS3 NAS4	NA synthesis	Cytosol/ Roots (NAS1/2) and shoots (NAS3/4)	Higher expression of *FRO2, IRT1*, and *FIT* in Fe-sufficient plants	High Fe accumulation in shoots Higher Fe in older leaves vs. younger leaves	Foliar application of Fe or NA
NRAMP3	Fe efflux	Vacuolar membrane/ Vasculature of roots and shoots	Overexpression of *NRAMP3* decreased *FRO2* and *IRT1*	No difference in Fe content, but *NRAMP3* overexpression reduces Mn and Zn accumulation	No obvious phenotype in *nramp3-1*
OPT3	Fe influx	Plasma membrane/ Phloem companion cells	Constitutive expression of *FRO2* and *IRT1*	High Fe accumulation in shoots Higher Fe in older leaves vs. younger leaves	Grafting Wt shoots onto *opt3* roots
NAS (*chln*)	NA synthesis	Cytosol/ Roots and shoots	Constitutive expression of *SlFRO*1 and *SlIRT1*	High Fe accumulation in shoots Higher Fe in older leaves vs. younger leaves	Foliar application of Fe or NA
Unknown (*brz*)	Unknown	Unknown	Constitutive expression of *PsFRO*1 and *PsIRT1*	High Fe accumulation in shoots Higher Fe in older leaves vs. younger leaves	Foliar application of Fe
Unknown (*dgl*)	Unknown	Unknown	Constitutive expression of *PsFRO*1 and *PsIRT1*	High Fe accumulation in older leaves	Grafting Wt shoots onto *dgl* roots

Vert et al. (2003) reported that Fe acts as a local inducer of *IRT1* and *FRO2* expression: expression of *IRT1* and *FRO2* is downregulated after prolonged Fe deficiency treatment (7 days)

while Fe re-supply to Fe-starved plants promotes accumulation of *IRT1* and *FRO2* transcripts, and the IRT1 protein. Furthermore, *IRT1/FRO2* expression in Fe-deficient conditions depends on the pool of apoplastic Fe. Removing the root apoplastic iron pool abolishes the transient induction of *IRT1* and *FRO2*, whereas increasing apoplastic iron enhances this response. Optimal cellular Fe is also required for regulated induction of *IRT1* and *FRO2*. Delayed induction of *IRT1* and lower ferric chelate reductase activity was reported in *fpn2-1* mutants, which lack the vacuolar transporter IREG2/FPN2 (Morrissey et al., 2009). The late response in mutant plants was suggested to be due to excess cellular Fe levels and misregulated local Fe sensing in the root (Morrissey et al., 2009).

Besides proper transport of Fe, the localization/production of its ligands, citrate and NA, are crucial for long-distance Fe signaling. Fe accumulation in *frd3* mutants is restricted to the apoplast (Green and Rogers 2004, Roschzttardtz et al., 2011), resulting in less Fe in the cytosol and constitutive expression of *IRT1* and *FRO2* (Rogers and Guerinot 2002, Green and Rogers 2004). Although it is possible that constitutive *IRT1* and *FRO2* expression is due to high apoplastic Fe, the *frd3* mutant is able to suppress Fe uptake genes if detached roots were placed in Fe-sufficient media, suggesting that a shoot-related signal is responsible for the constitutive Fe acquisition phenotype (Green and Rogers 2004). Accordingly, grafting *frd3* shoots onto wild-type roots reversed the constitutive expression of *IRT1* and *FRO2*, in contrast to grafts of wild-type shoots onto *frd3* roots (Green and Rogers 2004). It has long been speculated that movement of Fe from shoots to roots through the phloem suppresses Fe acquisition genes (Maas et al., 1988), and experiments described above suggest that the loss of citrate results in less cellular Fe in shoot tissue, which then induces *IRT1* and *FRO2* in roots.

In the cytoplasm and phloem, the predominant form of Fe is Fe-NA (Curie and Briat 2003).

Mutation of the NAS genes causes misregulated Fe signaling, as exemplified by upregulated *IRT1* and *FRO2* expression in a quadruple *NAS* mutants, *nas4x-2*, which is unable to produce NA (Schuler et al., 2012). The *nas4x-2* mutant has a severe interveinal chlorotic phenotype with dark green veins during all stages of growth and although *nas4x-2* mutants accumulates more Fe in shoot tissue compared to wild-type, Fe levels are higher in older *vs.* young leaves in the mutant, suggesting a defect in remobilization of Fe from source to sink tissues (Schuler et al., 2012). Accordingly, the *nas4x-2* plants are unable to produce siliques or seeds unless Fe or NA are applied to leaves (Schuler et al., 2012). Maas et al., (1988) suggested that phloem Fe suppresses Fe acquisition, and yet despite accumulation of Fe in phloem cells, upregulated expression of *IRT1*, *FRO2*, and *FIT* in the roots of the *nas4x-2* mutant suggests that roots of the mutant sense Fe deficiency (Schuler et al., 2012). Schuler et al. (2012) proposed that the phenotypes of the *nas4x-2* mutants are explained by the function of NA as a required chelate for Fe removal out of the phloem, where in root tissue, the lack of Fe supply to the cytosol explains higher expression on Fe acquisition genes.

As in *nas4x-2* mutants, a defect in the *OPT3* gene blocks shoot-to-root signaling in *opt3-2* mutant plants, which hyperaccumulate Fe in shoot tissue while overexpressing *IRT1* in roots (Stacey et al., 2008). OPT3 has been shown to participate in Fe homeostasis and Fe loading into seeds (Stacey et al., 2002, Stacey et al., 2008). However, the subcellular localization, cell-type expression pattern, and physiological substrate of OPT3 were not known at the time. Part of this dissertation addresses these questions in Chapter 5.

Other mutants displaying affected iron signaling

The tomato ***chl****oro****n****erva* (*chln*) mutant contains a defect in *NAS* (Ling et al., 2002) and similar

to *nas4x-2* mutants, *chln* develops chlorosis in the interveinal area of leaves, while the veins remain dark green and displays constitutive Fe uptake (Böhme and Sholtz 1960, Scholz et al., 1985, Garcia et al., 2013). In leaves, *chln* had a higher Fe symplastic content than the wild-type, and the *chln* mutant have higher symplastic Fe in older leaves compared to younger leaves (Becker et al., 1992), indicating that the *chln* mutant was unable to redistribute Fe from these pools from source to sink leaves. The chlorotic phenotype of *chln* is rescued by foliar application of NA (Böhme and Sholtz 1960), which also decreased constitutive Fe uptake (Scholz et al., 1985), indicating that NA is required for suppression of Fe acquisition genes. However, Garcia et al. (2013) showed that foliar application of Fe also suppressed Fe acquisition genes, indicating that both Fe and NA are required for proper shoot-to-root signaling in *chln*. Combining the physiological and genetic studies of the quadruple *A. thaliana nas4x-1* and *nas4x-2* mutants and the tomato *chln* mutant provide proof that NA is needed for long-distance signaling from shoots-to-roots.

Two pea (*Pisum sativum*) mutants, ***deg**enerated **l**eaflets* (*dgl*) and ***br**on**z**e* (*brz*) also have constitutive Fe uptake despite growth in sufficient Fe. The *brz* mutant displays bronzing of the leaves, starting from the lower leaf and moving to upper leaves during growth and like other mutants discussed, *brz* plants have a defect in remobilization of Fe from older to younger leaves, but accumulate more Fe overall compared to the wild-type (Kneen et al., 1990; Welch and Larue 1990). Grafting *brz* shoots onto wild-type roots show enhanced Fe translocation to shoot tissue (Welch and Larue 1990), suggesting that the *brz* shoot sends an Fe-deficient signal to the root. The *dgl* mutant also has a constitutive expression of *PsFRO1* and *PsIRT1* (Grusak and Pezeshgi 1996; Garcia et al., 2013) compared to the wild-type. Grafting *dgl* mutant shoots onto wild-type roots containing a wild-type shoot explant increased ferric reductase activity of the root (Grusak

and Pezeshgi 1996), and it was suggested that the *dgl* mutant lacked a promotive signal to induce Fe acquisition. However, foliar application of Fe onto *dgl* mutants lowered expression of *PsFRO2* and *PsIRT1* (Garcia et al., 2013), suggests that the *dgl* mutant is unable to send an Fe signal to root tissue *via* the phloem as a signal to repress Fe acquisition genes. Foliar application of Fe onto the *brz* mutant suppressed constitutive expression of *PsFRO1* and *PsIRT1*, suggesting that *brz* is able to move Fe into the phloem.

Vert et al. (2002) suggested two models for long distance Fe signaling: 1) a decrease of global iron in a plant causes a release of a signal of low symplastic Fe from the shoot and, combined with remobilization of root apoplastic Fe, promotes *IRT1* and *FRO2* expression and activity in the root; or 2) the expression of *IRT1* and *FRO2* is constitutive unless repressed by a signal of high symplastic Fe from the shoot. Overall, mutant studies in *A. thaliana*, tomato, and pea provide evidence in support of the second model as the predominant mechanism of Fe signaling in plants.

Conclusion

Much progress has been made regarding Fe homeostasis in terms of identifying vacuolar transporters and new transcription networks, as well as expanding existing knowledge on uptake and components of Fe deficiency response. Future research direction seems to be heading towards elucidating Fe signaling networks. In this regard, we have contributed to the current knowledge of long-distance signaling in the following publication:

Zhai, Z., Gayomba, S.R., Jung, H., Vimalakumari, N.K., Piñeros, M., Craft, E., Rutzke, M., Danku, J., Lahner, B., Punshon, T., Guerinot, M., Salt, D.E., Kochian, L.V., and Vatamaniuk, O.K. (2014) OPT3 is a phloem-specific iron transporter that is essential for shoot-to-root iron signaling and redistribution of iron and cadmium in *Arabidopsis thaliana*. *Plant Cell*. *Accepted*.

Overview of cadmium uptake, toxicity and basal resistance mechanisms

Cadmium (Cd) is a highly toxic transition metal of considerable biological and environmental concern. Although Cd is a natural component of the Earth's crust, anthropogenic activities during the last century significantly contributed to its emission into the environment, resulting in concerns that Cd may enter the food supply and cause devastating diseases (Jarup 2003, Waisburg 2003, Joseph 2009). Cadmium causes stunting and chlorosis in plants and affects major biochemical processes including redox balance, photosynthesis, and water status (Hasan et al*.,* 2009). Development of plants for successful heavy metal remediation and "Cd-safe crops" with increased density of essential minerals while decreased concentration of Cd rely on the knowledge of mechanisms that control Cd uptake and tissue partitioning.

Cadmium uptake and translocation in plants

Studies to date show that uptake and transport of the toxic, non-essential transition element Cd could be mediated by transporters for essential elements (*e.g.* Fe, Ca, Mn) due to either the broad substrate specificity of the transporter, or the similar ionic properties between Cd and essential metals (Eide et al., 1996, Thomine et al., 2000, Thomine et al., 2003) and Figure 3.

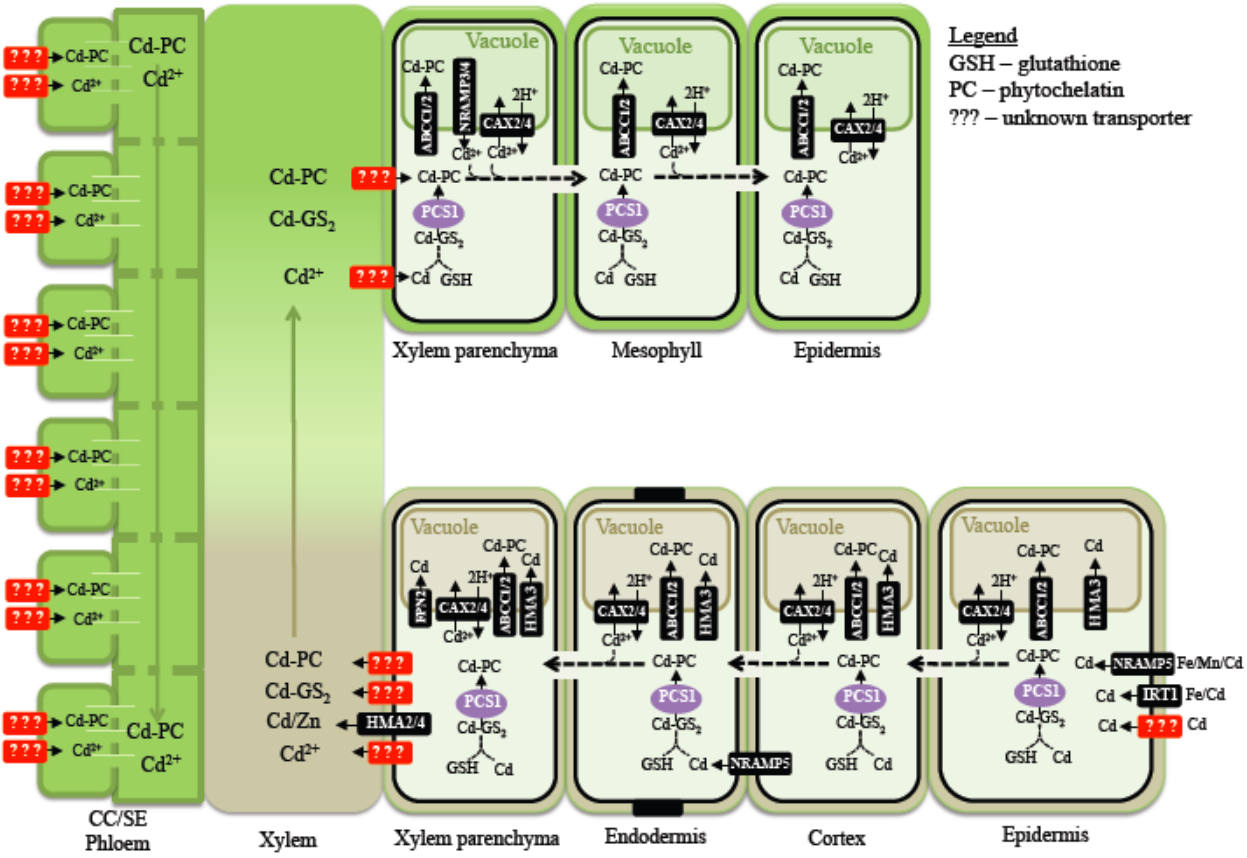

Figure 3. Overview of cadmium transport in *A. thaliana*. The major entry point of Cd into root epidermal cell is IRT1(Vert et al., 2002). In rice, NRAMP5 is the major entry pathway of Cd into the root (Ishimaru et al., 2012, Sasaki et al., 2012). Once in the cytosol, Cd ions form a bidentate chelate with glutathione, GSH, to form Cd-GS_2 complexes (Li et al., 1997). The blocked thiols of GSH activates PCS1 which catalyzes the synthesis of phytochelatins, PCs (Vatamaniuk et al., 2000). Cd-PC complexes, or Cd^{2+}, can travel through the plasmodesmata towards the stele and are loaded into xylem vessels by members of the P-type ATPase family, HMA2 or HMA4 (Hussain et al., 2004, Mills et al., 2003, Verret et al., 2004). Transporters mediating xylem reabsorption of Cd into shoot tissue remain unknown. Also unknown is how Cd enters the phloem, but Cd-PCs have been found in phloem sap (Mendoza-Cózatl et al., 2008). In the cytosol, Cd^{2+} can be sequestered into the vacuole by CAX2, CAX4, FPN2, HMA3, NRAMP3, and NRAMP4 in roots (Hussain et al., 2004, Morel et al., 2009, Chao et al., 2012, Hirschi et al., 2000, Korenkov et al., 2009, Wu et al., 2012, Molins et al., 2013). Note that NRAMP3 and NRAMP4 are not shown in root xylem parenchyma for simplicity. In shoots, vacuolar Cd transporters include of ABCC1, ABCC2, CAX2, CAX4, NRAMP3, and NRAMP4 (Park et al., 2012, Hussain et al., 2004, Morel et al., 2009, Chao et al., 2012, Molins et al., 2013).

After initial diffusion from the soil into the apoplast of root epidermal cells, the Fe transporter IRT1, is recognized as a main contributor to Cd uptake in *A. thaliana* and other

dicotyledonous plants (Vert et al., 2002). IRT1 expression is induced by Cd and studies have shown that Cd inhibits IRT1-dependent Fe(II) uptake (Eide et al., 1996, Connolly et al., 2002). Accordingly, *irt1-1* mutant plants are more tolerant to Cd than wild-type plants and accumulate less Cd in root tissue (Vert et al., 2002), while over-expression of *IRT1* increases sensitivity to Cd under Fe-deficient conditions (Connolly et al., 2002). Although Cd competes with Fe for uptake *via* IRT1 (Eide et al., 1996), increasing Fe levels rescues the Cd-sensitive phenotype of plants over-expressing *IRT1* (Connolly et al., 2002) and wild-type plants, compared to the *irt1-1* mutant (Vert et al., 2002).

The wheat (*Triticum aestivum*) Ca transporter, **L**ow-Affinity **C**ation **T**ransporter 1, TaLCT1, is expressed in roots and shoots (Schatman et al., 1994), and increases Cd sensitivity of *S. cerevisiae* by increasing Cd uptake suggesting that, in addition to Ca, TaLCT1 can mediate uptake of Cd as well (Clemens et al., 1998). However, over-expression of *TaLCT1* in tobacco resulted in more efficient Ca uptake, and greater tolerance to Cd (Antosiewicz and Hennig 2003). Further, transgenic plants contained less Cd and more Ca in root tissue compared to empty vector-expressing plants, suggesting that Ca competes with Cd uptake by TaLCT1 (Antosiewicz and Hennig 2003). These results suggest that under physiological conditions, LCT1 does not mediate Cd uptake.

In rice, *OsNRAMP5* functions as a multispecific transporter capable of mediating uptake of Mn, Fe, as well as Cd (Ishimaru et al., 2012, Sasaki et al., 2012). *OsNRAMP5* is predominantly expressed in roots and localizes to the plasma membrane (Ishimaru et al., 2012, Sasaki et al., 2012). Sasaki et al. (2012) detected OsNRAMP5 in root exodermis and endodermis cells through immunostaining using OsNRAMP5 antibodies, while Ishimaru et al. (2012) reported that *OsNRAMP5* is expressed at the epidermis, exodermis, and outer layers of the cortex and around

xylem cells in plants expressing an *NRAMP5*$_{promoter}$*-GUS* construct. Ishimaru et al. (2012) also reported less Mn and Fe in xylem sap of plants expressing an RNAi construct against *OsNRAMP5*, suggesting that OsNRAMP5 loads Mn and Fe into the xylem. Knockdown of *OsNRAMP5* resulted in greater Cd translocation into shoots (Ishimaru et al., 2012), in contrast to observations that *nramp5* plants accumulated less Cd in both roots and shoots (Sasaki et al., 2012). Sasaki et al. (2012) suggest that this discrepancy may be due to different Cd concentrations used in the growth media, but it is also possible that the rice ecotypes used in these studies had different *OsNRAMP5* expression levels, as found in *OsNRAMP1* expression levels in different rice ecotypes (Takahashi et al., 2011).

Once in the cell, Cd toxicity results from the displacement of endogenous co-factors from their cellular binding sites, thiol-capping of essential proteins, inhibition of DNA repair processes and interference with the antioxidant defense system, resulting in the generation of ROS (Clemens 2006, Stadtman 1990, Valko et al., 2005). Cd is detoxified in the cytosol by forming a bidentate Cd-GS_2 complex with GSH (Li et al*.,* 1997), which then facilitates synthesis of the strong Cd ligands, phytochelatins (PCs) (Rea 2012, Vatamaniuk et al., 2000). Plants unable to synthesize PCs in the *cad1* or ***cad****mium sensitive* mutant 1, (Howden and Cobbett 1992), are deficient in the phytochelatin synthase gene, *PCS1* (Vatamaniuk et al., 1999, Ha et al., 1999). The positive correlation between PC synthesis and Cd tolerance was demonstrated in an allelic series of *cad1* plants producing varying amounts of PCs (Howden et al., 1995). Cd-PC complexes, as well as free Cd ions, are either sequestrated into the vacuole in the root (described in the next section), or bypass the vacuole and instead load into xylem vessels of the root to travel into shoot with the transpiration stream (Hirschi et al., 2000, Morel et al., 2009, Park et al., 2012, Salt et al., 1995, Wong and Cobbett 2009). The Zn-transporting P-type ATPase proteins,

HMA2 and HMA4, mediate xylem loading of Cd (Hussain et al., 2004, Mills et al., 2003, Verret et al., 2004). Expression of *HMA4* decreases upon Cd exposure and the increased Cd tolerance of *HMA4*-expressing *S. cerevisiae* further support the notion that HMT4 is a metal efflux transporter (Mills et al., 2003). As in *S. cerevisiae*, over-expression of *HMA4* in the *A. thaliana* Wassilewskija (Ws) resulted in better root growth in plants exposed to Cd and increased Cd content in shoots, suggesting that improving root-to-shoot translocation of Cd increases tolerance of roots to this toxic element (Verret et al., 2004). Increased shoot accumulation of toxic elements should lead to increased sensitivity, but *A. thaliana* Ws ecotypes have enhanced Cd sequestration in leaf vacuoles by the HMA3 vacuolar Cd transporter (discussed in the next section). In *A. thaliana* Col-0, the loss of *HMA4* results in a mutant that has lower Cd translocation to shoot tissue (Verret et al., 2004) and increased Cd sensitivity of the root (Mills et al., 2005, Wong and Cobbett 2009), perhaps due to increased Cd and Zn accumulation in the root and less Zn in shoots. The mechanisms and transporters involved in Cd, Cd-GS_2, and/or Cd-PCs from xylem vessels to xylem parenchyma in the leaf are unknown. However, studies in Cd hyperaccumulating plants indicate that enhanced root-to-shoot translocation and vacuolar sequestration in leaf cells are an important component of Cd tolerance (Milner and Kochian, 2008, Verbruggen et al., 2009). A recent report identified a plasma membrane-localized phloem Cd transporter in *O. sativa* responsible for Cd-loading into grains (Uraguchi et al., 2011). A homologue of *TaLCT1* in rice, *OsLCT1*, is strongly expressed in leaf blades and nodes during grain ripening, with lower expression during the vegetative stage (Uraguchi et al., 2011). RNAi knockdown of *OsLCT1* resulted in decreased Cd content in phloem sap and grains, while Cd content in xylem sap showed no difference compared to empty vector-expressing plants (Uraguchi et al., 2011).

Vacuolar transporters

Vacuolar sequestration of toxic metals reduces their concentration within the cytoplasm and is a major mechanism of cellular Cd detoxification. The long-sought after Cd-PC vacuolar transporters, ABCC1 and ABCC2, belong to the **A**TP-**B**inding **C**assette, Sub-family **C** Transporter family and *abcc1* single and *abcc1abcc2* double mutants are sensitive to Cd and impaired in sequestering Cd in vacuoles (Park et al., 2012). Accumulation of Cd in shoot tissue was enhanced in both *abcc1* and *abcc1abcc2* mutants, and *ABCC1* over-expressing plants accumulated more Cd in both roots and shoots compared to wild-type plants (Park et al., 2012). However, *ABCC1* over-expressing plants had enhanced vacuolar sequestration and increased Cd load did not lead to sensitivity, unlike *abcc1* and *abcc1abcc2* mutants (Park et al., 2012). In addition to Cd, ABCC1 and ABCC2 also mediate transport of PCs complexed to the toxic metalloid, arsenic (Song et al., 2010).

As mentioned above, the P-type ATPase, HMA3, is localized to the vacuolar membrane and mediates Zn and Cd transport and rescues the Cd-sensitive phenotype of *S. cerevisiae* mutant cells lacking the vacuolar membrane-localized Cd-GS_2 transporter, YCF1 (Gravot et al., 2004). Studies in rice and *A. thaliana* ecotypes suggest that the combination of a functional HMA3 protein and its expression pattern dictates Cd root-to-shoot translocation and tolerance. *A thaliana* Col-0 and *A. thaliana* CS28181 ecotypes expresses *HMA3* primarily in the roots, but Col-0 *HMA3* is a pseudogene encoding a non-functional protein, whereas HMA3 in CS28181 is functional (Hussain et al., 2004, Morel et al., 2009, Chao et al., 2012). Retention of Cd in the root by vacuolar sequestration results in lower Cd accumulation in shoots of the CS28181 ecotype compared to Col-0 (Chao et al., 2012). *HMA3* in the *A. thaliana* Wassilewskija (Ws) ecotype encodes a functional protein (Hussain et al., 2004). Morel et al., (2009) observed that

that *hma3-1* mutants of the Ws ecotype were sensitive to Zn and Cd toxicity, while ectopic over-expression of *A. thaliana* Ws *HMA3* increased Cd tolerance (Morel et al., 2009). Increased tolerance was directly attributed to enhanced vacuolar sequestration of Cd in both roots and shoots, as the over-expression of *A. thaliana* Ws *HMA3* increased Cd accumulation in both tissues. *OsHMA3* in rice dictates Cd accumulation in two cultivars: the shoot Cd accumulating *indica* cultivar Anjana Dhan, and the root Cd accumulating *japonica* cultivar, Nipponbare (Ueno et al., 2010) and comparison of OsHMA3 between Nipponbare and Anjana Dhan showed that the HMA3 from Anjana Dhan is non-functional (Ueno et al., 2010). Thus, accumulation of Cd in shoots of Anjana Dhan is due to the lack of vacuolar sequestration in the root, allowing Cd movement into the xylem. In the Zn/Cd hyperaccumulator *Thlaspi caerulescens*, it is the level of *HMA3* expression that controls Cd accumulation in shoot tissue (Ueno et al., 2011). The *T. caerulescens* Ganges ecotype has higher expression of *TcHMA3* and greater Cd accumulation in shoots in contrast to the Prayon ecotype which accumulates and tolerates less Cd in the shoot (Lombi et al., 2002, Ueno et al., 2011). Studies of *HMA3* suggest that it is possible to control Cd accumulation in different tissues, making this gene a good candidate for creating plants both for Cd phytoremediation and Cd safe crops.

A vacuolar Ca^{2+}/H^{+} antiporter, **Ca**lcium E**x**changer 2, CAX2, was shown to transport Cd when expressed in tobacco (Hirschi et al., 2000). Tobacco plants expressing *CAX2* accumulated more Cd in root tissue and root tonoplast vesicles, although no phenotype was found when plants were grown on Cd-containing media (Hirschi et al., 2000). Tobacco plants specifically expressing *CAX2* and *CAX4* in roots accumulated less Cd in lower leaves, suggesting that enhanced vacuolar sequestration in roots confer protective functions in shoot tissue (Korenkov et al., 2009). Another vacuolar Zn transporter, **M**etal **T**olerance **P**rotein 3, MTP3, is expressed in

cortical and epidermal cells of roots and complements the Zn-sensitive phenotype of the *S. cerevisiae zrc1cot1* mutant strain (Arrivault et al., 2006). RNAi interference of the *MTP3* gene resulted in sensitivity to Zn toxicity, while over-expression confers tolerance (Arrivault et al., 2006). Although MTP3 was not yet shown to transport Cd, constitutive expression of *MTP3* in transgenic plants co-expressing *FIT* and *bHLH38*/*bHLH39* is thought to contribute to increased Cd tolerance in these lines (Wu et al., 2012). Like MTP3, it is unknown if FPN2/IREG2 transports Cd, but was highly expressed in transgenic plants co-expressing *FIT* and *bHLH38*/*bHLH39* and may contribute to Cd tolerance (Wu et al., 2012).

The vacuolar membrane NRAMP3 and NRAMP4 transporters that mediate Mn efflux from the vacuole highlight the importance of essential micronutrient release during Cd stress. The expression of *NRAMP3* and *NRAMP3* increases during Cd stress and although Cd accumulation in *nramp3nramp4* double mutants were similar to wild-type plants, *nramp3nramp4* plants are sensitive to Cd (Molins et al., 2013). This sensitivity is likely due to decreased chlorophyll levels and photosynthetic efficiency of *nramp3nramp4* mutants, probably from lower cytosolic Mn levels needed for PSII activity and function (Molins et al., 2013).

Conclusion

Studies of transporters involved in Cd uptake, translocation, and vacuolar sequestration have revealed much about Cd movement within the plant. Still unknown are transporters responsible for xylem reabsorption of Cd into shoot tissue and Cd loading in phloem tissue of dicot plants. It is possible that even more transporters are involved in Cd detoxification and studies listed above highlight the extent of cross-talk between Cd and essential metals. However, if the development of "cadmium safe" crops is the goal of these studies, the research must extend to how Cd affects

homeostasis of other metals. Thus far, the cross-talk between Fe and Cd are well known. Chapter 3 of this dissertation discusses cross-talk between Cd and Cu homeostasis, which was published under the following citation:

Gayomba, S. R., Jung, H., Yan, J., Danku, J., Rutzke, M. A., Bernal, M., Krämer, U., Kochian, L. V., Salt, D. E. and Vatamaniuk, O. K. (2013) The CTR/COPT-dependent copper uptake and SPL7-dependent copper deficiency responses are required for basal cadmium tolerance in *A. thaliana*. *Metallomics*, **5**, 1262-1275.

REFERENCES

Abdel-Ghany, S. E. and Pilon, M. (2008) MicroRNA-mediated systemic down-regulation of copper protein expression in response to low copper availability in *Arabidopsis*. *J Biol Chem*, **283**, 15932-15945.

Andrés-Colás, N., Perea-García, A., Puig, S. and Peñarrubia, L. (2010) Deregulated copper transport affects *Arabidopsis* development especially in the absence of environmental cycles. *Plant Physiol*, **153**, 170-184.

Andrés-Colás, N., Sancenón, V., Rodríguez-Navarro, S., Mayo, S., Thiele, D. J., Ecker, J. R., Puig, S. and Peñarrubia, L. (2006) The *Arabidopsis* heavy metal P-type ATPase HMA5 interacts with metallochaperones and functions in copper detoxification of roots. *Plant J*, **45**, 225-236.

Antosiewicz, D. M. and Hennig, J. (2003) Overexpression of *LCT1* in tobacco enhances the protective action of calcium against cadmium toxicity. *Environ Poll*, **129**, 237-245.

Angulo, J. F., Rouer, E., Mazin, A., Mattei, M. G., Tissier, A., Horellou, P., Benarous, R. and Devoret, R. (1991) Identification and expression of the cDNA of *KIN17*, a zinc-finger gene located on mouse chromosome 2, encoding a new DNA-binding protein. *Nuc Acids Res*, **19**, 5117-5123.

Arrivault, S., Senger, T. and Krämer, U. (2006) The *Arabidopsis* metal tolerance protein AtMTP3 maintains metal homeostasis by mediating Zn exclusion from the shoot under Fe deficiency and Zn oversupply. *Plant J*, **46**, 861-879.

Bauer, P., Ling, H. Q. and Guerinot, M. L. (2007) FIT. The FER-LIKE IRON DEFICIENCY TRANSCRIPTION FACTOR in *Arabidopsis*. *Plant Physiol Biochem*, **45**, 260-261.

Bauer, P., Thiel, T., Klatte, M., Bereczky, Z., Brumbarova, T., Hell, R. and Grosse, I. (2004) Analysis of sequence, map position, and gene expression reveals conserved essential genes for iron uptake in *Arabidopsis* and tomato. *Plant Physiol*, **136**, 4169-4183.

Becker, R., Grün, M. and Scholz, G. (1992) Nicotianamine and the distribution of iron into the apoplasm and symplasm of tomato (*Lycopersicon esculentum* Mill.) : I. Determination of the apoplasmic and symplasmic iron pools in roots and leaves of the cultivar Bonner Beste and its nicotianamine-less mutant *chloronerva*. *Planta*, **186**, 48-52.

Becker, R., Manteuffel, R., Neumann, D. and Scholz, G. (1998) Excessive iron accumulation in the pea mutants *dgl* and *brz*: subcellular localization of iron and ferritin. *Planta*, **207**, 217-223.

Bereczky, Z., Wang, H. Y., Schubert, V., Ganal, M. and Bauer, P. (2003) Differential regulation of nramp and irt metal transporter genes in wild type and iron uptake mutans of tomato. *J Biol Chem*, **278**, 24697-24704.

Bernal, M., Casero, D., Singh, V., Wilson, G. T., Grande, A., Yang, H., Dodani, S. C., Pellegrini, M., Huijser, P., Connolly, E. L., Merchant, S. S. and Krämer, U. (2012) Transcriptome sequencing identifies SPL7-regulated copper acquisition genes *FRO4*/*FRO5* and the copper dependence of iron homeostasis in *Arabidopsis*. *Plant Cell*, **24**, 738-761.

Bienfait, H. F., van den Briel, W. and Mesland-Mul, N. T. (1985) Free space iron pools in roots: generation and mobilization. *Plant Physiol*, **78**, 596-600.

Bittner, F. (2014) Molybdnum metabolism in plants and crosstalk to iron. *Front Plant Sci*, **5**, 28.

Böhme, H. and Sholtz, G. (1960) Versuche zur Normalisierung des Phänotyps der Mutante *chloronerva* von *Lycopersicon esculentum* Mill. *Die Kulturpflanze*, 8, 93-109.

Burkhead, J., Reynolds, K., Abdel-Ghany, S., Cohu C. and Pilon, M. (2009). Copper

homeostasis. New Phytol *182*, 799 - 816.
Buckhout, T. J., Yang, T. J. and Schmidt, W. (2009) Early iron-deficiency-induced transcriptional changes in *Arabidopsis* roots as revealed by microarray analysis. *BMC Genomics*, **10**, 147.
Chao, D.-Y., Silva, A., Baxter, I., Huang, Y. S., Nordborg, M., Danku, J., Lahner, B., Yakubova, E. and Salt, D. E. (2012) Genome-wide association studies identify Heavy Metal ATPase3 as the primary determinant of natural variation in leaf cadmium in *Arabidopsis thaliana*. *PloS Genetics*, **8**, e1002923.
Chen, Y. Y., Wang, Y., Shin, L. J., Wu, J. F., Shanmugam, V., Tsednee, M., Lo, J. C., Chen, C. C., Wu, S. H. and Yeh, K. C. (2013) Iron is involved in the maintenance of circadian period length in *Arabidopsis*. *Plant Physiol*, **161**, 1409-1420.
Chory, J., Peto, C. A., Ashbaugh, M., Saganich, R., Pratt, L. and Ausubel, F. (1989) Different roles for phytochrome in etiolated and green plants deduced from characterization of *Arabidopsis thaliana* mutants. *Plant Cell*, **1**, 867-880.
Chu, H. H., Chiecko, J., Punshon, T., Lanzirotti, A., Lahner, B., Salt, D. E. and Walker, E. L. (2010) Successful reproduction requires the function of *Arabidopsis* Yellow Stripe-Like1 and Yellow Stripe-Like3 metal-nicotianamine transporters in both vegetative and reproductive structures. *Plant Physiol*, **154**, 197-210.
Clemens, S. (2006) Toxic metal accumulation, responses to exposure and mechanisms of tolerance in plants. *Biochimie*, **88**, 1707-1719.
Clemens, S., Antosiewicz, D. M., Ward, J. M., Schachtman, D. P. and Schroeder, J. I. (1998) The plant cDNA *LCT1* mediates the uptake of calcium and cadmium in yeast. *Proc Natl Acad Sci U S A*, **95**, 12043-12048.
Clemens, S., Kim, E. J., Neumann, D. and Schroeder, J. I. (1999) Tolerance to toxic metals by a gene family of phytochelatin synthases from plants and yeast. *Embo J*, **18**, 3325-3333.
Cohu, C. M. and Pilon, M. (2007). Regulation of superoxide dismutase expression by copper availability. Physiol Plant *129*, 747-755.
Cohu, C. M., Abdel-Ghany, S. E., Gogolin Reynolds, K. A., Onofrio, A. M., Bodecker, J. R., Kimbrel, J. A., Niyogi, K. K. and Pilon, M. (2009) Copper delivery by the copper chaperone for chloroplast and cytosolic copper/zinc superoxide dismutases: regulation and unexpected phenotypes in an *Arabidopsis* mutant. *Mol Plant*, **2**, 1336-1350.
Colangelo, E. P. and Guerinot, M. L. (2004) The essential basic helix-loop-helix protein FIT1 is required for the iron deficiency response. *Plant Cell*, **16**, 3400-3412.
Connolly, E. L., Campbell, N. H., Grotz, N., Prichard, C. L. and Guerinot, M. L. (2003) Overexpression of the *FRO2* ferric chelate reductase confers tolerance to growth on low iron and uncovers posttranscriptional control. *Plant Physiol*, **133**, 1102-1110.
Connolly, E. L., Fett, J. P. and Guerinot, M.L. (2002) Expression of the IRT1 metal transporter is controlled by metals at the levels of transcript and protein accumulation. *Plant Cell*, **14**, 1347-1357.
Conte, S. S. and Walker, E. L. (2011) Transporters contributing to iron trafficking in plants. *Mol Plant*, **4**, 464-476.
Curie, C. and Briat, J.-F. (2003) Iron transport and signaling in plants. *Ann Rev Plant Biol*, **54**, 183-206.
Curie, C., Cassin, G., Couch, D., Divol, F., Higuchi, K., Le Jean, M., Misson, J., Schikora, A., Czernic, P. and Mari, S. (2009) Metal movement within the plant: contribution of nicotianamine and yellow stripe 1-like transporters. *Ann Bot*, **103**, 1-11.

Dancis, A., Haile, D., Yuan, D. S. and Klausner, R. D. (1994a) The *Saccharomyces cerevisiae* copper transport protein (Ctr1p). Biochemical characterization, regulation by copper, and physiological role in copper uptake. *J Biol Chem*, **14**, 25660-25667.

Dancis, A., Yuan, D. S., Haile, D., Askwith, C., Eide, D., Moehle, C., Kaplan, J. and Klausner, R. D. (1994b) Molecular characterization of a copper transport protein in *S. cerevisiae*: an unexpected role for copper in iron transport. *Cell*, **76**, 393-402.

Davis, S. J., Kurepa, J. and Vierstra, R. D. (1999) The Arabidopsis thaliana HY1 locus, required for phytochrome-chromophore biosynthesis, encodes a protein related to heme oxygenases. *Proc Natl Acad Sci U S A*, **96**, 6541-6546.

De Feo, C. J., Aller, S. G., Siluvai, G. S., Blackburn, N. J. and Unger, V. M. (2009) Three-dimensional structure of the human copper transporter hCTR1. *Proc Natl Acad Sci U S A*, **106**, 4237-4242.

De Feo, C. J., Aller, S. G. and Unger, V. M. (2007) A structural perspective on copper uptake in eukaryotes. *Biometals*, **20**, 705-716.

DiDonato, R. J., Roberts, L. A., Sanderson, T., Eisley, R. B. and Walker, E.L. (2004) *Arabidopsis* Yellow Stripe-Like2 (YSL2): a metal-regulated gene encoding a plasma membrane transporter of nicotianamine–metal complexes. *Plant J*, **39**, 403-414.

Duc, C., Cellier, F., Lobréaux, S., Briat, J. F. and Gaymard, F. (2009). Regulation of iron homeostasis in Arabidopsis thaliana by the clock regulator time for coffee. *J Biol Chem*, **284**, 36271-36281.

Durrett, T. P., Gassmann, W. and Rogers, E. E. (2007) The FRD3-mediated efflux of citrate into the root vasculature is necessary for efficient iron translocation. *Plant Physiol*, **144**, 197-205.

Eide, D., Broderius, M., Fett, J. and Guerinot, M. L. (1996) A novel iron-regulated metal transporter from plants identified by functional expression in yeast. *Proc Natl Acad Sci U S A*, **93**, 5624-5628.

Elich, T. D., McDonagh, A. F., Palma, L. A. and Lagarias, J. C. (1989) Phytochrome chromophore biosynthesis. Treatment of tetrapyrrole-deficient Avena explants with natural and non-natural bilatrienes leads to formation of spectrally active holoproteins. *J Biol Chem*, **264**, 183-189.

Feng, H., An, F., Zhang, S., Ji, Z., Ling, H. Q. and Zuo, J. (2006) Light-regulated, tissue-specific, and cell differentiation-specific expression of the *Arabidopsis* Fe(III)-chelate reductase gene *AtFRO6*. *Plant Physiol*, **140**, 1345-1354.

Fleming, C. A. and Trevors, J. T. (1989) Copper toxicity and chemistry in the environment: A review. *Water Air Soil Pollut*, **44**, 143-158.

GarcÍa, M. J., Lucena, C., Romera, F. J., Alcántara, E. and Pérez-Vicente, R. (2010) Ethylene and nitric oxide involvement in the up-regulation of key genes related to iron acquisition and homeostasis in *Arabidopsis*. *J Exp Bot*, **61**, 3885-3899.

GarcÍa, M. J., Romera, F. J., Stacey, M. G., Stacey, G., Villar, E., Alcántara, E. and Pérez-Vicente, R. (2013) Shoot to root communication is necessary to control the expression of iron-acquisition genes in Strategy I plants. *Planta*, **237**, 65-75.

Garcia-Molina, A., Andrés-Colás, N., Perea-García, A., Del Valle-Tascón, S., Peñarrubia, L. and Puig, S. (2011) The intracellular *Arabidopsis* COPT5 transport protein is required for photosynthetic electron transport under severe copper deficiency. *Plant J*, **65**, 848-860.

Garcia-Molina, A., Andrés-Colás, N., Perea-García, A., Neumann, U., Dodani, S.C., Huijser, P., Peñarrubia, L. and Puig, S. (2013) The *Arabidopsis* COPT6 transport protein functions in copper distribution under copper-deficient conditions.*Plant Cell Physiol*, **54**, 1378-1390.

Garcia-Molina, A., Xing, S. and Hujiser, P. (2014a) A conserved KIN17 curved DNA-binding domain protein assembles with SQUAMOSA PROMOTER BINDING PROTEIN-LIKE7 to adapt *Arabidopsis* growth and development to limiting copper availability. *Plant Physiol*, **162**, 828-840.

Garcia-Molina, A., Xing, S. and Hujiser, P. (2014b) The *Arabidopsis* KIN17 and its homologue KPL mediate different aspects of plant growth and development. *Plant Signal Behav*, **9**, pii: e2634.

Gayomba, S. R., Jung, H. I., Yan, J., Danku, J., Rutzke, M. A., Bernal, M., Krämer, U., Kochian, L. V., Salt, D. E. and Vatamaniuk, O.K. (2013) The CTR/COPT-dependent copper uptake and SPL7-dependent copper deficiency responses are required for basal cadmium tolerance in *A. thaliana*. *Metallomics*, **5**, 1262-1275.

Gong, J. M., Lee, D. A. and Schroeder, J. I. (2003) Long-distance root-to-shoot transport of phytochelatins and cadmium in *Arabidopsis*. *Proc Natl Acad Sci U S A*, **100**, 10118-10123.

Gravot, A., Lieutaud, A., Verret, F., Auroy, P., Vavasseur, A. and Richaud, P. (2004) AtHMA3, a plant P1B-ATPase, functions as a Cd/Pb transporter in yeast. *FEBS Lett*, **561**, 22-28.

Green, L. S. and Rogers, E. E. (2004) FRD3 controls iron localization in *Arabidopsis*. *Plant Physiol*, **136**, 2523-2531.

Grusak, M. A., and Pezeshgi, S. (1996) Shoot-to-root signal transmission regulates root Fe(III) reductase activity in the *dgl* mutant of pea. *Plant Physiol*, **110**, 329-334.

Ha, S. B., Smith, A. P., Howden, R., Dietrich, W. M., Bugg, S., O'Connell, M. J., Goldsbrough, P. B. and Cobbett, C. S. (1999) Phytochelatin synthase genes from *Arabidopsis* and the yeast *Schizosaccharomyces pombe*. *Plant Cell*, **11**, 1153-1164.

Hasan, S.A., Fariduddin, Q., Ali, B., Hayat, S. and Ahmad, A. (2009) Cadmium: toxicity and tolerance in plants. *J Environ Biol*, **30**, 165-174.

Heim, M. A., Jakoby, M., Werber, M., Martin, C., Weisshaar, B. and Bailey, P. C. (2003) The basic helix-loop-helix transcription factor family in plants: A genome-wide study of protein structure and functional diversity. *Mol Biol Evol*, **20**, 735-747.

Henriques, R., Jásik, J., Klein, M., Martinoia, E., Feller, U., Schell, J., Pais, M. S. and Koncz, C. (2002) Knock-out of *Arabidopsis* metal transporter gene IRT1 results in iron deficiency accompanied by cell differentiation defects. *Plant Mol Biol*, **50**, 587-597.

Himelblau, E. and Amasino, R. M. (2001) Nutrients mobilized from leaves of *Arabidopsis thaliana* during leaf senescence. *J Plant Physiol*, **158**, 1317-1323.

Hindt, M. N. and Guerinot, M. L. (2012) Getting a sense for signals: Regulation of the plant iron deficiency response. *Biochimi Biophys Acta,* **1823**, 1521-1530.

Hirschi, K. D., Korenkov, V. D., Wilganowski, N. L. and Wagner, G. J. (2000) Expression of *Arabidopsis* CAX2 in tobacco. Altered metal accumulation and increased manganese tolerance. *Plant Physiol*, **124**, 125-133.

Howden, R. and Cobbett, C. S. (1992) Cadmium-sensitive mutants of *Arabidopsis thaliana*. *Plant Physiol*, **100**, 100-107.

Howden, R., Goldsbrough, P. B., Andersen, C. R. and Cobbett, C. S. (1995) Cadmium-sensitive, *cad1* mutants of *Arabidopsis thaliana* are phytochelatin deficient. *Plant Physiol*, **107**, 1059-1066.

Hussain, D., Haydon, M. J., Wang, Y., Wong, E., Sherson, S. M., Young, J., Camakaris, J., Harper, J. F. and Cobbett, C. S. (2004) P-Type ATPase heavy metal transporters with roles in essential zinc homeostasis in *Arabidopsis*.*Plant Cell*, **16**, 1327-1339.

Ishimaru, Y., Kakei, Y., Shimo, H., Bashir, K., Sato, Y., Sato, Y., Uozumi, N., Nakanishi, H.,

and Nishizawa, N. K. (2011) A rice phenolic efflux transporter is essential for solubilizing precipitated apoplasmic iron in the plant stele. *J Biol Chem*, **286**, 24649-24655.

Ishimaru, Y., Kim, S., Tsukamoto, T., Oki, O., Kobayashi, T., Watanabe, S., Matsuhashi, S., Takahashi, M., Nakanishi, H., Mori, S. and Nishizawa, N. K. (2007) Mutational reconstructed ferric chelate reductase confers enhanced tolerance in rice to iron deficiency in calcareous soil. *Proc Natl Acad Sci U S A*, **104**, 7373-7378.

Ishimaru, Y., Takahashi, R., Bashir, K., Shimo, H., Senoura, T., Sugimoto, K., Ono, K., Yano, M., Ishikawa, S., Arao, T., Nakanishi, H. and Nishizawa, N. (2012) Characterizing the role of rice NRAMP5 in manganese, iron and cadmium transport. *Sci Rep*, **2**, 286.

Jakoby, M., Wang, H. Y., Reidt, W., Weisshaar, B. and Bauer, P. (2004). FRU (bHLH029) is required for induction of iron mobilization genes in *Arabidopsis thaliana*. *FEBS Lett*, **577**, 528-534.

Jarup, L. (2003) Hazards of heavy metal contamination. *Br Med Bull*, **68**, 167-182.

Jin, C. W., You, G. Y., He, Y. F., Tang, C., Wu, P. and Zheng, S. J. (2007) Iron deficiency-induced secretion of phenolics facilitates the reutilization of root apoplastic iron in red clover. *Plant Physiol*, **144**, 278-285.

Jung, H. I., Gayomba, S. R., Yan, J. and Vatamaniuk, O. K. (2014) *Brachypodium distachyon* as a model system for studies of copper transport in cereal crops. *Front Plant Sci*, **5**, 236.

Jung, H. I., Gayomba, S. R., Rutzke, M. A., Craft, E., Kochian, L. V. and Vatamaniuk, O. K. (2012). COPT6 is a plasma membrane transporter that functions in copper homeostasis in *Arabidopsis* and is a novel target of SQUAMOSA Promoter Binding Protein-Like 7. *J Biol Chem*, **287**, 33252-33267.

Jungmann, J., Reins, H. A., Lee, J., Romeo, A., Hassett, R., Kosman, D. and Jentschet, S. (1993) MAC1, a nuclear regulatory protein related to Cu-dependent transcription factors is involved in Cu/Fe utilization and stress resistance in yeast. *EMBO J*, **12**, 5051-5056.

Kampfenkel, K., Kushnir, S., Babiychuk, E., Inzé, D. and Van Montagu, M. (1995) Molecular characterization of a putative *Arabidopsis thaliana* copper transporter and its yeast homologue. *J Biol Chem*, **270**, 28479-28486.

Kim, B.-E., Nevitt, T. and Thiele, D.J. (2008) Mechanisms for copper acquisition, distribution and regulation. *Nat Chem Biol*, **4**, 176-185.

Kim, S. A., Punshon, T., Lanzirotti, A., Li, L., Alonso, J. M., Ecker, J. R., Kaplan, J. and Guerinot, M. L. (2006) Localization of iron in *Arabidopsis* seed requires the vacuolar membrane transporter VIT1. *Science*, **314**, 1295-1298.

Klatte, M., Schuler, M., Wirtz, M., Fink-Straube, C., Hell, R. and Bauer, P. (2009) The analysis of *Arabidopsis* nicotianamine synthase mutants reveals functions for nicotianamine in seed iron loading and iron deficiency responses. *Plant Physiol*, **150**, 257-271.

Klaumann, S., Nickolaus, S. D., Fürst, S. H., Starck, S., Schneider, S., Ekkehard Neuhaus, H. and Trentmann, O. (2011) The tonoplast copper transporter COPT5 acts as an exporter and is required for interorgan allocation of copper in *Arabidopsis thaliana*. *New Phytol*, **192**, 393-404.

Kneen, B. E., Larue, T. A., Welch, R. M. and Weeden, N. F. (1990) Pleiotropic Effects of *brz*: a mutation in *Pisum sativum* (L.) cv 'Sparkle' conditioning decreased nodulation and increased iron uptake and leaf necrosis. *Plant Physiol*, **93**, 717-722.

Knight, S. A., Labbé, S., Kwon, L. F., Kosman, D. J. and Thiele, D. J. (1996) A widespread transposable element masks expression of a yeast copper transport gene. *Genes Dev*, **10**, 1917-1929.

Kobayashi, T., Itai, R. N., Aung, M. S., Senoura, T., Nakanishi, H. and Nishizawa, N. K. (2012) The rice transcription factor IDEF1 directly binds to iron and other divalent metals for sensing cellular iron status. *Plant J*, **69**, 81-91.

Kobayashi, T., Nagasaka, S., Senoura, T., Itai, R. N., Nakanishi, H. and Nishizawa, N. K. (2013) Iron-binding Haemerythrin RING ubiquitin ligases regulate plant iron responses and accumulation. *Nat Commun*, **4**, 2792.

Korenkov, V., King, B., Hirschi, K. and Wagner, G. J. (2009) Root-selective expression of AtCAX4 and AtCAX2 results in reduced lamina cadmium in field-grown *Nicotiana tabacum* L. *Plant Biotechnol J*, **7**, 219-226.

Lanquar, V., Lelievre, F., Bolte, S., Hames, C., Alcon, C., Neumann, D., Vansuyt, G., Curie, C., Schroder, A., Krämer, U., Barbier-Brygoo, H. and Thomine, S. (2005) Mobilization of vacuolar iron by AtNRAMP3 and AtNRAMP4 is essential for seed germination on low iron. *EMBO J*, **24**, 4041-4051.

Larbi, A., Morales, F., Abadia, A. and Abadia, J. (2010) Changes in iron and organic acid concentrations in xylem sap and apoplastic fluid of iron-deficient *Beta vulgaris* plants in response to iron resupply. *J Plant Physiol*, **167**, 255-260.

Le Jean, M., Schikora, A., Mari, S., Briat, J. F. and Curie, C. (2005) A loss-of-function mutation in AtYSL1 reveals its role in iron and nicotianamine seed loading. *Plant J*, **44**, 769-782.

Lee, S., Moon, J. S., Ko, T. S., Petros, D., Goldsbrough, P. B. and Korban, S. S. (2003) Overexpression of *Arabidopsis* phytochelatin synthase paradoxically leads to hypersensitivity to cadmium stress. *Plant Physiol*, **131**, 656-663.

Li, Y., Dhankher, O. P., Carreira, L., Lee, D., Chen, A., Schroeder, J. I., Balish, R. S. and Meagher, R. B. (2004) Overexpression of phytochelatin synthase in *Arabidopsis* leads to enhanced arsenic tolerance and cadmium hypersensitivity.*Plant Cell Physiol*, **45**, 1787-1797.

Li, Z. S., Lu, Y. P., Zhen, R. G., Szczypka, M., Thiele, D. J. and Rea, P. A. (1997) A new pathway for vacuolar cadmium sequestration in *Saccharomyces cerevisiae*: YCF1-catalyzed transport of bis(glutathionato)cadmium. *Proc Natl Acad Sci U S A*, **94**, 42-47.

Ling, H. Q., Bauer, P., Bereczky, Z., Keller, B. and Ganal, M. (2002) The tomato *fer* gene encoding a bHLH protein controls iron-uptake responses in roots. *Proc Natl Acad Sci U S A*, **99**, 13938-13943.

Long, T. A., Tsukagoshi, H., Busch, W., Lahner, B., Salt, D. E. and Benfey, P. N. (2010) The bHLH transcription factor POPEYE regulates response to iron deficiency in *Arabidopsis* roots. *Plant Cell*, **22**, 2219-2236.

Lubkowitz, M. (2011) The oligopeptide transporters: A small gene family with a diverse group of substrates and functions? *Mol Plant*, **4**, 407-415.

Maas, F. M., van de Wetering, D. A., van Beusichem, M. L. and Bienfait, H. F. (1988) Characterization of phloem iron and its possible role in the regulation of Fe-efficiency reactions. *Plant Physiol*, **87**, 167-171.

Marschner, H. Mineral Nutrition of Higher Plants, 2nd ed.; Academic Press: Boston, MA, 1995.

Marschner, H. and Romheld, V. (1994) Strategies of plants for acquisition of iron. *Plant Soil*, **165**, 261-274.

Masson, C., Menaa, F., Pinon-Lataillade, G., Frobert, Y., Chevillard, S., Radicella, J. P., Sarasin, A. and Angulo, J. F. (2003) Global genome repair is required to activate KIN17, a UV-C-responsive gene involved in DNA replication. *Proc Natl Acad Sci U S A*, **100**, 616-621.

Mendel, R.R. and Kruse, T. (2012) Cell biology of molybdenum in plants and humans. *Biochim Biophys Acta*, **1823**, 1568-1579.

Merchant, S.S. (2010) The Elements of Plant Micronutrients. *Plant Physiol*, **154**, 512-515.
Mendoza-Cózatl, D. G., Butko, E., Springer, F., Torpey, J. W., Komives, E. A., Kehr, J. and Schroeder, J. I. (2008) Identification of high levels of phytochelatins, glutathione and cadmium in the phloem sap of *Brassica napus*. A role for thiol-peptides in the long-distance transport of cadmium and the effect of cadmium on iron translocation. *Plant J*, **54**, 249-259.
Miccoli, L., Frouin, I., Novac, O., Di Paola, D., Harper, F., Zannis-Hadjopoulos, M., Maga, G., Biard, D. S. and Angulo J. F. (2005) The human stress-activated protein kin17 belongs to the multiprotein DNA replication complex and associates *in vivo* with mammalian replication origins. *Mol Cell Biol*, **25**, 3814-3830.
Mills, R. F., Francini, A., Ferreira da Rocha, P. S., Baccarini, P. J., Aylett, M., Krijger, G. C. and Williams, L. E. (2005) The plant P1B-type ATPase AtHMA4 transports Zn and Cd and plays a role in detoxification of transition metals supplied at elevated levels. *FEBS Lett*, **579**, 783-791.
Mills, R. F., Krijger, G. C., Baccarini, P. J., Hall, J. L. and Williams, L. E. (2003) Functional expression of AtHMA4, a P1B-type ATPase of the Zn/Co/Cd/Pb subclass. *Plant J*, **35**, 164-176.
Milner, M. J. and Kochian, L. V. (2008) Investigating heavy-metal hyperaccumulation using *Thlaspi caerulescens* as a model system. *Ann Bot*, **102**, 3-13.
Mira, H., Martínez-García, F. and Peñarrubia, L. (2001) Evidence for the plant-specific intercellular transport of the *Arabidopsis* copper chaperone CCH. *Plant J*, **25**, 521-528.
Molins, H., Michelet, L., Lanquar, V., Agorio, A., Giraudat, J., Roach, T., Krieger-Liszkay, A. and Thomine, S. (2013) Mutants impaired in vacuolar metal mobilization identify chloroplasts as a target for cadmium hypersensitivity in *Arabidopsis thaliana*. *Plant Cell Environ*, **36**, 804-817.
Morel, M., Crouzet, J., Gravot, A., Auroy, P., Leonhardt, N., Vavasseur, A. and Richaud, P. (2009) AtHMA3, a P1B-ATPase allowing Cd/Zn/Co/Pb vacuolar storage in Arabidopsis. *Plant Physiol*, **149**, 894-904.
Morrissey, J., Baxter, I. R., Lee, J., Li, L., Lahner, B., Grotz, N., Kaplan, J., Salt, D. E. and Guerinot, M. L. (2009) The ferroportin metal efflux proteins function in iron and cobalt homeostasis in *Arabidopsis*.*Plant Cell*, **21**, 3326-3338.
Mukherjee, I., Campbell, N. H., Ash, J. S. and Connolly E. L. (2006) Expression profiling of the *Arabidopsis* ferric chelate reductase (FRO) gene family reveals differential regulation by iron and copper. *Planta*, **223**, 1178-1190.
Mustroph, A., Zanetti, M. E., Jang, C. J., Holtan, H. E., Repetti, P. P., Galbraith, D. W., Girke, T. and Bailey-Serres, J. (2009) Profiling translatomes of discrete cell populations resolves altered cellular priorities during hypoxia in *Arabidopsis*. *Proc Natl Acad Sci U S A*, **106**, 18843-18848.
Ooi, C. E., Rabinovich, E., Dancis, A., Bonifacino, J. S. and Klausner, R. D. (1996) Copper-dependent degradation of the *Saccharomyces cerevisiae* plasma membrane copper transporter Ctr1p in the apparent absence of endocytosis. *EMBO J*, **15**, 3515-3523.
Park, J., Song, W. Y., Ko, D., Eom, Y., Hansen, T. H., Schiller, M., Lee, T. G., Martinoia, E. and Lee, Y. (2012) The phytochelatin transporters AtABCC1 and AtABCC2 mediate tolerance to cadmium and mercury. *Plant J*, **69**, 278-288.
Peña, M. M., Puig, S. and Thiele, D. J. (2000) Characterization of the *Saccharomyces cerevisiae* high affinity copper transporter Ctr3. *J Biol Chem*, **27**, 33244-33251.
Perea-García, A., Garcia-Molina, A., Andrés-Colás, N., Vera-Sirera, F., Pérez-Amador, M. A.,

Puig, S. and Peñarrubia, L. (2013) *Arabidopsis* copper transport protein COPT2 participates in the cross talk between iron deficiency responses and low-phosphate signaling. *Plant Physiol*, **162**, 180-194.

Pomponi, M., Censi, V., Di Girolamo, V., De Paolis, A., di Toppi, L. S., Aromolo, R., Costantino, P. and Cardarelli, M. (2006) Overexpression of *Arabidopsis* phytochelatin synthase in tobacco plants enhances Cd(2+) tolerance and accumulation but not translocation to the shoot. *Planta*, **223**, 180-190.

Puig, S., Andrés-Colás, N., Garcia-Molina, A. and Peñarrubia, L. (2007) Copper and iron homeostasis in *Arabidopsis*: responses to metal deficiencies, interactions and biotechnological applications. *Plant Cell Environ*, **30**, 271-290.

Puig, S., Lee, J., Lau, M. and Thiele, D. J. (2002) Biochemical and genetic analyses of yeast and human high affinity copper transporters suggest a conserved mechanism for copper uptake. *J Biol Chem*, **277**, 26021-26030.

Ravet, K. and Pilon, M. (2013) Copper and iron homeostasis in plants: the challenges of oxidative stress. *Antioxid Redox Signal*, **19**, 919-932.

Rea, P.A. (2012) Phytochelatin synthase: of a protease a peptide polymerase made. *Physiol Plant*, **145**, 154-164.

Rees, E. M., Lee, J. and Thiele, D. J. (2004) Mobilization of intracellular copper stores by the ctr2 vacuolar copper transporter. *J Biol Chem*, **24**, 54221-54229.

Rellán-Álvarez, R., Abadia, J. and Alvarez-Fernandez, A. (2008) Formation of metal-nicotianamine complexes as affected by pH, ligand exchange with citrate and metal exchange. A study by electrospray ionization time-of-flight mass spectrometry. *Rapid Commun Mass Spectrom*, **22**, 1553-1562.

Rellán-Álvarez, R., Giner-Martínez-Sierra, J., Orduna, J., Orera, I., Rodríguez-Castrillón, J. Á., García-Alonso, J. I., Abadía, J. and Álvarez-Fernández, A. (2010) Identification of a tri-iron(III), tri-citrate complex in the xylem sap of iron-deficient tomato resupplied with iron: new insights into plant iron long-distance transport. *Plant Cell Physiol*, **51**, 91-102.

Robinson, N. J., Procter, C. M., Connolly, E. L. and Guerinot, M. L. (1999) A ferric-chelate reductase for iron uptake from soils. *Nature*, **397**, 694-697.

Rodríguez-Celma, J., Lin, W.-D., Fu, G.-M., Abadía, J., López-Millán, A.-F. and Schmidt, W. (2013) Mutually exclusive alterations in secondary metabolism are critical for the uptake of insoluble iron compounds by *Arabidopsis* and *Medicago truncatula*. *Plant Physiol*, **162**, 1473-1485.

Rogers, E. E. and Guerinot, M. L. (2002) FRD3, a member of the multidrug and toxin efflux family, controls iron deficiency responses in *Arabidopsis*. *Plant Cell*, **14**, 1787-1799.

Rogers, E. E., Eide, D. J. and Guerinot, M. L. (2000) Altered selectivity in an *Arabidopsis* metal transporter. *Proc Natl Acad Sci U S A*, **97**, 12356-12360.

Roschzttardtz, H., Conéjéro, G., Curie, C. and Mari, S. (2010) Straightforward histochemical staining of Fe by the adaptation of an old-school technique: identification of the endodermal vacuole as the site of Fe storage in *Arabidopsis* embryos. *Plant Sig Behav*, **5**, 56-57.

Roschzttardtz, H., Séguéla-Arnaud, M., Briat, J.-F., Vert, G. and Curie, C. (2011) The FRD3 citrate effluxer promotes iron nutrition between symplastically disconnected tissues throughout *Arabidopsis* development. *Plant Cell*, **23**, 2725-2737.

Salt, D. E., Prince, R. C., Pickering, I. J. and Raskin, I. (1995) Mechanisms of cadmium mobility and accumulation in Indian mustard. *Plant Physiol*, **109**, 1427-1433.

Sancenón, V., Puig, S., Mateu-Andres, I., Dorcey, E., Thiele, D. J. and Peñarrubia, L. (2004) The

Arabidopsis copper transporter COPT1 functions in root elongation and pollen development. *J Biol Chem*, **279**, 15348-15355.
Sancenón, V., Puig, S., Mira, H., Thiele, D. J. and Peñarrubia, L. (2003) Identification of a copper transporter family in *Arabidopsis thaliana*. *Plant Mol Biol*, **51**, 577-587.
Santi, S. and Schmidt, W. (2009) Dissecting iron deficiency-induced proton extrusion in *Arabidopsis* roots. *New Phytol*, **183**, 1072-1084.
Sasaki, A., Yamaji, N., Yokosho, K. and Ma, J. F. (2012) Nramp5 Is a major transporter responsible for manganese and cadmium uptake in Rice. *Plant Cell*, **24**, 2155-2167.
Schaaf, G., Honsbein, A., Meda, A. R., Kirchner, S., Wipf, D. and von Wirén, N. (2006) AtIREG2 encodes a tonoplast transport protein involved in iron-dependent nickel detoxification in *Arabidopsis* thaliana roots. *J Biol Chem*, **281**, 25532-25540.
Schaaf, G., Schikora, A., Haberle, J., Vert, G., Ludewig, U., Briat, J. F., Curie, C. and von Wiren, N. (2005) A putative function for the arabidopsis Fe-Phytosiderophore transporter homolog AtYSL2 in Fe and Zn homeostasis. *Plant Cell Physiol*, **46**, 762-774.
Schatman, D. P., Kumar, R., Schroeder, J. I. and Marsh, E. L. (1994) Molecular and functional characterization of a novel low-affinity cation transporter (LCT1) in higher plants. *Proc Natl Acad Sci U S A*, **94**, 11079-11084.
Scholz, G., Schlesier, G. and Seifert, K. (1985) Effect of nicotianamine on iron uptake by the tomato mutant '*chloronerva'*. *Physiol Plant*, **64**, 99-104.
Schuler, M., Rellán-Álvarez, R., Fink-Straube, C., Abadía, J. and Bauer, P. (2012) Nicotianamine functions in the phloem-based transport of iron to sink organs, in pollen development and pollen tube growth in *Arabidopsis*. *Plant Cell*, **24**, 2380-2400.
Schmidt, W. and Buckhout, T. J. (2011) A hitchhiker's guide to the *Arabidopsis* ferrome. *Plant Physiol Biochem*, **49**, 462-470.
Shin, L. J., Lo, J. C., Chen, G. H., Callis, J., Fu, H. and Yeh, K. C. (2013) IRT1 degredation factor1, a ring E3 ubiquitin ligase, regulates the degredation of iron-regulated transporter1 in *Arabidopsis*. *Plant Cell*, **25**, 3039-3051.
Shorrocks, V.M. and Alloway, B.J. (1988) *Copper in plant, animal and human nutrition* Potters Bar, Hertfordshire: Copper Development Association.
Sivitz, A., Grinvalds, C., Barberon, M., Curie, C. and Vert, G. (2011) Proteasome-mediated turnover of the transcriptional activator FIT is required for plant iron-deficiency response. *Plant J*, **66**, 1044-1052.
Song, W. Y., Park, J., Mendoza-Cozatl, D. G., Suter-Grotemeyer, M., Shim, D., Hortensteiner, S., Geisler, M., Weder, B., Rea, P. A., Rentsch, D., Schroeder, J. I., Youngsook, L. and Martinoia, E. (2010) Arsenic tolerance in Arabidopsis is mediated by two ABCC-type phytochelatin transporters. *Proc Natl Acad Sci U S A*, **107**, 21187-21192.
Stacey, M. G., Koh, S., Becker, J. and Stacey, G. (2002) AtOPT3, a member of the oligopeptide transporter family, is essential for embryo development in *Arabidopsis*. *Plant Cell*, **14**, 2799-2811.
Stacey, M. G., Osawa, H., Patel, A., Gassmann, W. and Stacey, G. (2006) Expression analyses of *Arabidopsis* oligopeptide transporters during seed germination, vegetative growth and reproduction. *Planta*, **223**, 291-305.
Stacey, M. G., Patel, A., McClain, W. E., Mathieu, M., Remley, M., Rogers, E. E., Gassmann, W., Blevins, D. G. and Stacey, G. (2008) The *Arabidopsis* AtOPT3 protein functions in metal homeostasis and movement of iron to developing seeds. *Plant Physiol*, **146**, 589-601.
Stadtman, E. R. (1990) Metal ion-catalyzed oxidation of proteins: biochemical mechanism and

biological consequences. *Free Radic Biol Med*, **9**, 315-325.
Takahashi, R., Ishimaru, Y., Nakanishi, H. and Nishizawa, N. K. (2011) The role of iron transporter OsNRAMP1 in cadmium uptake and accumulation in rice. *Plant Signal Behav*, **6**, 1813-1816.
Thimm, Q., Essigmann, B., Kloska, S., Altmann, T. and Buckhout, T. J. (2001) Response of *Arabidopsis* to iron deficiency stress as revealed by microarray analysis. *Plant Physiol*, **127**, 1030-1043.
Thomine, S., Lelièvre, F., Debarbieux, E., Schroeder, J. I. and Barbier-Brygoo, H. (2003) AtNRAMP3, a multispecific vacuolar metal transporter involved in plant responses to iron deficiency. *Plant J*, **34**, 685-695.
Thomine, S., Wang, R., Ward, J. M., Crawford, N. M. and Schroeder, J. I. (2000) Cadmium and iron transport by members of a plant metal transporter family in *Arabidopsis* with homology to NRAMP genes. *Proc Natl Acad Sci U S A*, **97**, 4991-4996.
Tissier, A., Kannouche, P., Biard, D. S., Timchenko, T., Mazin, A., Araneda, S., Allemand, I., Mauffrey, P., Frelat, G. and Angulo, J. F. (1995) The mouse Kin-17 gene codes for a new protein involved in DNA transactions and is akin to bacterial RecA protein. *Biochemie*, **77**, 854-860.
Ueno, D., Kono, I., Yokosho, K., Ando, T., Yano, M. and Ma, J. F. (2009) A major quantitative trait locus controlling cadmium translocation in rice (*Oryza sativa*). *New Phytol*, **182**, 644-653.
Ueno, D.m Koyama, E., Yamajl, N. and Ma, J. F. (2011) Physiological, genetic, and molecular characterization of a high-Cd-accumulating rice cultivar, Jarjan. *J Exp Bot*, **62**, 2265-2272.
Ueno, D., Yamaji, N., Kono, I., Huang, C. F., Ando, T., Yano, M. and Ma, J. F. (2010) Gene limiting cadmium accumulation in rice. *Proc Natl Acad Sci U S A*, **107**, 16500-16505.
Uraguchi, S., Kamiya, T., Sakamoto, T., Kasai, K., Sato, Y., Nagamura, Y., Yoshida, A., Kyozuka, J., Ishikawa, S. and Fujiwara, T. (2011) Low-affinity cation transporter (OsLCT1) regulates cadmium transport into rice grains. *Proc Natl Acad Sci U S A*, **108**, 20959-20964.
Valko, M., Morris, H. and Cronin, M. T. (2005) Metals, toxicity and oxidative stress. *Curr Med Chem*, **12**, 1161-1208.
Van Belleghem, F., Cuypers, A., Semane, B., Smeets, K., Vangronsveld, J., d'Haen, J. and Valcke, R. (2007) Subcellular localization of cadmium in roots and leaves of *Arabidopsis thaliana*. *New Phytol*, **173**, 495-508.
Varotto, C., Maiwald, D., Pesaresi, P., Jahns, P., Salamini, F. and Leister, D. (2002) The metal ion transporter IRT1 is necessary for iron homeostasis and efficient photosynthesis in Arabidopsis thaliana. *Plant J*, **31**, 589-599.
Vasconcelos, M. W., Li, G. W., Lubkowitz, M. A. and Grusak, M. A. (2008) Characterization of the PT clade of oligopeptide transporters in rice. *Plant Gen*, **1**, 77-88.
Vatamaniuk, O. K., Mari, S., Lu, Y. P. and Rea, P. A. (1999) AtPCS1, a phytochelatin synthase from *Arabidopsis*: isolation and in vitro reconstitution. *Proc Natl Acad Sci U S A*, **96**, 7110-7115.
Vatamaniuk, O. K., Mari, S., Lu, Y. P. and Rea, P. A. (2000) Mechanism of heavy metal ion activation of phytochelatin (PC) synthase: blocked thiols are sufficient for PC synthase-catalyzed transpeptidation of glutathione and related thiol peptides. *J Biol Chem*, **275**, 31451-31459.
Verbruggen, N., Hermans, C. and Schat, H. (2009) Molecular mechanisms of metal hyperaccumulation in plants. *New Phytol*, **181**, 759-776.

Verret, F., Gravot, A., Auroy, P., Leonhardt, N., David, P., Nussaume, L., Vavasseur, A. and Richaud, P. (2004) Overexpression of AtHMA4 enhances root-to-shoot translocation of zinc and cadmium and plant metal tolerance. *FEBS Lett*, **576**, 306-312.

Vert, G., Grotz, N., Dedaldechamp, F., Gaymard, F., Guerinot, M. L., Briat, J. F. and Curie, C. (2002). IRT1, an *Arabidopsis* transporter essential for iron uptake from the soil and for plant growth. *Plant Cell*, **14**, 1223-1233.

Vert, G. A., Briat, J.-F. and Curie, C. (2003) Dual regulation of the *Arabidopsis* high-affinity root iron uptake system by local and long-distance signals. *Plant Physiol*, **132**, 796-804.

Waisburg, M., Joseph, P., Hale, B. and Beyersmann, D. (2003) Molecular and cellular mechanisms of cadmium carcinogenesis. *Toxicology*, **192**, 95-117.

Wang, H. Y., Klatte, M., Jakoby, M., Bäumlein, H., Weisshaar, B. and Bauer, P. (2007) Iron deficiency-mediated stress regulation of four subgroup lb bHLH genes in *Arabidopsis thaliana*. *Planta*, **226**, 897-908.

Wang, N., Cui, Y., Liu, Y., Fan, H., Du, J., Huang, Z., Yuan, Y., Wu, H. and Ling, H. Q. (2013) Requirement and functional redundancy of lb subgroup bHLH proteins for iron deficiency responses and uptake in *Arabidopsis thaliana*. *Mol Plant*, **5**, 503-513.

Waters, B. M., Chu, H.-H., DiDonato, R. J., Roberts, L. A., Eisley, R. B., Lahner, B., Salt, D. E. and Walker, E. L. (2006) Mutations in *Arabidopsis* Yellow Stripe-Like1 and Yellow Stripe-Like3 reveal their roles in metal ion homeostasis and loading of metal ions in seeds. *Plant Physiol*, **141**, 1446-1458.

Welch, R. M. and Larue, T. A. (1990) Physiological characteristics of Fe accumulation in the 'Bronze' mutant of *Pisum sativum* L., cv 'Sparkle' E107 (*brz brz*). *Plant Physiol*, **93**, 723-729.

Wong, C. K. and Cobbett, C. S. (2008) HMA P-type ATPases are the major mechanism for root-to-shoot Cd translocation in *Arabidopsis thaliana*. *New Phytol*, **181**, 71-78.

Wu, H., Chen, C., Du, J., Liu, H., Cui, Y., Zhang, Y., He, Y., Wang, Y., Chu, C., Feng, Z., Li, J. and Ling, H. Q. (2012) Co-Overexpression FIT with AtbHLH38 or AtbHLH39 in *Arabidopsis*-enhanced cadmium tolerance via increased cadmium sequestration in roots and improved iron homeostasis of shoots. *Plant Physiol*, **158**, 790-800.

Wu, X., Sinani, D., Kim, H. and Lee, J. (2009) Copper transport activity of yeast Ctr1 is down-regulated via its C terminus in response to excess copper. *J Biol Chem*, **284**, 4112-4122.

Xiao, Z., Loughlin, F., George, G. N., Howlett, G. J. and Wedd, A. G. (2004) C-terminal domain of the membrane copper transporter Ctr1 from *Saccharomyces cerevisiae* binds four Cu(I) ions as a cuprous-thiolate polynuclear cluster: sub-femtomolar Cu(I) affinity of three proteins involved in copper trafficking. *J Am Chem Soc*, **126**, 3081-3090.

Yamaguchi-Iwai, Y., Serpe, M., Haile, D., Yang, W., Kosman, D. J., Klausner, R. D. and Dancis, A. (1997) Homeostatic regulation of copper uptake in yeast via direct binding of MAC1 protein to upstream regulatory sequences of *FRE1* and *CTR1*. *J Biol Chem*, **272**, 17711-17718.

Yamasaki, H., Abdel-Ghany, S. E., Cohu, C. M., Kobayashi, Y., Shikanai, T. and Pilon, M. (2007). Regulation of copper homeostasis by micro-RNA in *Arabidopsis*. J Biol Chem *282*, 16369-16378.

Yamasaki, H., Hayashi, M., Fukazawa, M., Kobayashi, Y. and Shikanai, T. (2009). SQUAMOSA Promoter Binding Protein-Like7 is a central regulator for copper homeostasis in *Arabidopsis*. Plant Cell *21*, 347-361.

Yang, T. J., Lin, W. D. and Schmidt, W. (2010) Transcriptional profiling of the *Arabidopsis* iron

deficiency response reveals conserved transition metal homeostasis networks. *Plant Physiol*, **154**, 810-819.

Yonkovich, J., McKenndry, R., Shi, X. and Zhu, Z. (2002) Copper ion-sensing transcription factor Mac1p post-translationally controls the degradation of its target gene product Ctr1p. *J Biol Chem*, **277**, 23981-23984.

Yuan, Y., Wu, H., Wang, N., Li, J., Zhao, W., Du, J., Wang, D. and Ling, H. Q. (2008) FIT interacts with AtbHLH38 and AtbHLH39 in regulating iron uptake gene expression for iron homeostasis in *Arabidopsis*. *Cell Res*, **18**, 385-397.

Yuan, M., Chu, Z., Li, X., Xu, C. and Wang, S. (2010) The bacterial pathogen *Xanthomonas oryzae* overcomes rice defenses by regulating host copper redistribution. *Plant Cell*, **22**, 3164-3176.

Yuan, M., Li, X., Xiao, J. and Wang, S. (2011) Molecular and functional analyses of COPT/Ctr-type copper transporter-like gene family in rice. *BMC Plant Biol,* **11**, 69.

Zhang, H. and Forde, B. G. (1998) An *Arabidopsis* MADS box gene that controls nutrient-induced changes in root architecture. *Science*, **279**, 407-409.

Zhang, Y., Xu, Y. H., Yi, H. Y. and Gong, J. M. (2012) Vacuolar membrane transporters OsVIT1 and OsVIT2 modulate iron translocation between flag leaves and seeds in rice. *Plant J*, **72**, 400-410.

Zheng, L., Yamaji, N., Yokosho, K. and Ma, J. F. (2012). YSL16 is a phloem-localized transporter of the copper-nicotianamine complex that is responsible for copper distribution in rice. *Plant Cell*, **24**, 3767-3782.

CHAPTER II

COPT6 is a Plasma Membrane Transporter that Functions in Copper Homeostasis in *Arabidopsis* and is a Novel Target of SQUAMOSA Promoter Binding Protein-Like 7

Abstract

Among the mechanisms controlling copper homeostasis in plants is the regulation of its uptake and tissue partitioning. Here we characterized a newly identified member of the conserved CTR/COPT family of copper transporters in *Arabidopsis thaliana*, COPT6. We showed that COPT6 resides at the plasma membrane and mediates copper accumulation when expressed in the *Saccharomyces cerevisiae* copper uptake mutant. Although the primary sequence of COPT6 contains the family conserved domains, including methionine-rich motifs in the extracellular amino terminal domain and a second transmembrane helix (TM2), it is different from the founding family member, *S. cerevisiae* Ctr1p. This conclusion was based on the finding that although the positionally conserved Met_{106} residue in the TM2 of COPT6 is functionally essential, the conserved Met_{27} in the amino terminal domain is not. Structure-function studies revealed that the amino terminal domain is dispensable for COPT6 function in copper replete conditions but is important under copper limiting conditions. In addition, COPT6 interacts with itself and with its homolog, COPT1, unlike Ctr1p that interacts only with itself. Analyses of the expression pattern showed that while *COPT6* is expressed in different cell types of different plant organs, the bulk of its expression is located in the vasculature. We also show that *COPT6* expression is regulated by copper availability that, in part, is controlled by a master regulator of copper homeostasis, SPL7. Finally, studies using the *A. thaliana copt6-1* mutant and plants overexpressing *COPT6* revealed its essential role during copper limitation and excess.

Introduction

Copper is a redox active transition element that serves as an essential micronutrient for all living organisms (Burkhead et al., 2009; Prohaska 2000; Pugi et al., 2007). It acts as a cofactor for enzymes involved in electron transfer reactions and thus, participates in important biological processes such as respiration, photosynthesis and scavenging of oxidative stress. In addition, copper is involved in the perception of ethylene, nitrogen metabolism, molybdenum cofactor synthesis, cell wall remodeling and response to pathogens in plants (Burkhead et al., 2009; Gavnholt et al., 2002; Yuan et al., 2010). However, free copper ions are toxic to cells in excess due their ability to promote the formation of free radicals through the Fenton reaction and increased malfunction of important proteins, either through thiol capping or displacement of metal co-factors of metalloenzymes (Burkhead et al., 2009, Stadtman 1990; Gaetke and Chow 2003; Merchant 2010). Therefore, organisms have evolved sophisticated mechanisms for maintaining copper homeostasis to prevent deficiency while avoiding toxicity.

Response to copper deficiency in plants includes reallocation of intracellular copper and induction of the expression of copper uptake systems. In *Arabidopsis thaliana*, this regulation is largely attributable to the activity of the transcription factor SPL7 (*SQUAMOSA* promoter binding protein–like7) and its downstream targets, microRNAs (Abdel-Ghany and Pilon 2008; Sunkar and Zhu 2006; Yamasaki et al., 2007; Yamasaki et al, 2007; Kliebenstein et al., 1998). When copper is limited, SPL7 up-regulates expression of *miRNA398,* which in turn down-regulates expression of two main isoforms of the major copper enzymes, the cytosol Cu/Zn superoxide dismutase (SOD), *CSD1,* and the chloroplast stroma SOD, *CSD2* (Abdel-Ghany and Pilon 2008; Sunkar and Zhu 2006; Yamasaki et al., 2007; Yamasaki et al, 2007; Kliebenstein et al., 1998). As *CSD1* and *CSD2* transcripts and the activity of the encoded proteins decrease, their

superoxide scavenging functions are replaced by an increase in gene expression and total enzyme activity of a plastid-localized Fe-SOD, FSD1 (Yamasaki et al., 2007; Cohu and Pilon 2007). The miRNA-mediated Cu economy model has been proposed, where energy-related electron transport functions receive priority in copper delivery over the major copper enzymes (Burkhead et al., 2009; Yamasaki et al., 2007; Ravet et al., 2011; Abdel-Ghany et al, 2005).

Simultaneously, plants regulate copper homeostasis by controlling its uptake into cells. Copper uptake in plants, the green alga *Chlamydomonas reinhardtii,* yeast, *Drosophila* and humans is maintained mainly through the tight regulation of the expression and stability of copper transporters of the CTR/COPT family (Dancis et al, 1994; Peña et al., 2000; Rees et al., 2004; Andrés-Colás et al., 2010; Page et al., 2009; Sancenón et al., 2004; Sancenón et al., 2003; Kampfenkel et al., 1995; Dancis et al., 19941). The founding members, Ctr1p, Ctr2p and Ctr3p, were identified in *Saccharomyces cerevisiae* (Dancis et al, 1994a; Peña et al., 2000; Rees et al., 2004; Andrés-Colás et al., 2010; Page et al., 2009; 17-19, Dancis et al, 1994b). Ctr1p and Ctr3p localize to the plasma membrane, are functionally redundant, and mediate high-affinity copper uptake from the external medium during copper deficiency (Dancis et al., 1994a; Dancis et al., 1994b). Expression of the *CTR1* gene is subject to copper metalloregulation: it is transcriptionally induced under copper deficient conditions *via* a transcription factor, Mac1, and is post-transcriptionally degraded under copper replete conditions (Ooi et al., 1996; Yonkovich et al., 2002; Jungmann et al., 1993). Ctr2p is located on the vacuolar membrane and mobilizes copper from the vacuole during copper deficiency (Rees et al., 2004). CTR/COPT family members have conserved structural features that include three putative transmembrane helices (TMs), with the N- and C-termini located towards the extracellular space and cytosol respectively, methionine-rich N-terminal motifs (Mets motifs), and M*XXX*M and G*XXX*G motifs

located in TM2 and TM3, respectively (De Feo et al., 2007; De Feo et al., 2009; Puig et al., 2002; Peñarrubia et al., 2010). Two methionine residues, Met_{127} in the Mets motif of the N-terminus and Met_{260} in the M*XXX*M motif of TM2 in *S. cerevisiae* Ctr1p, are conserved among the majority of CTR/COPT family members and, based on studies of yeast and human Ctr1p, are essential for copper transport (Puig et al., 2002). The C-terminus may contain cysteine-rich C*X*C motifs, which are suggested to bind copper ions for transfer to cytosolic copper chaperones, or to downregulate Ctr1p activity in response to toxic copper levels (Puig et al., 2002; Wu et al., 2009; Xiao and Wedd 2002). CTR/COPT proteins homotrimerize to form a pore within the membrane to transport copper across the lipid bilayer, but can also form heterocomplexes with other CTR/COPT family members and/or other proteins (Yuan et al., 2010; De Feo et al., 2007; Lee et al., 2002; Yuan et al., 2011).

In plants, the CTR/COPT family is best characterized in *A. thaliana* and *Oryza sativa* and is represented by six and seven members, respectively (Peñarrubia et al., 2010; Yuan et al., 2011). *A. thaliana*, COPT1 and COPT2 fully suppress the copper deficiency-associated respiratory defect of the *S. cerevisiae ctr1ctr3* mutant, while COPT3 and COPT5 partially complement this phenotype (Sancenón et al., 2004; Sancenón et al., 2003; Kampfenkel et al., 1995). Subsequent studies showed that COPT1 localizes to the plasma membrane, mediates copper influx and, similar to CTR proteins from other organisms, is highly specific for copper (I) (Andrés-Colás et al., 2010; Sancenón et al., 2003). Studies in *A. thaliana* showed that COPT1 plays a predominant role in copper acquisition from the soil *via* root tips (Andrés-Colás et al., 2010; Sancenón et al., 2003). In contrast, COPT5 localizes to the tonoplast and pre-vacuolar compartment and functions by remobilizing copper from these organelles during copper deficiency (Garcia-Molina et al., 2011; Klaumann et al., 2011). Expression of *COPT1* and *COPT2* mRNA is upregulated in

copper-deficient conditions (Sancenón et al., 2004) and these responses are controlled by the transcription factor, SPL7 (Yamasaki et al., 2009). COPT6 is a newly identified member of the CTR/COPT family of *A. thaliana* transporters (Peñarrubia et al., 2010), and its function in copper homeostasis has not been yet elucidated.

We show that COPT6 is a plasma membrane copper uptake transporter that is distinct from its *S. cerevisiae* counterpart, Ctr1p, and plays important role in *A. thaliana* during copper deficiency and excess.

Results

The COPT6 polypeptide contains the key features of the CTR/COPT family

The *A. thaliana* genome possesses six genes encoding putative CTR/COPT transporters that are designated COPT1 to 6. Of the six family members, COPT6 has been identified in the *A. thaliana* genome only recently (Peñarrubia et al., 2010), thus making COPT6 the least studied member of the *A. thaliana* CTR/COPT family. Analysis of the amino acid sequence identity and similarity of COPT6 to other CTR/COPT family members of *A. thaliana* disclosed that COPT2 and COPT1 are the closest COPT6 homologs sharing 75%/79% sequence identity/similarity and 71%/75% identity/similarity, respectively (Figure 1).

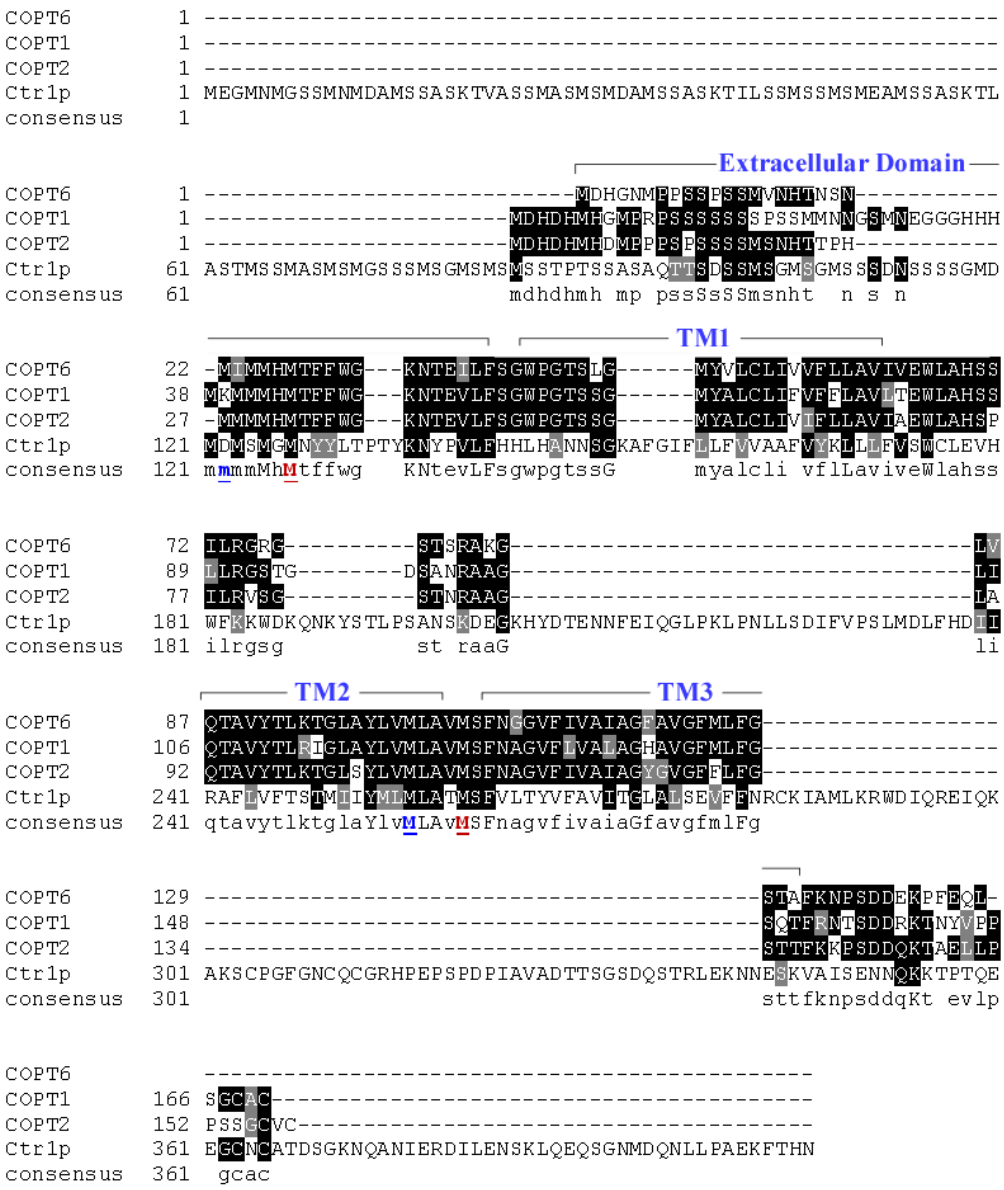

Figure 1. Alignment of the deduced amino acid sequence of COPT6 (GenBank accession number AT2G26975.1) and its homologs from *A. thaliana, COPT1 and COPT2* (GenBank accession numbers AT5G59030.1 and AT3G46900.1, respectively) and *S. cerevisiae* Ctr1p (YPR124W). Conserved methionine amino acid residues subjected to site-directed mutagenesis are indicated in red and blue in the consensus line. Red color indicates positionally conserved methionine residues that are essential for functional activity of *S. cerevisiae* Ctr1p. Also shown are the extracellular amino terminal domain and transmembrane helices (**TM1**, **TM2,** and **TM3**).

In addition, COPT6 clusters in one clade with COPT1 and COPT2 when their amino acid sequences are subjected to phylogenetic analysis (Figure 2A) suggesting that COPT6 may have similar functions to COPT1 and COPT2 in copper homeostasis.

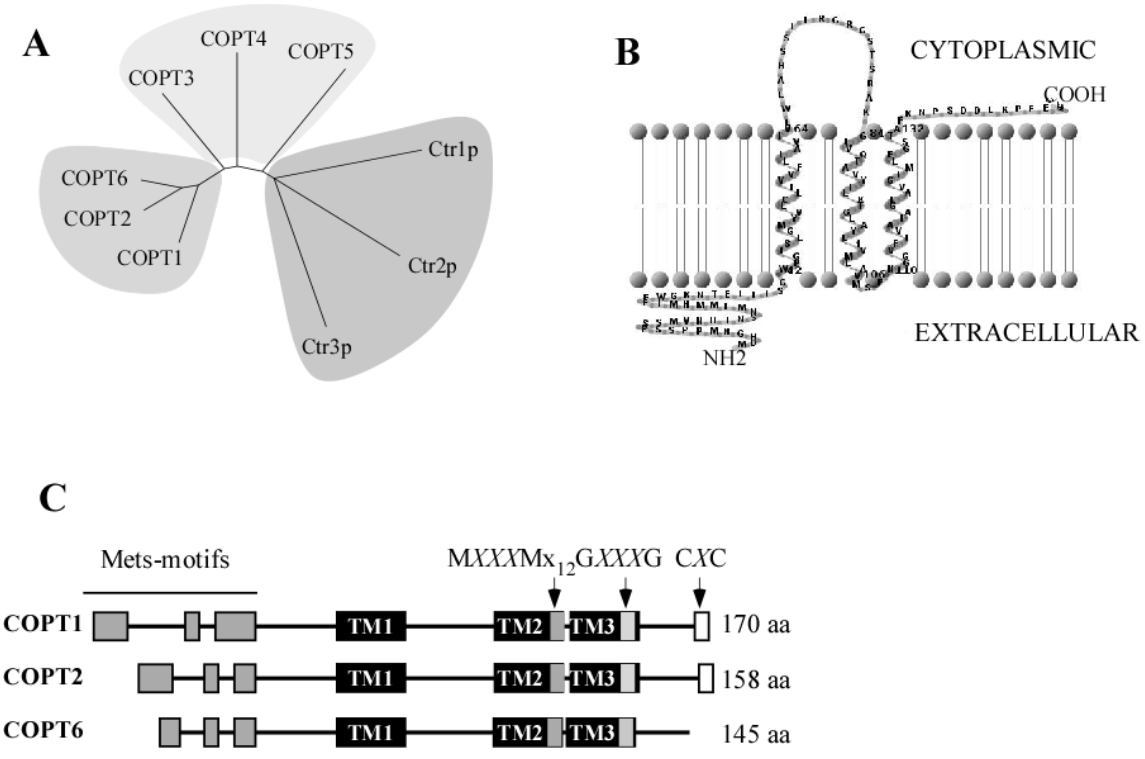

Figure 2. *In silico* analysis of the putative *A. thaliana* copper transporter, COPT6. A. A phylogenetic tree of *A. thaliana* COPT proteins and *S. cerevisiae* Ctr1p, Ctr2p and Ctr3p. **B.** Schematic representation of the membrane topology of the full-length COPT6 polypeptide. Based on the predicted topology (TMHMM software, version 2.0 [http://www.cbs.dtu.dk/services/TMHMM-2.0/] and TMRPres2D [http://biophysics.biol.uoa.gr/TMRPres2D/download.jsp]), the N-terminus is located outside (**Extracellular**), whereas the C-terminus is inside the cell (**Cytoplasmic**). **C**. A schematic diagram showing conserved motifs in the primary sequence of COPT1, COPT2 and COPT6. The conserved features include three transmembrane domains (**TM1**, **TM2**, **TM3**, black bars), methionine-rich motifs in the predicted extracellular domain (**Mets-motifs**, grey bars), and M*XXX*M, G*XXX*G and C*X*C motifs (**M*XXX*M$_{12}$G*XXX*G**, grey bars and **C*X*C**, white bars) in TM2, TM3 and the C-terminus hydrophilic domain, respectively. Note, that **C*X*C** motif is absent in the COPT6 polypeptide. M, G and C are methionine, glycine and cysteine amino acid residues, respectively, and *X* is any amino acid residue.

Computer algorithm-assisted analysis of the COPT6 polypeptide membrane topology and conserved motif organization revealed an extracellular amino terminal domain, a membrane domain encompassing three transmembrane (TM) helices, where TM2 and TM3 are separated by 3 amino acids, and an intracellular C-terminal domain (Figure 2B). The COPT6 polypeptide includes the M*XXX*M-x_{12}-G*XXX*G signature of CTR/COPT proteins: its amino terminus and TM2 contains Mets and M*XXX*M (*X* representing any amino acid) motifs, respectively, while TM3 harbors the G*XXX*G motif (Figure 2C). These features are conserved in the majority of the CTR/COPT proteins and are also present in COPT1 and COPT2. However, unlike COPT1 and COPT2, COPT6 does not possess the cysteine-rich C*X*C motif at the C-terminus (Figure 2C).

Heterologously expressed COPT6 complements the growth defect of the triple *ctr1ctr2ctr3* *S. cerevisiae* mutant on non-fermentable growth medium

Despite the presence of key motifs conserved in the CTR/COPT family, COPT6 lacks the C*X*C motif at the C-terminus (Figure 2C), which was shown to play an important role in copper homeostasis in Ctr1p (Puig et al., 2002; Wu et al., 2009; Xiao et al., 2002). This motif is also present in *A. thaliana* homologues COPT1 and COPT2, prompting us to test whether the lack of *CXC* motif in COPT6 still results in a protein capable of transporting copper. In this regard, *S. cerevisiae* strains harboring mutations in copper uptake genes have been used as a versatile and well-defined model system for functional analysis of putative copper transporters from various species. Yeast lacking copper uptake systems cannot grow on non-fermentable carbon sources such as glycerol and ethanol (YPEG medium) due to low levels of intracellular copper. This deficiency results in the inability of cytochrome *c* oxidase to obtain its copper cofactor that, in turn, causes a defect in the mitochondrial respiratory chain unless copper is exogenously

supplied to the media (Dancis et al., 1994a; Glerum et al., 1996).

The function of COPT6 in copper transport was tested through complementation studies in the *S. cerevisiae ctr1ctr2ctr3* triple mutant strain, which lacks high-affinity plasma membrane transporters Ctr1p and Ctr3p, and a vacuolar-membrane transporter, Ctr2p (19). Growth of *ctr1ctr2ctr3* mutant and wild-type strains expressing an empty *YES3-Gate* vector and the *ctr1ctr2ctr3* mutant transformed with *YES3-Gate* harboring the *COPT6* cDNA insert was compared on medium with glucose (YNB-URA) or ethanol/glycerol (YPEG) as a carbon source. All yeast alleles were able to grow on YNB-Ura (Figure 3A). As shown previously (Rees et al., 2004), *ctr1ctr2ctr3* cells did not grow on YPEG medium unless the medium was supplemented with exogenous copper (Figure 3A). In contrast, *ctr1ctr2ctr3* cells expressing *COPT6* grew on YPEG regardless of copper supplementation, and their growth was comparable to that of wild-type cells transformed with the empty vector (Figure 3A).

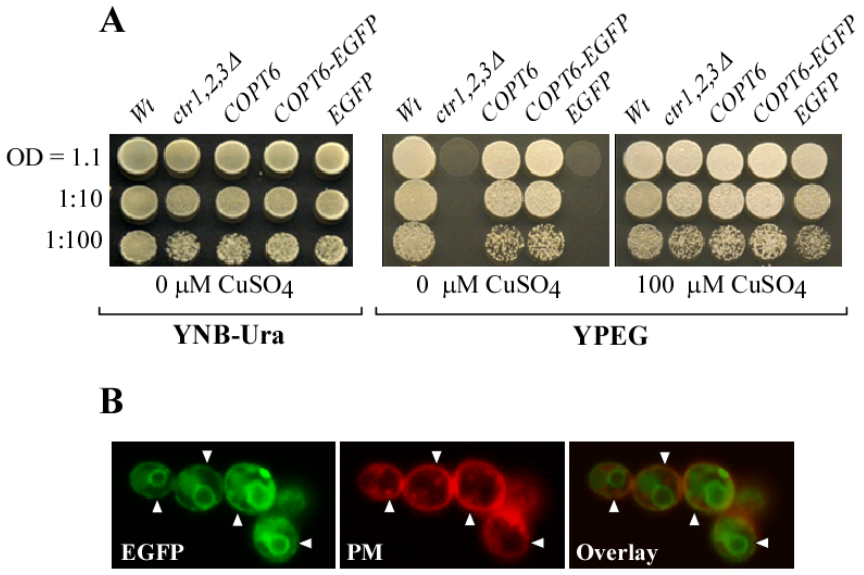

Figure 3. COPT6 rescues growth defect of the *ctr1ctr2ctr3 S. cerevisiae* triple mutant on ethanol/glycerol medium (YPEG). A. The wild-type SEY6210 strain, transformed with the empty vector (**Wt**), and the *ctr1ctr2ctr3* mutant transformed with the empty vector (***ctr1,2,3Δ***) or the vector containing *COPT6* (***COPT6***), or *COPT6-EGFP* (***COPT6-EGFP***), or *EGFP* ***(EGFP)*** cDNA inserts were grown overnight in liquid medium to an OD_{600nm} = 1.1. Cells were then serially 10-fold diluted (indicated on the left), and spotted either onto solid YNB-URA medium (**YNB-URA**) or YPEG (**YPEG**) with indicated concentrations of $CuSO_4$. **B**. Microphotographs of EGFP- and FM 4-64-mediated fluorescence (**EGFP** and **PM**, respectively) derived from *S. cerevisiae* expressing *COPT6-EGFP* construct and stained with FM 4-64 dye. Superimposed EGFP- and FM 4-64-fluorescent images (**Overlay**) show that COPT6-EGFP-localizes at the plasma membrane. A fraction of COPT6-EGFP is also present at ER and inside the vacuole (see the explanation in the main body of the manuscript).

To determine the subcellular localization of COPT6 in the heterologous system, we fused it at the C-terminus to EGFP of the *YES3-EGFP-Gate* vector and transformed this construct, or the empty vector expressing EGFP only, into the *ctr1ctr2ctr3* mutant. The COPT6-EGFP construct was functional because, unlike the empty vector, it rescued growth of the *ctr1ctr2ctr3* mutant on YPEG medium (Figure 3A). The COPT6-EGFP-mediated fluorescence was observed at the cell periphery (Figure 3B) where it overlapped with FM 4-64 dye, which stained the plasma membrane after short-term labeling conducted in low temperatures (Udvardi et al., 2008; Pfaffl et al., 2002; Vida and Emr 1995; Ueda et al., 2001; Bolte et al., 2004). These data suggested that

COPT6-EGFP localizes to the plasma membrane in the heterologous system. A fraction of COPT6-EGFP degraded, resulting in EGFP accumulation inside the vacuole and in endoplasmic reticulum (Figure 3B) as frequently observed for overexpressed plasma membrane proteins (Baekgaard et al., 2010; Jahn et al., 2002). Nevertheless, the plasma membrane-localized COPT6-EGFP was sufficient to complement the growth defect of the *ctr1ctr2ctr3* mutant on YPEG medium (Figure 3A).

The ability of heterologously expressed *COPT6* to rescue the growth defect of the *ctr1ctr2ctr3* mutant on YPEG medium, along with its plasma membrane localization, suggest that COPT6 is involved in copper uptake.

Heterologously expressed *COPT6* facilitates copper accumulation in *ctr1ctr2ctr3 S. cerevisiae* cells

To ascertain that COPT6 rescues the growth defect of the *ctr1ctr2ctr3* mutant on YPEG medium by transporting copper, we analyzed copper content of the *ctr1ctr2ctr3* mutant expressing the *YES3-Gate* vector with or without the *COPT6* cDNA and wild-type cells expressing the *YES3-Gate* vector. Yeast cells were grown on YNB-URA medium supplemented with the indicated concentrations of $CuSO_4$, and copper content was analyzed by ICP-MS. We found that empty vector expressing wild-type cells accumulated 20.7 ± 0.5 ppb of copper when grown on YNB-URA. In contrast, the *ctr1ctr2ctr3* mutant accumulated 6-fold less copper than the empty vector-expressing wild-type (Figure 4).

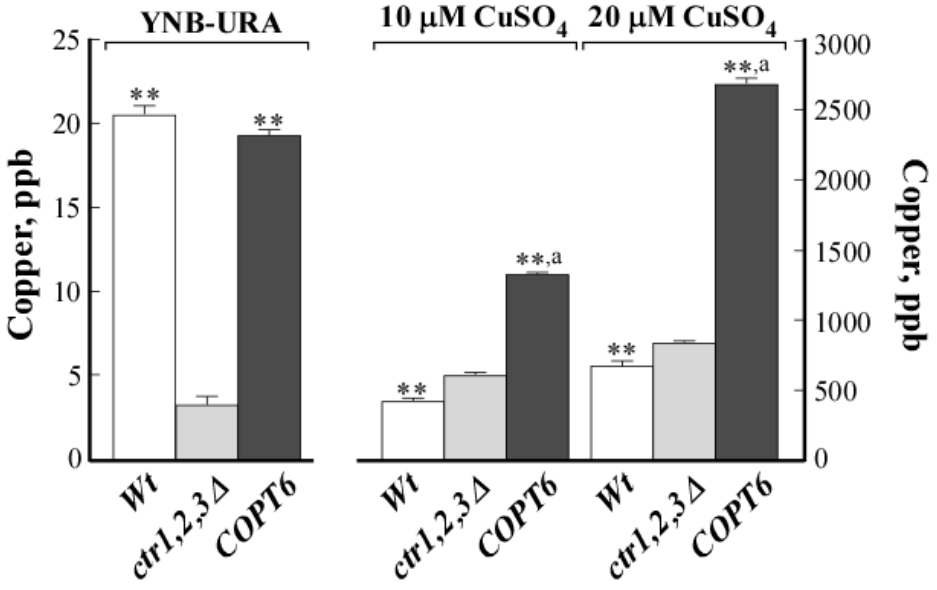

Figure 4. Copper content of the vector-transformed *S. cerevisiae* wild-type (Wt) and *ctr1ctr2ctr3* mutant cells (*ctr1,2,3Δ*) and *ctr1ctr2ctr3* mutant cells transformed with the vector containing the *COPT6* cDNA insert (*COPT6*). Yeast cells were cultured in liquid YNB-URA medium that originally contained 0.25 μM $CuSO_4$ (**YNB-URA**), or on YNB-URA supplemented with additional concentrations of $CuSO_4$, as indicated. Copper content was analyzed by ICP-MS. Statistical significance of differences was determined using the ANOVA Single Factor Analysis. The asterisks (**) indicate statistically significant differences of the mean values from the vector-transformed *ctr1ctr2ctr3* mutant ($p \leq 0.001$; n = 5). Letters (^{a}) indicate statistically significant differences ($p \leq 0.001$) of the mean values from the vector-expressing wild-type cells. Error bars indicate S.E.

These data are consistent with previous findings showing that CTR proteins are important for copper transport (Dancis et al., 1994a; Dancis et al., 1994b; Puig et al., 2002). Expression of *COPT6* in the *ctr1ctr2ctr3* mutant increased its ability to accumulate copper to the level of the wild-type strain (Figure 4). Supplementing YNB-URA with the indicated concentrations of copper increased copper accumulation in all yeast alleles (Figure 3). Nevertheless, *ctr1ctr2ctr3* cells expressing *COPT6* accumulated 2- and 3-fold more copper when grown at 10 μM and 20 μM $CuSO_4$,, respectively, than mutant cells expressing the empty vector, and 3- and 4-fold more copper than the empty vector-expressing wild-type (Figure 4). These data indicate unambiguously that *A. thaliana* COPT6 is a copper uptake transporter.

A positionally conserved methionine residue in TM2 (Met_{106}), but not a positionally conserved amino-terminal methionine residue (Met_{27}) is essential for COPT6 function

Elegant genetic and biochemical studies have shown that positionally conserved methionine residues within the hydrophilic N-terminal extracellular domain of *S. cerevisiae* Ctr1p, $Met_{127,}$ and in TM2, Met_{260}, are important for extracellular copper binding and uptake, respectively (Puig et al., 2002). To test whether the corresponding residues in COPT6 (Met_{27} in the amino terminus and Met_{106} in TM2, Figure 1) are also essential for function, we converted Met_{27} and Met_{106} in the full-length COPT6 wild-type protein to alanine, M27A and M106A, respectively, and transformed these mutant alleles into the *ctr1ctr2ctr3* mutant. Concurrently, the *ctr1ctr2ctr3* mutant was transformed with full-length Ctr1p or the previously described point mutants with Met_{127} and Met_{260} substituted to leucine or alanine (M127L or M260A, respectively) as controls (Puig et al., 2002). We then compared the ability of wild-type COPT6, wild-type Ctr1p and their mutant alleles to suppress the growth defect of the *ctr1ctr2ctr3* mutant on YPEG medium.

We found that all yeast alleles grew well on YPEG medium supplemented with 100 μM $CuSO_4$ (Figure 5). As expected, expression of the full-length wild-type COPT6 and Ctr1p complemented the growth defect of the *ctr1ctr2ctr3* mutant on YPEG medium; however expression of M106A-substituted COPT6 did not (Figure 5).

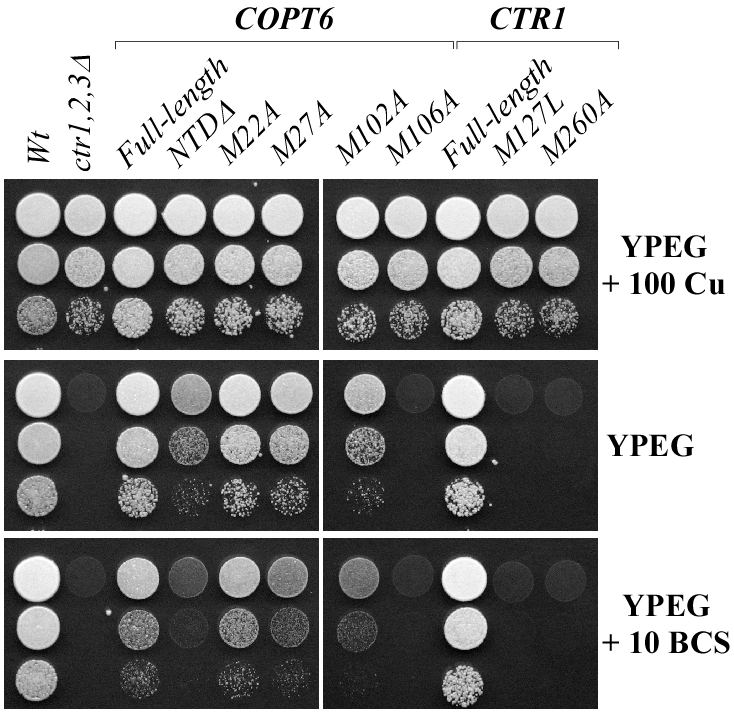

Figure 5. The conserved Met_{106} residue within the TM2 is essential for COPT6 function. *S. cerevisiae* wild-type (**Wt**) and *ctr1ctr2ctr3* mutant cells (*ctr1,2,3Δ*) were transformed with the empty vector. *ctr1ctr2ctr3* mutant cells were also transformed with the vector containing the full-length *COPT6,* or *S. cerevisiae CTR1* cDNA inserts (***COPT6*** and ***CTR1****,* respectively), or *COPT6* lacking the extracellular N-terminal domain (*NTD*Δ), or Met-to-Ala substituted *COPT6* alleles (***M22A, M27A, M102A,*** and ***M106A***) or Met-to-Leu, Met-to-Ala substituted *CTR1* alleles (***M127L, M260A***). Yeast alleles were grown, diluted as indicated on Figure 3, and spotted on YPEG medium with or without 100 μM $CuSO_4$ (**100 Cu**), or 10 μM BCS (**10 BCS**), as indicated on the right.

Consistent with previous findings (Puig et al., 2002), the Ctr1p mutant allele with a point mutation in a corresponding Met_{260} residue (M260A) also did not complement the growth defect of the *ctr1ctr2ctr3* mutant on YPEG (Figure 5). We also tested whether the adjacent conserved Met_{102} residue in TM2 of COPT6 is essential for COPT6 function. However, substituting Met_{102} to alanine did not appear to alter COPT6 function since the *ctr1ctr2ctr3* mutant expressing M102A allele grew on YPEG medium as well as mutant cells expressing the wild-type COPT6 or Ctr1p (Figure 5). These results show that the function of one of two methionine residues within the TM2 is conserved throughout the CTR/COPT proteins in yeast and plants.

Consistent with previous findings of the essential role of a positionally conserved Met_{127} residue in the amino terminus of Ctr1p (31), expression of the M127L mutant allele of Ctr1p did not complement the respiratory deficiency of the *ctr1ctr2ctr3* mutant on the YPEG medium (Figure 5). Surprisingly, substitution of a corresponding Met_{27} (M27A) residue in COPT6 complemented the *ctr1ctr2ctr3* mutant growth defect on YPEG medium, suggesting that this residue in the N-terminus of COPT6 is not required for COPT6 function. In addition, mutation of the semi-conserved, adjacent Met_{22} (M22A) in the amino terminus (Figure 1) also complemented the growth defect of the *ctr1ctr2ctr3* mutant on YPEG medium. These data suggest that unlike Ctr1p, the tested conserved Met residues of the amino terminus in COPT6 are not essential for its function.

The methionine-rich amino terminus is required for COPT6 function under conditions of copper limitation

Previous studies suggested that Met_{127} within the methionine-rich regions (Mets motifs) of the amino terminus of Ctr1p is involved in extracellular copper binding prior to its transport into the cell (Puig et al., 2002). Our data indicate that the corresponding positionally conserved Met_{27} or adjacent semi-conserved Met_{22} are dispensable for COPT6 function. To determine the function of the amino terminus of COPT6, we decided to generate a COPT6 mutant allele without its extracellular N-terminal domain (NTDΔ). We then tested the respiratory competence of the *ctr1ctr2ctr3* mutant expressing NTDΔ-COPT6 compared to the mutant expressing full-length COPT6 or Ctr1p proteins. Surprisingly, cells expressing NTDΔ-COPT6 were still able to grow on YPEG medium (Figure 5), suggesting that the N-terminal region of COPT6 is not absolutely essential for the function of the transporter. However, we noticed that the cell density of NTDΔ-

COPT6 expressing cells on YPEG medium was lower than that of expressing the full-length COPT6 or Ctr1p (Figure 5). We then tested if limiting bioavailable copper through the addition of a specific copper chelator, bathocuproine disulfonic acid (BCS), to the YPEG medium would alter the growth of cells expressing NTDΔ-COPT6. We found that the growth of cells expressing NTDΔ-COPT6 was severely impacted when extracellular bioavailable copper was limited by the addition of BCS (Figure 4, YPEG + 10 BCS). These results suggest that the extracellular N-terminal domain of COPT6 plays an important role in copper homeostasis under copper-limiting conditions. Future studies will reveal the specific amino acid residue(s) involved in copper binding.

COPT6 localizes to the plasma membrane in *A. thaliana* protoplasts

Members of the CTR/COPT family in different species associate with different endomembranes including the plasma membrane or endosomal vesicles/vacuoles, and contribute to copper homeostasis either by copper uptake from the external media or copper release from internal compartments during deficiency (Rees et al., 2004; Andrés-Colás et al., 2010; van den Berghe et al., 2007; Bellemare et al., 2002). Our studies of the subcellular localization of COPT6 in *S. cerevisiae* showed that in this heterologous system it localizes to the plasma membrane. Subsequently, we sought to determine its localization in *A. thaliana*. The coding sequence of *COPT6* was fused at the C-terminus to *EGFP* in the *SAT6-EGFP-N1-Gate* vector and transiently expressed under the control of the constitutive cauliflower mosaic virus (CaMV) *35S* promoter in *A. thaliana* protoplasts. As a control, protoplasts were transfected with the empty *SAT6-EGFP-N1-Gate* vector.

EGFP-mediated fluorescence was present at the periphery of COPT6-EGFP transfected

protoplasts and did not overlap with chlorophyll autofluorescence (Figure 6A). To ascertain the plasma membrane localization of COPT6-EGFP, transfected protoplasts were co-stained with FM 4-64. After the short-term labeling at 4^{o}C, FM4-64 stained the plasma membrane (Figure 6B FM 4-64+Chl) and FM 4-64-mediated fluorescence overlapped with COPT6-EGFP-mediated fluorescence but not with chlorophyll-mediated fluorescence (Figure 6B). In protoplasts transfected with the empty vector, EGFP was present as a soluble protein in the cytosol and its fluorescence did not overlap with chlorophyll autofluorescence (Figure 6C). These results are consistent with the plasma membrane localization of COPT6.

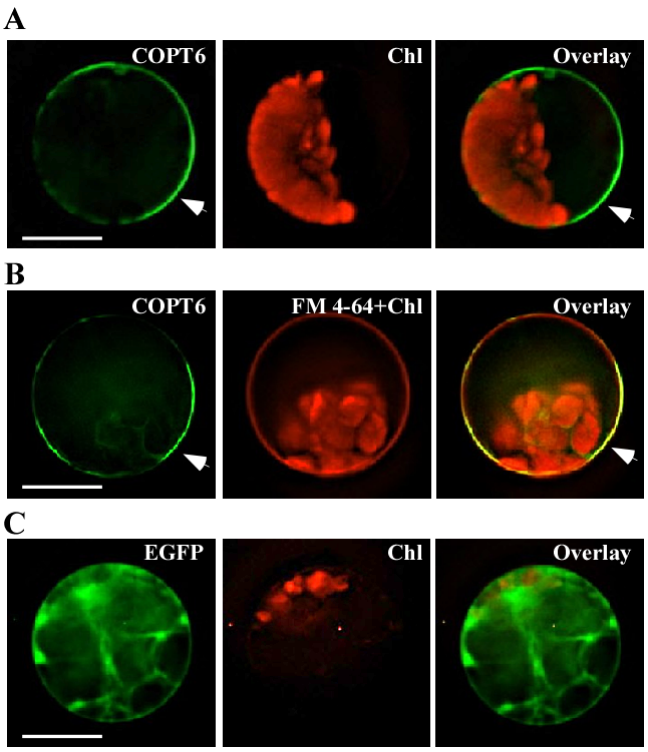

Figure 6. Subcellular localization of COPT6 in *A. thaliana* protoplasts. *A. thaliana* leaf protoplasts were transfected with the vector expressing the *COPT6-EGFP* fusion (**A, B**) or vector expressing *EGFP* without the *COPT6* cDNA insert (**C**). To visualize the plasma membrane, *COPT6-EGFP* transfected protoplasts were co-stained with FM 4-64 (**B**). EGFP-mediated fluorescence, derived from COPT6-EGFP (**COPT6**) or EGFP (**EGFP**), FM 4-64-mediated fluorescence and chlorophyll autofluorescence (**FM 4-64+Chl** and **Chl**, respectively) were visualized using FITC or rhodamine filter sets. Superimposed images of COPT6-EGFP-, FM 4-64-mediated fluorescence and chlorophyll autofluorescence (**Overlay**) were created to demonstrate that green fluorescence derived from COPT6-EGFP-colocalizes with FM 4-64. Scale bar = 10 µm.

We also co-transfected protoplasts with the *SAT6-EGFP-N1-Gate* vector containing a COPT6-EGFP fusion and *BIN20* vector containing a plasma membrane marker, PIP2A, fused to mCherry (Nelson et al., 2007). Fluorescence signals originated from COPT6-EGFP and PIP2A-mCherry co-localized at the periphery of transfected protoplasts (Figure 7), suggesting that COPT6 similar to PIP2A localizes to the plasma membrane.

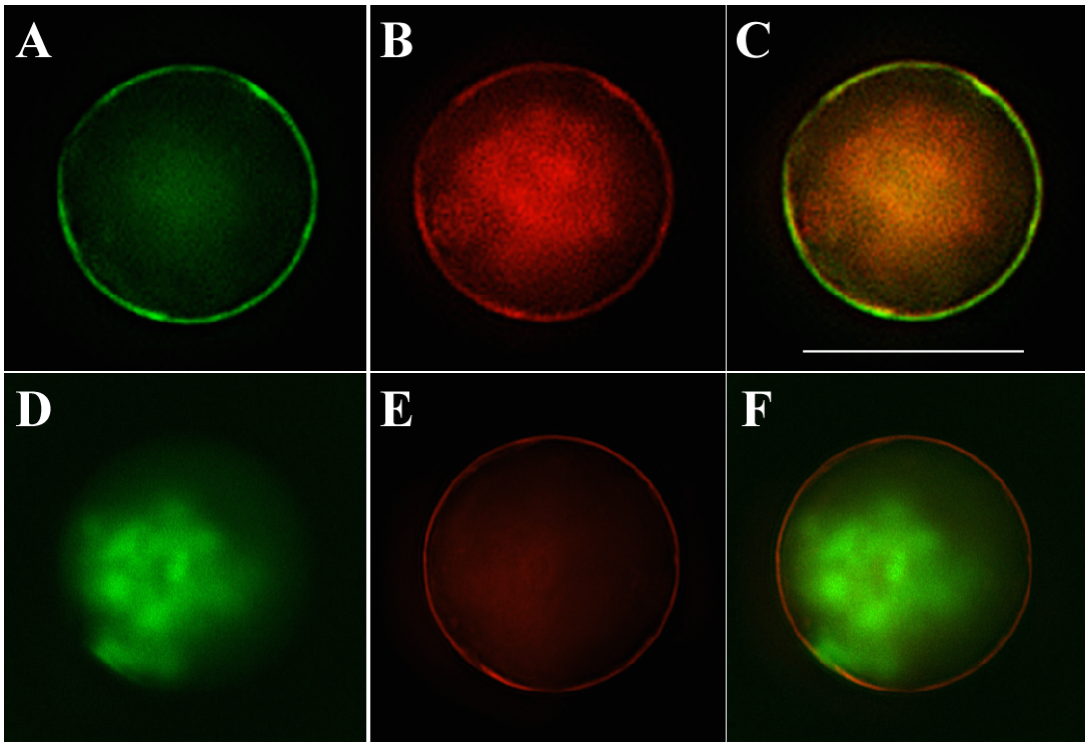

Figure 7. **Subcellular localization of COPT6 in *A. thaliana* protoplasts.** Protoplasts were isolated from 14-day old seedlings and co-transfected with the *SAT6-EGFP-N1* vector containing a COPT6-EGFP fusion and the *BIN20* vector containing a plasma membrane marker, PIP2A, fused to mCherry (**A**-**C**), or with the *BIN20-PIP2A-mCherry* construct (**D**-**F**). EGFP- or mCherry-mediated fluorescence were visualized through FITC (**A, D**) or Rhodamine (**B, E**) filter sets of an Axio Imager M2 microscope equipped with a motorized Z-drive (Zeiss). Superimposed images of COPT6-EGFP-, and PIP2A-mCherry-mediated fluorescence (**C, F**) were created to demonstrate that COPT6-EGFP-colocalizes with PIP2A-mCherry. Z-stack (1.3 µm-thick) images of protoplasts were collected with an AxioCam MR Camera and 3D deconvoluted using an inverse filter algorithm of the Zeiss AxioVision 4.8 software. Scale bar = 20 µm

Analyses of the *copt6-1* mutant and transgenic plants ectopically expressing *COPT6*

Our studies in *S. cerevisiae* showed that COPT6 is involved in copper uptake (Figures 3A and 4). To study the role of COPT6 *in planta*, we used a T-DNA insertion allele, *copt6-1* (SALK 083438) and two transgenic lines, $35S_{pro}$-*COPT6-1* and $35S_{pro}$-*COPT6-2*. Wild-type plants and a transgenic line expressing the *EarlyGate201* vector without the *COPT6* cDNA insert ($35S_{pro}$) were used as controls for the *copt6-1* mutant or *COPT6* overexpressing lines, respectively.

Sequencing of the *copt6-1* genomic DNA fragment revealed a T-DNA insertion 110 bp upstream of the *COPT6* start codon. qRT-PCR analysis disclosed 10- and 8-fold decrease of *COPT6* mRNA in roots and shoots, respectively, in the *copt6-1* allele (Figure 8A). In contrast, transcript abundance of *COPT6* was 1,000- and 30-fold higher in roots and shoots of $35S_{pro}$-*HA-COPT6-1* transgenic plants compared to plants expressing the empty vector (Figure 8B). Expression of *COPT6* in the $35S_{pro}$-*HA-COPT6-2* transgenic line was 7,000- and 170-times higher in roots and shoots, respectively (Figure 8B).

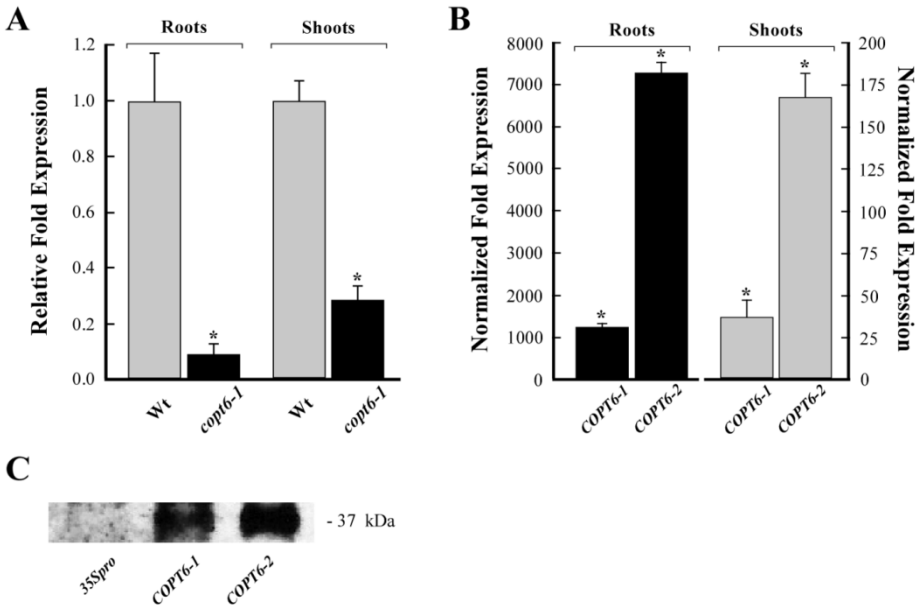

Figure 8. Characterization of the *copt6-1* mutant allele and transgenic lines ectopically expressing *$35S_{pro}$-HA-COPT6*. **A**. Quantitative real-time (qRT)-PCR analysis of 10-day-old *copt6-1* seedlings (***copt6-1***) indicates a 10- and 8-fold decrease of the abundance of the *COPT6* transcript in roots and shoots, respectively, compared to the wild-type (**Wt**) seedlings. **B.** Abundance of the *COPT6* transcript in roots and shoots of two transgenic lines, $35S_{pro}$-*HA-COPT6-1* (***COPT6-1***) and $35S_{pro}$-*HA-COPT6* (***COPT6-2***). Results are presented relative to the expression of *COPT6* in plants transformed with the empty vector, designated as 1. Error bars indicate S.E. (n = 9). Asterisks indicate statistically-significant differences ($p \leq 0.05$) of the mean values. **C**. Immunoblot analysis of the COPT6-HA polypeptide in transgenic plants expressing *EarleyGate201* vector lacking the cDNA insert (***$35S_{pro}$***) and two lines (***COPT6-1*** and ***COPT6-2***) expressing $35S_{pro}$-*HA-COPT6.* The apparent molecular weight of COPT6-HA is indicated on the right.

SDS-PAGE and immunoblot analyses of total membrane proteins isolated from leaves of transgenic plants revealed the anti-HA antibody reactive protein with an apparent molecular mass of ~37 kDa in extracts from *35S$_{pro}$-HA-COPT6-1* and *35S$_{pro}$-HA-COPT6-2* transgenic lines but not from the empty vector-expressing plants (Figure 8C). Consistent with the qRT-PCR results (Figure 8B), the level of anti-HA immuno-reactive polypeptide was higher in the *35S$_{pro}$-HA-COPT6-2* line than in the *35S$_{pro}$-HA-COPT6-1* line (Figure 8C). It is noteworthy that the molecular mass of COPT6-HA is considerably larger than its predicted size of 16.9 kDa. It is possible that this aberrant migration is a consequence of posttranslational modifications, i.e. *O*-glycosylation, that was shown for the COPT6 homolog from *S. cerevisiae*, Ctr1p (Puig et al., 2002).

COPT6* plays an important role in copper homeostasis in *A. thaliana

Wild-type, the *copt6-1* mutant and transgenic plants were germinated and grown on solid half-strength Murashige and Skoog (½ MS) medium (Cu sufficient conditions, Figure 9A). To limit copper availability, ½ MS was supplemented with the indicated concentration of BCS (Figure 9C). To impose copper toxicity, ½ MS was supplemented with 45 μM $CuCl_2$ (Figure 9D).

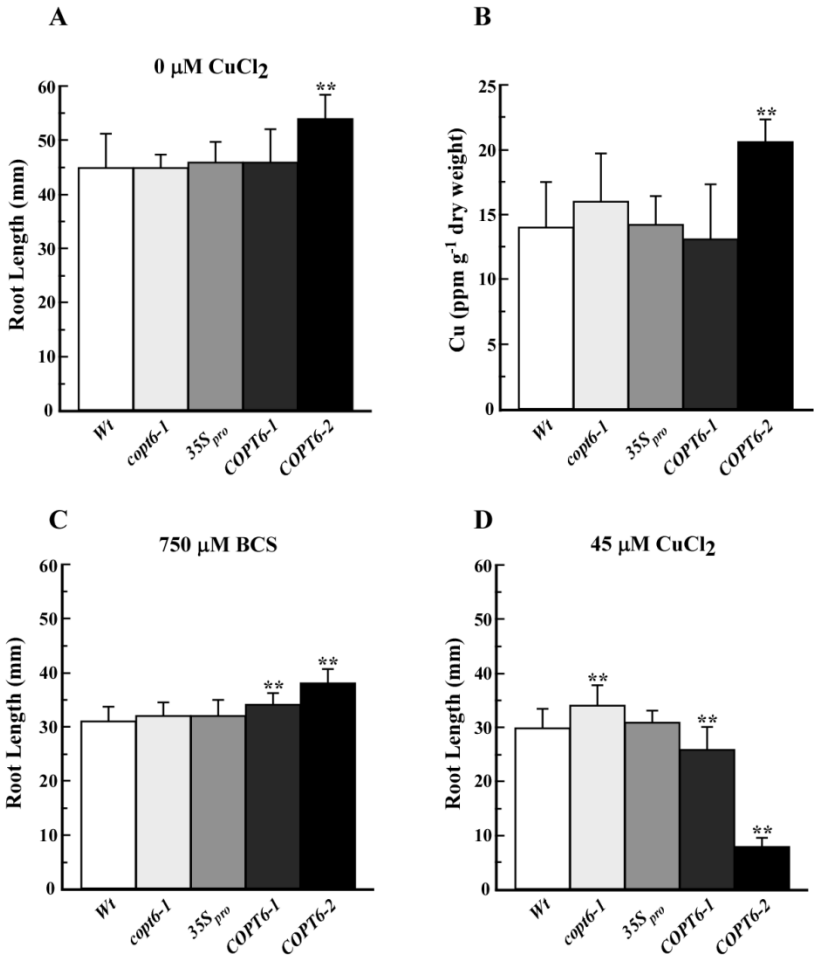

Figure 9. **Altered expression of *COPT6* in the *copt6-1* mutant and *COPT6* transgenic plants affects their response to copper limitation and excess.** Root length of wild-type (**Wt**), the *copt6-1* mutant ***(copt6-1)***, two transgenic lines overexpressing *35S$_{pro}$-HA-COPT6* (*COPT6-1* and *COPT6-2*), and plants transformed with the empty vector (*35S$_{pro}$)* grown in ½ MS (0 μM $CuCl_2$, **A**), or in ½ MS supplemented with 750 μM BCS (**C**) or 45 μM $CuCl_2$ (**D**). **B**. Copper content in shoots of different plant lines grown hydroponically. Plant lines are designated as in (**A**). Asterisks indicate statistically-significant differences (** = $p \leq 0.001$) of the mean values (ANOVA).

These concentrations of $CuCl_2$ and BCS were selected based on morphological and molecular phenotypes associated with copper excess or deficiency (Figure 10).

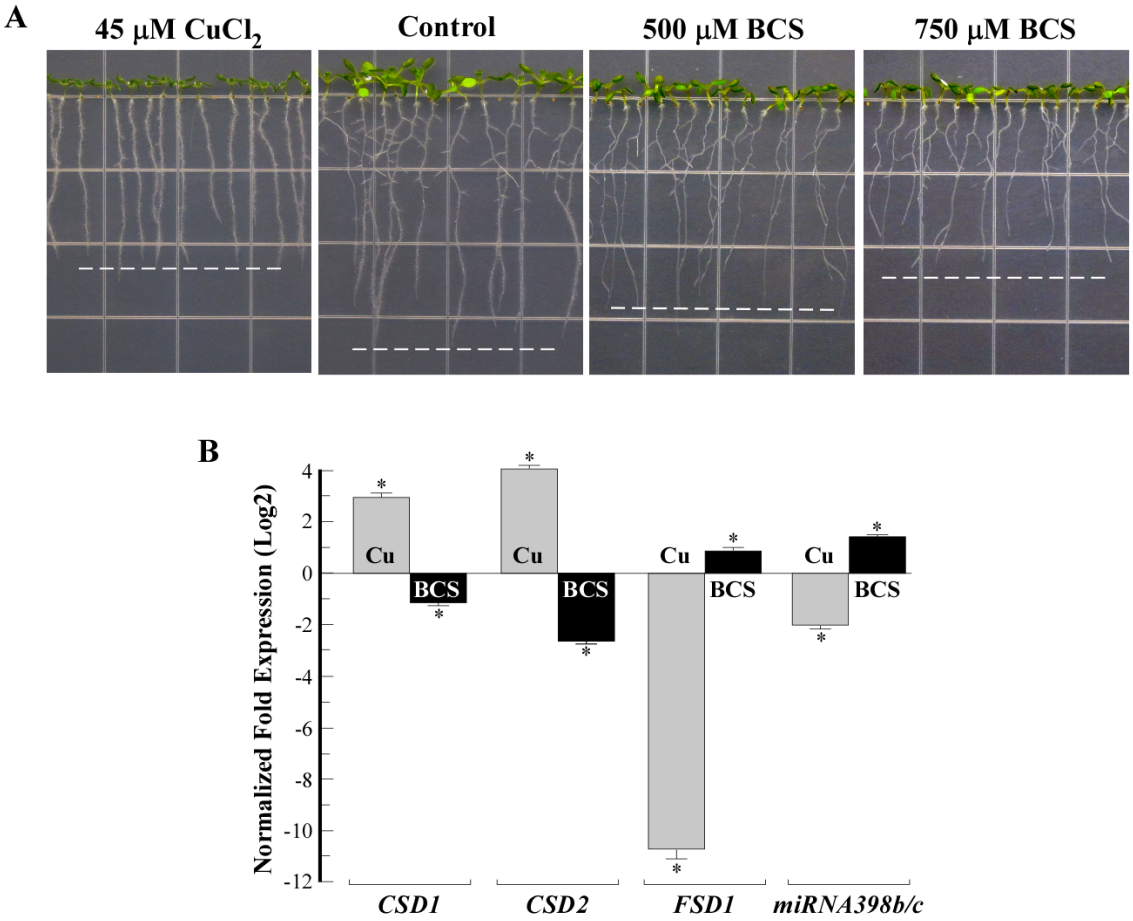

Figure 10. **Effect of copper availability on growth (A) and transcript abundances of copper responsive genes in shoots of *A. thaliana* wild-type (B).** Seeds were germinated and grown for 10 days on ½ MS without (**Control**) or with 45 μM $CuCl_2$ (**45 μM $CuCl_2$**) or 500 or 750 μM BCS (**500 μM BCS** or **750 μM BCS**, respectively) before seedlings were photographed and shoots were collected for RNA isolation and cDNA synthesis. Note the decreased root length of seedlings (indicated by the white dashed line in **A**) grown on medium with excess copper or BCS. **B**. Transcript abundances of genes encoding Cu/Zn-SODs, *CSD1* and *CDS2* (***CSD1*** and ***CSD2***, respectively), Fe-SOD (***FSD1***) and miRNA398b/c (***miR398b*/c**). Data were normalized to expression of *Actin 2* and are shown relative to their expression in control conditions. Error bars indicate S.E. ($n = 9$). Asterisks indicate statistically-significant differences ($p \leq 0.05$) of the mean values from corresponding control samples.

Copper toxicity and deficiency inhibits root growth of *A. thaliana* (Burkhead et al., 2009, Murphy et al, 1995, Lequeux et al., 2010) and alters expression of the *miRNA398* and its targets, cytosol- and plastid-localized Cu/ZnSODs, *CSD1* and *CSD2*, and Fe-containing SOD, *FSD1* in shoots of *A. thaliana*. Specifically, the abundance of *miRNA398* mRNA increases during copper

deficiency, while mRNA abundance of its targets, *CSD1* and *CSD2*, decreases (Abdel-Ghany et al., 2008; Sunkar and Zhu 2006; Yamasaki et al., 2007). The superoxide scavenging functions of CSD1 and CSD2 during copper deficiency are replaced by an increase in gene expression *FSD1* (Yamasaki et al., 2007; Abdel-Ghany et al., 2005). These morphological and molecular phenotypes of copper excess or deficiency were observed in *A. thaliana* seedlings grown in the presence of 45 μM $CuCl_2$ or 750 μM BCS (Figure 10A and B).

Root length of 10-day-old seedlings was used as a measure of tolerance or sensitivity to these growth conditions. The average lengths of primary roots of the *copt6-1* mutant and the *35S$_{pro}$-COPT6-1* transgenic line cultured at ½ MS were the same as of their corresponding controls, the wild-type and the empty vector expressing plants, respectively (Figure 9A). We also did not find statistically significant differences in copper accumulation in roots (not shown) or shoots (Figure 9B) of these plant lines. In contrast, roots of *35S$_{pro}$-COPT6-2* transgenic line, which manifested the highest level of the *COPT6* transcript and polypeptide (Figure 8B, C), were 1.2-fold longer then empty vector expressing plants (Figure 9A). While internal copper content of roots of this plant line did not differ from the other plant lines (not shown), its shoots accumulated 1.5-fold more copper then the empty vector expressing plants (Figure 9B). These data suggest that significantly increased expression of *COPT6* in these plants was beneficiary for plants even at copper sufficient conditions.

We then tested the response of different plant lines to copper limitation or excess. As would be expected for copper limiting conditions, primary roots were shorter in all plant lines grown on ½ MS supplemented with BCS than on ½ MS without supplements (Figure 9A, C). However, there was no difference between the root length of the *copt6-1* mutant and wild-type plants in copper limiting conditions (Figure 9C). This result was not very surprising because of the

possible functional redundancy of *COPT6* with other COPT family members. In contrast, roots of *35S$_{pro}$-COPT6-1* and *35S$_{pro}$-COPT6-2* transgenic plants grown in copper limiting conditions were 1.3 and 1.4-fold longer, respectively, compared to the empty vector expressing plants (Figure 9C) suggesting that overexpression of *COPT6* was beneficiary for plant growth also when copper is scarce.

Supplementation of ½ MS medium with a toxic concentration of $CuCl_2$ inhibited root growth of all plant lines in comparison with ½ MS without supplementation (Figure 9A, D). *COPT6* overexpressing transgenics and the *copt6-1* mutant showed opposite responses to toxic copper: roots of plants overexpressing *COPT6* were significantly shorter, while roots of the *copt6-1* mutant were longer when compared to corresponding controls (Figure 9D). It is important to note that the sensitivity of *COPT6* over-expressing plants to copper excess correlated with the level of *COPT6* overexpression: the *35S$_{pro}$-COPT6-2* line was more markedly sensitive and overexpressed *COPT6* to a higher degree compared to *35S$_{pro}$-COPT6-1*.

The improved growth of *COPT6* transgenics in copper limiting conditions and their increased sensitivity to copper excess and the decreased sensitivity of the *copt6-1* mutant to copper excess not only show that COPT6 functions in copper homeostasis in *planta* but also further support the notion that tight control of the expression of copper transporters is needed for preventing copper deficiency while avoiding toxicity.

Expression of *COPT6* is regulated by copper status

Regulation of the mRNA expression of CTR/COPT family members by copper status is among the major mechanisms of the control of copper homeostasis in the cell. Therefore, we sought to determine whether the abundance of *COPT6* mRNA in *A. thaliana* would be altered in response

to changes in copper supply as well. Wild-type *A. thaliana* (Col-0) seedlings were grown on ½ MS medium without (control), with 45 μM of $CuCl_2$ (copper excess) or 500 μM of BCS (copper deficiency).

Analyses of *COPT6* transcript abundance in *A. thaliana* cultured on control ½ MS medium showed that *COPT6* is mainly expressed in leaves (Figure 11A). The transcript abundance of *COPT6* increased in both roots and shoots of BCS-treated *A. thaliana* wild-type plants (Figure 11B). In contrast, copper excess affected the transcript abundance of *COPT6* only in shoots, but not roots (Figure 11B). Based on these results we concluded that *COPT6* expression is differentially regulated in roots and leaves of *A. thaliana* in response to alterations in copper availability.

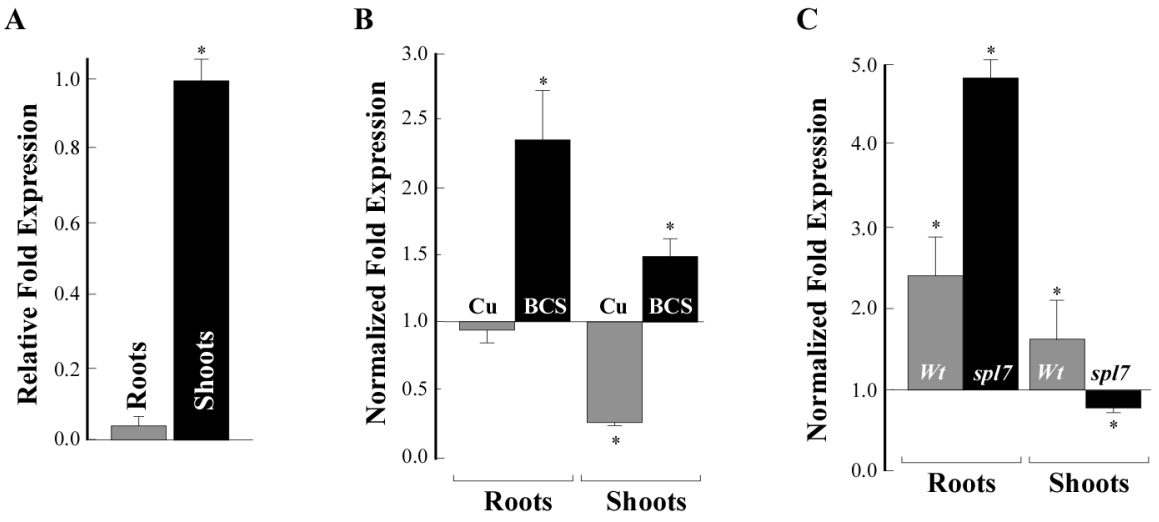

Figure 11. **Quantitative real-time (qRT) PCR analysis of *COPT6* transcript abundance in 10-day-old *A. thaliana* seedlings**. **A.** Relative transcript abundance of *COPT6* in roots (**Roots**) and shoots (**Shoots**) of seedlings grown on ½ MS agar plates. **B.** Analysis of the *COPT6* mRNA expression in response to copper status in wild-type plants. Roots and shoots were collected from seedlings germinated and grown on ½ MS agar plates without addition or with 45 μM $CuCl_2$ (**Cu**) or 500 μM bathocuproine disulfonate (**BCS**). Results are presented relative to the expression of *COPT6* in the wild-type grown without added Cu or BCS, designated as 1. **C.** Analysis of the *COPT6* expression in the *spl7-1* mutant in response to copper limitation. Roots and shoots were collected from wild-type (**Wt**) and *spl7-1* mutant (***spl7***) seedlings germinated and grown on ½ MS agar plates without addition or with 500 μM BCS. Transcript abundance of *COPT6* in tissues of the wild-type and the *spl7*-1 mutant grown in the presence of BCS is presented relative to its expression in corresponding plant lines grown without BCS that is designated as 1. Error bars indicate S.E. (*n = 9-18*). Asterisks indicate statistically significant differences ($p \leq 0.05$) of the mean values from corresponding control samples.

Expression of *COPT6* depends, in part, on SPL7

A recent microarray study revealed that upregulation of the expression of many copper-deficiency responsive genes in *A. thaliana*, including *COPT1* and *COPT2,* is attributable to the activity of the transcription factor, SPL7 (Yamasaki et al., 2009). SPL7 activates the transcription if its targets *via* binding to the GTAC motif (*alias* Copper-Responsive Elements [CuRE]) in the transcription regulation regions of copper-responsive genes (Yamasaki et al., 2009, Quinn et al., 1995). Since *COPT6* is not represented on the Agilent *Arabidopsis* 3 Oligo Microarray used in (Yamasaki et al., 2009), we sought to determine whether the transcriptional

response of *COPT6* to low copper availability (Figure 11B) is controlled by SPL7 as well.

In this regard, we identified two GTAC motifs in a region of <200 bp upstream of the *COPT6* start codon using the PLACE prediction software (http://www.dna.affrc.go.jp/PLACE/signalscan.html), suggesting that *COPT6* might be an SPL7 target. We then used the *spl7-1* mutant allele of *A. thaliana* (Yamasaki et al., 2009) and tested whether decreasing copper availability by supplementing the growth medium with BCS would upregulate *COPT6* expression in this mutant background as it did in the wild-type (Figure 11B). It was found that the transcript abundance of *COPT6* was still significantly increased in roots of the BCS-treated *spl7-1* mutant (Figure 11C). In contrast, expression of *COPT6* mRNA was not upregulated in shoots of the BCS-treated *spl7-1* mutant (Figure 11C). Based on these findings, we concluded that SPL7 is essential for the transcriptional response of *COPT6* to copper limitation in shoots, while other transcription regulators might be involved in its response in roots of *A. thaliana.*

The expression pattern of COPT6 in *A. thaliana*

To investigate the sites of *COPT6* action in *A. thaliana*, the *COPT6* promoter sequence ($COPT6_{pro}$) was fused to the *uidA* reporter gene encoding *β*-glucuronidase (*GUS*), and this $COPT6_{pro}$-*GUS* construct was transformed into wild-type *A. thaliana*. From three transgenic lines exhibiting the same pattern of GUS activity, we selected one representative line for subsequent studies. Consistent with results of qRT-PCR analysis (Figure 11A), the majority of GUS activity was observed in leaves of young seedlings (Figure 12A).

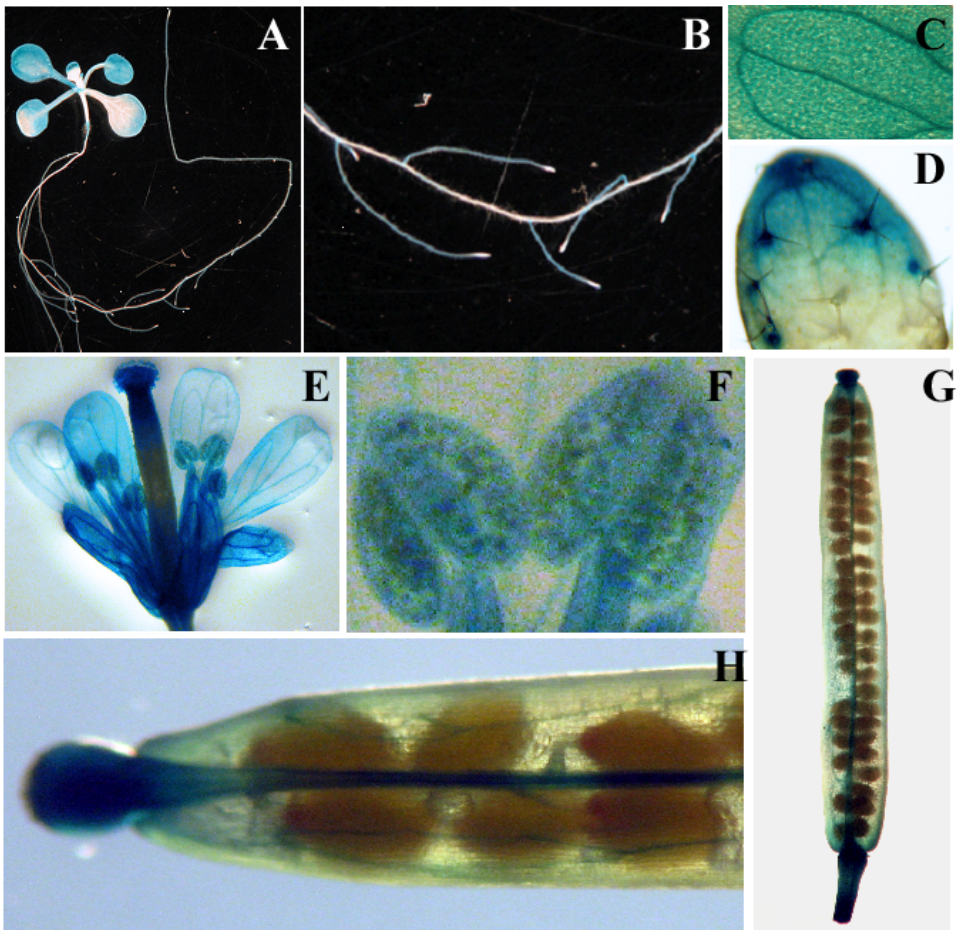

Figure 12. Histochemical analysis of the expression pattern of *COPT6* in *A. thaliana* transformed with the *COPT6$_{pro}$-GUS* construct. A. Representative expression patterns of *COPT6$_{pro}$-GUS* in a 10-day-old seedling. Note the strong GUS activity in lateral roots and vascular tissues of cotyledons (close-up images **B** and **C**, respectively), trichomes, and trichome basal cells (shown in a close-up image of a first true leaf [**D**]). **E.** Staining pattern in a flower, **F.** A close-up of an anther and a filament of a stamen; a young silique (**G)**, and close-up of a silique (**H)**.

While the GUS staining was observed throughout different cell types of lateral roots, it was absent in the primary root and at the root tips of lateral roots (Figure 12B). We also observed strong GUS staining in the vasculature in leaves, in leaf trichomes and trichome basal cells (Figure 12C, D). The histochemical analysis of mature plants revealed that *COPT6* is also expressed in sepals and petals of inflorescence (Figure 12E). Analysis of the *COPT6$_{pro}$* activity in reproductive organs disclosed *COPT6$_{pro}$* activity in stigma and ovary, pollen grains and

filaments of stamens (Figure 12E, F). GUS activity in young siliques was less abundant and was primarily located in a gynophore, vasculature, a central replum, funiculus, style and stigma surfaces (Figure 12G, H). Since the bulk of $COPT6_{pro}$ activity is concentrated in the shoots and reproductive organs, it is tempting to suggest that COPT6 may play a primary role in Cu delivery and/or re-distribution in aboveground tissues.

COPT6 interacts with itself and with COPT1 at the plasma membrane

CTR/COPT proteins exist as homo- and/or hetero-complexes on the cellular membranes (5,29,30,35,36). Here we tested whether COPT6 would interact with itself by using split-ubiquitin-based membrane yeast two-hybrid (MYTH) and bimolecular fluorescence complementation (BiFC) and approaches (Kittanakom et al, 2009, Schutze et al., 2009, Bracha-Drori et al., 2004).

In the MYTH approach, modified ubiquitin is split into C- and N-terminal halves (Cub and NubG) and is fused to membrane-bound bait or prey proteins, respectively. Interactions of bait and prey proteins cause Cub and NubG to reconstitute ubiquitin. The presence of reconstituted ubiquitin is recognized by ubiquitin specific proteases (UBPs) that release an artificial transcription factor, PLV, (ProteinA-LexA-VP16) which is fused to the C-terminus of ubiquitin (CubPLV). Interactions are monitored by the PLV-induced expression of *lexA*-driven reporter genes, *ADE2, HIS3* and *lacZ* (Kittanakom et al., 2009, Obrdlik et al., 2004).

Interactions using the MYTH approach can only be detected when CubPLV and Nub fusions are located in the cytosol (Kittanakom et al., 2009). Based on computer algorithm analysis of the predicted membrane topology, the C-terminus of COPT6 is in the cytosol, whereas the N-terminus is located extracellularly (Figure 2B). Therefore, in order to detect COPT6-COPT6

interactions, NubG and CubPLV were fused to the C-terminus of the full-length COPT6, generating COPT6-NubG and COPT6-CubPLV, and co-expressed in *S. cerevisiae*. To detect false positives due to self-activation, COPT6-CubPLV was co-expressed with pNubG lacking the *COPT6* cDNA insert. Our data show that regardless of whether interactions were monitored as colony formation on selective media (SC) or by *β*-galactosidase activity, interactions occurred only in cells that co-expressed COPT6-CubPLV and COPT6-NubG constructs (Figure 13A). These interactions were not caused by self-activation because they did not occur in cells that co-expressed COPT6-CubPLV and pNubG (Figure 13A).

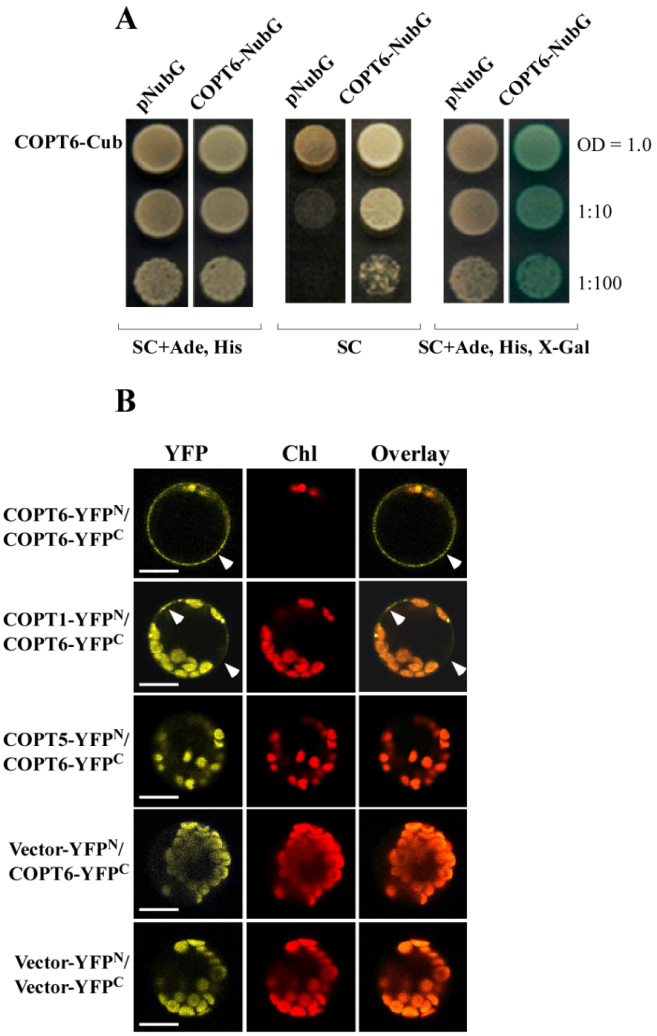

Figure 13. COPT6-COPT6 protein-protein interactions. A. COPT6 interacts with itself in MYTH system. Shown are yeast cells co-expressing COPT6-CubPLV construct (**COPT6-PLV**) with NubG lacking COPT6 cDNA insert (pNubG) or with COPT6 fused to NubG (**COPT6-NubG**). Growth was monitored for 2 days under conditions indicated below each panel; concentrations of yeast cells are indicated on the right. Shown are representative results of at least three biological replicates. SC = synthetic complete medium; Ade = adenine; His = histidine; X-gal = bromo-chloro-indolyl-galactopyranoside. **B.** Epifluorescence images of YFP fluorescence complementation. Protoplasts were co-transfected with plasmids containing COPT6-YFP^N and COPT6-YFP^C *(***COPT6-YFP^N/COPT6-YFP^C***)* or COPT1-YFP^N and COPT6-YFP^C *(***COPT1-YFP^N/COPT6-YFP^C***),* or COPT5-YFP^N and COPT6-YFP^C *(***COPT5-YFP^N/COPT6-YFP^C***)*, or with empty vector-YFP^N and COPT6-YFP^C (**Vector-YFP^N/COPT6-YFP^C**) or empty vector-YFP^N and vector-YFP^C (**Vector-YFP^N/Vector-YFP^C**). Chlorophyll autofluorescence, visible in yellow (**YFP**) and red filter sets (**Chl**) does not overlap with yellow fluorescence of reconstituted YFP in superimposed images (**Overlay**), indicating COPT6-COPT6 and COPT1-COPT6 protein-protein interactions due to assembly of split YFP. Scale bar = 10 μm.

The BiFC method is based on the observation that N- and C-terminal halves of enhanced yellow fluorescent protein, YFP^N and YFP^C, respectively, reconstitute a functional fluorophore when brought into proximity by two interacting proteins fused to the YFP fragments (Schutze et al., 2009, Bracha-Drori et al., 2004). For BiFC assays, the full-length COPT6 was fused at the C-terminus with the N- or C-terminal halves of YFP to generate COPT6-YFP^N or COPT6-YFP^C, and both constructs were co-transfected into *A. thaliana* protoplasts. For negative controls, protoplasts were co-transfected with YFP^N and YFP^C vectors without the *COPT6* insert (Vector-YFP^N/Vector-YFP^C) or with COPT5-YFP^N and COPT6-YFP^C (COPT5-YFP^N/COPT6-YFP^C). COPT5 has been shown to localize to the vacuolar membrane (Garcia-Molina et al., 2011, Klaumann et al., 2011) and should not interact with the plasma membrane-localized COPT6 protein. Interactions were visualized by following the fluorescence pattern of the reconstituted YFP fluorophore. Strong yellow fluorescence was observed at the plasma membrane only in COPT6-YFP^N and COPT6-YFP^C co-transfected protoplasts, but not in protoplasts co-transfected with Vector-YFP^N/Vector-YFP^C or COPT6-YFP^C/Vector-YFP^N (Figure 13B). Chlorophyll autofluorescence was also detected using the YFP filter set, but it did not overlap with yellow fluorescence associated with the plasma membrane in COPT6-YFP^N/COPT6-YFP^C co-expressing protoplasts. These results suggest that COPT6 interacts with itself at the plasma membrane in BiFC assays.

We also tested if COPT6 will form heterologous interactions with COPT1, which is located at the plasma membrane and has a well-established role in copper homeostasis (Sancenón et al., 2004, Sancenón et al., 2003). Protoplasts co-transfected with COPT1-YFP^N and COPT6-YFP^C (COPT1-YFP^N/COPT6-YFP^C) showed a faint yellow fluorescence pattern at the plasma

membrane, which did not overlap with chlorophyll autofluorescence (Figure 13B). This suggests that COPT6 interacts with COPT1. Collectively these results show that COPT6 at a minimum interacts with itself and COPT1 at the plasma membrane.

Discussion

The essential, yet potentially toxic nature of copper exemplifies the careful balance required to prevent deficiency while avoiding toxicity in most organisms. Among the central mechanisms in controlling copper homeostasis is the regulation of copper uptake. In this manuscript, we characterized COPT6, a newly identified member of the CTR/COPT family in *A. thaliana*. The primary sequence of COPT6 contains the family-conserved methionine-rich motifs of which residues corresponding to Met_{27} and Met_{106} in COPT6 are important in *S. cerevisiae* Ctr1p for copper binding and transport functions, respectively. In addition, the carboxyl terminus of Ctr1p and two closest COPT6 homologs, COPT1 and COPT2 contain the C*X*C motif (Figure 2C). This motif in Ctr1p is also involved in copper binding and transfer to cytosolic copper chaperones, and in protein degradation during copper excess (Puig et al., 2002; Wu et al., 2009; Xiao et al., 2002). In contrast, the primary sequence of COPT6 lacks the C*X*C motif (Figure 2C). Nevertheless, COPT6 suppresses the copper-deficient phenotype of the *ctr1ctr2ctr3* mutant and confers copper accumulation (Figures 3 and 4), suggesting that the C*X*C motif is not important for its transport activity. Whether it plays a regulatory role under copper excess as was proposed for *S. cerevisiae* Ctr1p (Puig et al., 2002, Wu et al., 2009, Xiao et al., 2002), is yet to be determined.

Consistent with the role of the positionally conserved methionine residue in TM2 of the CTR/COPT proteins (Puig et al., 2002), the positionally conserved Met_{106} in TM2 is required for

COPT6 function (Figure 5). However, it was surprising to find that the conserved Met_{27} in the N-terminal extracellular domain, as well as the extracellular domain itself are dispensable for COPT6 function when copper was still available in the medium. We found, however, that the extracellular domain is required for COPT6 function when availability of external copper was depleted by addition of BCS (Figure 5), suggesting that this domain is important for COPT6 function during high-affinity copper uptake under copper limitation. Since the positionally conserved Met_{27} and adjacent semi-conserved Met_{22} were dispensable for COPT6 function in the presence of BCS in the medium (Figure 5), we suggest that other residues within the extracellular domains may be involved in copper coordination. In this regard, the N-terminus of COPT6 contains five methionine and three histidine residues in addition to Met_{22} and Met_{27} (Figure 1), which can also coordinate copper ions prior their transport *via* COPT6.

The role of COPT6 in copper homeostasis *in planta* was tested by using an *A. thaliana* knockdown allele, *copt6-1,* and two transgenic lines ectopically expressing *COPT6*, *$35S_{pro}$-HA-COPT6-1* and *$35S_{pro}$-HA-COPT6-2*. Knocking down or overexpressing COPT6 had opposite effects on plant growth during copper limitation or excess: *copt6-1* plants were more sensitive to copper limitation while more tolerant to copper toxicity (Figure 9C, D). Furthermore, as expected, *$35S_{pro}$-HA-COPT6-1* and *$35S_{pro}$-HA-COPT6-2* plants were more tolerant to copper limitation but more sensitive to copper excess (Figure 9C, D). Given that our studies in yeast show that COPT6 is an uptake transporter, it is likely that the observed responses of the mutant and transgenic plants to copper availability result from impaired copper uptake and/or partitioning in the mutant and increased copper transport and/or tissue partitioning in transgenic lines.

The transcript abundance of *COPT6* is significantly higher in leaves than in roots (Figure

11A), suggesting its primary role in maintaining copper homeostasis of above-ground tissues. We also found that the transcript abundance of *COPT6* decreases in leaves but not in roots when copper concentration in external medium reaches its toxic limits (Figure 11B), suggesting that *COPT6* expression must be tightly controlled in leaves to protect photosynthetic apparatus from copper overload. We hypothesize that *COPT6* expression in roots is not altered by high copper because it is already relatively low under control conditions, and thus COPT6 contribution to copper uptake would be minimal under copper replete or excess conditions. In contrast, because of the low expression in roots under control conditions, *COPT6* expression is upregulated under copper limiting conditions to provide an adequate copper supply to plants (Figure 11A,B).

The histochemical analysis of the spatial distribution of the *COPT6* promoter activity in transgenic plants expressing the $COPT6_{pro}$-*GUS* construct shows that although *COPT6* is expressed in different cell types, its expression is concentrated in the vasculature (Figure 12), where the majority of plant copper is stored to ensure rapid remobilization in response to increased copper demand (Garcia-Molina et al., 2011). Therefore, it is tempting to speculate that COPT6 is involved in copper partitioning between different plant organs for its delivery to copper-requiring functions. Since *COPT6* is also expressed in different cell types of lateral roots except for root tips (Figure 12), its function in copper uptake from external solution cannot be excluded. In addition, the finding that *COPT6* transcript abundance increases in roots and leaves of *A. thaliana* under copper deficient conditions (Figure 8B), further support the suggestion that COPT6-mediated copper influx might be important when copper availability is limited.

Similar to *S. cerevisiae* Ctr1p, COPT6 interacts with itself on the plasma membrane (Figure 13). However, unlike Ctr1p, that does not form heterocomplexes with its closest homolog, a plasma membrane transporter Ctr3p (31), COPT6 interacts with COPT1 (Figure 13B). However,

since COPT6 functions in copper uptake without COPT1 in *S. cerevisiae* (Figure 3 and 4), the biological significance of COPT6-COPT1 interactions is yet to be determined. It is possible that COPT1-COPT6 interactions are important for copper uptake in specific *A. thaliana* cell types, *e.g.* in trichomes and/or pollen that co-express *COPT6* and *COPT1* (Figure 12 and Sancenón et al., 2004).

The transcriptional response of some of the CTR/COPT family members is under tight transcriptional control exerted by Mac1 or SPL7 transcriptional factors in *S. cerevisiae* and *A. thaliana* respectively (Yamasaki et al., 2009, Yonokovich et al., 2002, Jungmann et al., 1993). Microarray analysis revealed that *A. thaliana COPT1* and *COPT2* are among the SPL7 targets (Yamasaki et al., 2009). Since COPT6 was not represented on the Agilent Arabidopsis 3 Oligo Microarray used in (Yamasaki et al., 2009), but is subjected to transcriptional regulation by copper status (Figure 11B), we tested whether *COPT6* is among the SPL7 targets as well. Our studies using the *spl7-1* mutant of *A. thaliana* revealed that the transcript abundance of *COPT6* increases independently of SPL7 in roots of *A. thaliana* (Figure 11C), suggesting involvement of other transcription factors in this organ. In contrast, the *COPT6* transcriptional response to copper limitations in the shoot absolutely depends on SPL7 (Figure 11C). Although the transcriptional regulation region of *COPT6* contains two CuRE elements essential for SPL7 binding, whether COPT6 is a direct SPL7 target is not known. It is noteworthy that SPL7 is expressed mainly in roots where it suggested to sense copper availability (Yamasaki et al., 2009). Nevertheless, many SPL7 targets (Yamasaki et al., 2009), including *COPT6,* are induced by copper deficiency in shoots, suggesting a complex mechanism of SPL7-dependent regulation of the transcriptional copper deficiency response.

COPT6 has been annotated as a vacuolar membrane protein based on studies of the *A.*

thaliana vacuole proteome (Carter et al., 2004). However, our data showing that 1) COPT6-EGFP, heterologously expressed in *S. cerevisiae* and transiently expressed in *A. thaliana* protoplasts is associated with the plasma membrane; 2) COPT6 interacts with the plasma membrane-localized COPT1 but not with vacuolar-membrane localized COPT5 in BiFC assays; 3) heterologously expressed COPT6 complements the *S. cerevisiae* copper uptake mutant, and 4) transgenic plants that overexpress COPT6 are more sensitive to copper excess, are consistent with the suggestion that COPT6 localizes to the plasma membrane and is involved in copper uptake rather than in vacuolar sequestration. To reconcile our experimental data with results of (Carter et al., 2004) we suggest that the detection of COPT6 in the vacuolar proteome may reflect a vacuolar-mediated degradation pathway of COPT6 as was shown for its *S. cerevisiae* counterpart Ctr1p (Liu et al., 2007)

To conclude, COPT6 is a plasma membrane copper uptake transporter and is a novel SPL7 target that is essential for maintaining plant growth during extreme copper conditions acting, possibly, by controlling copper uptake and partitioning to copper requiring functions.

Materials and Methods

Plant Materials and Growth Conditions

All plant lines used in the study were in the *A. thaliana* Columbia (Col-0) background. Seeds of the *copt6-1* (SALK 083438) T-DNA insertion allele were obtained from the *Arabidopsis* Biological Resource Center (Alonso et al., 2003). Seeds of the *spl7-1* mutant were obtained from Dr. Shikanai (Kyoto University, Japan) and this mutant is described in (Yamasaki et al., 2009). Before growing different *A. thaliana* lines on solid medium, seeds were surface-sterilized with 75% (v/v) ethanol before soaking in a solution containing 1.8% bleach (made-up by diluting a

household Clorox) and 0.1% Tween-20. Sterilized seeds were rinsed with sterile water and sowed on half-strength Murashige and Skoog (1/2 MS) medium (pH 5.7) with 0.1% sucrose (w/v) and 0.7% agar (w/v, Sigma A1296) supplemented with or without 45 μM $CuCl_2$ or indicated concentrations of the specific copper chelator, bathocuproine disulfonate (BCS). After stratification at 4°C for 2 days in darkness, seeds were germinated and seedlings grown vertically for 10-days (at 22°C; 12-h light/12-h dark photoperiod at photosynthetic photon flux density of 120 μmol $m^{-2}s^{-1}$) before subsequent analyses.

RNA extraction and cDNA synthesis

Root and shoot tissues from 10-day-old seedlings grown under indicated conditions were separated and flash-frozen in liquid nitrogen before homogenization in liquid nitrogen using a mortar and a pestle. Total RNA was isolated using TRIZOL reagent (Invitrogen), according to the manufacturer's instructions. Genomic DNA in total RNA samples was digested with DNAse *I* (Roche) prior to first strand cDNA synthesis using QPCR cDNA Synthesis kit (BioRad).

Plasmid construction

The following vectors, *YES3* (Lu et al., 1997) and *SAT6-N1-EGFP* (Tzfira et al., 2005) were modified into Gateway destination vectors with the Gateway® Vector Conversion System (Invitrogen) and designated accordingly as *YES3-Gate*, and *SAT6-N1-EGFP-Gate*.

To generate the *YES3-EGFP* vector, the EGFP DNA sequence was amplified from the *SAT6-N1-EGFP* vector using primer pairs that generated *Sma*I restriction enzyme recognition sites at 5′ and 3′ ends of the PCR product (Table 1). The PCR product was then subcloned into *Sma*I/*Sma*I restriction enzyme sites of the *YES3* vector. The resulting *YES3-EGFP* was converted into *YES3-*

EGFP-Gate with the Gateway® Vector Conversion System (Invitrogen).

The *COPT6* cDNA with or without the stop codon was amplified by RT-PCR from RNA isolated from *A. thaliana* leaves. The primers (Table 1) added *attB* sites on resulting PCR products, which were then introduced into corresponding vectors by recombination cloning (Invitrogen).

Table 1. **List of oligos.** Nucleotide sequence marked in bold indicate *attB* sites. Asterisk (*) indicates primers with a stop codon. Underlined nucleotides indicate a Met to Ala point mutation.

Name	Sequence	Purpose
LBb1.3	attttgccgatttcggaac	Genotyping
LP*copt6-1*	agggtttctcgtcatcagagg	Genotyping
RP*copt6-1*	ttcgttttgtccttgttttcg	Genotyping
F*COPT6*$_{pro}$	**ggggacaagtttgtacaaaaaagcaggct**tcacctttttttctttcagtaagactaatcggag	GUS fusion
R*COPT6*$_{pro}$	**ggggaccactttgtacaagaaagctgggt**cgataagtttctgaaatttttgtttgggac	GUS fusion
F*COPT6*-CDS	**ggggacaagtttgtacaaaaaagcaggct**tcaccatggatcatggtaacatgccacc	Cloning primer
R*COPT6*-CDS*	**ggggaccactttgtacaagaaagctgggt**ctcatagttgttcgaagggtttctcg	Cloning for YES3-Gate
R*COPT6*-CDS	**ggggaccactttgtacaagaaagctgggt**ctagttgttcgaagggtttctcgtc	Cloning for YES3-GFP-Gate, SAT6-N1, UC-SPYNE, UC-SPYCE, MetYCgate, NXgate33-3HA and XNgate21-3HA
F*CTR1*-sub	g**ggggacaagtttgtacaaaaaagcaggcttcacc**atggaaggtatgaatatgggtagc	Subcloning *CTR1* inserts from 416TEF into YES3-Gate
R*CTR1*-sub	**ggggaccactttgtacaagaaagctgggtc**ttagttatgagtgaatttttcggccgg	
F*COPT1*	**ggggacaagtttgtacaaaaaagcaggct**tcaccgccaagaacaaagaaaccatggatca	Cloning for UC-SPYNE
R*COPT1*	**ggggaccactttgtacaagaaagctgggtc**acaagcacaacctgaggga	
F*COPT5*	**ggggacaagtttgtacaaaaaagcaggct**tcaccatgatgcacatgaccttctactggg	Cloning for UC-SPYNE
R*COPT5*	**ggggaccactttgtacaagaaagctgggtc**agcacatggacatggatcatccg	
F*COPT6*-M27-deletion	**ggggacaagtttgtacaaaaaagcaggct**tcaccatgactttcttctggggaaagaac	Deletion primer
F*COPT6*-M22A	ggtaaatcataccaattccaacgctatcatgatgcatatgactttc	Point mutation primer
R*COPT6*-M22A	gaaagtcatatgcatcatgatagcgttggaattggtatgatttacc	Point mutation primer
F*COPT6*-M27A	ccaacatgatcatgatgcatgctactttcttctggggaaagaac	Point mutation primer
R*COPT6*-M27A	gttctttccccagaagaaagtagcatgcatcatgatcatgttgg	Point mutation primer
F*COPT6*-M102A	caggccttgcttatctcgtggctctcgccgttatgtcctttaac	Point mutation primer
R*COPT6*-M102A	gttaaaggacataacggcgagagccacgagataagcaaggcctg	Point mutation primer
F*COPT6*-M106A	cgtgatgctcgccgttgcttcctttaacggtggag	Point mutation primer
R*COPT6*-M106A	ctccaccgttaaaggaagcaacggcgagcatcacg	Point mutation primer
F*COPT6*	atcgtcgtcttcctccttgctgtt	qRT-PCR
R*COPT6*	agcaaggcctgtcttgagtgtgta	qRT-PCR
F*SPL7*	gagctggagggctatatccg	qRT-PCR
R*SPL7*	ggaagaggctcgatgactgt	qRT-PCR
F*miR398b/c*	ggatctcgacagggttgatatg	qRT-PCR
R*miR398b/c*	aagagctcagcaggggtgacctg	qRT-PCR
F*FSD1*	acttacagcttcccaagacac	qRT-PCR
R*FSD1*	tgctgtgaatccccttgtg	qRT-PCR
F*CSD1*	ttctggccttaagcctggtc	qRT-PCR
R*CSD1*	cgacatgctggtgatctagg	qRT-PCR
F*CSD2*	catgacacacggagctccag	qRT-PCR
R*CSD2*	gagctggagggctatatccg	qRT-PCR
F*ACTIN2*	gacctttaactctcccgcta	qRT-PCR
R*ACTIN2*	ggaagagagaaaccctcgta	qRT-PCR

Site-directed mutagenesis of *COPT6* was performed directly on a *YES3-Gate-COPT6* vector with QuickChange® II Site-Directed Mutagenesis Kit (Stratagene). The mutagenic oligonucleotides (Table 1) were designed to substitute conserved methionines to alanine codons in the Mets motif of the predicted extracellular domain or TM2 of COPT6, or to delete 81 bp corresponding to 27 amino acids of the extracellular amino-terminal domain (Figure 1). Mutagenesis was confirmed by sequencing the cDNA regions encompassing each mutation.

The cDNA encoding the full-length CTR1p and CTR1p with M127L and M260A point mutations were amplified by PCR from the *416TEF* vector (courtesy of Dr. Dennis Thiele, Duke University) using primer pairs (Table 1). All inserts were introduced into the *DONR222* entry vector before recombination with the *YES3-Gate* destination vector mentioned above.

Functional complementation of the *S. cerevisiae* copper uptake deficient *ctr1ctr2ctr3* mutant strain

S. cerevisiae SEY6210 (*MATa ura3-52 leu2-3,-112 his3Δ200 trp1Δ901 lys2-801 suc2Δ9)* wild-type and *ctr1ctr2ctr3* triple mutant (*MATa ura3-52 his3Δ200 trp1-901 ctr1::ura3::Knr ctr2::HIS3 ctr3::TRP1)* strains that were used for functional complementation assays were the generous gift of Dr. Dennis Thiele (Duke University). Yeast cells were transformed with the *YES3-Gate-COPT6* vector or *YES3-Gate* lacking the cDNA insert using the Frozen-EZ yeast Transformation II Kit (Zymo Research). Transformants were selected for uracil prototrophy on YNB medium containing 0.67% (w/v) Yeast Nitrogen Base without amino acids (Difco), 0.077% (w/v) CSM-Ura, 0.05% (w/v) NaCl, 2% glucose, 2% (w/v) agar.

Respiration competence was evaluated by testing the ability of transformants to grow on the

non-fermentable carbon sources, glycerol and ethanol (Dancis et al., 1994a, Puig et al., 2002). Transformants were grown in liquid YNB-Ura to an OD_{600nm} = 1.0-1.1, serially-10-fold diluted and spotted onto YPEG media containing 1% (w/v) yeast extract, 2% (w/v) bacto-peptone, 3% (v/v) glycerol 2% (v/v) ethanol and 2% (w/v) agar and the indicated concentrations of $CuSO_4$. Plates were incubated for 3 days at 30°C.

Quantitative real-Time (qRT)-PCR and data analysis

Prior to qRT-PCR analysis, primer and cDNA concentrations were optimized to reach the target and normalizing genes amplification efficiency of 100 ± 10%. One microliter of 15-fold diluted cDNA was used as a template for qRT-PCR in a total volume of 10 µL containing 500 nM of each PCR primer, 50 mM KCl, 20 mM Tris-HCl, pH 8.4, 0.2 mM each dNTP and 1.25 units of iTaq DNA polymerase in iQ SYBR Green Supermix (BioRad). PCR was carried out using CFX96 Real-Time PCR system (BioRad). The thermal cycling parameters were as follows: denaturation at 95°C for 3 min, followed by 39 cycles of 95°C for 10 s, 55°C for 30 s. Amplicon dissociation curves, *i.e.* melting curves, were recorded after cycle 39 by heating from 60°C to 95°C with 0.5°C increments and an average ramp speed of 3.3°C s^{-1}. Real-time PCR experiments were conducted using three independent biological samples, each consisting of three technical replicates (Udvardi et al., 2008), unless indicated otherwise. Data were normalized to the expression of *ACTIN 2*. The fold difference ($2^{-\Delta\Delta Ct}$) was calculated using the CFX Manager Software, version 1.5 (BioRad). Statistical analysis was performed using the Relative Expression Software Tool (REST, Qiagen [Pfaffl et al., 2002]).

Subcellular localization and fluorescent microscopy

For studies of subcellular localization in *S. cerevisiae*, COPT6 was fused at C-terminus with the EGFP in the *YES3-EGFP-Gate* vector and expressed under the control of the constitutive phosphoglycerate kinase (*PGK*) gene promoter. The resulting COPT6-EGFP construct and the empty *YES3-EGFP-Gate* vector were transformed into *S. cerevisiae ctr1ctr2ctr3* triple mutants using the Frozen-EZ yeast Transformation II Kit (Zymo Research). Plasma membranes were stained with FM 4-64 dye, an endocytic marker that is also used to visualize the plasma membrane after short-term staining at 0^{o}C (Vida and Emr 1995, Ueda et al., 2001, Bolte et al., 2004). Three milliliters of overnight culture were pelleted by centrifugation and concentrated cells were resuspended in 1 mL of ice-cold liquid YPD media containing 2% peptone (w/v), 1% yeast extract (w/v) and 2% glucose (v/v), pH 6.0. The sample was cooled on ice for 5-10 min before adding 3 µL of DMSO and FM 4-64 at a final concentration of 7.5 µM. The sample was incubated at 4°C before dispensing on pre-cooled slides topped with 1% agarose for visualization. Epifluorescence images were collected using an Axio Imager M2 microscope (Zeiss).

For studies of the subcellular localization of COPT6 in *Arabidopsis* protoplasts, the full-length *COPT6* cDNA without the stop codon was fused at the C-terminus with the modified green fluorescent protein (EGFP) using the *SAT6-N1-EGFP-Gate* vector and expressed under the control of the cauliflower mosaic virus (CaMV) *35S* promoter. The resulting $35S_{pro}$*-COPT6-EGFP* construct or *SAT6-N1-Gate*, lacking the cDNA insert were transfected into *A. thaliana* protoplasts isolated from leaf mesophyll tissue using previously established procedures (Zhai et al., 2009a, Zhai et al., 2009b, Jung et al., 2011). Plasma membranes were stained with 50 μM FM 4-64 as described (Ueda et al., 2011). EGFP- and FM 4-64- mediated fluorescence, and

chlorophyll autofluorescence were visualized using FITC (for EGFP) or rhodamine (FM 4-64 and chlorophyll) filter sets of the Axio Imager M2 microscope equipped with the motorized Z-drive (Zeiss). Z-stack (1.3 μm-thick) images were collected with the high-resolution AxioCam MR Camera and then 3D deconvoluted using an inverse filter algorithm of the Zeiss AxioVision 4.8 software. Images were processed using the Adobe Photoshop software package, version 12.0.

Bimolecular fluorescence complementation (BiFC) assays and confocal microscopy

The vectors used in the BiFC assay, *UC-SPYNE* and *UC-SPYCE*, contained the N- or C-terminal fragments of yellow fluorescent protein, YFP^N or YFP^C, respectively, allowing expression of fused proteins under the control of the *35S* promoter (Walter et al., 2004). To generate COPT6-YFP^N and COPT6-YFP^C fusion constructs, the C-terminus of the *COPT6* coding sequence was fused with YFP^N or YFP^C in the *UC-SPYNE* or *UC-SPYCE* vectors, respectively. The coding regions of *COPT1* and *COPT5* were amplified without stop codons and used to generate COPT1-YFP^N and COPT5-YFP^N. The resulting constructs and *UC-SPYNE* and *UC-SPYCE* vectors lacking cDNA inserts were co-transfected in the indicated combinations into *A. thaliana* leaf protoplasts as described (Zhai et al., 2009a, Zhai et al., 2009b, Jung et al., 2011). Protoplasts were analyzed using a Zeiss 710 confocal microscope. The YFP fluorophore was excited with 514 nm laser and the emission was recorded in the range of 524-595 nm and 650-715 nm, for YFP and chlorophyll, respectively. To allow comparison of the relative brightness between different BiFC experiments, the zoom, pinhole, detector gain, amplifier offset, frame size, scan speed, scan average, and laser power were kept consistent between samples. Images were processed using the Zen 2009 LE software of the Zeiss 710 confocal microscope and the Adobe Photoshop software package, version 12.0.

Split-ubiquitin membrane yeast two-hybrid system (MYTH)

Vectors, *S. cerevisiae* strains THY.AP4 (*MATa leu2-3,112 ura3-52 trp1-289 lexA::HIS3 lexA::ADE2 lexA::lacZ)* and THY.AP5 (*MATα URA3 leu2-3,112 trp1-289 his3-Δ1 ade2Δ::loxP)* for MYTH were obtained from the Frommer lab (Stanford University) depository at *Arabidopsis* Biological Resource Center (ABRC) http://www.arabidopsis.org/abrc/index.jsp. The full-length *COPT6* cDNA was introduced into MetYCgate and pXNgate21-3HA vectors by *in vivo* cloning in yeast as described (Kittanakom et al., 2009, Obrdlik et al., 2004) to generate bait COPT6-CubPLV and prey COPT6-NubG constructs in THY.AP4 and THY.AP5 strains, respectively. In both cases, C- and N-terminal fragments of ubiquitin were placed at the C-terminus of COPT6. Protein interactions were selected in diploid cells after 2 days of growth on SC medium lacking adenine and histidine. Interactions were verified using *β*-galactosidase assays, as detailed in (Kittanakom et al., 2009, Kim et al., 2010).

Histochemical analysis

To examine the pattern of *COPT6* expression *in planta*, a 1083 bp fragment of the genomic sequence upstream of the *COPT6* start codon was amplified by PCR using primer pairs listed in Table 1. The resulting PCR product was cloned by recombination into the *GUS1-Gate* vector upstream of *uidA*, encoding the *β*-glucuronidase (*GUS*) reporter gene. The $COPT6_{pro}$-*GUS* construct was transformed into wild-type *A. thaliana* (Clough and Bent 1998). Histochemical staining was performed with 1 mM X-Gluc (5-bromo-4-chloro-3-indolyl-β-D-glucuronide) as described (Jefferson et al., 1987) with 20 min (for seedlings) or 3-hour (for mature plants) incubation period at 37°C. Staining patterns were analyzed using the Zeiss 2000

stereomicroscope. Images were collected using a Canon PowerShot S3 IS digital camera and a CS3IS camera adapter. Images were processed using the Adobe Photoshop software package, version 12.0.

Generation of transgenic lines

The full-length *COPT6* cDNA was introduced by recombination cloning into *EarleyGate201* destination vector (Earley et al., 2006) where *COPT6* was fused at the N-termini to the human influenza hemagglutinin (HA) epitope tag under the control of the *35S* promoter. The resulting *$35S_{pro}$-COPT6-HA* construct or the *EarleyGate201* vector lacking the cDNA insert were transformed into wild-type *A. thaliana via* floral dip method (Clough and Bent 1998). Based on results of qRT-PCR analyses of T2 transgenic lines, two homozygous lines overexpressing *COPT6-HA, $35S_{pro}$-COPT6-1-HA* and *$35S_{pro}$-COPT6-2-HA,* and one line expressing the empty vector, *$35S_{pro}$*, were selected for subsequent experiments.

SDS-PAGE and western blot analysis

Two grams of leaf tissue were taken from 35-day-old transgenic plants grown on soil and ground in liquid nitrogen using a mortar and pestle before the addition of extraction buffer containing 50 mM Tris-HCl, pH 7.5, 2 mM EDTA, 150 mM NaCl, 10 % glycerol, 2% polyvinylpolypyrrolidone, 0.25% Triton-X 100, 5 mM DTT, 1 mM PMSF, 0.2 mM AEBSF, 1 μg/ml leupeptin, 1 μg/ml aprotinin, and 1 μg/ml pepstatin. Total protein extracts were cleared from cellular debris by centrifugation at 4,000 × *g* for 10 min at 4 °C. The supernatant was centrifuged at 100,000 × *g* for 1 hour at 4 °C and pellet containing total membrane proteins was reconstituted in extraction buffer and stored at -80^{o}C. Aliquots of proteins (20 μg/lane) were

subjected to SDS-PAGE on 12% (w/v) gels and electrotransferred to nitrocellulose filters in Towbin buffer containing 0.05% SDS (Towbin et al., 1979). For detection of the influenza hemagglutinin-HA epitope nitrocellulose filters were probed with a primary polyclonal anti-HA antibody (1:2,000 dilution, Sigma) and a secondary HR-conjugated IgG antibody (1:10,000 dilution, GE Healthcare). In both cases, immunoreactive bands were visualized with ECL using the LumiGLO system (KPL).

Analyses of copper content

S. cerevisiae wild-type SEY6210 and *ctr1ctr2ctr3* mutant cells transformed with *YES3-Gate* vector, and the *ctr1ctr2ctr3* mutant transformed with *YES3-Gate-COPT6* were grown overnight at 30^{o}C to an OD_{600nm}=1.2 in liquid YNB medium supplemented with CSM-URA and 2% glucose. Hundred microliter aliquots of the overnight culture were diluted into 20 ml of the same medium supplemented with indicated concentrations of $CuSO_4$, and grown for 18h at 30^{o}C. Cells were then harvested by centrifugation, washed with deionized water before copper in cell walls was desorbed in a buffer containing 1 mM EDTA and 100 μM BCS, pH8.0. Cells were then washed two more times with deionized water, dried, digested by heating with a combination of purified concentrated nitric and perchloric acids and finally dissolved in 10 ml of 5% nitric acid. Copper content in processed yeast and plant samples was analyzed by inductively coupled plasma mass spectroscopy (ICP-MS, Agilent 7500) (Lahner et al., 2003). Copper at mass 63 was measured using helium as the collision gas at 5.0 ml per minute to reduce potential polyatomic interferences from sodium-argon ions, which also has a mass at 63.

For analyses of copper content in *A. thaliana*, 10-day-old seedlings of different plant lines grown as described above were transferred to *Arabidopsis* hydroponic solution described in

(Arteca and Arteca 2000) and grown at 22^{o}C and 12-h light/12-h dark photoperiod at photosynthetic photon flux density of 120 μmol $m^{-2}s^{-1}$. Roots and shoots of 30-day-old plants were harvested and roots were desorbed by washing with 10 mM EDTA followed by washing in a solution of 0.3 mM BCS and 5.7 mM sodium dithionite before rinsing with deionized water (Cailliatte et al., 2010). Shoots were rinsed with deionized water. Root and shoot tissues were dried, processed and analyzed for copper content as described above.

REFERENCES

Abdel-Ghany, S. E. and Pilon, M. (2008) MicroRNA-mediated systemic down-regulation of copper protein expression in response to low copper availability in *Arabidopsis*. *J Biol Chem*, **283**, 15932-15945.

Abdel-Ghany, S. E., Muller-Moule, P., Niyogi, K. K., Pilon, M. and Shikanai, T. (2005) Two P-type ATPases are required for copper delivery in *Arabidopsis thaliana* chloroplasts. *Plant Cell*, **17**, 1233-1251.

Alonso, J. M., Stepanova, A. N., Leisse, T. J., Kim, C. J., Chen, H., Shinn, P., Stevenson, D. K., Zimmerman, J., Barajas, P., Cheuk, R., Gadrinab, C., Heller, C., Jeske, A., Koesema, E., Meyers, C. C., Parker, H., Prednis, L., Ansari, Y., Choy, N., Deen, H., Geralt, M., Hazari, N., Hom, E., Karnes, M., Mulholland, C., Ndubaku, R., Schmidt, I., Guzman, P., Aguilar-Henonin, L., Schmid, M., Weigel, D., Carter, D. E., Marchand, T., Risseeuw, E., Brogden, D., Zeko, A., Crosby, W. L., Berry, C. C. and Ecker, J. R. (2003) Genome-wide insertional mutagenesis of *Arabidopsis thaliana*. *Science*, **301**, 653-657.

Andrés-Colás, N., Perea-García, A., Puig, S. and Peñarrubia, L. (2010) Deregulated copper transport affects *Arabidopsis* development especially in the absence of environmental cycles. *Plant Physiol*, **153**, 170-184.

Arteca, R. N. and Arteca, J. M. (2000) A novel method for growing *Arabidopsis thaliana* plants hydroponically. *Physiol Plant*, **108**, 188-193.

Bækgaard, L., Mikkelsen, M. D., Sørensen, D. M., Hegelund, J. N., Persson, D. P., Mills, R. F., Yang, Z., Husted, S., Andersen, J. P., Buch-Pedersen, M. J., Schjoerring, J. K., Williams, L. E. and Palmgren, M. G. (2010) A combined zinc/cadmium sensor and zinc/cadmium export regulator in a heavy metal pump. *J Biol Chem*, **285**, 31243-31252.

Bellemare, D. R., Shaner, L., Morano, K. A., Beaudoin, J., Langlois, R. and Labbe, S. (2002) Ctr6, a vacuolar membrane copper transporter in *Schizosaccharomyces pombe*. *J Biol Chem*, **277**, 46676-46686.

Bolte, S., Talbot, C., Boutte, Y., Catrice, O., Read, N. D. and Satiat-Jeunemaitre, B. (2004) FM-dyes as experimental probes for dissecting vesicle trafficking in living plant cells. *J Microsc*, **214**, 159-173.

Bracha-Drori, K., Shichrur, K., Katz, A., Oliva, M., Angelovici, R., Yalovsky, S. and Ohad, N. (2004) Detection of protein-protein interactions in plants using bimolecular fluorescence complementation. *Plant J*, **40**, 419-427.

Burkhead, J., Reynolds, K., Abdel-Ghany, S., Cohu, C. and Pilon, M. (2009) Copper homeostasis. *New Phytol*, **182**, 799 – 816.

Cailliatte, R., Schikora, A., Briat, J.-F., Mari, S. and Curie, C. (2010) High-affinity manganese uptake by the metal transporter NRAMP1 is essential for *Arabidopsis* growth in low manganese conditions. *Plant Cell*, **22**, 904-917.

Carter, C., Pan, S., Zouhar, J., Avila, E. L., Girke, T. and Raikhel, N. V. (2004) The vegetative vacuole proteome of *Arabidopsis thaliana* reveals predicted and unexpected proteins. *Plant Cell*, **16**, 3285-3303.

Cohu, C. M. and Pilon, M. (2007) Regulation of superoxide dismutase expression by copper availability. *Physiol Plant*, **129**, 747–755.

Clough, S. J. and Bent, A. F. (1998) Floral dip: a simplified method for *Agrobacterium*-mediated transformation of *Arabidopsis thaliana*. *Plant J*, **16**, 735-743.

Dancis, A., Haile, D., Yuan, D. S. and Klausner, R. D. (1994) Biochemical characterization,

regulation by copper, and physiological role in copper uptake. *J Biol Chem*, **269**, 25660-25667.

Dancis, A., Yuan, D., Haile, D., Askwith, C., Eide, D., Moehle, C., Kaplan, J. and Klausner, R. (1994) Molecular characterization of a copper transport protein in *S. cerevisiae*: an unexpected role for copper in iron transport. *Cell*, **76**, 393 – 402.

De Feo, C. J., Aller, S. G., Siluvai, G. S., Blackburn, N. J. and Unger, V. M. (2009) Three-dimensional structure of the human copper transporter hCTR1. *Proc Natl Acad Sci U S A*, **106**, 4237-4242.

De Feo, C., Aller, S. and Unger, V. (2007) A structural perspective on copper uptake in eukaryotes. *Biometals*, **20**, 705-716.

Earley, K. W., Haag, J. R., Pontes, O., Opper, K., Juehne, T., Song, K. and Pikaard, C. S. (2006) Gateway-compatible vectors for plant functional genomics and proteomics. *Plant J*, **45**, 616-629.

Gaetke, L. M. and Chow, C. K. (2003) Copper toxicity, oxidative stress, and antioxidant nutrients. *Toxicology*, **189**, 147-163.

Garcia-Molina, A., Andrés-Colás, N., Perea-García, A., del Valle-Tascón, S., Peñarrubia, L. and Puig, S. (2011) The intracellular *Arabidopsis* COPT5 transport protein is required for photosynthetic electron transport under severe copper deficiency. *Plant J*, **65**, 848-860.

Gavnholt, B. and Larsen, K. (2002) Molecular biology of plant laccases in relation to lignin formation. *Physiol Plant*, **116**, 273-280.

Glerum, D. M., Shtanko, A. and Tzagoloff, A. (1996) Characterization of *COX17*, a yeast gene involved in copper metabolism and assembly of cytochrome oxidase. *J Biol Chem*, **271**, 14504-14509.

Jahn, T. P., Schulz, A., Taipalensuu, J. and Palmgren, M. G. (2002) Post-translational modification of plant plasma membrane H(+)-ATPase as a requirement for functional complementation of a yeast transport mutant. *J Biol Chem*, **277**, 6353-6358.

Jefferson, R. A., Kavanagh, T. A. and Bevan, M. W. (1987) GUS fusions: beta-glucuronidase as a sensitive and versatile gene fusion marker in higher plants. *EMBO J*, **6**, 3901.

Jung, H. I., Zhai, Z. and Vatamaniuk, O. K. (2011) Direct transfer of synthetic double-stranded RNA into protoplasts of *Arabidopsis thaliana*. *Methods Mol Biol*, **744**, 109-127.

Jungmann, J., Reins, H. A., Lee, J., Romeo, A., Hassett, R., Kosman, D. and Jentsch, S. (1993) MAC1, a nuclear regulatory protein related to Cu-dependent transcription factors is involved in Cu/Fe utilization and stress resistance in yeast. *EMBO J*, **12**, 5051-5056.

Kampfenkel, K., Kushnir, S., Babiychuk, E., Inze, D. and Van Montagu, M. (1995) Molecular characterization of a putative *Arabidopsis thaliana* copper transporter and its yeast homologue. *J Biol Chem*, **270**, 28479-28486.

Kim, S., Selote, D. S. and Vatamaniuk, O. K. (2010) The N-terminal extension domain of the *C. elegans* half-molecule ABC transporter, HMT-1, is required for protein-protein interactions and function. *PLoS One*, **5**, e12938.

Kittanakom, S., Chuk, M., Wong, V., Snyder, J., Edmonds, D., Lydakis, A., Zhang, Z., Auerbach, D. and Stagljar, I. (2009) Analysis of membrane protein complexes using the split-ubiquitin membrane yeast two-hybrid (MYTH) system. *Methods Mol Biol*, **548**, 247-271.

Klaumann, S., Nickolaus, S. D., Fürst, S. H., Starck, S., Schneider, S., Ekkehard Neuhaus, H. and Trentmann, O. (2011) The tonoplast copper transporter COPT5 acts as an exporter and is required for interorgan allocation of copper in *Arabidopsis thaliana*. *New Phytol*, **192**, 393-

404.
Kliebenstein, D. J., Monde, R.-A. and Last, R. L. (1998) Superoxide dismutase in *Arabidopsis*: an eclectic enzyme family with disparate regulation and protein localization. *Plant Physiol*, **118**, 637-650.
Lahner, B., Gong, J., Mahmoudian, M., Smith, E. L., Abid, K. B., Rogers, E. E., Guerinot, M. L., Harper, J. F., Ward, J. M., McIntyre, L., Schroeder, J. I. and Salt, D. E. (2003) Genomic scale profiling of nutrient and trace elements in *Arabidopsis thaliana*. *Nat Biotechnol*, **21**, 1215-1221.
Lee, J., Peña, M. M., Nose, Y., and Thiele, D. J. (2002). Biochemical characterization of the human copper transporter Ctr1. *J Biol Chem*, **277**, 4380-4387.
Lequeux, H., Hermans, C., Lutts, S., and Verbruggen, N. (2010). Response to copper excess in *Arabidopsis thaliana*: Impact on the root system architecture, hormone distribution, lignin accumulation and mineral profile. *Plant Physiol Biochem*, **48**, 673-682.
Liu, J., Sitaram, A. and Burd, C. G. (2007) Regulation of copper-dependent endocytosis and vacuolar degradation of the yeast copper transporter, Ctr1p, by the Rsp5 ubiquitin ligase. *Traffic*, **8**, 1375-1384.
Lu, Y. P., Li, Z. S. and Rea, P. A. (1997) AtMRP1 gene of *Arabidopsis* encodes a glutathione S-conjugate pump: isolation and functional definition of a plant ATP-binding cassette transporter gene. *Proc Natl Acad Sci U S A*, **94**, 8243-8248.
Merchant, S. S. (2010) The elements of plant micronutrients. *Plant Physiol*, **154**, 512-515.
Murphy, A. and Taiz, L. (1995) A new vertical mesh transfer technique for metal-tolerance studies in *Arabidopsis* (ecotypic variation and copper-sensitive mutants). *Plant Physiol*, **108**, 29-38.
Nelson, B. K., Cai, X. and Nebenfuhr, A. (2007) A multicolored set of in vivo organelle markers for co-localization studies in *Arabidopsis* and other plants. *Plant J*, **51**, 1126-1136.
Obrdlik, P., El-Bakkoury, M., Hamacher, T., Cappellaro, C., Vilarino, C., Fleischer, C., Ellerbrok, H., Kamuzinzi, R., Ledent, V., Blaudez, D., Sanders, D., Revuelta, J. L., Boles, E., Andre, B. and Frommer, W. B. (2004) K+ channel interactions detected by a genetic system optimized for systematic studies of membrane protein interactions. *Proc Natl Acad Sci U S A*, **101**, 12242-12247.
Ooi, C. E., Rabinovich, E., Dancis, A., Bonifacino, J. S. and Klausner, R. D. (1996) Copper-dependent degradation of the *Saccharomyces cerevisiae* plasma membrane copper transporter Ctr1p in the apparent absence of endocytosis. *EMBO J*, **15**, 3515-3523.
Page, M. D., Kropat, J., Hamel, P. P. and Merchant, S. S. (2009) Two *Chlamydomonas* CTR copper transporters with a novel cys-met motif are localized to the plasma membrane and function in copper assimilation. *Plant Cell*, **21**, 928-943.
Peña, M. M., Puig, S. and Thiele, D. J. (2000) Characterization of the *Saccharomyces cerevisiae* high affinity copper transporter Ctr3. *J Biol Chem*, **275**, 33244-33251.
Peñarrubia, L., Andrés-Colás, N., Moreno, J. and Puig, S. (2010) Regulation of copper transport in *Arabidopsis thaliana*: a biochemical oscillator? *J Biol Inorganic Chem*, **15**, 29 – 36.
Pfaffl, M. W., Horgan, G. W. and Dempfle, L. (2002) Relative expression software tool (REST) for group-wise comparison and statistical analysis of relative expression results in real-time PCR. *Nucleic Acids Res*, **30**, e36.
Prohaska, J. (2000). Long-term functional consequences of malnutrition during brain development: copper. *Nutrition*, **16**, 502-504.
Puig, S., Andrés-Colás, N., Garcia-Molina, A. and Peñarrubia, L. (2007) Copper and iron

homeostasis in *Arabidopsis*: responses to metal deficiencies, interactions and biotechnological applications. *Plant Cell Environ*, **30**, 271-290.

Puig, S., Lee, J., Lau, M. and Thiele, D. (2002) Biochemical and genetic analyses of yeast and human high affinity copper transporters suggest a conserved mechanism for copper uptake. *J Biol Chem*, **277**, 26021 – 26030.

Quinn, J. M. and Merchant, S. (1995) Two copper-responsive elements associated with the *Chlamydomonas* Cyc6 gene function as targets for transcriptional activators. *Plant Cell*, **7**, 623-638.

Ravet, K., Danford, F. L., Dihle, A., Pittarello, M. and Pilon, M. (2011) Spatiotemporal analysis of copper homeostasis in *Populus trichocarpa* reveals an integrated molecular remodeling for a preferential allocation of copper to plastocyanin in the chloroplasts of developing leaves. *Plant Physiol*, **157**, 1300-1312.

Rees, E. M., Lee, J. and Thiele, D. J. (2004) Mobilization of intracellular copper stores by the ctr2 vacuolar copper transporter. *J Biol Chem*, **279**, 54221-54229.

Sancenón, V., Puig, S., Mateu-Andres, I., Dorcey, E., Thiele, D. J. and Peñarrubia, L. (2004) The *Arabidopsis* copper transporter COPT1 functions in root elongation and pollen development. *J Biol Chem*, **279**, 15348-15355.

Sancenón, V., Puig, S., Mira, H., Thiele, D. J. and Peñarrubia, L. (2003) Identification of a copper transporter family in *Arabidopsis thaliana*. *Plant Mol Biol*, **51**, 577-587.

Schutze, K., Harter, K. and Chaban, C. (2009) Bimolecular fluorescence complementation (BiFC) to study protein-protein interactions in living plant cells. *Methods Mol Biol*, **479**, 189-202.

Stadtman, E. R. (1990) Metal ion-catalyzed oxidation of proteins: biochemical mechanism and biological consequences. *Free Radic Biol Med*, **9**, 315-325.

Sunkar, R., Kapoor, A. and Zhu, J.-K. (2006) Posttranscriptional induction of two Cu/Zn superoxide dismutase genes in *Arabidopsis* is mediated by downregulation of miR398 and important for oxidative stress tolerance. *Plant Cell*, **18**, 2051-2065.

Towbin, H., Staehelin, T. and Gordon, J. (1979) Electrophoretic transfer of proteins from polyacrylamide gels to nitrocellulose sheets: procedure and some applications. *Proc Natl Acad Sci U S A*, **76**, 4350-4354.

Tzfira, T., Tian, G. W., Lacroix, B., Vyas, S., Li, J., Leitner-Dagan, Y., Krichevsky, A., Taylor, T., Vainstein, A. and Citovsky, V. (2005) pSAT vectors: a modular series of plasmids for autofluorescent protein tagging and expression of multiple genes in plants. *Plant Mol Biol*, **57**, 503-516.

Udvardi, M. K., Czechowski, T. and Scheible, W.-R. (2008) Eleven golden rules of quantitative RT-PCR. *Plant Cell*, **20**, 1736-1737.

Ueda, T., Yamaguchi, M., Uchimiya, H. and Nakano, A. (2001) Ara6, a plant-unique novel type Rab GTPase, functions in the endocytic pathway of *Arabidopsis thaliana*. *EMBO J*, **20**, 4730-4741.

van den Berghe, P. V. E., Folmer, D. E., Malingre, H. E. M., van Veurden, E., Klomp, A. E. M., van de Sluis, B., Merkx, M., Berger, R. and Klomp, L. W. J. (2007) Human copper transporter 2 is localized in late endosomes and lysosomes and facilitates cellular copper uptake. *Biochem J*, **407**, 49-59.

Vida, T. A. and Emr, S. D. (1995) A new vital stain for visualizing vacuolar membrane dynamics and endocytosis in yeast. *J Cell Biol*, **128**, 779-792.

Walter, M., Chaban, C., Schütze, K., Batistic, O., Weckermann, K., Näke, C., Blazevic, D.,

Grefen, C., Schumacher, K., Oecking, C., Harter, K. and Kudla, J. (2004) Visualization of protein interactions in living plant cells using bimolecular fluorescence complementation. *Plant J*, **40**, 428-438.

Wu, X., Sinani, D., Kim, H. and Lee, J. (2009) Copper transport activity of yeast Ctr1 is down-regulated via its C terminus in response to excess copper. *J Biol Chem*, **284**, 4112-4122.

Xiao, Z. and Wedd, A. G. (2002) A C-terminal domain of the membrane copper pump Ctr1 exchanges copper(I) with the copper chaperone Atx1. *Chem Commun (Camb)*, **21**, 588-589.

Yamasaki, H., Abdel-Ghany, S. E., Cohu, C. M., Kobayashi, Y., Shikanai, T. and Pilon, M. (2007) Regulation of copper homeostasis by micro-RNA in *Arabidopsis*. *J Biol Chem*, **282**, 16369-16378.

Yamasaki, H., Hayashi, M., Fukazawa, M., Kobayashi, Y. and Shikanai, T. (2009) SQUAMOSA Promoter Binding Protein-Like7 is a central regulator for copper homeostasis in *Arabidopsis*. *Plant Cell*, **21**, 347-361.

Yonkovich, J., McKenndry, R., Shi, X. and Zhu, Z. (2002) Copper ion-sensing transcription factor Mac1p post-translationally controls the degradation of its target gene product Ctr1p. *J Biol Chem*, **277**, 23981-23984.

Yuan, M., Chu, Z., Li, X., Xu, C. and Wang, S. (2010) The bacterial pathogen *Xanthomonas oryzae* overcomes rice defenses by regulating host copper redistribution. *Plant Cell*, **22**, 3164-3176.

Yuan, M., Li, X., Xiao, J. and Wang, S. (2011) Molecular and functional analyses of COPT/Ctr-type copper transporter-like gene family in rice. *BMC Plant Biol*, **11**, 69.

Zhai, Z., Jung, H. I. and Vatamaniuk, O. K. (2009a) Isolation of protoplasts from tissues of 14-day-old seedlings of *Arabidopsis thaliana*. *J Vis Exp*, **30**, pii: 1149.

Zhai, Z., Sooksa-nguan, T. and Vatamaniuk, O. K. (2009b) Establishing RNA interference as a reverse-genetic approach for gene functional analysis in protoplasts. *Plant Physiol*, **149**, 642-652.

CHAPTER III

The CTR/COPT-dependent Copper Uptake and SPL7-dependent Copper Deficiency Responses are Required for Basal Cadmium Tolerance in *A. thaliana*

Abstract

Copper (Cu) homeostasis in plants is maintained by at least two mechanisms: 1) the miRNA-dependent reallocation of intracellular Cu among major Cu-enzymes and important energy-related functions; 2) the regulation of the expression of Cu transporters including members of the CTR/COPT family. These events are controlled by the transcription factor SPL7 in *Arabidopsis thaliana*. Cadmium (Cd), on the other hand, is a non-essential and a highly toxic metal that interferes with homeostasis of essential elements by competing for cellular binding sites. Whether Cd affects Cu homeostasis in plants is unknown. We found that Cd stimulates Cu accumulation in roots of *A. thaliana* and increases mRNA expression of three plasma membrane-localized Cu uptake transporters, *COPT1*, *COPT2* and *COPT6.* Further analysis of Cd sensitivity of single and triple *copt1copt2copt6* mutants, and transgenic plants ectopically expressing *COPT6* suggested that Cu uptake is an essential component of Cd resistance in *A. thaliana*. Analysis of the contribution of the SPL7-dependent pathway to Cd-induced expression of *COPT1*, *COPT2* and *COPT6* showed that it occurs, in part, through mimicking the SPL7-dependent transcriptional Cu deficiency response. This response also involves components of the Cu reallocation system, *miRNA398*, *FSD1*, *CSD1* and *CSD2*. Furthermore, seedlings of the *spl7-1* mutant accumulate up to 2-fold less Cu in roots than the wild-type, are hypersensitive to Cd, and are more sensitive to Cd than the triple *copt1copt2copt6* mutant. Together these data show that exposure to excess Cd triggers SPL7-dependent Cu deficiency responses that include Cu

uptake and reallocation that are required for basal Cd tolerance in *A. thaliana*.

Introduction

Copper (Cu) is an essential, redox-active transition metal that serves as a cofactor for enzymes involved in electron transfer reactions and thus, participates in important biological processes including respiration, photosynthesis and scavenging of oxidative stress (Burkhead et al., 2009, Ravet and Pilon 2013) However, Cu also promotes formation of free radicals through Fenton reactions and inactivates essential proteins via thiol-capping, and thus, free Cu ions are toxic to cells in excess (Ravet and Pilon 2013, Stadtman et al., 1990). Cu homeostasis in plants is maintained mainly through the tight regulation of Cu uptake, root-to-shoot partitioning and accumulation in chloroplasts as well as by the redistribution of Cu between major Cu-containing enzymes and important Cu-requiring energy-related functions (Burkhead et al., 2009, Ravet and Pilon 2013). Cu uptake in plants, the green alga *Chlamydomonas reinhardtii,* yeast, *Drosophila* and humans is maintained through the regulation of the expression and stability of Cu transporters of the CTR/COPT family (Dancis et al., 1994, Peña et al., 2004, Andrés-Colás et al., 2010, Page et al., 2009, Sancenón et al., 2003, Kampfenkel et al., 2995, Jung et al., 2012, Puig et al., 2002). The plant CTR/COPT family in *Arabidopsis thaliana* and *Oryza sativa* is represented by six and seven members, respectively (Puig et al., 2002, Peñarrubia et al., 2010). *A. thaliana* COPT1, COPT2 and COPT6 are highly homologous and cluster in one clade on phylogenetic tree (Jung et al., 2012). Heterologous expression of *A. thaliana COPT1*, *COPT2* and *COPT6* also fully suppress the Cu deficiency-associated respiratory defect of the *Saccharomyces cerevisiae ctr1ctr2ctr3* mutant lacking the plasma membrane and the vacuolar membrane-localized Cu transporters, while COPT3 and COPT5 partially complement this phenotype (Sancenón et al.,

2003, Kampfenkel et al., 2995, Jung et al., 2012). Subsequent studies showed that COPT1 and COPT6 are plasma membrane-localized Cu uptake transporters (Andrés-Colás et al., 2010, Sancenón et al., 2003, Jung et al., 2012, Sancenón et al., 2004). COPT1 plays a predominant role in copper acquisition from the soil into root tips (Andrés-Colás et al, 2010, Sancenón et al., 2004), while COPT6 might contribute primarily to Cu distribution in photosynthetic tissues under normal growth conditions and to Cu uptake into roots under Cu deficiency (Jung et al., 2012). In contrast, COPT5 localizes to the tonoplast and pre-vacuolar compartment and functions by remobilizing Cu from these organelles during Cu deficiency (Garcia-Molina et al., 2011, Klaumann et al., 2011). Expression of *COPT1, COPT2* and *COPT6* is upregulated in Cu-deficient conditions (Jung et al., 2012, Sancenón et al., 2004), and these responses are controlled by the master regulator of Cu homeostasis in *A. thaliana*, the transcription factor, SPL7 (*SQUAMOSA* promoter binding protein-like7) (Jung et al., 2012, Yamasaki et al., 2009).

Cu homeostasis is also maintained through the "Cu economy" and "metal-switch" mechanisms, which include re-allocation of Cu within the cell to meet the demands of Cu-essential functions and the replacement of Cu-containing enzymes with functionally equivalent iron (Fe)-enzymes (Ravet et al., 2011, Ravet et al., 2013). For example, plastocyanin is the major Cu-containing protein in higher plants and is essential for photosynthesis (Weigel et al., 2003). During Cu deficiency, plastocyanin photosynthetic electron transport activity is maintained by the re-allocation of Cu from two Cu/Zn superoxide dismutases (SOD), CSD1 and CSD2, that are major Cu proteins located in the cytosol and plastid, respectively (Bowler et al., 1994, Cohu et al., 2009, Kliebenstein et al., 1998). As *CSD1* and *CSD2* transcripts and the activity of the encoded proteins decreases, their superoxide scavenging functions are replaced by an increase in gene expression and total enzyme activity of the Fe-containing SOD, FSD1 (Cohu and Pilon

2007, Yamasaki et al., 2007). These responses also depend on SPL7, and its downstream target, *miRNA398* (Yamasaki et al., 2007, Yamasaki et al., 2009, Sunkar and Zhu 2006). In addition to the SPL7-dependent mechanisms, Cu content and plastocyanin abundance in chloroplasts are controlled by two P-type ATPases. PAA1/HMA6 (P-type ATPase of *Arabidopsis* 1/Heavy-metal-associated 6) is a Cu transporter located in the inner chloroplast envelope (Shikanai et al., 2003), and PAA2/HMA8 is a Cu transporter located in the thylakoid membrane (Abdel-Ghany et al., 2005). PAA2/HMA8 is also subject to feedback control by Cu availability and plastocyanin levels (Tapken et al., 2012). These homeostatic mechanisms allow the most important Cu-requiring functions to remain active allowing plants to thrive in environments with a wide range of Cu concentrations.

While substantial progress has been made towards understanding how plants maintain Cu homeostasis, how it is controlled in an environment that also contains non-essential and potentially toxic elements such as cadmium (Cd), is not completely understood. Although Cd is a natural component of the Earth's crust, it is increasingly emitted into the environment as industrial and consumer waste, and from application of fertilizers, pesticides and insecticides, posing a threat to crop productivity, and human health (Jarup 2003). Cd causes stunting and chlorosis in plants and affects their major biochemical processes including redox balance, photosynthesis, and water status (Das et al., 1997, Hasan et al., 2009). At the cellular level, Cd toxicity results from the displacement of endogenous co-factors from their cellular binding sites, thiol-capping of essential proteins, inhibition of DNA repair processes and interference with the antioxidant defense system, resulting in the generation of reactive oxygen species (ROS) (Stadtman 1990, Clemens et al., 2006, Valko et al., 2005). Uptake of Cd into plant roots is mediated by transporters and channels for essential elements (*e.g.* iron [Fe], zinc [Zn], calcium

[Ca] and manganese [Mn]) due to either the broad substrate specificity of the transporter, or the similar ionic properties of essential and nonessential heavy metals (Clemens et al., 1998, Eide et al., 1996, Cohen et al., 1998, Sasaki et al., 2012). Cadmium is detoxified in the cytosol by forming a complex with the thiol tripeptide glutathione (GSH) (Li et al., 1997) and its derivatives, phytochelatins (PCs) (Vatamaniuk et al., 2000, Grill et al., 1985, Cobbett et al., 2000). These complexes as well as free Cd ions are then either sequestrated into the vacuole, or bypass the vacuole and instead load into xylem vessels of the root to travel into shoot with the transpiration stream (Hirshi et al., 2000, Morel et al., 2009, Park et al., 2012, Wong et al., 2009, Salt et al., 1995).

Competition of Cd with essential metals for cellular uptake sites as well as binding sites in metalloenzymes disrupts homeostasis of essential elements. In this regard, effects of Cd on the Fe status of plants is the best understood. In *A. thaliana*, Cd upregulates the mRNA expression of the Fe uptake system including the root ferric chelate reductase, *FRO2*, and a plasma membrane-localized Fe(II) transporter, *IRT1* (Robinson et al., 1999, Eide et al., 1996). In addition, transgenic *A. thaliana* plants overexpressing *IRT1* accumulate more Cd (Eide et al., 1996, Connolly et al., 2002). Therefore, it is suggested that Cd might compete with Fe(II) for uptake in Cd-polluted soils, thus causing Fe deficiency (Vert et al., 2002). Consistent with this suggestion, exposure of the Cd/Zn hyperaccumulator, *Thlaspi caerulescens* (*Ganges* population) to Cd inhibited Fe uptake (Kupper and Kochian 2010). The effect of Cd on homeostasis of other essential elements has not yet been investigated. In this regard, recent work in *S. cerevisiae* has shown that Cd negatively affects Cu metabolism by reducing transcript levels of a member of the CTR/COPT family, a high-affinity Cu uptake transporter, *CTR1* (Heo et al., 2010). Whether Cd affects Cu homeostasis in plants, is currently unknown.

Here, we show that Cd stimulates Cu accumulation in roots of *A. thaliana* and increases expression of genes encoding Cu transporters, COPT1, COPT2 and COPT6. Further analysis of Cd sensitivity of single and triple *copt1copt2copt6* mutants, and transgenic plants ectopically expressing *COPT6* suggested that Cu uptake is an essential component of Cd resistance in *A. thaliana*. Cd also elicited the transcriptional Cu deficiency responses by increasing expression *miRNA398* precursors and the Fe-SOD encoding gene*, FSD1*, while decreasing expression of genes encoding Cu/Zn SODs, *CSD1* and *CSD2.* We also found that these transcriptional responses depend on SPL7. Furthermore, seedlings of the *spl7-1* mutant accumulate up to 2-fold less Cu in roots, are hypersensitive to Cd, and are more sensitive to Cd than the *copt1copt2copt6* triple mutant. Together these data suggest that maintaining Cu homeostasis though CTR/COPT-dependent Cu uptake into roots and SPL7-dependent intracellular Cu reallocation, are essential for basal Cd resistance in *A. thaliana*.

Results

Cadmium promotes copper accumulation in roots of *A. thaliana.*

To test if Cd alters Cu accumulation in roots and shoots of *A. thaliana*, hydroponically-grown wild-type plants were exposed to two Cd-treatment regimens: high Cd (25 μM) for 3 days or low Cd (1 and 2.5 μM) for 10 days. As would be expected, both treatments led to Cd accumulation in roots and shoots (Table 1) and mild Cd toxicity symptoms, primarily chlorosis of younger leaves (not shown).

Table 1. Accumulation of cadmium in *A. thaliana.* Plants were grown hydroponically for two weeks before transferring to a fresh medium containing the indicated concentrations of $CdCl_2$ for the indicated time. Plants were harvested at the bolting stage. Roots and shoots were collected and Cd content was analysed by ICP-MS. Shown are arithmetic means ± S.D. (*n* = 2-4)

	Cadmium Accumulation (µg g^{-1} dry biomass)	
Growth conditions	**Root**	**Shoot**
25 µM $CdCl_2$; 3 days	2212.1 ± 174.3	1565.6 ± 145.1
1 µM $CdCl_2$; 10 days	789.9 ±59.4	291.7 ±14.0
2.5 µM $CdCl_2$; 10 days	1259.8 ± 62.7	715.9 ± 1.1

Exposure of plants to Cd led to significant accumulation of Cu in *A. thaliana* regardless of the treatment regimens (Table 2).

Table 2. Accumulation and root-to-shoot distribution ratio for copper in *A. thaliana*. Plants were grown hydroponically for three weeks before transferring to fresh medium containing the indicated concentrations of $CdCl_2$ for the indicated number of days. Plants were harvested at bolting stage. Total copper is the sum of root and shoot content in plants grown without supplemental Cd (Control) or with the indicated concentrations of $CdCl_2$, for times shown in Table 1. Shown are means ± S.D. (n = 4).

Conditions	**Total copper concentration (root + shoot), µg g^{-1} dry biomass**	**Root-to-shoot ratio**
Control (for 3 day Cd exposure)	13.40 ± 1.50	1.40 ± 0.30
25 µM $CdCl_2$ (3 days)	54.67 ± 14.50	8.23 ± 3.45
Control (for 10 day Cd exposure)	17.88 ± 0.55	2.35 ± 0.06
1 µM $CdCl_2$ (10 days)	52.82 ± 2.86	7.28 ± 1.26
2.5 µM $CdCl_2$ (10 days)	74.00 ± 5.16	10.00 ± 1.79

Analysis of Cu content in roots and shoots showed that roots of plants grown in 25 µM Cd for three days or 1 or 2.5 µM Cd for 10 days accumulated 4.5-, 3.7- and 5.3-fold more Cu, respectively, than roots of wild-type plants cultured at control conditions (Figure 1). In contrast, the effect of Cd on shoot Cu accumulation was not statistically significant except for long-term exposure to 2.5 µM Cd, upon which shoots of *A. thaliana* had accumulated 1.3-fold more Cu than shoots of plants grown under standard conditions (Figure 1B). Analyses of root-to-shoot

distribution ratios showed that Cd significantly affected Cu partitioning into roots; the root-to-shoot distribution ratio was 3- to 6-fold higher in plants grown under different Cd-treatment than in plants grown under control conditions (Table 2). Together, these data suggest that Cd stimulates Cu uptake into roots but does not facilitate its root-to-shoot translocation.

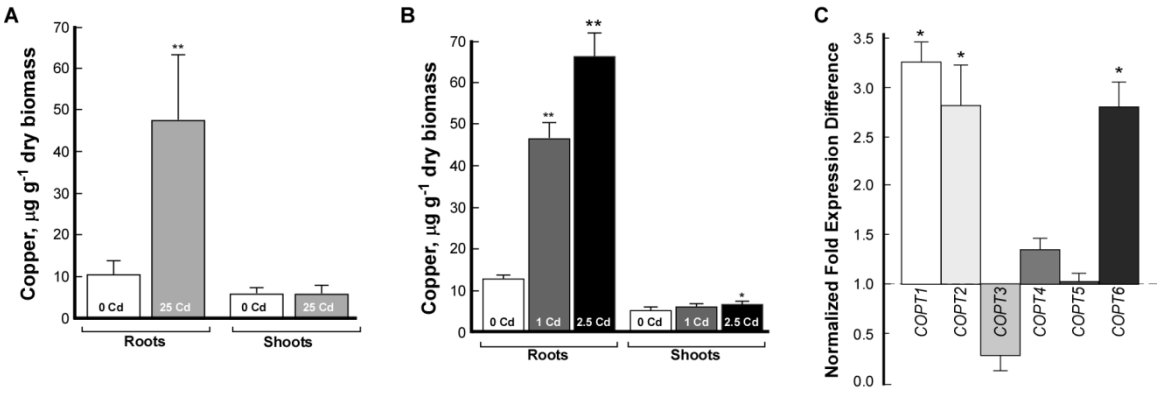

Figure 1. Cadmium promotes copper accumulation in roots of *A. thaliana*. Hydroponically grown *A. thaliana* wild-type plants were exposed to 25 µM $CdCl_2$ for 3 days (**A**) or to 1 or 2.5 µM $CdCl_2$ for 10 days (**B**). Root and shoot tissues were collected and subjected to ICP-MS elemental analysis. Statistical significance of measurements was determined using the ANOVA Single Factor Analysis. Error bars indicate S.D. The asterisks indicate statistically significant differences (*$p \leq 0.05$; **$p \leq 0.01$; n = 3-4). **C**. Normalized fold-expression difference of the effect of Cd on the expression of *COPT* genes in roots of *A. thaliana*. Error bars indicate S.E. *(n = 9)*. Statistically-significant differences of the mean values between control (untreated conditions) and Cd-treated plants are indicated as *($p \leq 0.05$). Results are presented relative to the expression of genes in control conditions, designated as 1.

Expression of *COPT1*, *COPT2*, and *COPT6* is differentially regulated by cadmium

We next tested if the increased Cu uptake into roots of Cd-grown *A. thaliana* (Figure 1) was associated with altered expression of members of the CTR/COPT family of Cu transporters. Wild-type plants were germinated and grown with or without 50 µM $CdCl_2$ for 10 days and transcript abundance was analyzed in roots by quantitative real-time (qRT)-PCR. We found that of the six family members, expression of *COPT1, COPT2* and *COPT6* was significantly higher in roots of plants grown in the presence of Cd than in roots of plants grown under control

conditions (Figure 1C). It is noteworthy that of the six family members, COPT1, COPT2 and COPT6 are the closest homologs and cluster in one clade on a phylogenetic tree (Jung et al., 2012). Together, these results suggest that COPT1, COPT2 and/or COPT6 might serve similar roles in response to Cd and might contribute to Cd-promoted Cu accumulation into roots of *A. thaliana*.

COPT2 localizes to the plasma membrane

COPT1 and COPT6 localize to the plasma membrane and are involved in cellular Cu uptake (Andrés-Colás et al., 2010, Page et al., 2009, Jung et al., 2012). To elucidate the subcellular localization of COPT2, its coding sequence was fused to that of EGFP of the *SAT6-EGFP-N1* vector (Tzfira et al., 2005) and co-transformed into onion cells with the *BIN20* vector expressing the *A. thaliana* plasma membrane protein, PIP2A, tagged with mCherry (Nelson et al., 2007). We found that COPT2-EGFP co-localized with PIP2A-mCherry at the cell periphery of intact onion cells (Figure 2A). To ensure the plasma membrane localization of COPT2-EGFP, the onions cells were plasmolyzed by incubating in a hypertonic solution created by 20% sucrose that forced the cytoplasm and accompanying plasma membrane to shrink from the cell wall. Both signals from COPT2-EGFP and PIP2A-mCherry co-localized at the plasma membrane of plasmolyzed cells (Figure 2B). On this basis we concluded that COPT2 localizes to the plasma membrane in *A. thaliana*.

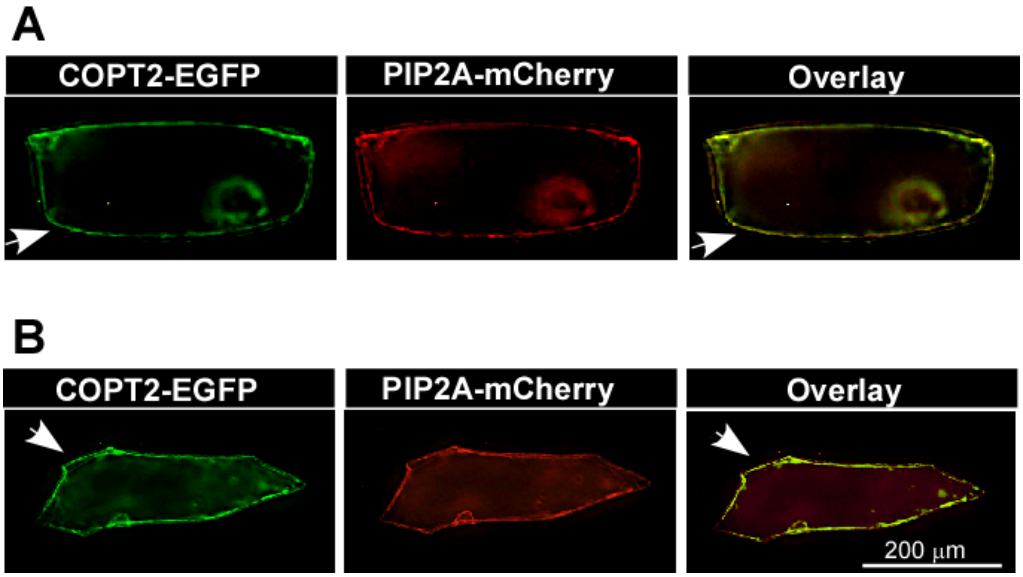

Figure 2. Subcellular localization of a chimeric COPT2-EGFP fusion protein. A. Onion cells were co-transformed with COPT2 fused to EGFP in the *SAT6-N1-EGFP-Gate* vector (**COPT2-EGFP**) and a plasma membrane marker, PIP2A fused to mCherry in the *BIN20* vector (**PIP2A-mCherry**). **B**. Onion cells transiently co-expressing COPT2-EGFP and PIP2A-mCherry were plasmolyzed in 20% sucrose solution for 10 min before imaging. EGFP- and mCherry-mediated fluorescence was visualized using FITC and Rhodamine filter sets respectively. Arrows point to plasma membrane localization of COPT2-EGFP. Superimposed images (**Overlay**) of COPT2-EGFP-, and PIP2A-mCherry-mediated fluorescence were generated to demonstrate the co-localization of COPT2-EGFP with PIP2A-mCherry (**A**, **B**). Our data are consistent with recent findings that COPT2 localizes to the plasma membrane when transiently expressed in *A. thaliana* protoplasts (Perea-García et al., 2013).

Cadmium toxicity and copper availability affect the expression pattern of *COPT2* in *A. thaliana*

Analyses of the expression pattern of *COPT1* and *COPT6* in *A. thaliana* and their response to Cu availability suggest that COPT1 is primarily involved in Cu acquisition *via* the root tip while COPT6 might primarily contribute to Cu distribution in photosynthetic tissues under standard growth conditions and to Cu uptake and root-to-shoot partitioning under Cu limitation (Jung et al., 2012; Sancenón et al., 2004). To investigate the sites of *COPT2* action in *A. thaliana*, the 1.8 kb genomic fragment upstream of the *COPT2* open reading frame ($COPT2_{pro}$) was fused to the

uidA reporter gene encoding *β*-glucuronidase (*GUS*), and the $COPT2_{pro}$-*GUS* construct was transformed into wild-type *A. thaliana*. From three transgenic lines exhibiting similar pattern of GUS activity, we selected one representative line for subsequent studies. Histochemical analysis of $COPT2_{pro}$ activity in plants grown under standard conditions revealed weak GUS staining in cotyledons and the root-to-hypocotyl junction but not in the main root of young seedlings (Figure 3A). The intensity of staining increased in cotyledons and leaves of older seedlings and was present in the lateral roots, but not the main root or roots tips, of 14-day-old seedlings (Figure 3E, inset). Weak staining in younger leaves and increased staining in older leaves of plants cultured under standard conditions is consistent with the increased demand for copper at different stages of plant development. Within the leaf, GUS staining was observed in mesophyll cells as well as in the vasculature of cotyledons and leaves (Figure 3K). Analysis of the $COPT2_{pro}$ activity in reproductive organs disclosed GUS staining in the stigma of siliques (Figure 3I, young siliques; 3J, older siliques) and in the vasculature and funiculus in older siliques (Figure 3J, L, M), and stigma and pollen grains of flowers (Figure 3N).

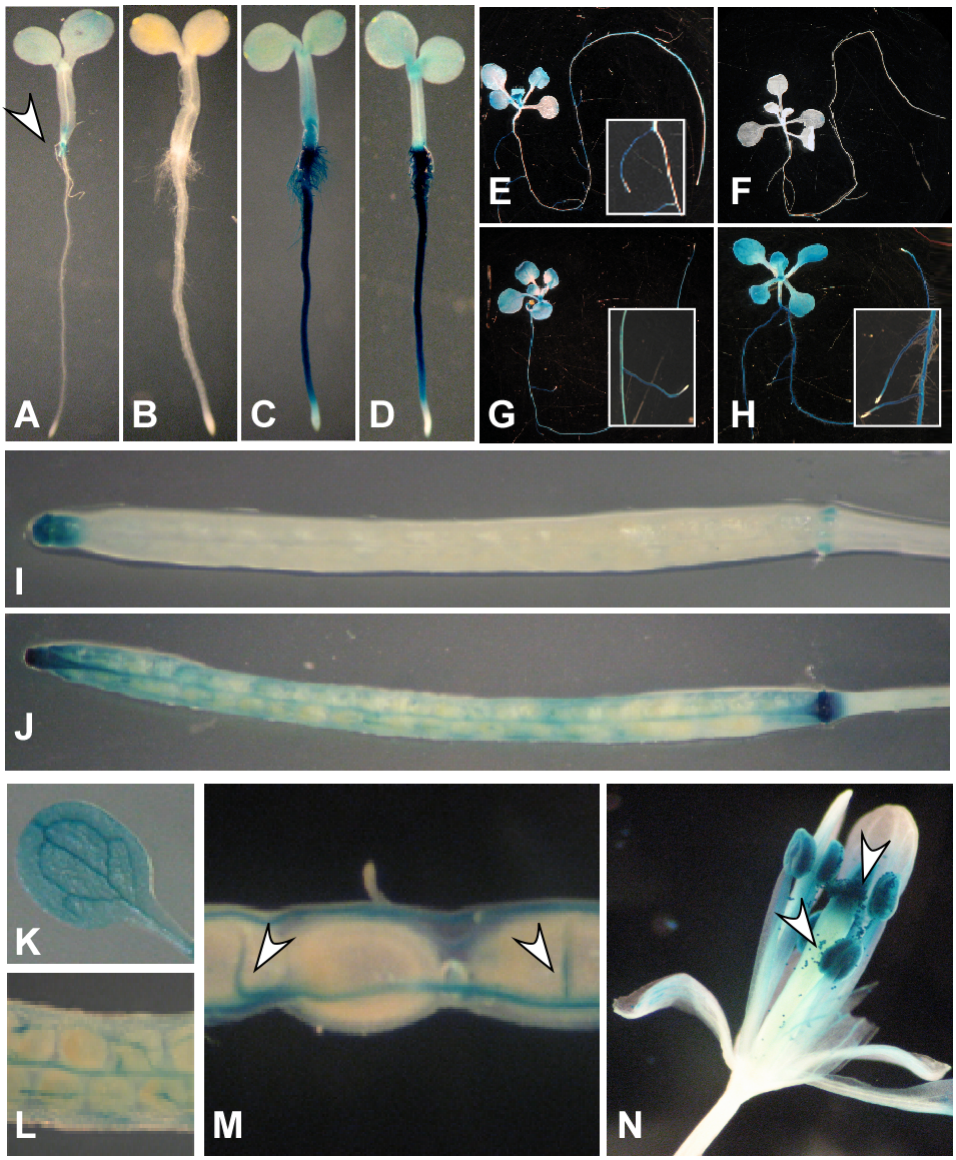

Figure 3. Histochemical analysis of the expression pattern of *COPT2* in *A. thaliana* transformed with the *$COPT2_{pro}$-GUS* construct. Plants were grown for 4 (**A-D**) or 14 days (E-H) on solid ½ MS media without (**A, E**) or with 3 µM $CuSO_4$ (**B** and **F**), or with 500 µM BCS (**C** and **G**), or with 50 µM $CdCl_2$ (**D** and **H**). Note the absence of GUS staining in 4-day and 14-day-old seedlings of plants cultured on ½ MS supplemented with 3 µM $CuSO_4$ (**B** and **F**), compared to control conditions (**A** and **E**), and intense GUS staining when plants were grown on ½ MS supplemented with 500 µM BCS (**C** and **G**) or with 50 µM Cd (**D** and **H**). GUS staining was observed throughout leaves and cotyledons and was concentrated in the vasculature (**K**). This staining pattern is consistent with findings from recent studies of *COPT2* expression. [79] To visualize the $COPT2_{pro}$ activity in reproductive organs (**I, J, L-N**), plants were grown on soils. *COPT2* expression is detected in the stigma of siliques (**I**, a young silique; **J**, an older silique) and in the vasculature of older siliques (**L** – is a close-up of **J**). Siliques were peeled to show the presence of *COPT2* expression in the funiculus (**M**, arrowheads). $COPT2_{pro}$ activity was also detected in the stigma and pollen grains of flowers (**N**, arrowheads).

Activity of *COPT2*$_{pro}$ was altered by Cu availability and Cd toxicity. We noticed that GUS staining was completely abolished by the supplementation of the growth medium with 3 μM Cu (Figure 3B and F). In contrast, GUS staining significantly increased in response to Cu limitation in roots of young (Figure 3C) as well as older seedlings (Figure 3G), and was present in the main root as well as in lateral roots (Figure 3 G, inset). GUS staining was not observed in root tips of the main or lateral roots. *COPT2*$_{pro}$ activity was moderately increased in leaves of older plants under Cu limitation (Figure 3G). Exposure to Cd mimicked Cu deficiency response by increasing *COPT2*$_{pro}$ activity in roots and to a much lesser extent in leaves of *COPT2*$_{pro}$*-GUS* transgenic plants (Figure 3D, H). Given that Cu and Cd alter *COPT2* expression in the root and that Cd toxicity increase Cu accumulation in roots of *A. thaliana* (Figure 1), and that COPT2 localizes to the plasma membrane (Figure 2), it is possible that COPT2 is primarily involved in Cu uptake into the root.

Heterologously expressed COPT2 and COPT6 alleviate cadmium hypersensitivity of *ctr1ctr2ctr3 S. cerevisiae* cells by mediating copper accumulation

Since we have shown that COPT6 is a Cu uptake transporter (Jung et al., 2012) and since COPT2 is implicated in Cu uptake (Sancenón et al., 2003), it is possible that the Cd-mediated increase in expression of genes encoding them was necessary for maintaining Cu uptake and partitioning to combat Cd toxicity. To test this hypothesis we used an *S. cerevisiae* strain (Rees et al., 2004) harboring mutations in Cu uptake genes, *ctr1ctr2ctr3*. This strain has been used as a versatile and well-defined model system for functional analysis of putative copper transporters from various species, and it has been shown that inhibited Cu uptake into yeast cells is associated with Cd sensitivity (Heo et al., 2010).

We heterologously expressed *COPT2* and *COPT6* in the *S. cerevisiae ctr1ctr2ctr3* strain, and compared Cd sensitivity between wild-type cells expressing the empty *YES3-Gate* vector and *ctr1ctr2ctr3* cells expressing empty *YES3-Gate* or *YES3-Gate* with the *COPT2* or *COPT6* cDNA insert. We found that lack of Ctr1p, Ctr2p and Ctr3p expression substantially increased Cd sensitivity of yeast cells (Figure 4A). In contrast, heterologous expression of either COPT2 or COPT6 fully abolished their Cd sensitivity (Figure 4A).

We then tested whether Cd sensitivity responses exhibited by the *ctr1ctr2ctr3* mutant expressing the empty vector or COPT2 or COPT6 were associated with Cu accumulation. Cells were cultured in liquid medium with or without the indicated concentration of Cd for 24 h. Consistent with previous findings, empty vector-expressing *ctr1ctr2ctr3* cells cultured under standard conditions accumulated less Cu than wild-type cells (Figure 4B and (Dancis et al., 1994a, Jung et al., 2012, Puig et al., 2002, Dancis et al., 1994b). Expression of COPT2 or COPT6 complemented this Cu accumulation defect (Figure 4B). Cd treatment significantly decreased Cu accumulation in wild-type and even more so in *ctr1ctr2ctr3* cells (Figure 4B). In contrast, expression of COPT2 and COPT6 in the *ctr1ctr2ctr3* mutant not only fully rescued the Cu accumulation defect but even increased internal Cu concentration by 1.7-fold compared to Cu concentration in Cd-treated wild-type cells (Figure 4B).

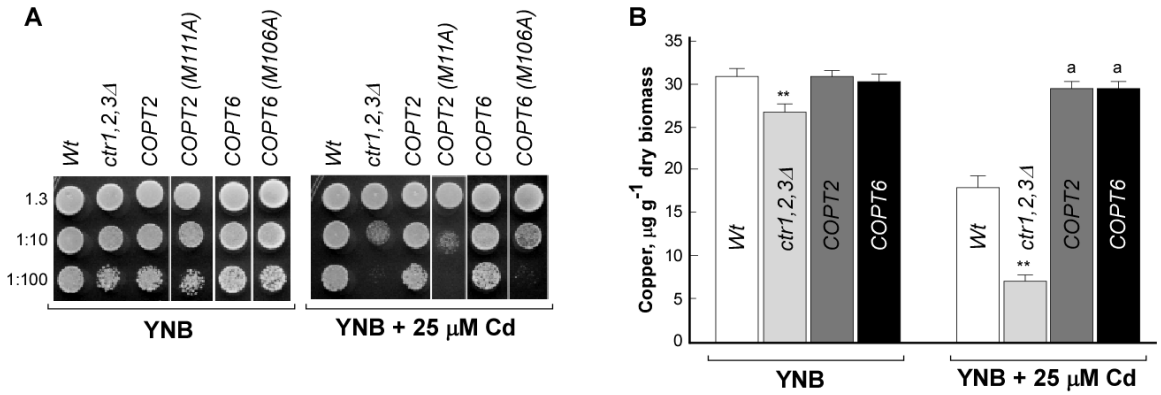

Figure 4. COPT2 and COPT6 suppress cadmium sensitivity of the *S. cerevisiae ctr1ctr2ctr3* triple mutant and facilitate copper accumulation. A. BY4741 wild-type transformed with the empty *YES3-GATE* vector (**Wt**), the *ctr1ctr2ctr3* cells transformed with the empty *YES3-GATE* vector (***ctr1,2,3Δ***) or the vector containing a wild-type *COPT2* or *COPT6* cDNA insert (***COPT2, COPT6***) or Met-to-Ala substituted *COPT2* and *COPT6* alleles (**COPT2 [M111A], COPT6 [M106A]**) were grown overnight in liquid YNB medium without uracil (YNB) to an $OD_{600\ nm}$ of 1.3 (indicated on the left). Aliquots of cell suspensions were spotted onto solid YNB medium supplemented with the indicated concentration of $CdCl_2$. **B.** Yeast cells designated as in (**A**) were cultured in liquid YNB-URA medium with or without indicated concentration of $CdCl_2$. Copper content was analyzed by ICP-MS. Statistical significance of differences was determined using the ANOVA Single Factor Analysis. The asterisks (**) indicate statistically significant differences from the wild-type cells expressing the empty vector or from the *ctr1ctr2ctr3* mutant expressing *COPT2* or *COPT6*. A letter "a" indicates statistically significant differences between the wild-type expressing the empty vector and the *ctr1ctr2ctr3* mutant expressing *COPT2* or *COPT6* ($p \leq 0.001$; n = 5). Error bars indicate S.D.

To ensure that the ability of COPT2 and COPT6 to rescue Cd sensitivity is associated with Cu accumulation, we generated Cu transport incompetent mutant alleles of COPT2 and COPT6 by replacing positionally conserved methionine residues within the TMD2, Met_{111} and Met_{106} in COPT2 and COPT6, respectively, with alanine residues. These positionally conserved residues within the TMD2 are essential for the Cu transport ability of COPT6 and its homolog from yeast, CTR1p (Jung et al., 2012, Puig et al., 2002). We then compared the ability of M111A- and M106A-substituted COPT2 and COPT6 to suppress Cd sensitivity in *ctr1ctr2ctr3* cells. If COPT2 and COPT6 alleviated Cd sensitivity by transporting Cu into yeast cells, and if the positionally conserved Met_{111} residue in COPT2 plays the same role in Cu uptake as the

corresponding residues in Ctr1p and COPT6 (Jung et al., 2012, Puig et al., 2002), then *ctr1ctr2ctr3* cells expressing these mutant alleles should be sensitive to Cd. As predicted, *ctr1ctr2ctr3* cells expressing M111A-substituted COPT2 or M106A-substituted COPT6 were as sensitive to Cd as cells expressing the empty vector (Figure 4A). Together, these data suggested that heterologously expressed COPT2 and COPT6 rescue Cd sensitivity of the *ctr1ctr2ctr3* mutant by facilitating Cu accumulation. In addition, demonstration that heterologously expressed *COPT2* mediates Cu accumulation in yeast cells and that Met_{111} is essential for COPT2 transport function (Figure 4) substantiate a previous suggestion that COPT2 is involved in Cu uptake (Sancenón et al., 2004).

The *A. thaliana copt1-1* single mutant and the *copt1copt2copt6* triple mutant show differential sensitivity to cadmium

We then proceeded with analyses of the role of COPT1, COPT2 and COPT6 in Cd resistance using *A. thaliana* mutants. The *copt6-1* mutant has been previously characterized with respect to the location of the T-DNA insertion and the sensitivity to Cu availability (Jung et al., 2012). We also obtained two T-DNA insertion alleles, SALK_147451C and SALK_152053 (*alias copt2-1* and *copt2-2*, respectively) possessing T-DNA insertions 89 and 455 bp upstream of the *COPT2* start codon, respectively (Figure 5A), and a *copt1-1* allele (SALK_067183) bearing a T-DNA insertion upstream of the *COPT1* start codon (Figure 6). Homozygous plants were identified (Figures 5B and 6B) and effect of T-DNA insertions on *COPT1* and *COPT2* transcripts abundance for both alleles were assessed by RT-PCR. We found that the abundance of *COPT1* and *COPT2* transcripts was significantly lower in *copt1-1* and was below the limit of detection in both *copt2* allelic mutants, when compared to transcripts present in wild-type plants (Figures 5C

and 6C).

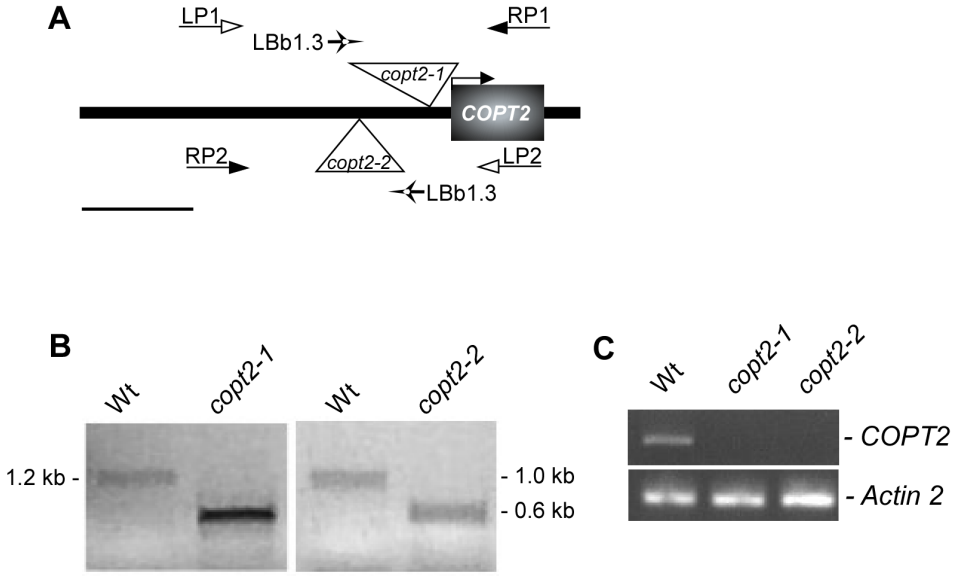

Figure 5. Basic characterization of *copt2-1* and *copt2-2* alleles. A. Genomic structure of *COPT2* (start codon indicated by horizontal black arrow on the black box labeled *COPT2*). Note that *COPT2* does not contain introns. Triangles indicate T-DNA insertions located 89 and 455 bp in the genomic region upstream of *COPT2* ORF in the *copt2-1 (**copt2-1**)* and *copt2-2 (**copt2-2**)* alleles, respectively. Positions of primers used for genotyping the *copt2-1* allele are indicated as arrows above and for the *copt2-2* allele below the schematic representation of the genomic structure of *COPT2*. Note that the T-DNA insertion for *copt2-1* is oriented towards the *COPT2* coding region, while the T-DNA insertion within the *copt2-2* allele is oriented in the opposite direction. Scale bar = 500 bp. **B**. Comparison of PCR products using both LBb1.3 + RP1/2 and LP1/2 + RP1/2 primer combinations and genomic DNA (gDNA) isolated from *copt2-1 (**copt2-1**)* and *copt2-2 (**copt2-2**)* mutant plants, respectively, shows that both mutants bear homozygous T-DNA insertions, in contrast to wild-type plants (**Wt**). LBb1.3 + RP1/2 primers used to detect T-DNA insertions produce a ~0.6 kb product for *copt2-1* and *copt2-2*, suggesting a presence of T-DNA inserts. Primer pairs LP1/RP1 and LP2/RP2 detect genomic fragments lacking the T-DNA insert and thus, PCR products of the indicated size are present in the gDNA from the wild-type but not from homozygous *copt2-1* or *copt2-2* alleles. **C**. RT-PCR detection of full-length *COPT2* (***COPT2***) transcripts (482 bp, 27 cycles) using COPT2-F and COPT2-R (Table 3) in roots of 14-day old Wt, *copt2-1* and *copt2-2* seedlings show the lack of the detectable *COPT2* transcript, in contrast to wild-type plants. *Actin2* (***Actin 2***) was used as a loading control and detected using qPCR primers (141 bp Table 4). Note: 30 cycles show a faint band in *copt2-1* seedlings (not shown).

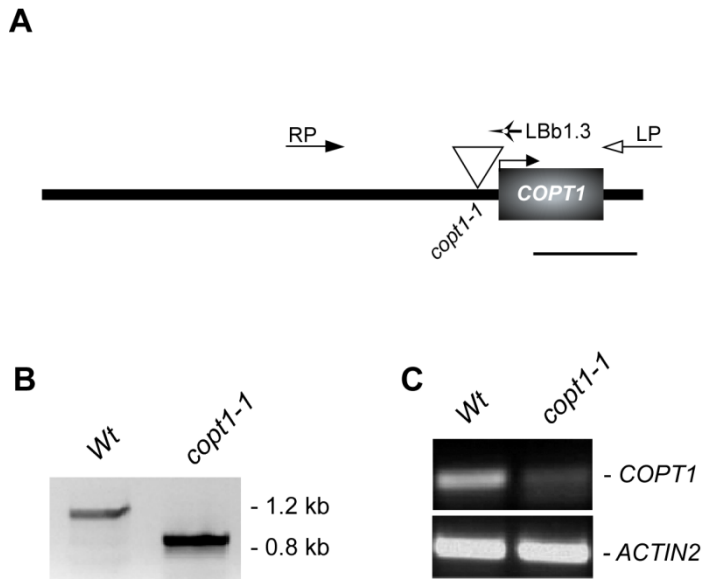

Figure 6. A. Genomic structure of *COPT1* (start codon indicated by horizontal black arrow). Note that *COPT1* does not contain introns. Gray arrowheads indicate a T-DNA insertion with a predicted location 93 bp in the promoter region of *COPT1* in the *copt1-1* mutant, according to the flanking sequence associated with the SALK_067183 allele. Arrowheads seen above the genomic structure indicate LP (**LP**), RP (**RP**), LBb1.3 (**LBb1.3**) primer positions. Scale bar = 500 bp. **B**. Comparison of PCR products using both LBb1.3 + RP and LP + RP primer combinations in gDNA isolated from *copt1-1* ***(copt1-1)*** mutant plants indicate that the *copt1-1* allele contains homozygous T-DNA insertions, in contrast to wild-type plants (**Wt**). LBb1.3 + RP primers used to detect T-DNA produce a ~0.8 kb product while LP + RP primers used to detect non-T-DNA bearing plants result in a 1.2 kb product.

We then tested Cd sensitivity of *copt1-1*, *copt2-1*, *copt2-2* and *copt6-1* knock-out plants. In the medium without Cd, no difference was found in growth of roots and shoots of different mutant alleles as compared to the wild-type (Figure 7A). In the medium supplemented with 50 μM $CdCl_2$, only *copt1-1* exhibited increased sensitivity as evident by 1.12-fold decrease in growth of the primary root, while we did not detect statistically significant differences in root or shoot growth between the wild-type and *copt2-1* (and *copt2-2*, not shown) or the wild-type and the *copt6-1* mutant (Figure 7B). We conclude that decreased expression of *COPT1* in the *copt1-1* mutant increases its Cd sensitivity, while the absence of *COPT2* or *COPT6* alone does not affect the growth of *A. thaliana* on Cd-containing medium.

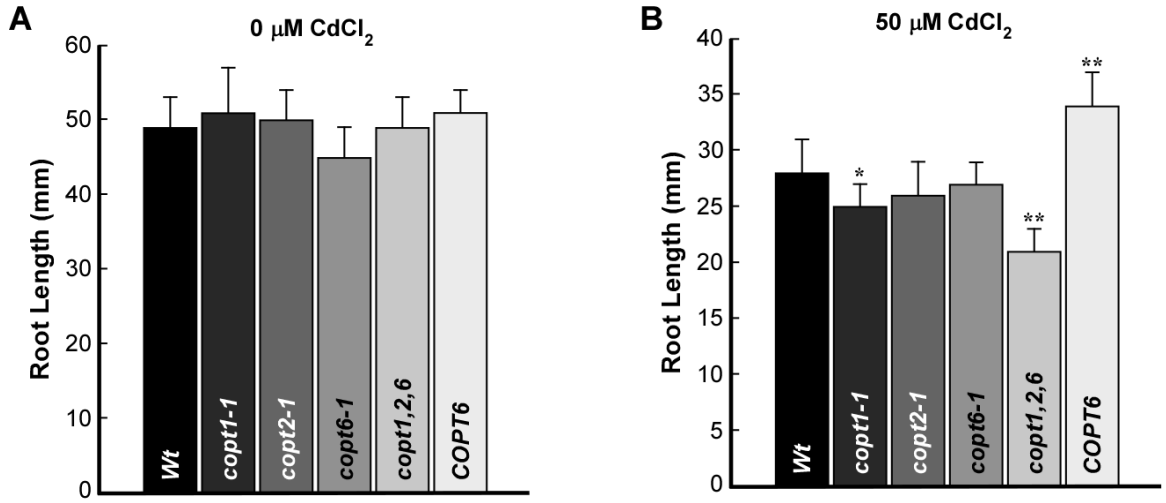

Figure 7. Function of COPT1, COPT2 and COPT6 is required for cadmium-resistance in *A. thaliana*. A. Root lengths of the 10-day-old wild-type (**Wt**), *copt1-1* (***copt1-1***), *copt2-1* (***copt2-1***), *copt6-1* (***copt6-1***), *copt1copt2copt6* (***copt1,2,6***) mutants, and transgenic plants overexpressing *COPT6* (***COPT6***), all grown in ½ MS without Cd (**0 μM $CdCl_2$**). **B**. Root lengths of seedlings from the same lines but grown with Cd (**50 μM $CdCl_2$**). Asterisks indicate statistically significant differences between the wild-type and mutants or the transgenic line (*p ≤ 0.01, **p ≤ 0.001). Error bars indicate S.D. Representative results from three independent experiments are shown.

High similarity between COPT1, COPT2 and COPT6 protein sequences (Jung et al., 2012) suggests possible redundancy within plasma membrane-localized COPT family members, and the lack of phenotype of single *copt2-1* and *copt6-1* mutants grown on Cd prompted us to generate a triple mutant lacking *COPT1*, *COPT2* and *COPT6* simultaneously. RT-PCR analysis disclosed decreased transcript abundance of all three genes in the *copt1copt2copt6* triple mutant in comparison with the wild-type (Figure 8). When grown in control conditions (no Cd), no significant differences were found in root lengths of all lines (Figure 7A). Growth on Cd containing medium (50 μM) produced shorter root lengths for all lines (Figure 7B), which is consistent with effects of Cd toxicity. Furthermore, we observed that root lengths of

copt1copt2copt6 triple mutants were 1.4-fold shorter than in wild-type plants and 1.2-fold shorter than in the single *copt1-1* mutant (Figure 7B). These data suggest that COPT1, COPT2 and COPT6 play essential role in Cd resistance. The synergistic effect of *copt1-1* with *copt2-1* and *copt6-1* alleles suggests that these genes may act in different steps and/or tissues of Cu uptake. For example, in accordance with tissues-specificity of expression of *COPT* genes (Jung et al., 2012, Sancenón et al., 2004) and Figure 3, COPT1 and COPT2 may be necessary for initial Cu uptake into root epidermal cells, while COPT6 may also act in Cu partitioning and distribution in photosynthetic tissues to prevent Cu essential functions from Cd toxicity.

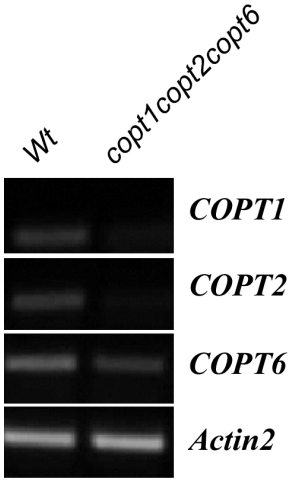

Figure 8. RT-PCR comparison of the transcript abundance of *COPT1, COPT2* and *COPT6* in the wild-type (*Wt*) and a triple *copt1copt2copt6* mutant of *A. thaliana.* Plants were grown on solid ½ MS medium for 10 days prior RNA extraction and cDNA synthesis. *COPT1 (**COPT1**), COPT2 (**COPT2**)* and *COPT6 (**COPT6**)* transcripts were detected using qPCR primer pairs (Table 4) and *Actin2* (***ACTIN2***) as a loading control. Reactions were run for 27 cycles before detection.

A. thaliana transgenic plants overexpressing *COPT6* are more tolerant to cadmium

We next tested if increased Cu uptake due to overexpression of COPT transporters would increase Cd tolerance. We used transgenic *A. thaliana* ectopically expressing *COPT6* (Jung et al., 2012). Of two previously characterized lines we used *$35S_{pro}$-COPT6-2*, because high *COPT6*

mRNA and protein level of this line correlated with its ability to confer increased Cu accumulation in shoots and increased growth under Cu limited conditions (Jung et al., 2012). Based on comparison of the root lengths of different plant lines grown in the presence of Cd (Figure 7B), *35S$_{pro}$-COPT6-2* transgenic plants were 1.2-, 1.4-, and 1.6-fold more tolerant to Cd than wild-type, *copt1-1* or *copt1copt2copt6* mutants respectively. Together, our data show that COPT-mediated Cu uptake and tissue partitioning are essential for basal Cd resistance in *A. thaliana*.

Cadmium exposure elicits the transcriptional copper deficiency response in roots of *A. thaliana*

Studies in *C. reinhardtii* revealed that exposure to nickel (Ni) mimics Cu deficiency response under Cu-replete conditions by acting on the transcription factor, Crr1, a homolog of *A. thaliana* SPL7 (Yamasaki et al., 2009, Kropat et al., 2005). Similarly, Ni exposure elicits Cu deficiency responses in the Ni hyperaccumulator, *Alyssum inflatum* (Ghasemiet et al., 2009). In contrast, Ni does not alter the transcription of Cu-deficiency responsive genes under Cu-replete conditions in *A. thaliana;* instead it mimics Cu in response to Cu deficiency (Yamaskai et al., 2009). Our finding that Cd induces expression of SPL7 targets, *COPT1*, *COPT2* and *COPT6* in roots of *A. thaliana* suggests that effect of Cd on Cu homeostasis might be distinct from the effect of Ni in this species. To explore this further, we sought to determine if Cd induces the SPL7-dependent Cu-deficiency response, which could explain the increased expression of *COPT1*, *COPT2* and *COPT6*.

SPL7 is predominantly expressed in roots where it induces the expression of *miRNA398* upon Cu deficiency (Yamasaki et al., 2007, Yamasaki et al., 2007). Mature *miRNA398* targets the

cytosol- and plastid-localized Cu/ZnSOD genes, *CSD1* and *CSD2*, respectively, for degradation in order to reallocate Cu to plastocyanin (Cohu et al., 2009). When this occurs, the functions of CSD1 and CSD2 are replaced by the Fe-SOD enzyme, FSD1, whose expression is induced during Cu deficiency *via* SPL7 as well (Cohu et al., 2009, Palmer et al., 2009, Puig et al., 2007). Therefore, if Cd exposure mimics Cu deficiency, then transcript abundance of *miRNA398* isoforms *b* and *c* would increase in Cd-treated plants. Accordingly, *CSD1* and *CSD2* expression and activity of the encoded proteins would decrease, while *FSD1* expression and FSD1 activity would increase to replace CSD1 and CSD2 functions in Cd-treated plants.

To test our predictions, we compared the transcript abundance of *miRNA398* precursor isoforms *b* and *c* (hereafter designated *miRNA398 b/c*), *CSD1, CSD2* and *FSD1* in roots of Cd-treated *vs.* untreated plants. Although it was shown that *SPL7* and *CRR1* do not transcriptionally respond to alterations in Cu status (Yamasaki et al., 2009, Kropat et al., 2005), their transcriptional regulation by other metals has not been analyzed, prompting us to test if Cd would alter the expression of *SPL7* as well.

Comparison of *SPL7* transcript abundance in roots of Cd-treated *vs.* untreated plants did not reveal statistically significant differences (Figure 9A), suggesting that similar to Cu, Cd does not affect *SPL7* expression. In contrast, expression of *miR398b/c* was significantly increased, while expression of *CSD1* and *CSD2* decreased in roots of Cd-grown seedlings (Figure 9A). Accordingly, *FSD1* expression was increased in roots of Cd-exposed seedlings (Figure 9A). Consistent with gene expression, Cd exposure significantly decreased Cu/ZnSOD activity and increased Fe-SOD activity in roots of *A. thaliana* (Figure 9B). These data show that Cd causes a Cu deficiency response at the level of gene expression and that induction of *COPT1, COPT2* and *COPT6* expression could be a component of this response.

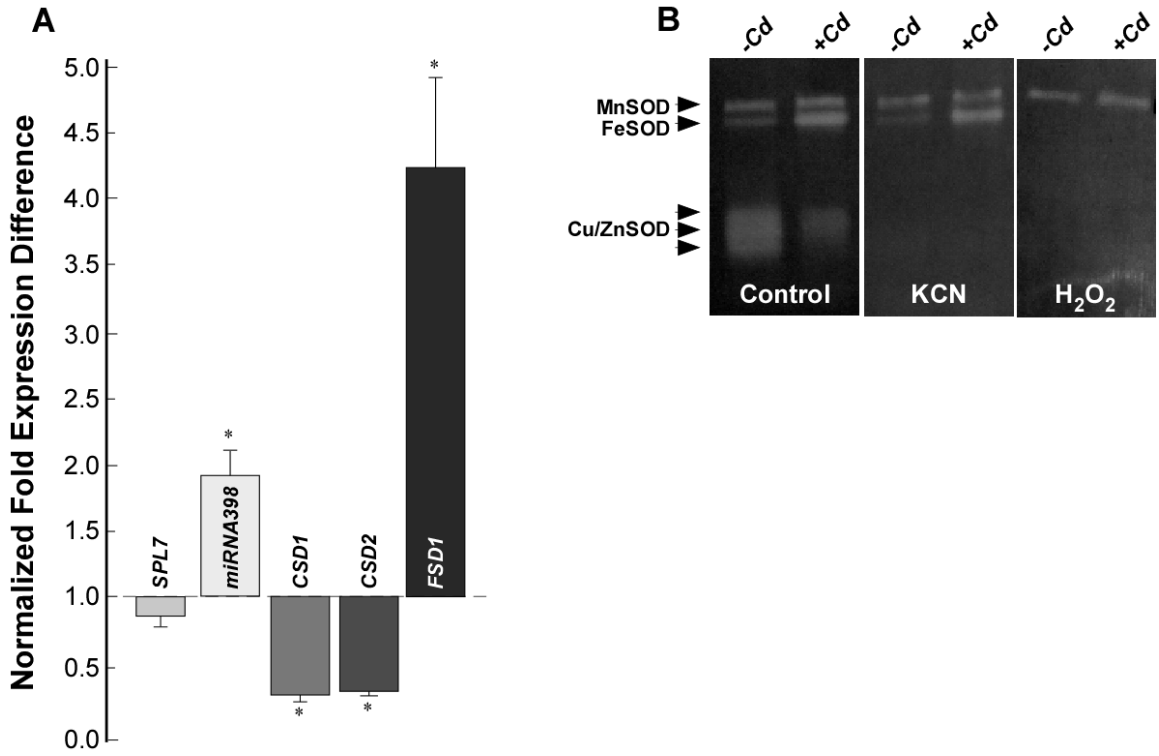

Figure 9. Cadmium exposure induces the copper deficiency response in *A. thaliana*. A. Quantitative real-time (qRT)-PCR analysis of the effects of Cd exposure on transcript levels of Cu-regulated genes in roots of 10-day-old seedlings cultured on solid medium with 50 μM $CdCl_2$. Error bars show S.E. (*n = 4*). Results are presented relative to the expression of genes in control (no added cadmium) conditions. **B.** SOD isozyme activity in roots of 10-day old seedlings cultured on solid medium without (**-Cd**) or with 50 μM $CdCl_2$ (**+Cd**). Assays for SOD activity were conducted using NBT (**Control**). Cu/Zn SOD isozyme activities were repressed by adding KCN (**KCN**), whereas Cu/Zn and FeSOD activities were repressed with H_2O_2 (**H_2O_2**). Positions of the mitochondrial Mn-containing SOD, Fe-containing SOD and Cu/ZnSODs, are indicated. Note the decrease of Cu/ZnSOD and increase of FeSOD activities in roots of seedlings grown with $CdCl_2$.

The effect of cadmium on the expression on copper-responsive genes depends, in part, on SPL7

To test if the effect of Cd on the expression of the above Cu-responsive genes depends on SPL7, we used the *A. thaliana spl7-1* mutant that bears a T-DNA insertion in the fifth intron, resulting

in loss-of-function due to a truncated protein (Yamasaki et al., 2009). We compared expression of *COPT1*, *COPT2*, *COPT6*, *miRNA398b/c* precursors, *CSD1, CSD2* and *FSD1* in roots of *spl7-1* mutant *vs.* wild-type plants grown with or without Cd. We found that while expression of *COPT1* was not altered by *spl7-1* mutation in roots of seedlings grown without Cd, expression of *COPT2*, *COPT6*, *FSD1* and *miRNA398* was downregulated in the mutant compared to the wild-type, both grown without Cd (Figure 10A). In contrast, expression of *CSD1* and *CSD2* was upregulated in the *spl7-1* mutant *vs.* wild-type, both grown on medium without Cd. As we found previously (Figure 9A), Cd caused transcriptional Cu deficiency response as evident by upregulation of the expression of *COPT1, COPT2, COPT6, FSD1*, and *miRNA398* and down-regulation of the expression of *CSD1* and *CSD2,* and this effect was abolished in the *spl7-1* mutant (Figure 10B). Compared to transcript levels in Cd-treated wild-type plants, Cd-stimulated increase of transcript abundance of *COPT1* and *COPT6* was diminished by 1.4- and 1.5-fold respectively in the *spl7-1* mutant, but unlike *COPT2*, was not abolished completely. This result was not entirely surprising since our recent studies showed that while *COPT6* expression is under SPL7 control in shoots, its expression depends only partially on SPL7 in roots (Jung et al., 2012). With respect to *COPT1*, our data suggest that while its transcriptional response to Cu deficiency depends on SPL7 (Yamasaki et al., 2009), other factors in addition to SPL7 may regulate its transcriptional response to Cd toxicity (Figure 10B). Taken together our results strongly support the conclusion that Cd elicits transcriptional Cu deficiency response in Cu-replete conditions and that this response, in part, depends on SPL7.

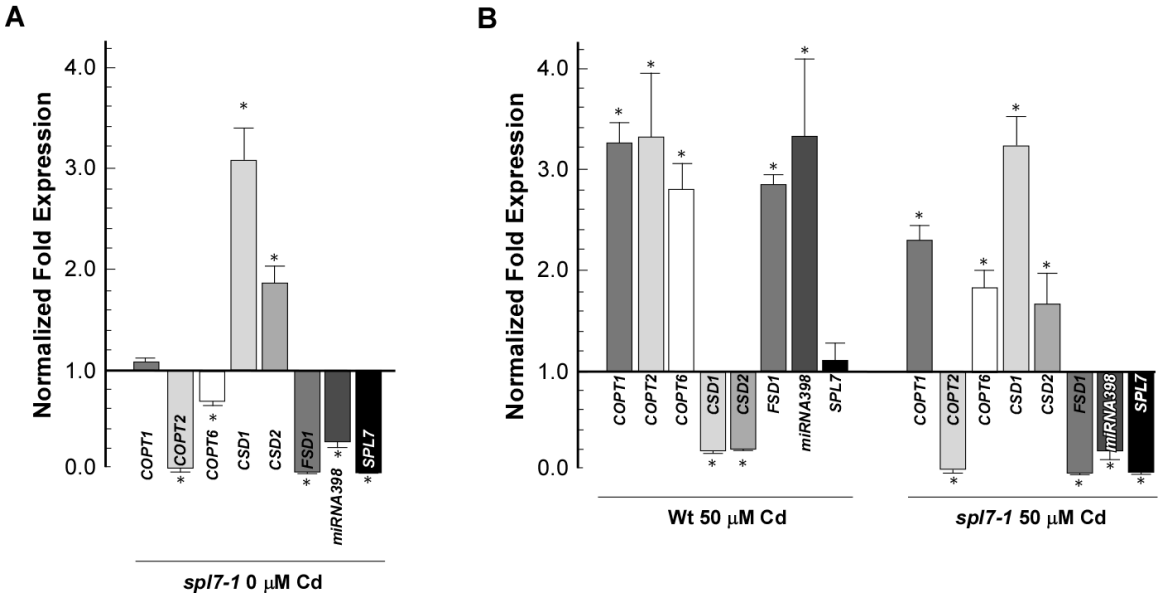

Figure 10. qRT-PCR comparison of the transcript abundance of *COPT1, COPT2, COPT6, CSD1, CSD2, FSD1* and *miR398b/c* precursors in roots of wild-type (Wt) and *spl7-1* (*spl7*) seedlings grown at control conditions (A) *vs.* cultured with $CdCl_2$ (B). All results are presented relative to the expression of genes in wild-type plants under control conditions. Error bars indicate S.E. (*n = 6*). Asterisks (*) indicate statistically significant differences from wild-type grown under control conditions, designated as 1.

The *A. thaliana spl7-1* mutant is sensitive to cadmium

SPL7 maintains Cu homeostasis in *A. thaliana* by at least two mechanisms: 1) by the reallocation of intracellular Cu among the major Cu-enzymes (*e.g.* Cu/ZnSODs) to preserve important Cu-demanding energy-related functions (*e.g*. plastocyanin) and 2) *via* the regulation of Cu uptake and Cu root-to-shoot partitioning. Since Cd altered both components in an *SPL7*-dependent manner, we hypothesized that both, *SPL7*-dependent Cu uptake and Cu reallocation are important for Cd resistance. Therefore, we predicted that the *spl7-1* mutant will be more sensitive to Cd than the *copt1copt2copt6* mutant because of the additive effect of both mechanisms, the compromised COPT-dependent Cu uptake as well as Cu reallocation in the *spl7-1* mutant. To test this hypothesis, we compared growth of the *spl7-1* mutant *vs.* the wild-type, both germinated and grown for 10 days on ½ MS solid medium with or without 50 μM

$CdCl_2$. Consistent with previous findings (Yamasaki et al., 2009, Bernal et al., 2012), roots of the *spl7-1* mutant were shorter than roots of wild-type plants when plants were grown under standard conditions, possibly because the Cu concentration in standard MS medium is within the mild Cu deficiency range (Yamasaki et al., 2009, Abdel-Ghany et al., 2005, Andrés-Colás et al., 2013). Therefore we supplemented the control medium with increasing concentrations of Cu (Figure 11A). We found that supplementing the MS medium with as low as 0.1 μM Cu rescued the short-root phenotype of the *spl7-1* mutant (Figure 11A).

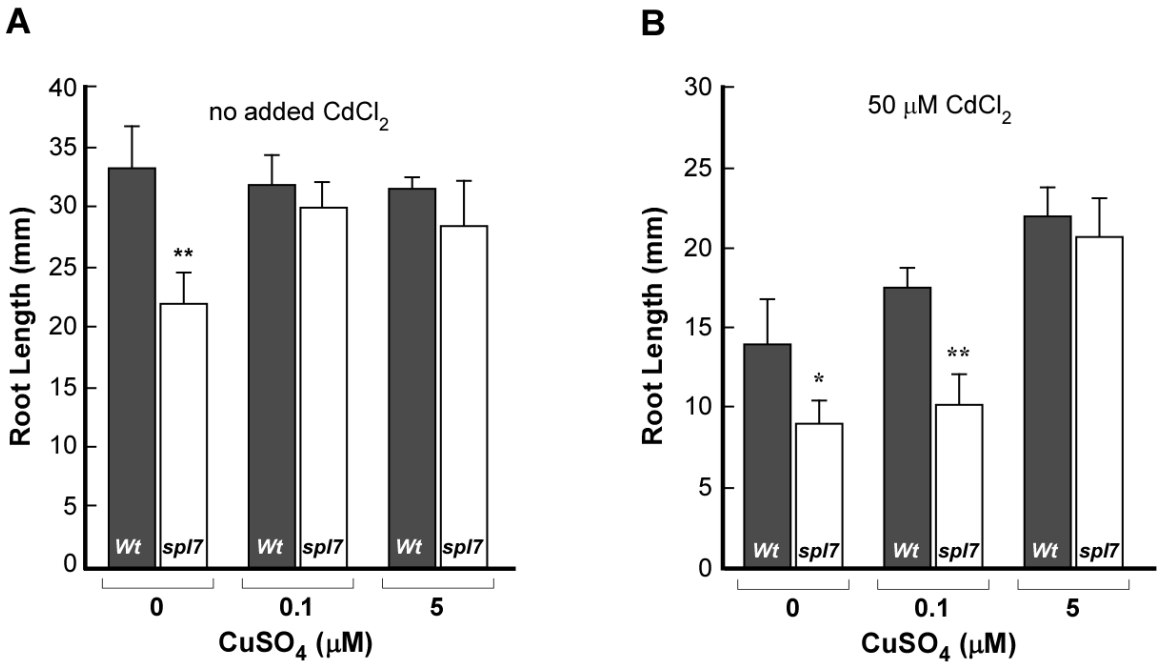

Figure 11. Root lengths of the 10-day-old wild-type (Wt) and the *spl7-1* mutant (*spl7*) grown on ½ MS supplemented with the indicated concentrations of $CuSO_4$ without (A) or with (B) 50 μM $CdCl_2$. Note that 0.1 μM $CuSO_4$ rescues the short-root phenotype of *spl7-1* seedlings under standard conditions but not under Cd stress. Asterisks indicate statistically significant differences between the wild-type and the *spl7-1* mutant where $*p \leq 0.05$, $**p \leq 0.001$. Error bars indicate S.D. Shown are representative results of three independent experiments.

We then tested the effect of Cd on the root growth of the *spl7-1* mutant. We also

supplemented medium with the indicated concentrations of Cu to distinguish the effect of Cd toxicity from mild Cu deficiency on root growth of the mutant (Figure 11B). In medium without additional Cu, Cd inhibited root growth of wild-type and *spl7-1* mutant plants with roots of the *spl7-1* mutant being 1.5-fold shorter than roots of the wild-type, suggesting an increased sensitivity of the *spl7-1* mutant to Cd (Figure 11B). Although 0.1 μM Cu complemented the short-root phenotype of the *spl7-1* mutant under control conditions (Figure 11A), the addition of Cd to medium containing 0.1 μM Cu significantly decreased root growth of the *spl7-1* mutant in comparison to root growth in wild-type plants with roots of the *spl7-1* mutant being 1.8-fold shorter than roots of the wild-type (Figure 11B). When Cd-grown plants were also supplemented with higher concentrations of Cu (5 μM), partial rescue of root growth in both the wild-type and the *spl7-1* mutant was observed and the root length of the *spl7-1* mutant was indistinguishable from the wild-type (Figure 11B).

The *spl-1* mutant was more sensitive to Cd than the *copt1copt2copt6* mutant as evident from the 1.8 and 1.4-fold decrease in root length of *spl7-1* and the *copt1copt2copt6* mutant respectively *vs.* the wild-type. Together, these results suggest that the SPL7-dependant pathway, which includes COPT-dependent Cu uptake and tissue distribution, as well as Cu reallocation, is essential for basal Cd tolerance in *A. thaliana*.

The *spl7-1* mutant accumulates less copper under cadmium stress than the wild-type

To test whether the increased Cd sensitivity of roots of the *spl7-1* mutant is associated with an altered ability to accumulate and/or partition Cu into shoots, we compared Cu concentrations in roots and shoots of Cd-treated wild-type and *spl7-1* mutant plants. When plants were grown under control (Cu sufficient, no Cd) conditions no difference was found in the Cu concentrations

between roots of wild-type and *spl7-1* plants (Figure 12A); however, shoots of *spl7-1* plants accumulated 1.7-fold less Cu compared to the wild-type (Figure 12B). The latter observation suggests that Cu translocation into leaves is impaired in the *spl7-1* mutant grown under standard conditions.

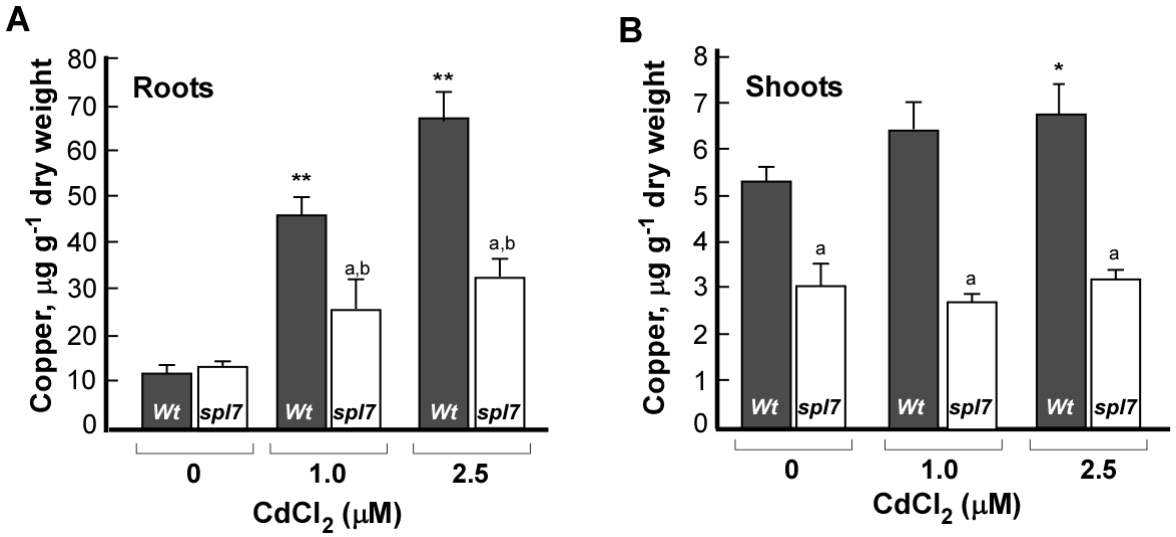

Figure 12. Cadmium decreases copper accumulation in the *spl7-1* mutant. Wild-type (Wt) and *spl7-1* mutant (*spl7*) plants were grown hydroponically before indicated concentrations of $CdCl_2$ were added to the culture medium. Roots (**A**) and shoots (**B**) were collected after 10 days and Cu concentrations were analyzed by ICP-MS. Error bars indicate S.D. Asterisks indicate statistically significant differences between the wild-type grown without *vs.* with Cd (*$p \leq 0.05$; ** $p \leq 0.001$); a letter "a" indicates statistically significant differences between wild-type and *spl7-1* plants ($p \leq 0.05$); a letter "b" indicates statistically significant differences between *spl7-1* plants grown without *vs.* with Cd ($p \leq 0.05$).

As we showed previously (Figure 1), Cd stimulated Cu accumulation in roots of wild-type plants (Figure 12A). Although Cd also stimulated Cu accumulation in roots of the *spl7-1* mutant, the Cu concentration was significantly lower in roots of the *spl7-1* mutant compared to the wild-type (1.8- and 2-fold lower) when grown on 1, or 2.5 μM $CdCl_2$, respectively (Figure 12A). In contrast, Cd treatment did not alter accumulation of Cu in shoots of wild-type and *spl7-1* plants (Figure 12B). Taken together, these data support our hypothesis that increased sensitivity of roots of *spl7-1* seedlings to Cd is a result of their reduced ability to enhance root Cu

accumulation or mount other Cu deficiency responses in response to Cd exposure. Thus, the SPL7-dependent pathway plays an essential role in basal Cd tolerance of *A. thaliana*.

Discussion

This manuscript addresses the effect of Cd on homeostasis of the essential micronutrient Cu in the model plant, *A. thaliana.* We found that Cd stimulates Cu uptake into *A. thaliana* roots (Figure 1A, B) and increases mRNA abundance of genes encoding plasma membrane-localized Cu uptake transporters of the CTR-COPT family, COPT1, COPT2 and COPT6 (Figure 1C) suggesting that Cu accumulation through these transporters might be an essential component of Cd resistance. This suggestion was further validated by finding that the *copt1-1* single mutant is sensitive to Cd and the sensitivity is even more pronounced in the triple *copt1copt2copt6* mutant. We hypothesized that the synergistic effect of *copt1-1* with *copt2-1* and *copt6-1* alleles is due to these genes acting in different steps and/or tissues of Cu uptake.

Aside from upregulation of *COPT1*, *COPT2* and *COPT6*, Cd induces the SPL7-dependent transcriptional Cu deficiency response in *Arabidopsis* roots by altering expression of the intracellular Cu reallocation system including *miRNA398*, *CSD1*, *CSD*2 and *FeSOD1*. Given that roots of the *spl7-1* mutant accumulate 2-fold less Cu than roots of the wild-type (Figure 12A), the mutant is Cd sensitive (Figure 11B), and is more Cd sensitive than the triple *copt1copt2copt6* mutant (Figure 7B), we concluded that at a minimum both, the SPL7-dependent Cu uptake and intracellular Cu reallocation and/or other SPL7-dependent processes are important for basal Cd resistance in *A. thaliana*.

We propose several, not-mutually exclusive mechanistic scenarios for crosstalk between Cd and Cu homeostasis (Figure 13).

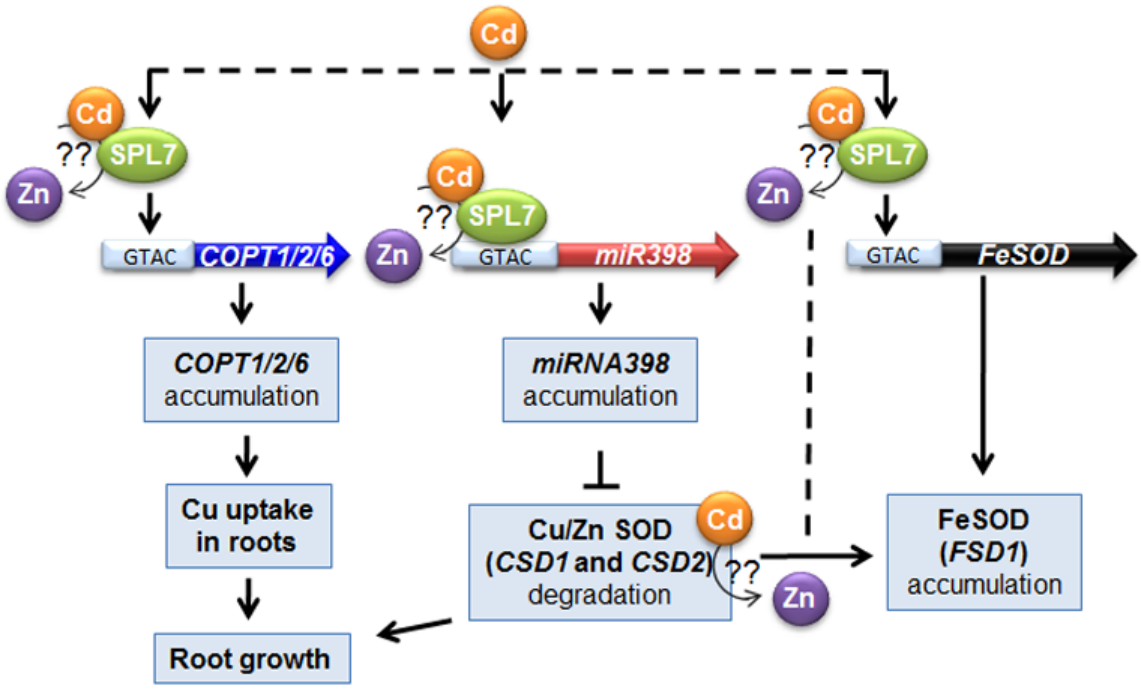

Figure 13. A model depicting possible scenarios of the effect of cadmium on SPL7-dependent regulation of copper homeostasis. Cd elicits SPL7-dependent Cu deficiency responses by altering expression of *COPT1, COPT2, COPT6, CSD1, CSD2, miRNA398 b/c* precursors and *FSD1*. It is possible that Cd acts directly on SPL7 either *via* the Zn-containing SBP domain and/or other sites resulting in SPL7 binding to the GTAC core sequences in promoters of its targets. Note, that binding of the SBP domain to the GTAC motifs in the promoter of *miRNA398c* was shown (Yamasaki et al., 2009). Although we identified GTAC motifs in promoters of *COPT* genes and *FSD1* using PLACE prediction software (Jung et al., 2012, Higo et al., 1999, Prestridge et al., 1991), whether SPL7 regulates their expression directly, or indirectly, is unknown. It is also possible that Cd alters cellular Cu availability and/or reallocation among Cu metalloenzymes (as exemplified here with Cu/Zn SODs), which, if sensed as Cu deficiency, will elicit the SPL7-dependent Cu-deficiency response. As a result, *COPT1, COPT2, COPT6, CSD1*, *CSD2*, *miRNA398* and *FSD1* are differentially expressed and Cu is reallocated from CSD1 and CSD2 to other important Cu-requiring functions in order to maintain their activity and root growth under Cd stress.

It is possible that Cd exposure mimics Cu deficiency by acting directly on SPL7. In this regard, the His and Cys residues located within the SBP DNA-binding domain in SPL7 may act as Zn and Cu(I) ligands, similar to its homolog in *C. reinhardtii*, CRR1 (Kropat et al., 2005, Sommer et al., 2010). Furthermore, Zn binding is essential for the binding of the SBP domain of CRR1 to Cu-responsive elements (CuRE) in promoters of its targets (Kropat et al., 2005,

Sommer et al., 2010). Whether similar events occur in the SPL7-dependent pathway is not known. Nevertheless, because of the chemical similarity of Cd^{2+} and Zn^{2+} ions (Clemens 2006, Stohs et al., 1995), it is tempting to speculate that Cd may act on SPL7 *via* its Zn-binding pockets in the SBP-domain to turn on expression of SPL7 targets. It is also possible that Cd acts at other sites in SPL7 to activate expression of its targets even in Cu-replete cells. Finally, it is possible that Cd does not act directly on SPL7, but instead, Cd alters cellular Cu availability and/or reallocation among Cu-requiring metalloenzymes, which, if perceived as Cu deficiency, would elicit the SPL7-dependent Cu-deficiency responses. SPL7-dependent Cu-deficiency responses could then stimulate a global response resulting in increased expression of genes responsible for Cu uptake, *COPT1* and *COPT6*. Indeed, the requirement of Cu during Cd toxicity can be attributed to increased Cu uptake by the *spl7-1* mutant when exposed to Cd (Figure 12A). Regardless of which of these scenarios operate in *A. thaliana*, the demonstration that COPT-dependent Cu uptake and SPL7-dependent Cu homeostasis are essential for Cd resistance opens novel avenues for functional studies and for the identification of components of the regulatory networks underlying crosstalk between Cd resistance and Cu homeostasis.

Materials and Methods

Plant materials and growth conditions

All plant lines used in the study were in the *A. thaliana* Columbia (Col-0) background. Seeds of the *spl7-1* mutant were obtained from Dr. Shikanai (Kyoto University, Japan) and this mutant is described in (Yamasaki et al., 2009). *COPT1* and *COPT2* mutant alleles, SALK_067183 (*alias copt1-1*), SALK_147451C (*alias copt2-1*) and SALK_152053 (*alias copt2-2*) were obtained from the *Arabidopsis* Biological Resource Center (Alonso et al., 2003). Mutants bearing

homozygous T-DNA insertions were selected by PCR using genomic DNA as a template and the LBb1.3 and RP or LB and RP primer pairs (Table 3) to select plants homozygous for *copt1-1*, *copt2-1* and *copt2-2* mutations. To generate a triple *copt1-1copt2-1copt6-1* mutant, the *copt2-1* allele was crossed into the previously described *copt6-1* mutant (Jung et al., 2012), and after the homozygous double mutant was selected by PCR, the *copt1-1* mutant was crossed into the *copt2-1copt6-1* double mutant. The homozygous *copt1-1copt2-1copt6-1* mutant (from then on *copt1copt2copt6)* was selected by PCR using genomic DNA as a template and the LBb1.3 and appropriate RP or LB and RP primer pairs (Table 3).

Seeds of different plant lines were surface-sterilized in 75% (v/v) ethanol and a solution containing 1.8% sodium hypochlorite (made-up by diluting a household Clorox solution), 0.1% (v/v) Tween-20, and seeds of uniform size were sown on half-strength Murashige and Skoog (1/2 MS) medium (pH 5.7) (Murashige and Skoog 1962) with 0.1% (w/v) sucrose and 0.7% agar (w/v, Sigma A1296) supplemented with or without indicated concentrations of $CuSO_4$ or $CdCl_2$. After stratification at 4°C for 2 days in darkness, seeds were germinated and seedlings grown vertically for 10-days. Wild-type and *spl7-1* mutant plants shown in Figure 8 were grown at 22^{o}C, 14-h light/10-h dark photoperiod at photon flux density of 87 μmol $m^{-2}s^{-1}$; *copt1-1*, *copt2-1*, *copt6-1* single mutants and *copt1copt2copt6* triple mutants along with wild-type plants were grown in 22^{o}C; 12-h light/12-h dark photoperiod at photon flux density of 88 μmol $m^{-2}s^{-1}$.

Histochemical analysis

To examine the pattern of *COPT2* expression in *A. thaliana,* the 1.8 kb genomic sequence upstream of the *COPT2* translational start codon was amplified by nested PCR first using the NEST-COPT2-promoter-F and COPT2-R primer pairs (Table 3) before a second round of PCR

using the COPT2-promoter-F and COPT2-promoter-R primers (Table 3).

Table 3. Cloning primers used in this study

Name	**5´ → 3´**
COPT2-F	GCCGCCTCGAGCATTAGTATCATGGATCATGATCAC
COPT2-R	GCGGCGAATTCACAAACGCAGCCTGAAGAC
att*B*-*COPT2*-F	TCGTCGGGGACAACTTTGTACAAAAAAGTTGGATTAGTATCATGGATCATGAT CACATG
att*B*-*COPT2*-R	GGCGGCCGCACAACTTTGTACAAGAAAGTTGGGTTGTTCAACAAACGCAGCCT
COPT2-M111A-F	GGTGATGCTCGCTGTTGCTTCCTTTAACGCAGGTGT
COPT2-M111A-R	ACACCTGCGTTAAAGGAAGCAACAGCGAGCATCACC
COPT2-1-LP	CTGTGTCGTGAGGTTTTGAGG
COPT2-1-RP	TCTTGAGTGTGTACACAGCGG
COPT2-2-LP	GAGACAGAGAGCGTACATGCC
COPT2-2-RP	TTTATGGGGAATTCCCAAAAG
COPT1-LP	TCCTCCTCCTCACATTCACAC
COPT1-RP	CCTACATTACCCGATTTGCTG
LBb1.3	ATTTTGCCGATTTCGGAAC

The resulting amplicon was fused to the bacterial *uidA* gene encoding β-glucuronidase (GUS) of the *GUS1-Gate* vector (Jung et al., 2012). The resulting construct was transformed into wild-type *A. thaliana* by the floral dip method (Clough and Bent 1998). Independent homozygous transgenic lines were selected for tolerance to 50 µg/L of kanamycin. For analyses of the $COPT2_{pro}$ activity, transgenic plants were grown on solid ½ MS supplemented with 1% (w/v) sucrose, 50 µg/L kanamycin and the indicated concentrations of $CuSO_4$ or $CdCl_2$ for 4 or 14-days before histochemical staining. Flowers and siliques were selected from plants grown on soil and with 100 ppm of Jack's 21-5-20 fertilizer, used once every two weeks. Staining was performed for 12 to 16 h with 1 or 0.5 mM X-Gluc (5-bromo-4-chloro-3-indolyl-β-D-glucuronide) as previously described (Jefferson et al., 1987). Staining patterns were analyzed using a Zeiss 2000 stereomicroscope. Images were collected using a Canon PowerShot S3 IS digital camera and a CS3IS camera adapter. Images were processed using the Adobe Photoshop software package, version 12.0.

Subcellular localization and fluorescent microscopy

The full-length *COPT2* cDNA without the stop codon was fused at the C-terminus with the modified green fluorescent protein (EGFP) under the control of the cauliflower mosaic virus (CaMV) *35S* promoter of the *SAT6-N1-EGFP-Gate* vector (Jung et al., 2012). The resulting construct and the plasma membrane marker, PIP2A, fused to mCherry in the *BIN20* vector (Nelson et al, 2007) were introduced into onion epidermal cells by biolistic transformation (Wyatt et al., 1999). Briefly, 2 µg of each construct in 10 µl distilled water was mixed with 10 µl of solution containing 50 mg/ml of 1.0 µm gold particles, 10 µl of 2.5 mM $CaCl_2$, and 4 µl of 0.1 M spermidine. The mixture was incubated for 30 min at room temperature. Gold particles coated with plasmid DNA were rinsed with cold ethanol and then gently suspended in 20 µl of ethanol. Onion pieces were placed onto agar plates containing 1× MS medium and bombarded using a double-barreled extension of the Bio-Rad He/1000 particle delivery system (PDS-1000/He [Bio-Rad]) with 1100 p.s.i. rupture discs under a vacuum of 0.04 bar. Onion pieces were left to recover after bombardment in the dark at 25°C for 16 h. Onion skin epidermal layers were peeled from the onion pieces and placed on glass slides for analyses. When indicated, onion epidermal cells were plasmolyzed by incubating in 20% (w/v) sucrose solution for 10 minutes. Z-stack (1.3 µm-thick) images were collected with the high-resolution AxioCam MR Camera and then 3D deconvoluted using an inverse filter algorithm of the Zeiss AxioVision 4.8 software. Images were processed using the Adobe Photoshop software package, version 12.0.

Yeast strains and growth conditions

S. cerevisiae strains used in this study were the *ctr1ctr2ctr3* triple mutant (*MATa ura3-52 his3Δ200 trp1-901 ctr1::ura3::Knr ctr2::HIS3 ctr3::TRP1)* and its isogenic wild-type, SEY6210

(*MATa ura3-52 leu2-3,-112 his3Δ200 trp1Δ901 lys2-801 suc2Δ9)* (the generous gift of Dr. Dennis Thiele [Duke University]). Yeast cells were cultured at 30°C on YNB medium containing 6.7% (w/v) Yeast Nitrogen Base without amino acids (Difco), 0.7 % CSM-Ura (w/v), 0.08% (w/v) uracil, 0.5% (w/v) NaCl, 2% (w/v) glucose and 2% (w/v) agar. cDNA corresponding to the full-length open reading frame (ORF) of *COPT2* was amplified from *A. thaliana* RNA by reverse transcription (RT) PCR using primer pairs that introduced *att*B1 and *att*B2 sites and 5′ and 3′ end of *COPT2* cDNA, respectively (Table 3). The resulting PCR product was introduced by recombination cloning (Gateway, Invitrogen) into the *yeast-E. coli* shuttle vector *YES3-Gate* vector (Jung et al., 2012).

Site-directed mutagenesis of *COPT2* was performed directly on a *YES3-Gate-COPT2* vector with QuickChange® II Site-Directed Mutagenesis Kit (Stratagene). The mutagenic oligonucleotides (Table 3) were designed to substitute conserved Met codons with Ala codons in the TMD2 of COPT2. Mutagenesis was confirmed by sequencing the cDNA region encompassing the mutation before yeast transformation.

YES3-Gate-COPT2, YES3-Gate-COPT2 (M111A), YES3-Gate-COPT6 and *YES3-Gate-COPT6 (M106A)* (Jung et al., 2012) constructs or *YES3-Gate* lacking cDNA inserts were transformed into yeast cells using the Frozen-EZ yeast Transformation II Kit (Zymo Research). Transformants were selected for uracil prototrophy on YNB medium. For analysis of Cd sensitivity, transformants were grown in liquid YNB-Ura media to an OD_{600nm} = 1.0-1.3. Cells then were serially diluted 10-fold with the same media and spotted onto solid YNB-Ura plates supplemented with indicated concentrations of $CdCl_2$.

RNA extraction and cDNA synthesis

Root and shoot tissues from 10-day-old seedlings grown with or without 50 μM $CdCl_2$ were separated and flash-frozen before homogenization in liquid nitrogen. Samples were collected between 7 and 8 Zeitgeber time, where Zeitgeber hour 1 is defined as the first hour of light after the dark period. Total RNA was isolated using TRIZOL reagent (Invitrogen), according to the manufacturer's instructions. Genomic DNA in total RNA samples was digested with DNAse *I* (Roche) prior to first strand cDNA synthesis using AffinityScript™ QPCR cDNA Synthesis kit according to manufacturer's recommendations (Agilent Technologies).

Quantitative real-time (qRT)-PCR and data analysis

Prior to qRT-PCR analysis, primers (Table 4) and cDNA concentration were optimized to reach the target and normalization genes amplification efficiency of 100 ± 10%. Two μL of 15-fold diluted cDNA was used as a template for quantitative PCR in a total volume of 15 μL containing 300 nM of each PCR primer, 50 mM KCl, 20 mM Tris-HCl, pH 8.4, 0.2 mM each dNTP and 1.25 units of iTaq DNA polymerase in iQ SYBR Green Supermix (BioRad), containing 3 mM $MgCl_2$, SYBR Green I, 20 nM fluorescein, and stabilizers. PCR was carried out using the CFX96 Real-Time PCR system (BioRad). The thermal cycling parameters were as follows: denaturation at 95°C for 3 min, followed by 39 cycles of 95°C for 10 s, 55°C for 30 s. Amplicon dissociation curves, *i.e.* melting curves, were recorded after cycle 39 by heating from 60°C to 95°C with 0.5°C increments and an average ramp speed of 3.3°C s^{-1}. Real-time PCR experiments were conducted using three independent biological samples, each consisting of three technical replicates (Udvardi et al., 2008), unless indicated otherwise. Data were normalized to the expression of two reference genes encoding ACTIN-2 (AT3G18780) and F-box protein

(AT5G15710), since their transcripts are stable in Cd treated *A. thaliana* (Remans et al., 2008). The fold difference ($2^{-\Delta\Delta Ct}$) was calculated using the CFX Manager Software, version 1.5 (BioRad). Statistical analysis was performed using the Relative Expression Software Tool (REST, Qiagen and Pfaffl et al., 2002).

Table 4. qPCR primers used in this study

Gene	5′ → 3′
Actin 2-F	GACCTTTAACTCTCCCGCTA
Actin 2-R	GGAAGAGAGAAACCCTCGTA
COPT1-F	CATGTCGTTTAACGCCGGTGTGTT
COPT1-R	CCGGAAAGTTTGGCTTCCGAACAA
COPT2-F	TGGTGATGCTCGCTGTTATGTCCT
COPT2-R	TCTGGTCATCGGAGGGTTTCTTGA
COPT3-F	AATGTATTGGGTCTGTCTCGCCGT
COPT3-R	GCCACGAAGACTCCTCCATTGAA
COPT4-F	AGACCGTCACTGTTACACCCAACA
COPT4-R	AGTGCATACATCCCACGGTCAGAA
COPT5-F	ATCAATACCTCGAGAATCGCCGCA
COPT5-R	AGCTGCAAGCATCAGCAAGTAACC
COPT6-F	ACACTCAAGACAGGCCTT
COPT6-R	CGAAGAGCATGAAACCCAC
SPL7-F	GAGCTGGAGGGCTATATCCG
SPL7-R	GGAAGAGGCTCGATGACTGT
miR398b/c-F	GGATCTCGACAGGGTTGATATG
miR398b/c-F	AAGAGCTCAGCAGGGGTGACCTG
FSD1-F	ACTTACAGCTTCCCAAGACAC
FSD1-R	TGCTGTGAATCCCCTTGTG
CSD1-F	TTCTGGCCTTAAGCCTGGTC
CSD1-R	CGACATGCTGGTGATCTAGG
CSD2-F	CATGACACACGGAGCTCCAG
CSD2-R	GAGCTGGAGGGCTATATCCG
F-box-F	TTTCGGCTGAGAGGTTCGAGT
F-box-R	GATTCCAAGACGTAAAGCAGATCAA

Primer pairs used for qRT-PCR were selected for specificity to *COPT1*, *COPT2* and *COPT6* cDNA and validated by subjecting primers to the BLAST tool (TAIR). The *COPT1* forward and reverse qRT-PCR primers have E-values of 2e-06 each, with no match to other *COPT* genes and amplify from the 426-510 bp region of the *COPT1* transcript. The *COPT2* transcript is amplified from the 326-445 region and both forward and reverse qRT-PCR primers have E-values of 2e-06

to *COPT2*. Although the *COPT2* qRT-PCR forward primer aligns to *COPT6* with an E-value of 0.007, the combination of the *COPT2* qRT-PCR primers would amplify only from the *COPT2* transcript. The qRT-PCR primers for *COPT6* amplify from the 405-513 bp region of the *COPT6* transcript. The E-value of the forward primer is 0.003 to *COPT6* and 0.81 to *COPT2*. The reverse primer has an E-value of 0.001 to *COPT6* and no alignment to other *COPT* genes. Thus, the pairing of the *COPT6* primer pairs would amplify only from the *COPT6* transcript.

Analyses of copper content

For analyses of Cu content in *A. thaliana*, 10-day-old seedlings were grown vertically on ½ MS solid medium before being transferred to *Arabidopsis* hydroponic solution described in (Arteca and Arteca 2000). Plants were then grown at 22^{o}C and 12-h light/12-h dark photoperiod at photosynthetic photon flux density of 120 μmol $m^{-2}s^{-1}$ for 10-20 days before $CdCl_2$ was added to the medium. Roots and shoots of 30-day-old plants were harvested and roots were desorbed by washing with 10 mM EDTA for 5 min followed by washing in a solution of 0.3 mM BCS and 5.7 mM sodium dithionite for 10 min before rinsing with deionized water as described (Jung et al., 2012). *S. cerevisiae* alleles were grown and cells were collected for analysis of Cu content by inductively coupled plasma mass spectroscopy (ICP-MS, Agilent 7500) (Jung et al., 2012, Lahner et al., 2003).

SOD isozyme activity gels

Root and shoot tissues from 10-day-old *A. thaliana* seedlings grown vertically on ½ MS plates supplemented with 0 or 50 μM $CdCl_2$ were harvested and immediately frozen in liquid nitrogen. Total proteins were extracted by homogenizing plant tissues with 100 mM potassium phosphate

buffer (pH of 7.5), supplemented with 2 mM EDTA, 1% PVP-40, and 1 mM phenylmethylsulfonyl fluoride. After pelleting cell debris at 15,000 × *g* for 20 min at 4°C, aliquots of soluble proteins (100 μg) were loaded onto 12% (v/v) non-denaturing polyacrylamide gels and subjected to electrophoresis at 120 V for 3 h. Inhibition of the reduction of a colorless nitro blue tetrazolium (NBT) to a blue formazan was used for visualizing the activity of SOD isoforms on gels (Beauchamp and Fridovich 1971, Flohé and Otting 1984). The SOD isozymes were identified by differential inhibition using 2 mM KCN to inhibit Cu/ZnSOD (Geller and Winge 1984) or 3 mM H_2O_2 to inhibit Cu/ZnSOD and FeSOD (Shikanai et al., 2003). Quantification of SOD activity bands in non-denaturing polyacrylamide gels was conducted using the *GelQuant* software, version 2.7 (DNR Bio-Imaging Systems).

Accession numbers for genes used in this study (accession numbers are in parenthesis) are as follows: *COPT1* (AT5G59030), *COPT2* (AT3G46900), *COPT3* (AT5G59040), *COPT4* (AT2G37925), *COPT5* (AT5G20650), *COPT6* (AT2G26975), *SPL7* (AT5G18830), *CSD1* (AT1G08830), *CSD2* (AT2G28190), *FSD1* (AT4G25100), *miR398b* (AT5G14545), *miR398c* (AT5G14565), *Actin-2* (AT3G18780) and F-box protein (AT5G15710).

REFERENCES

Abdel-Ghany, S. E., Muller-Moule, P., Niyogi, K. K., Pilon, M. and Shikanai, T. (2005) Two P-type ATPases are required for copper delivery in *Arabidopsis thaliana* chloroplasts. *Plant Cell*, **17**, 1233-1251.

Alonso, J. M., Stepanova, A. N., Leisse, T. J., Kim, C. J., Chen, H., Shinn, P., Stevenson, D. K., Zimmerman, J., Barajas, P., Cheuk, R., Gadrinab, C., Heller, C., Jeske, A., Koesema, E., Meyers, C. C., Parker, H., Prednis, L., Ansari, Y., Choy, N., Deen, H., Geralt, M., Hazari, N., Hom, E., Karnes, M., Mulholland, C., Ndubaku, R., Schmidt, I., Guzman, P., Aguilar-Henonin, L., Schmid, M., Weigel, D., Carter, D. E., Marchand, T., Risseeuw, E., Brogden, D., Zeko, A., Crosby, W. L., Berry C. C. and Ecker, J. R. (2003) Genome-wide insertional mutagenesis of *Arabidopsis thaliana*. *Science*, **301**, 653-657.

Andrés-Colás, N., Perea-García, A., Mayo de Andres, S., Garcia-Molina, A., Dorcey, E., Rodriguez-Navarro, S., Perez-Amador, M. A., Puig, S. and Peñarrubia, L. (2013) Comparison of global responses to mild deficiency and excess copper levels in *Arabidopsis* seedlings. *Metallomics*, **5**, 1234-1246.

Andrés-Colás, N., Perea-García, A., Puig, S. and Peñarrubia, L. (2010) Deregulated copper transport affects *Arabidopsis* development especially in the absence of environmental cycles. *Plant Physiol*, **153**, 170-184.

Arteca, R.N. and Arteca, J. M. (2000) A novel method for growing *Arabidopsis thaliana* plants hydroponically. *Physiol Plant*, **108**, 188-193.

Beauchamp, C. and Fridovich, I. (1971) Electrophoretic detection of ascorbate oxidase activity by photoreduction of nitroblue tetrazolium. *Anal Biochem*, **44**, 276-287.

Bernal, M., Casero, D., Singh, V., Wilson, G. T., Grande, A., Yang, H., Dodani, S. C., Pellegrini, M., Huijser, P., Connolly, E. L., Merchant, S. S. and Krämer, U. (2012) Transcriptome sequencing identifies SPL7-regulated copper acquisition genes *FRO4*/*FRO5* and the copper dependence of iron homeostasis in *Arabidopsis*. *Plant Cell*, **24**, 738-761.

Bowler, C., Van Camp, W., Van Montagu, M., Inzé, D. and Asada, K. (1994) Superoxide dismutase in plants. *Crit Rev Plant Sci*, **13**, 199 - 218.

Burkhead, J., Reynolds, K., Abdel-Ghany, S., Cohu C. and Pilon, M. (2009) Copper homeostasis. *New Phytol*, **182**, 799 - 816.

Clemens, S. (2006) Toxic metal accumulation, responses to exposure and mechanisms of tolerance in plants. Biochimie *88*, 1707-1719.

Clemens, S., Antosiewicz, D. M., Ward, J. M., Schachtman, D. P. and Schroeder, J. I. (1998) The plant cDNA *LCT1* mediates the uptake of calcium and cadmium in yeast. *Proc Natl Acad Sci U S A*, **95**, 12043-12048.

Clough, S. J. and Bent, A. F. (1998) Floral dip: a simplified method for *Agrobacterium*-mediated transformation of *Arabidopsis thaliana*. *Plant J*, **16**, 735-743.

Cobbett, C. S. (2000) Phytochelatins and their roles in heavy metal detoxification. *Plant Physiol*, **123**, 825-832.

Cohen, C. K., Fox, T. C., Garvin, D. F. and Kochian, L. V. (1998) The role of iron-deficiency stress responses in stimulating heavy-metal transport in plants. *Plant Physiol*, **116**, 1063-1072.

Cohu, C. M., Abdel-Ghany, S. E., Gogolin Reynolds, K. A., Onofrio, A. M., Bodecker, J. R., Kimbrel, J. A., Niyogi, K. K. and Pilon, M. (2009) Copper delivery by the copper chaperone for chloroplast and cytosolic copper/zinc-superoxide dismutases: regulation and unexpected

phenotypes in an *Arabidopsis* mutant. *Mol Plant*, **2**, 1336-1350.
Cohu, C. M. and Pilon, M. (2007) Regulation of superoxide dismutase expression by copper availability. *Physiol Plant*, **129**, 747-755.
Connolly, E. L., Fett., J. P. and Guerinot, M.L. (2002) Expression of the IRT1 metal transporter is controlled by metals at the levels of transcript and protein accumulation. *Plant Cell*, **14**, 1347-1357.
Dancis, A., Haile, D., Yuan, D. S. and Klausner, R. D. (1994) Biochemical characterization, regulation by copper, and physiological role in copper uptake. *J Biol Chem*, **269**, 25660-25667.
Dancis, A., Yuan, D., Haile, D., Askwith, C., Eide, D., Moehle, C., Kaplan, J. and Klausner, R. (1994) Molecular characterization of a copper transport protein in *S. cerevisiae*: an unexpected role for copper in iron transport. *Cell*, **76**, 393 – 402.
Das, P., Samantaray, S. and Rout, G. R. (1997) Studies on cadmium toxicity in plants: A review. *Environ Poll*, **98**, 29-36.
Eide, D., Broderius, M., Fett J. and Guerinot, M. (1996). A novel iron-regulated metal transporter from plants identified by functional expression in yeast. *Proc Natl Acad Sci U S A*, **93**, 5624 - 5628.
Flohé, L. and Otting, F. (1984) Superoxide dismutase assays. Methods in Enzymology: Oxygen Radicals in Biological Systems. Ed. Packer L. (Academic, New York) vol. 105, pp. 93-104.
Garcia-Molina, A., Andrés-Colás, N., Perea-García, A., del Valle-Tascón, S., Peñarrubia, L. and Puig, S. (2011) The intracellular *Arabidopsis* COPT5 transport protein is required for photosynthetic electron transport under severe copper deficiency. *Plant J*, **65**, 848-860.
Geller, B. L. and Winge, D. R. (1984) Subcellular distribution of superoxide dismutases in rat liver. *Methods Enzymol*, **105**, 105-114.
Ghasemi, R., Ghaderian, S. M. and Krämer, U. (2009) Interference of nickel with copper and iron homeostasis contributes to metal toxicity symptoms in the nickel hyperaccumulator plant Alyssum inflatum. *New Phytol*, **184**, 566-580.
Grill, E., Winnacker, E. L. and Zenk, M. H. (1985) Phytochelatins: the principal heavy-metal complexing peptides of higher plants. Science *230*, 674-676.
Hasan, S.A., Fariduddin, Q., Ali, B., Hayat, S. and Ahmad, A. (2009) Cadmium: toxicity and tolerance in plants. *J Environ Biol*, **30**, 165-174.
Heo, D. H., Baek, I. J., Kang, H. J., Kim, J. H., Chang, M., Jeong, M. Y., Kim, T. H., Choi, I. D. and Yun, C. W. (2010) Cadmium regulates copper homoeostasis by inhibiting the activity of Mac1, a transcriptional activator of the copper regulon, in *Saccharomyces cerevisiae*. *Biochem J*, **431**, 257-265.
Higo, K., Ugawa, Y., Iwamoto, M. and Korenaga, T. (1999) Plant cis-acting regulatory DNA elements (PLACE) database: 1999. *Nucleic Acids Res*, **27**, 297-300.
Hirschi, K. D., Korenkov, V. D., Wilganowski, N. L. and Wagner, G. J. (2000) Expression of *Arabidopsis* CAX2 in tobacco. Altered metal accumulation and increased manganese tolerance. *Plant Physiol*, **124**, 125-133.
Jarup, L. (2003) Hazards of heavy metal contamination. *Br Med Bull*, **68**, 167-182.
Jefferson, R. A., Kavanagh, T. A. and Bevan, M. W. (1987) GUS fusions: beta-glucuronidase as a sensitive and versatile gene fusion marker in higher plants. *EMBO J*, **6**, 3901.
Jung, H. I., Gayomba, S. R., Rutzke, M. A., Craft, E., Kochian, L. V. and Vatamaniuk, O. K. (2012) COPT6 is a plasma membrane transporter that functions in copper homeostasis in *Arabidopsis* and is a novel target of SQUAMOSA Promoter Binding Protein-Like 7. *J Biol*

Chem, **287**, 33252-33267.
Kampfenkel, K., Kushnir, S., Babiychuk, E., Inze, D. and Van Montagu, M. (1995) Molecular characterization of a putative *Arabidopsis thaliana* copper transporter and its yeast homologue. *J Biol Chem*, **270**, 28479-28486.
Klaumann, S., Nickolaus, S. D., Fürst, S. H., Starck, S., Schneider, S., Ekkehard Neuhaus, H. and Trentmann, O. (2011) The tonoplast copper transporter COPT5 acts as an exporter and is required for interorgan allocation of copper in *Arabidopsis thaliana*. *New Phytol*, **192**, 393-404.
Kliebenstein, D. J., Monde, R.-A. and Last, R. L. (1998) Superoxide dismutase in *Arabidopsis*: an eclectic enzyme family with disparate regulation and protein localization. *Plant Physiol*, **118**, 637-650.
Kropat, J., Tottey, S., Birkenbihl, R. P., Depage, N., Huijser, P. and Merchant, S. (2005) A regulator of nutritional copper signaling in *Chlamydomonas* is an SBP domain protein that recognizes the GTAC core of copper response element. *Proc Natl Acad Sci U S A*, **102**, 18730-18735.
Küpper, H. and Kochian, L. V. (2010) Transcriptional regulation of metal transport genes and mineral nutrition during acclimatization to cadmium and zinc in the Cd/Zn hyperaccumulator, *Thlaspi caerulescens* (Ganges population) *New Phytol*, **185**, 114-129.
Lahner, B., Gong, J., Mahmoudian, M., Smith, E. L., Abid, K. B., Rogers, E. E., Guerinot, M. L., Harper, J. F., Ward, J. M., McIntyre, L., Schroeder, J. I. and Salt, D. E. (2003) Genomic scale profiling of nutrient and trace elements in *Arabidopsis thaliana*. *Nat Biotechnol*, **21**, 1215-1221.
Li, Z. S., Lu, Y. P., Zhen, R. G., Szczypka, M., Thiele, D. J. and Rea, P. A. (1997) A new pathway for vacuolar cadmium sequestration in *Saccharomyces cerevisiae*: YCF1-catalyzed transport of bis(glutathionato)cadmium. *Proc Natl Acad Sci U S A*, **94**, 42-47.
Morel, M., Crouzet, J., Gravot, A., Auroy, P., Leonhardt, N., Vavasseur, A. and Richaud, P. (2009) AtHMA3, a P1B-ATPase allowing Cd/Zn/Co/Pb vacuolar storage in *Arabidopsis*. *Plant Physiol*, **149**, 894-904.
Murashige T. and Skoog, F. (1962) A revised medium for rapid growth and bio assays with tobacco tissue cultures. *Physiol Plant*, **15**, 473-497.
Nelson, B. K., Cai, X. and Nebenführ, A. (2007) A multicolored set of in vivo organelle markers for co-localization studies in *Arabidopsis* and other plants. *Plant J*, **51**, 1126-1136.
Page, M. D., Kropat, J., Hamel, P. P. and Merchant, S. S. (2009) Two *Chlamydomonas* CTR copper transporters with a novel cys-met motif are localized to the plasma membrane and function in copper assimilation. *Plant Cell*, **21**, 928-943.
Palmer, C. M. and Guerinot, M. L. (2009). Facing the challenges of Cu, Fe and Zn homeostasis in plants. *Nat Chem Biol*, **5**, 333-340.
Park, J., Song, W. Y., Ko, D., Eom, Y., Hansen, T. H., Schiller, M., Lee, T. G., Martinoia, E. and Lee, Y. (2012) The phytochelatin transporters AtABCC1 and AtABCC2 mediate tolerance to cadmium and mercury. *Plant J*, **69**, 278-288.
Peña, M.M., Puig, S. and Thiele, D. J. (2000) Characterization of the *Saccharomyces cerevisiae* high affinity copper transporter Ctr3. *J Biol Chem*, **27**, 33244-33251.
Peñarrubia, L., Andrés-Colás, N., Moreno, J. and Puig, S. (2010) Regulation of copper transport in *Arabidopsis thaliana*: a biochemical oscillator? *J Biol Inorganic Chem*, **15**, 29 - 36.
Perea-García, A., Garcia-Molina, A., Andrés-Colás, N., Vera-Sirera, F., Pérez-Amador, M. A., Puig, S. and Peñarrubia, L. (2013) *Arabidopsis* copper transport protein COPT2 participates

in the cross talk between iron deficiency responses and low-phosphate signaling. *Plant Physiol*, **162**, 180-194.
Pfaffl, M. W., Horgan, G. W. and Dempfle, L. (2002) Relative expression software tool (REST) for group-wise comparison and statistical analysis of relative expression results in real-time PCR. *Nucleic Acids Res*, **30**, e36.
Prestridge, D. S. (1991) SIGNAL SCAN: a computer program that scans DNA sequences for eukaryotic transcriptional elements. *Comput Appl Biosci*, **7**, 203-206.
Puig, S., Andrés-Colás, N., Garcia-Molina, A. and Peñarrubia, L. (2007) Copper and iron homeostasis in *Arabidopsis*: responses to metal deficiencies, interactions and biotechnological applications. *Plant Cell Environ*, **30**, 271-290.
Puig, S., Lee, J., Lau, M. and Thiele, D. J. (2002) Biochemical and genetic analyses of yeast and human high affinity copper transporters suggest a conserved mechanism for copper uptake. *J Biol Chem*, **277**, 26021-26030.
Ravet, K. and Pilon, M. (2013) Copper and iron homeostasis in plants: the challenges of oxidative stress. *Antioxid Redox Signal*, **19**, 919-932.
Ravet, K., Danford, F. L., Dihle, A., Pittarello, M. and Pilon, M. (2011) Spatiotemporal analysis of copper homeostasis in *Populus trichocarpa* reveals an integrated molecular remodeling for a preferential allocation of copper to plastocyanin in the chloroplasts of developing leaves. *Plant Physiol*, **157**, 1300-1312.
Rees, E. M., Lee, J. and Thiele, D. J. (2004) Mobilization of intracellular copper stores by the ctr2 vacuolar copper transporter. *J Biol Chem*, **279**, 54221-54229.
Remans, T., Smeets, K., Opdenakker, K., Mathijsen, D., Vangronsveld, J. and Cuypers, A. (2008) Normalisation of real-time RT-PCR gene expression measurements in *Arabidopsis thaliana* exposed to increased metal concentrations. *Planta*, **227**, 1343-1349.
Robinson, N. J., Procter, C. M., Connolly, E. L. and Guerinot, M. L. (1999) A ferric-chelate reductase for iron uptake from soils. *Nature*, **397**, 694-697.
Salt, D. E., Prince, R. C., Pickering, I. J. and Raskin, I. (1995) Mechanisms of cadmium mobility and accumulation in Indian mustard. *Plant Physiol*, **109**, 1427-1433.
Sancenón, V., Puig, S., Mateu-Andres, I., Dorcey, E., Thiele, D. J. and Peñarrubia, L. (2004) The *Arabidopsis* copper transporter COPT1 functions in root elongation and pollen development. *J Biol Chem*, **279**, 15348-15355.
Sancenón, V., Puig, S., Mira, H., Thiele, D. J. and Peñarrubia, L. (2003) Identification of a copper transporter family in *Arabidopsis thaliana*. *Plant Mol Biol*, **51**, 577-587.
Sasaki, A., Yamaji, N., Yokosho, K. and Ma, J. F. (2012) Nramp5 is a major transporter responsible for manganese and cadmium uptake in rice. *Plant Cell*, **24**, 2155-2167.
Scott, A., Wyatt, S., Tsou, P. L., Robertson, D. and Allen, N. S. (1999) Model system for plant cell biology: GFP imaging in living onion epidermal cells. *Biotechniques*, **26**, 1125, 1128-1132.
Shikanai, T., Muller-Moule, P., Munekage, Y., Niyogi, K. K. and Pilon, M. (2003) PAA1, a P-type ATPase of *Arabidopsis*, functions in copper transport in chloroplasts. *Plant Cell*, **15**, 1333-1346.
Sommer, F., Kropat, J., Malasarn, D., Grossoehme, N. E., Chen, X., Giedroc, D. P. and Merchant, S. S. (2010) The CRR1 nutritional copper sensor in *Chlamydomonas* contains two distinct metal-responsive domains. *Plant Cell*, **22**, 4098-4113.
Stadtman, E. R. (1990) Metal ion-catalyzed oxidation of proteins: biochemical mechanism and biological consequences. *Free Radic Biol Med*, 9, 315-325.

Stohs, S. J. and Bagchi, D. (1995) Oxidative mechanisms in the toxicity of metal ions. *Free Radic Biol Med*, **18**, 321-336.

Sunkar, R., Kapoor, A. and Zhu, J.-K. (2006) Posttranscriptional induction of two Cu/Zn superoxide dismutase genes in *Arabidopsis* is mediated by downregulation of miR398 and important for oxidative stress tolerance. *Plant Cell*, **18**, 2051-2065.

Tapken, W., Ravet, K. and Pilon, M. (2012) Plastocyanin controls the stabilization of the thylakoid Cu-transporting P-type ATPase PAA2/HMA8 in response to low copper in *Arabidopsis*. *J Biol Chem*, **287**, 18544-18550.

Tzfira, T., Tian, G. W., Lacroix, B., Vyas, S., Li, J., Leitner-Dagan, Y., Krichevsky, A., Taylor, T., Vainstein, A. and Citovsky, V. (2005) pSAT vectors: a modular series of plasmids for autofluorescent protein tagging and expression of multiple genes in plants. *Plant Mol Biol*, **57**, 503-516.

Udvardi, M. K., Czechowski, T. and Scheible, W.-R. (2008) Eleven golden rules of quantitative RT-PCR. *Plant Cell*, **20**, 1736-1737.

Valko, M., Morris, H. and Cronin, M. T. (2005) Metals, toxicity and oxidative stress. *Curr Med Chem*, **12**, 1161-1208.

Vatamaniuk, O. K., Mari, S., Lu, Y. P. and Rea, P. A. (2000) Mechanism of heavy metal ion activation of phytochelatin (PC) synthase: blocked thiols are sufficient for PC synthase-catalyzed transpeptidation of glutathione and related thiol peptides. *J Biol Chem*, **275**, 31451-31459.

Vert, G., Grotz, N., Dedaldechamp, F., Gaymard, F., Guerinot, M. L., Briat, J.-F. and Curie, C. (2002) IRT1, an *Arabidopsis* transporter essential for iron uptake from the soil and for plant growth. *Plant Cell*, **14**, 1223-1233.

Weigel, M., Varotto, C., Pesaresi, P., Finazzi, G., Rappaport, F., Salamini, F. and Leister, D. (2003) Plastocyanin is indispensable for photosynthetic electron flow in *Arabidopsis thaliana*. *J Biol Chem*, **278**, 31286-31289.

Wong, C. K. and Cobbett, C. S. (2009) HMA P-type ATPases are the major mechanism for root-to-shoot Cd translocation in *Arabidopsis thaliana*. *New Phytol*, **181**, 71-78.

Yamasaki, H., Abdel-Ghany, S. E., Cohu, C. M., Kobayashi, Y., Shikanai, T. and Pilon, M. (2007) Regulation of copper homeostasis by micro-RNA in *Arabidopsis*. *J Biol Chem*, **282**, 16369-16378.

Yamasaki, H., Hayashi, M., Fukazawa, M., Kobayashi, Y. and Shikanai, T. (2009) SQUAMOSA Promoter Binding Protein-Like7 is a central regulator for copper homeostasis in *Arabidopsis*. *Plant Cell*, **21**, 347-361.

Yuan, M., Li, X., Xiao, J. and Wang, S. (2011) Molecular and functional analyses of COPT/Ctr-type copper transporter-like gene family in rice. *BMC Plant Biol*, **11**, 69.

CHAPTER IV

Brachypodium distachyon as a Model System for Studies of Copper Transport in Cereal Crops

Abstract

Copper (Cu) is an essential micronutrient that performs a remarkable array of functions in plants including photosynthesis, cell wall remodeling, flowering, and seed set. Of the world's major cereal crops, wheat, barley, and oat are the most sensitive to Cu deficiency. Cu deficient soils include alkaline soils, which occupy approximately 30% of the world's arable lands, and organic soils that occupy an estimated 19% of arable land in Europe. We used *Brachypodium distachyon* (brachypodium) as a proxy for wheat and other grain cereals to initiate analyses of the molecular mechanisms underlying their increased susceptibility to Cu deficiency. In this report, we focus on members of the CTR/COPT family of Cu transporters because their homologs in *A. thaliana* are transcriptionally upregulated in Cu-limited conditions and are involved either in Cu uptake from soils into epidermal cells in the root, or long-distance transport and distribution of Cu in photosynthetic tissues. We found that of five COPT proteins in brachypodium, BdCOPT3 and BdCOPT4 localize to the plasma membrane and are transcriptionally upregulated in roots and leaves by Cu deficiency. We also found that BdCOPT3, BdCOPT4, and BdCOPT5 confer low affinity Cu transport, in contrast to their counterparts in *A. thaliana* that confer high affinity Cu transport. These data suggest that increased sensitivity to Cu deficiency in some grass species may arise from lower efficiency and, possibly, other properties of components of Cu uptake and tissue partitioning systems and reinforce the importance of using brachypodium as a model for the comprehensive analyses of Cu homeostasis in cereal crops.

Introduction

Copper (Cu) is an essential micronutrient for all organisms because it acts as a cofactor for enzymes participating in important biological processes such as respiration, photosynthesis, and scavenging of oxidative stress (Burkhead et al*.,* 2009, Merchant 2010, Ravet and Pilon 2013). In addition to these functions, plants also employ Cu for the perception of ethylene, nitrogen metabolism, molybdenum cofactor synthesis, cell wall remodeling, response to pathogens, flowering, and seed set (Burkhead et al*.,* 2009, Marschner 1995, Mendel and Kruse 2012, Ravet and Pilon 2013, Shorrocks and Alloway 1988). This remarkable array of functions is attributed to the ability of Cu to change its oxidation state ($Cu^{2+} \leftrightarrow Cu^{+}$). However, the same property imposes toxicity when free Cu ions accumulate in cells in excess because of their ability to promote oxidative stress (Valko et al*.,* 2005). Copper availability, and thus crop productivity on agricultural soils depend on soil type and agricultural practices (Marschner 1995, Shorrocks and Alloway 1988, Solberg et al*.,* 1999). For example, Cu deficiency develops on alkaline soils due to low solubility of Cu at high pH, and on organic soils due to Cu binding to organic matter (Marschner 1995, Shorrocks and Alloway 1988, Solberg et al*.,* 1999). While Cu deficiency can be remedied by the application of Cu-based fertilizers, this strategy is not environmentally friendly, and the repeated use of fertilizers, as well as Cu-based pesticides, has led to the build-up of toxic levels of Cu in soils (Marschner 1995, Shorrocks and Alloway 1988). In this regard, organic farming has emerged as a preferred production system that relies on using natural fertilizers; however natural fertilizers increase soil organic matter and thus, further reduce Cu bioavailability. Sensitivity to Cu bioavailability in soils varies among crops species. Of the major cereal crops, wheat is regarded as the most sensitive to Cu deficiency (Shorrocks and Alloway 1988, Solberg et al*.,* 1999). In contrast, crops like canola have not shown Cu deficiency

symptoms or responded to Cu fertilizer when grown on soils that would cause Cu deficiency in wheat or barley (Solberg et al., 1999). Higher sensitivity of some cereal crops to Cu deficiency compared to other crop species has been recognized in farm reports and fact sheets from some states in the United States and different countries in the world. Among the major cereal crops, sensitivity to Cu deficiency is reported to be in the following rank order, from greater sensitivity to least sensitive: winter wheat > spring wheat > flax > barley > oats > triticale > rye (Shorrocks and Alloway 1988, Solberg et al., 1999). Remarkably, the molecular mechanisms that underlie this tendency are unknown.

Plants tightly regulate Cu homeostasis to prevent deficiency while avoiding toxicity. This regulation includes transcriptional control of genes encoding proteins that are involved in Cu uptake, trafficking, tissue partitioning, and reallocation among Cu requiring enzymes. Of known Cu transporters, members of the CTR/COPT family are among the main contributors to initial Cu uptake in plants, the green alga *Chlamydomonas reinhardtii,* yeast, *Drosophila*, and humans (Merchant 2010, Nevitt et al., 2012, Ravet and Pilon 2013). The plant CTR/COPT family is best characterized in *Arabidopsis thaliana* and *Oryza sativa*, where it is represented by six and seven members, respectively (Peñarrubia et al., 2010, Yuan et al., 2011). *A. thaliana* COPT1, COPT2, and COPT6 are transcriptionally regulated by Cu deficiency, localize to the plasma membrane, mediate Cu uptake, and complement the growth defect of the *S. cerevisiae* Cu uptake mutant lacking functional Cu transporters, Ctr1p, Ctr2p, and Ctr3p (*ctr1ctr3* or *ctr1ctr2ctr3*) (Andrés-Colás et al., 2010, Garcia-Molina et al., 2013, Gayomba et al., 2013, Jung et al., 2012, Perea-García et al., 2013, Sancenón et al., 2004). COPT1 and COPT2 function primarily in Cu uptake into the root, while COPT6 also contributes to Cu partitioning in photosynthetic tissues (Garcia-Molina et al., 2013, Jung et al., 2012). In contrast, COPT5 localizes to the tonoplast and the pre-

vacuolar compartment and functions by remobilizing Cu from these organelles during Cu deficiency (Garcia-Molina et al., 2011, Klaumann et al., 2011). CTR/COPT proteins homotrimerize to form a pore within the membrane to transport Cu across the lipid bilayer, but can also form heterocomplexes with other CTR/COPT family members and/or other proteins (De Feo et al., 2009, Lee et al., 2002, Yuan et al., 2010, Yuan et al., 2011). Studies in *A. thaliana* have shown that while COPT6 interacts with COPT1, this interaction is not required for the ability of COPT6 or COPT1 to complement the Cu uptake deficiency phenotype of the *S. cerevisiae ctr1ctr2ctr3* mutant strain (Jung et al., 2012). Unlike CTR/COPT transporters from *A. thaliana,* CTR/COPT transporters from *O. sativa* complement the Cu uptake mutant of yeast only when are co-expressed with another OsCOPT member, and OsCOPT7 is the only high-affinity Cu transporter in the *O. sativa* CTR/COPT family (Yuan et al., 2010, Yuan et al., 2011). These findings suggest that some properties of CTR/COPT transporters are distinct between grass and non-grass species. These differences are not entirely surprising, given that *A. thaliana* is only distantly related to the *Poaceae* family and lacks many biological features of monocotyledonous grass crops (Brkljacic et al., 2011).

A member of the grass species, *Brachypodium distachyon* (from then on referred to as brachypodium) has emerged as a valuable experimental model for the study of small-grain cereals due to its less complex and fully sequenced genome, the continued development of numerous genetic resources, including efficient protocols for *Agrobacterium*-mediated transformation (Vogel and Hill 2008), whole genome TILLING mutant alleles (Brkljacic et al., 2011, Thole et al., 2012), a T-DNA insertion mutant collection (http://brachypodium.pw.usda.gov/TDNA/ [Bragg et al., 2012]), as well as other attributes such as short life cycle (8-12 weeks), small stature (15-20 cm), diploid accessions, self-fertility, and

simple growth requirements (Brkljacic et al., 2011). Because brachypodium and wheat grains have similar structure, brachypodium is an attractive model for molecular, genetic, and genomic studies of Cu homeostasis of wheat (Brkljacic et al., 2011, Mochida et al., 2011, Mur et al., 2011). Furthermore, root anatomy of brachypodium and wheat is similar and is distinct from the root anatomy of another *Poaceae* family member, *O. sativa*, which is specialized for overcoming anaerobic conditions associated with submerged roots, and thus, it is suggested that brachypodium and wheat may have similar root-related genes, including those that are involved in mineral ion uptake (Chochois et al., 2012). Hence, brachypodium becomes a preferred model for studies of ion homeostasis, as was recently demonstrated by the analyses of brachypodium Yellow Stripe-Like (YSL) proteins, which are involved in uptake and internal translocation of iron (Fe)(Yordem et al., 2011).

Members of the CTR/COPT family of Cu transporters are the best characterized in both *A. thaliana* and rice, but corresponding members in brachypodium have not yet been characterized, and are not fully annotated, according to database collections such as the National Center for Biotechnology Information (NCBI, http://www.ncbi.nlm.nih.gov/). In contrast, a specialized database for *A. thaliana* membrane proteins, ARAMEMNON 7.0 (http://aramemnon.botanik.uni-koeln.de/ [Schwacke et al., 2003]) has a more complete annotation of putative membrane proteins of *A. thaliana* and provides their homologs from other species, including brachypodium, based on amino acid similarity and motif organization. According to *in silico* predictions using ARAMEMNON 7.0, we have identified five putative CTR/COPT family members in brachypodium and provided the initial characterization of their function in Cu homeostasis. We have also developed growth conditions for studies of Cu homeostasis in brachypodium as a model for small grain cereals and established protocols for the isolation and transfection of

protoplasts isolated from brachypodium mesophyll cells. We used these procedures, along with functional complementation assays in the *S. cerevisiae ctr1ctr2ctr3* mutant strain, gene expression analyses, and yeast-two-hybrid assays of protein-protein interactions to study members of the CTR/COPT family of Cu transporters in brachypodium.

Results

The predicted COPT transporters of brachypodium share conserved features of the CTR/COPT family

To identify putative members of the CTR/COPT family in brachypodium, we used the Plant Membrane Protein database, ARAMEMNON 7.0 (http://aramemnon.botanik.uni-koeln.de/ [Schwacke et al*.,* 2003]), which has the most complete annotation of putative CTR/COPT transporters based on amino acid similarity and motif organization of CTR/COPT proteins in different species. We found that the brachypodium genome possesses five genes that encode putative CTR/COPT transporters *Bradi1g24180*, *Bradi1g24190*, *Bradi2g51210*, *Bradi4g31330*, *Bradi5g09580,* designated *COPT1* through *COPT5* (*alias BdCOPT1-BdCOPT5*) (Table 1). *BdCOPT1* and *BdCOPT2* are located on chromosome 1, while *BdCOPT3*, *BdCOPT4*, and *BdCOPT5* are found on chromosome 2, 4, and 5, respectively (Table 1).

Table 1. The proposed nomenclature and accession numbers of putative brachypodium COPT transporters annotated at different databases.

Suggested nomenclature	MIPS/ ARAMEMNON	NCBI	UniPROT	Chromosome
BdCOPT1	*Bradi1g24180*	*not annotated*	*I1GT99*	I
BdCOPT2	*Bradi1g24190*	*not annotated*	*I1GTA0*	I
BdCOPT3	*Bradi2g51210*	*XP_003569917.1*	*I1HS28*	II
BdCOPT4	*Bradi4g31330*	*XP_003578182.1*	*I1IQG8*	IV
BdCOPT5	*Bradi5g09580*	*not annotated*	*I1IXK4*	V

Based on the *BdCOPT* gene structures in the ARAMEMNON 7.0 database, *BdCOPT1*, *BdCOPT3, BdCOPT4*, and *BdCOPT5* lack introns, similar to *COPT* genes in rice (Yuan et al*.,*

2011) and *A. thaliana* (http://arabidopsis.org). In contrast, *BdCOPT2* possesses two introns (Figure 1A).

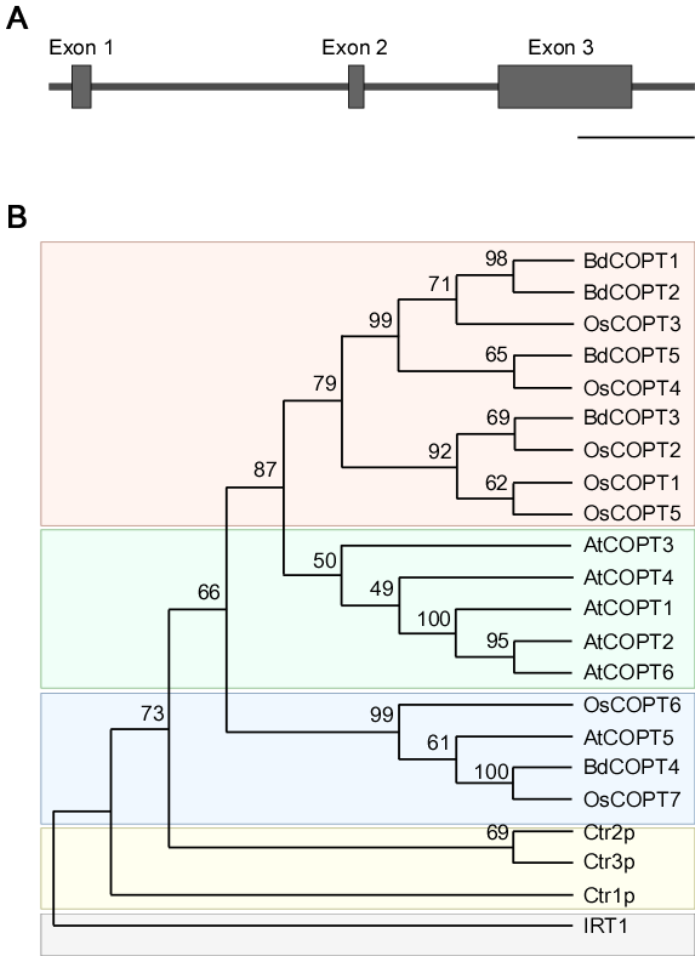

Figure 1. Gene structure of *BdCOPT2* and phylogenetic analysis of the brachypodium COPT family. (A) Gene structure of *BdCOPT2*. Note the presence of introns, which are absent in other plant CTR/COPT members. Scale bar = 500 bp. (**B**) A phylogenetic tree of CTR/COPT members of *A. thaliana* (designated as AtCOPT1-6), *O. sativa* (designated as OsCOPT1-7), brachypodium (designated as BdCOPT1-5), and *S. cerevisiae* (designated as Ctr1p-CTR3p). The *A. thaliana* protein, IRT1, is included as an outgroup.

BdCOPTs share 16% to 69% amino acid sequence identity and 30% to 73% sequence similarity to each other (Table 2). Phylogenetic analysis revealed that a majority of CTR/COPT proteins from brachypodium and *O. sativa* cluster together and are separate from CTR/COPTs from *A. thaliana* (Figure 1B). One exception is BdCOPT4, which forms a separate cluster along with AtCOPT5, OsCOPT7, and OsCOPT6 (Figure 1B). BdCOPT4 is highly similar (65%) to

AtCOPT5, whereas other BdCOPT proteins share 38% to 54% similarity to their counterparts in *A. thaliana* (Table 3). Similar to *OsCOPT* members (Yuan et al*.,* 2011), the nucleotide sequence of *BdCOPT* genes are GC-rich, ranging from GC content of 67.9% (*BdCOPT2*) to 73.2% (*BdCOPT3*), in contrast to an average GC content of 50% in *A. thaliana COPT*s.

Table 2. **Percentage of amino acid identity (similarity) among putative COPT proteins in brachypodium.**

	BdCOPT1	**BdCOPT2**	**BdCOPT3**	**BdCOPT4**	**BdCOPT5**
BdCOPT1	100 (100)	69 (73)	40 (48)	21 (30)	43 (51)
BdCOPT2	-	100 (100)	34 (42)	16 (26)	38 (46)
BdCOPT3	-	-	100 (100)	27 (35)	42 (50)
BdCOPT4	-	-	-	100 (100)	31 (42)
BdCOPT5	-	-	-	-	100 (100)

Table 3. **Amino acid length (aa length), molecular mass (shown in kDa), and percentage of amino acid identity (similarity) of putative brachypodium COPT (BdCOPT1-5) transporters in comparison to their homologues in *A. thaliana* (AtCOPT1-6).**

	aa length/ kDa	**AtCOPT1**	**AtCOPT2**	**AtCOPT3**	**AtCOPT4**	**AtCOPT5**	**AtCOPT6**
BdCOPT1	183/18.8	40.0 (47.1)	36.7 (47.5)	38.4 (49.0)	34.5 (43.4)	28.1 (41.8)	42.8 (54.5)
BdCOPT2	214/22.5	35.9 (44.7)	34.2 (45.6)	36.4 (47.0)	33.1 (46.2)	26.0 (38.4)	41.4 (53.8)
BdCOPT3	162/16.6	41.4 (53.7)	40.5 (53.8)	36.4 (48.3)	34.5 (48.3)	30.8 (40.4)	43.4 (53.8)
BdCOPT4	151/15.8	31.1 (45.0)	29.8 (44.4)	29.1 (42.4)	26.9 (38.6)	57.5 (65.1)	31.0 (44.1)
BdCOPT5	159/16.3	42.1 (51.6)	38.0 (46.2)	39.7 (51.0)	34.5 (45.5)	28.1 (39.7)	40.7 (52.4)

CTR/COPT family members possess conserved structural features that include three putative transmembrane helices (TMs), the N- and C-termini located towards the extracellular space and cytosol respectively, N-terminally-located methionine-rich motifs (Mets motifs), and M*XXX*M-X_{12}-G*XXX*G motifs located within TM2 and TM3, respectively (De Feo et al*.,* 2007, De Feo et al*.,* 2009, Peñarrubia et al*.,* 2010, Puig et al*.,* 2002). Importantly, M*XXX*M motifs of TM2 in Ctr1p of *S. cerevisiae,* and COPT2 and COPT6 of *A. thaliana* contain a positionally conserved Met residue that is essential for the ability of these proteins to transport Cu (Gayomba et al*.,* 2013, Jung et al*.,* 2012, Puig et al*.,* 2002). Some CTR/COPT proteins also contain the C-terminal

cysteine-rich C*X*C motif, which is suggested to bind Cu ions for transfer to cytosolic Cu chaperones, or to downregulate Ctr1p activity in response to toxic Cu levels (Puig et al*.,* 2002, Wu et al*.,* 2009, Xiao et al*.,* 2004). This motif is present in *A. thaliana* COPT1 and COPT2, but is absent in COPT6; nevertheless, COPT6 is a functional Cu transporter (Jung et al*.,* 2012).

Computer algorithm-assisted analysis of membrane topology and motif organization in brachypodium CTR/COPT proteins revealed that all BdCOPTs, except for BdCOPT3, are predicted to contain the classical three TMs (Figure 2) with N-terminal domains oriented towards the extracellular space, while C-terminal domains are predicted to be located in the cytosol. In contrast, BdCOPT3 is predicted to have two transmembrane domains, with both N- and C-termini located in the cytosol. While polypeptides of all BdCOPT included the N-terminal Mets motifs, the distribution of M*XXX*M-X_{12}-G*XXX*G motifs varied within different BdCOPT polypeptides (Figure 2). For example, M*XXX*M motifs and thus, positionally conserved essential Met residues, were located within TM2 in BdCOPT3, BdCOPT4 and BdCOPT5, but outside of TM2 in BdCOPT1 and BdCOPT2. Although the predicted membrane topology of BdCOPT proteins has to be validated experimentally, the location of essential positionally conserved Met residues of the M*XXX*M motif outside of the predicted membrane domain suggest that BdCOPT1 and BdCOPT2 might not mediate Cu transport. The C-terminal C*X*C motif is present in BdCOPT3 as a CC motif and in BdCOPT4 as a C*X*C motif, but is absent in BdCOPT1, BdCOPT2, and BdCOPT5 (Figure 2).

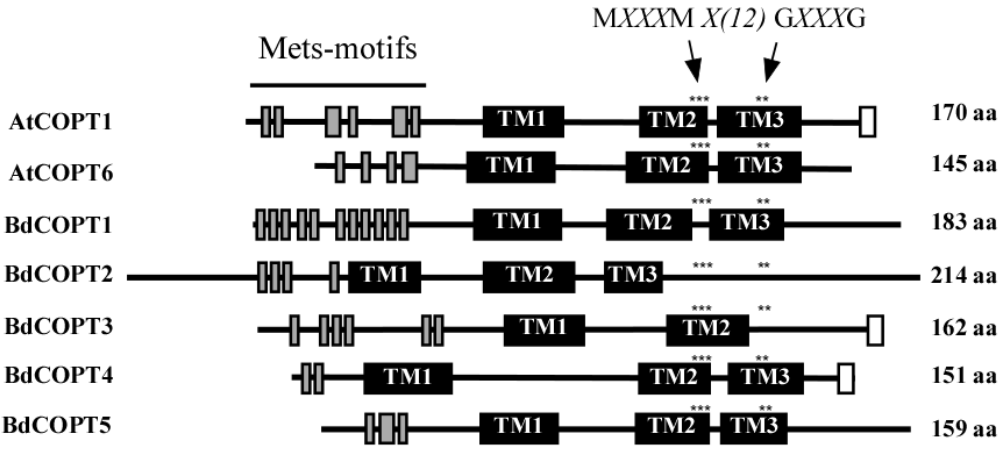

Figure 2. A diagram showing conserved motifs within the primary sequence of BdCOPT proteins and their homologues in *A. thaliana,* AtCOPT1 and AtCOPT6. Topology predictions are based on the TMHMM software, version 1.0. Shown are methionine-rich motifs within the predicted N-terminal domain (**Mets-motifs**, gray bars), transmembrane domains (**TM1**, **TM2**, and **TM3**; black bars) and cysteine-rich motifs within the predicted C-terminal domain (white bars). Asterisks *** and ** indicate the location of conserved M*XXX*M and G*XXX*G motifs. Note that BdCOPT3 has a unique structure of two transmembrane domains and that BdCOPT3 and BdCOPT4 have cysteine-rich domains in the C-terminal domain.

BdCOPT3 and *BdCOPT4* respond transcriptionally to Cu status

To determine whether *BdCOPT* genes respond transcriptionally to Cu status of the plant like their counterparts in *A. thaliana* and *O. sativa*, we first developed growth conditions under which Cu limitation would minimally affect the growth and development of brachypodium. Seeds were germinated in perlite irrigated with a modified hydroponic medium supplemented with 0.25 μM $CuSO_4$ (Figure 3 and Methods) and grown for 7 days before transferring to hydroponic medium to grow further for 18 days under the following conditions: 1) control conditions (0.25 μM $CuSO_4$); 2) Cu limited conditions (0 μM $CuSO_4$); 3) Cu deficiency (0 μM $CuSO_4$ and supplemented with 500 μM of the Cu chelator, bathocuproine disulfonate (BCS); and 4) Cu excess (3 μM $CuSO_4$).

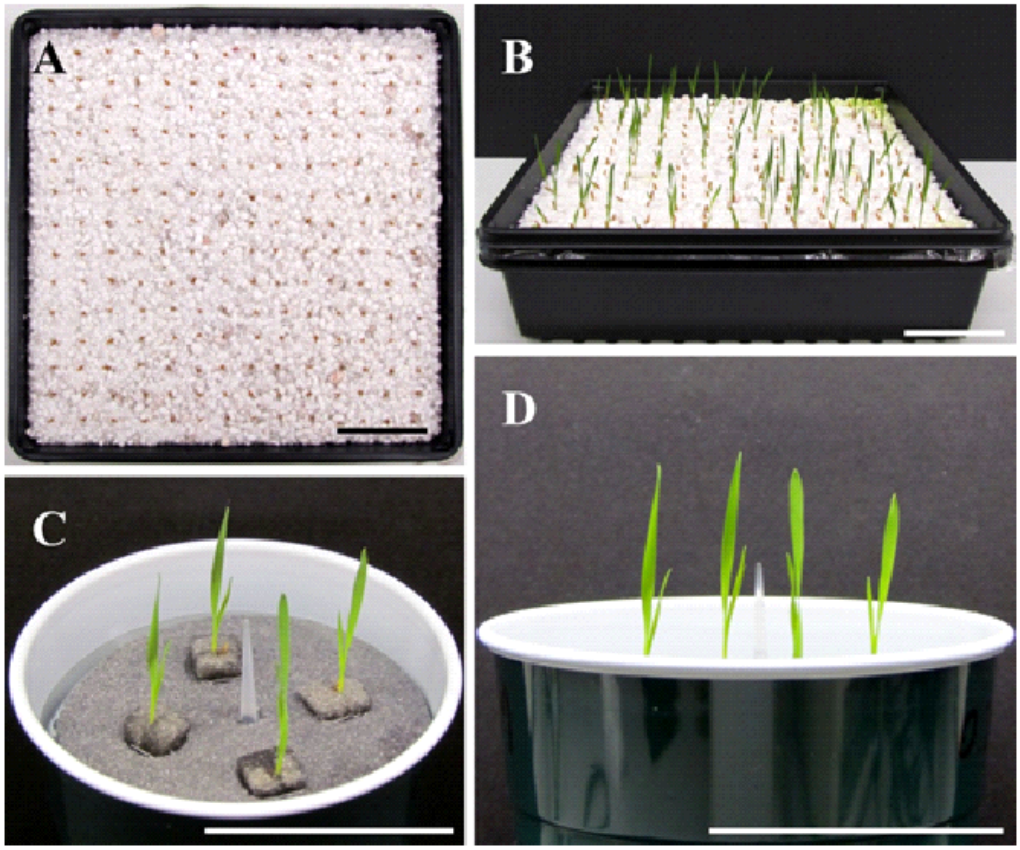

Figure 3. Establishing growth conditions for brachypodium. Plants were grown on the standard nutrient solution (see Table 1) at 22°C and 12-h light/12-h dark photoperiod at photosynthetic photon flux density of 150 µmol photons $m^{-2}s^{-1}$. The glume and lemma of seeds were removed and seeds were sown on rinsed perlite (**A**). Seven-day-old seedlings grown on perlite irrigated with standard nutrient solution (**B**). Seven-day-old seedlings were transferred from perlite to hydroponic medium and shown from above (**C**) and from the side view (**D**). Scale bar = 5 cm.

While there were no signs of chlorosis in leaves of plants grown under Cu deficiency or Cu excess (Figure 4A), plants grown under Cu deficiency had decreased height, and shoot and root dry weight compared to plants grown under control conditions (Figure 4B). Plants grown under Cu excess had decreased shoot and root dry weight, but were of the same height as control plants. Cu limitation did not significantly alter plant growth or shoot and root biomass (Figure 4B).

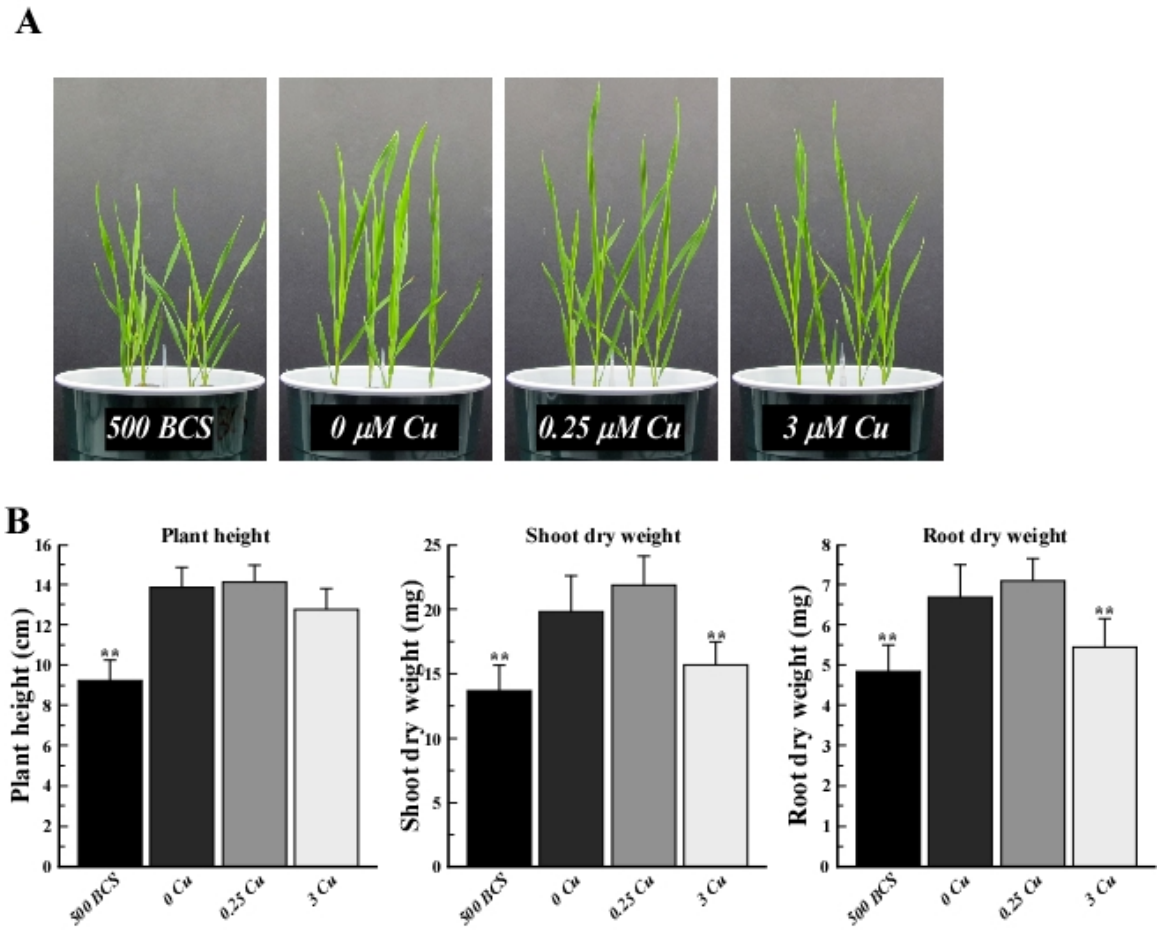

Figure 4. Phenotypes of brachypodium seedlings grown under different copper conditions. **(A)** Twenty five-day-old plants grown in hydroponic solution without $CuSO_4$ and supplemented with 500 μM BCS (**500 BCS**), or indicated concentrations of $CuSO_4$. (**B)** Plants from (A) were used to measure height (**Plant height**), shoot dry weight (**Shoot dry weight**) and root dry weight (**Root dry weight**). Asterisks (**) indicate statistically significant differences ($p \leq 0.01$, ANOVA) of the mean values of treatments compared to control conditions (0.25 μM $CuSO_4$). Error bars show S.D. (n = 3).

We then analyzed the steady-state levels of *BdCOPT* mRNAs in different plant tissues of brachypodium grown under the Cu regimes described above. Expression studies in roots (Figure 3A) revealed that Cu limitation increased mRNA expression of *BdCOPT3* and *BdCOPT4*. Cu deficiency increased *BdCOPT3* and *BdCOPT4* expression even further and, in addition, increased expression of *BdCOPT1*. There were no statistically significant differences in mRNA expression levels of *BdCOPT2* and *BdCOPT5* in root tissue of plants grown under these conditions (Figure 5A). In roots of plants grown under Cu toxicity, *BdCOPT4* was the only gene

whose expression was responsive to this treatment (Figure 5A). In young leaves (Figure 5B), Cu limitation elevated the abundance of *BdCOPT3* and *BdCOPT4* transcripts, which increased even further under Cu deficiency. In young leaves of plants grown under Cu toxicity, expression of *BdCOPT4* decreased, but expression of *BdCOPT2* increased. Expression studies in old leaves (Figure 5C) of plants grown in Cu limited or Cu deficient conditions showed an increase of the abundance of *BdCOPT3* and *BdCOPT4* transcripts. In contrast, both, Cu toxic and Cu limited conditions, increased expression of *BdCOPT1*, while expression of *BdCOPT2* and *BdCOPT5* were downregulated under Cu deficiency.

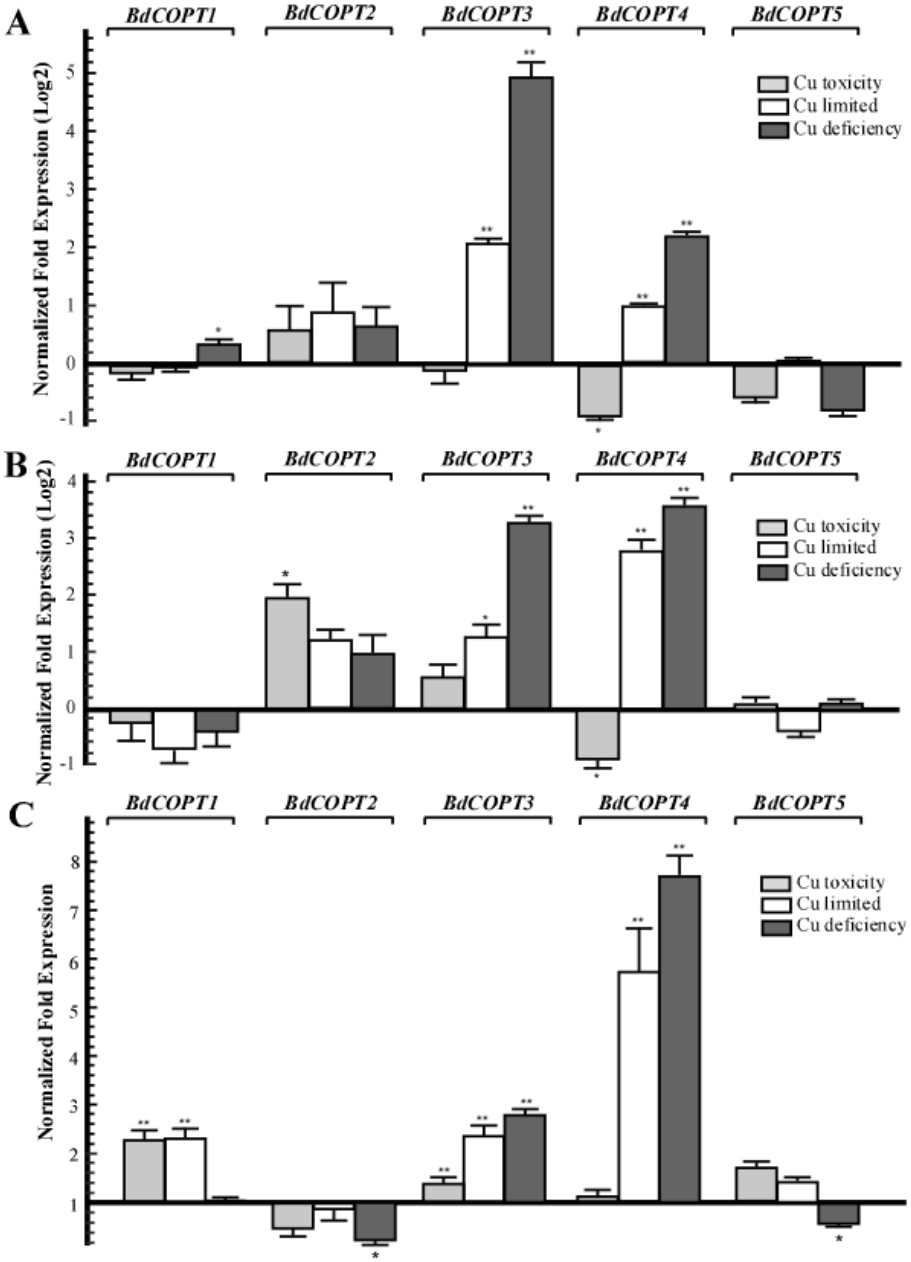

Figure 5. Quantitative real-time (qRT)-PCR analysis of the effect of copper on expression *COPT1* through *5* in roots (A), young leaves (B), and older leaves (C) of brachypodium. For all treatments, seven-day-old wild-type seedlings were transferred to hydroponic solutions and were grown for 18 days in medium that, in addition to macro- and micronutrients, contained either 0.25 μM $CuSO_4$ (control conditions), 0 μM $CuSO_4$ (**Cu limited**), 0 μM $CuSO_4$ + 500 μM BCS (**Cu deficiency**), or 3 μM $CuSO_4$ (**Cu toxicity**). Error bars show S.E. (n = 9). Differences of the mean values between control and treated plants are indicated as * ($p \leq 0.05$) or ** ($p \leq 0.001$). Results are presented relative to the expression of genes under control conditions.

To summarize, of five *BdCOPT* genes, *BdCOPT3* and *BdCOPT4*, are the most responsive to fluctuations in Cu availability, and changes in their expression are most prominent in roots and

young leaves. *BdCOPT2* is significantly upregulated under Cu toxicity only in young leaves, while *BdCOPT1* is regulated by Cu mainly in old leaves. Expression of *BdCOPT5* was the least responsive to Cu availability and was downregulated only by Cu deficiency and only in old leaves.

Heterologously expressed *BdCOPT3*, *BdCOPT4*, and *BdCOPT5* partially rescue growth defects of the *S. cerevisiae ctr1ctr2ctr3* copper uptake mutant on non-fermentable growth medium

We next tested whether BdCOPT proteins are involved in Cu transport. In this regard, the *S. cerevisiae ctr1ctr2ctr3* mutant, which lacks high-affinity plasma membrane-localized Cu uptake transporters Ctr1p and Ctr3p, and the vacuolar membrane-localized Ctr2p, is deficient in Cu uptake and release of Cu from the vacuole, and has been successfully used to identify Cu transport capabilities of CTR/COPT transporters from higher plants (Barhoom et al., 2008, Garcia-Molina et al., 2011, Gayomba et al., 2013, Johnson et al., 2007, Jung et al., 2012, Kampfenkel et al., 1995, Klaumann et al., 2011, Nagalakshmi et al., 2010, Yuan et al., 2010, Yuan et al., 2011, Zhang and Li 2013). Analyses of Cu transport capabilities using yeast as a heterologous system is based on the fact that cells lacking functional Cu uptake systems are unable to deliver Cu to cytochrome *c* oxidase in the mitochondrial respiratory chain, preventing cell growth on non-fermentable carbon sources such as glycerol and ethanol (YPEG medium), unless high concentrations of exogenous Cu are added to the growth medium (Dancis et al., 1994b, Glerum et al., 1996, Zhu et al., 2012). Therefore, we expected that if BdCOPT proteins act as high-affinity Cu transporters, then their expression in the *S. cerevisiae ctr1ctr2ctr3* mutant would promote Cu uptake and suppress growth defects of the mutant on non-fermentable

medium.

Here, we focused on analyses of BdCOPT1, BdCOPT3, BdCOPT4, and BdCOPT5 due to difficulty in cloning of BdCOPT2. As a positive control, we used the previously characterized CTR/COPT transporter from *A. thaliana*, AtCOPT6 (Jung et al., 2012). We found that all yeast lines grew at the same rates on standard medium (YNB-Ura) supplied with glucose as a carbon source or on YPEG medium supplemented with 100 μM $CuSO_4$ (Figure 6). In contrast, only the empty vector-expressing wild-type cells and *ctr1ctr2ctr3* cells expressing *AtCOPT6* grew well on YPEG medium (Figure 6), suggesting that none of BdCOPTs tested were able to rescue the growth defect of the *S. cerevisiae* mutant on YPEG medium. However, addition of a low concentration of Cu (10 μM $CuSO_4$) to YPEG medium allowed *BdCOPT3* (Figure 6B), *BdCOPT4* (Figure 6C) and *BdCOPT5* (Figure 6D) but not *BdCOPT1* (Figure 6A) to complement partially the growth defect of *ctr1ctr2ctr3* cells. These results suggest that transport capabilities of brachypodium COPT transporters differ from their counterparts in *A. thaliana*.

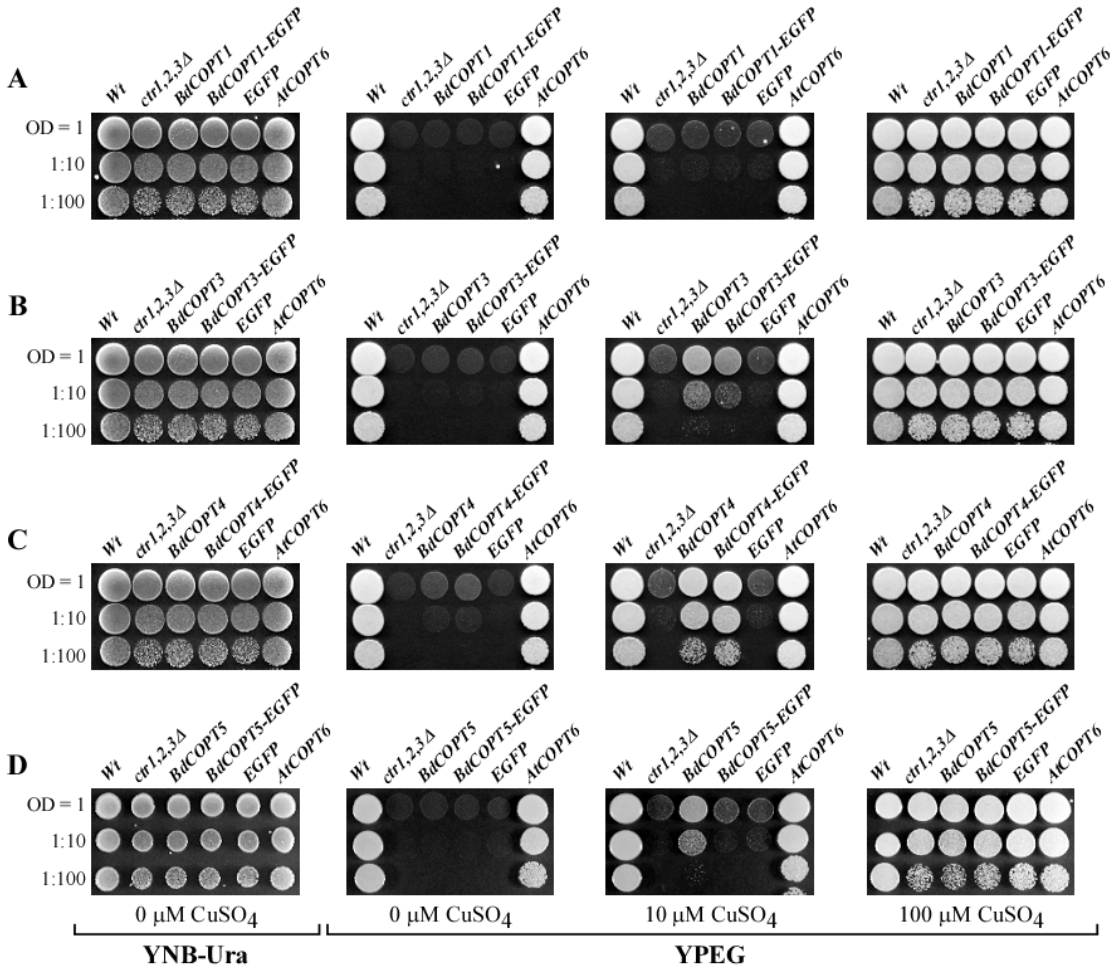

Figure 6. *BdCOPT3*, *BdCOPT4* and *BdCOPT5* rescue the growth defect of the *S. cerevisiae ctr1ctr2ctr3* triple mutant on ethanol/glycerol medium (YPEG). The *ctr1ctr2ctr3* mutant was transformed with the YES3-Gate vector harboring *BdCOPT1* (**A**), *BdCOPT3* (**B**), *BdCOPT4* (**C**), and *BdCOPT5* (**D**) along with corresponding EGFP-fusions and spotted onto YPEG plates supplemented with the indicated concentrations of $CuSO_4$. As negative controls, the *ctr1ctr2ctr3* mutant strain was transformed with the empty YES3-Gate (***ctr1,2,3*Δ**) or empty YES3-EGFP-Gate vector (**EGFP**). The isogenic wild-type, SEY6210, transformed with the empty YES3-Gate vector (**Wt**) and *ctr1ctr2ctr3* cells transformed with YES3-Gate harboring the *A. thaliana COPT6* (***AtCOPT6*)** cDNA insert were used as positive controls.

BdCOPT3 and BdCOPT4 localize to the plasma membrane in *S. cerevisiae* cells and brachypodium protoplasts.

S. cerevisiae Ctr1p and Ctr3p localize to the plasma membrane and contribute to Cu uptake into the cell (Dancis et al*.,* 1994a, Peña et al*.,* 2000), while Ctr2p localizes to the vacuolar membrane

and remobilizes Cu from this internal store upon Cu deficiency (Rees et al., 2004). To determine whether BdCOPTs rescue growth defects of the *S. cerevisiae ctr1ctr2ctr3* mutant by facilitating Cu uptake into the cell from the external medium or by vacuolar remobilization, we determined their subcellular localization in yeast cells as well as in brachypodium protoplasts.

For studies in *S. cerevisiae*, we inserted *BdCOPT3*, *BdCOPT4*, and *BdCOPT5* cDNAs without the stop codon into the YES3-EGFP-Gate vector to generate translational C-terminal EGFP fusions. We then verified whether the BdCOPT-EGFP constructs were functional by expressing them in the *ctr1ctr2ctr3* mutant and assessing the growth of transformed cells on YPEG media. We found that expression of BdCOPT3-, and BdCOPT4-EGFP fusions in *ctr1ctr2ctr3* cells resulted in growth phenotypes mirroring results of cells expressing un-tagged proteins (Figure 6B, C). However, the BdCOPT5-EGFP construct was unable to rescue growth of *ctr1ctr2ctr3* cells, suggesting that fusing EGFP with BdCOPT5 resulted in the loss of its activity (Figure 6D). Since unfunctional BdCOPT5-EGFP might mislocalize in yeast cells as well as in brachypodium protoplasts, this construct was omitted from subsequent study. We did not analyze the subcellular localization of BdCOPT1 for the same reason. Fluorescent microscopy revealed that EGFP-mediated fluorescence in BdCOPT3-EGFP and BdCOPT4-EGFP expressing cells localized mainly to the cell periphery and the distribution of the EGFP signal was distinct in *S. cerevisiae* cells expressing the EGFP-only vector (Figure 7). These data suggest that BdCOPT3 and BdCOPT4 localize to the plasma membrane in this heterologous system.

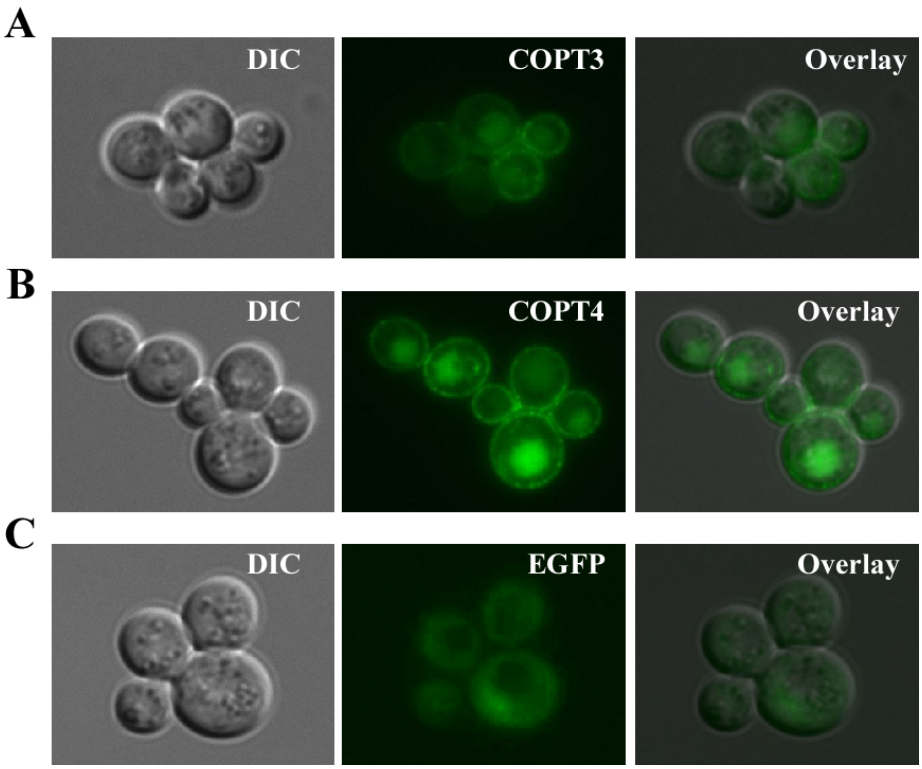

Figure 7. Subcellular localization of BdCOPT3-EGFP (A) or BdCOPT4-EGFP (B) fusions or EGFP (C) in *S. cerevisiae ctr1ctr2ctr3* cells. Superimposed images (**Overlay)** from differential interference contrast microscopy (**DIC**) and EGFP-mediated fluorescence (**EGFP**) show that BdCOPT3 and BdCOPT4 localize to the plasma membrane and that the pattern of fluorescence of EGFP-fused proteins is distinct from EGFP.

We next analyzed the subcellular localization of BdCOPT3 and BdCOPT4 in brachypodium using transient expression in protoplasts. After establishing a procedure for the isolation of viable protoplasts from brachypodium (Figure 8), we transfected protoplasts with BdCOPT3-EGFP or BdCOPT4-EGFP constructs with C-terminal EGFP fusions expressed from the CaMV promoter of the SAT-N1-EGFP-Gate vector, or with the empty SAT-N1-EGFP-Gate vector.

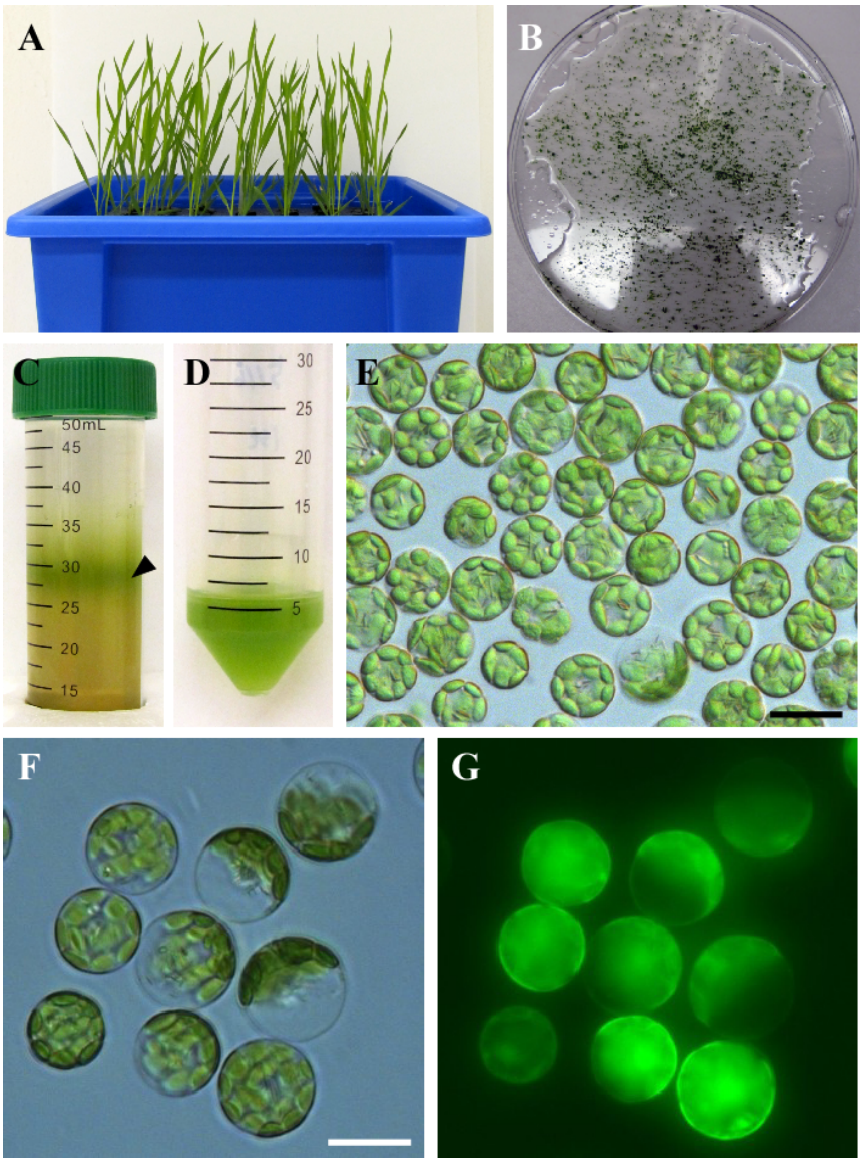

Figure 8. Isolation of protoplasts from brachypodium. Hydroponically grown 25-day-old plants (**A**) were used for the isolation of protoplasts from leaf tissue. Chopped brachypodium leaves in filter-sterilized TVL solution are shown in (**B**). Enzymatic digestion of the cell wall and fractionation by sucrose density gradient yielded protoplasts at the interface of the enzyme solution and W5 solution (**C**, black arrow). Protoplasts were collected and purified from sucrose density gradient solution (**D**) and visualized under microscopy using bright-field filter sets (**E**). In our method, 0.2 g of leaf tissue from 25-day-old seedlings yields 5×10^{6}-10^{7} protoplasts. Close-up of brachypodium protoplasts through bright-field (**F**) and FITC (**G**) filter sets to assess protoplast viability after staining with the membrane-permeable non-fluorescent dye, fluorescein diacetate. After diffusion into viable protoplasts fluorescein diacetate is hydrolyzed into a polar compound, causing the cytoplasm of the cell to fluoresce under the FITC filter set. Scale bar = 20 µm.

We found that EGFP-mediated fluorescence originating from BdCOPT3-EGFP or BdCOPT4-EGFP constructs was located at the periphery of transfected protoplasts and did not overlap with chlorophyll-mediated autofluorescence (Figure 9A, B and 11 3A, B). Furthermore, fluorescence from BdCOPT3- and BdCOPT4-EGFP constructs was distinct from the fluorescence pattern exhibited by protoplasts transfected with the empty EGFP vector (Figure 9C and Figure 10C). We note that internally-localized EGFP-mediated fluorescence is likely an artifact of the degradation of the BdCOPT-EGFPs. We then co-stained protoplasts expressing BdCOPT3- or BdCOPT4-EGFP with the lipophylic dye, FM4-64, which selectively labels the plasma membrane under low-temperature conditions (Vida and Emr 1995). We found strict co-localization of BdCOPT3- or BdCOPT4-EGFP and FM4-64-mediated fluorescence (Figure 9A, B), suggesting that BdCOPT3 and BdCOPT4 are located at the plasma membrane.

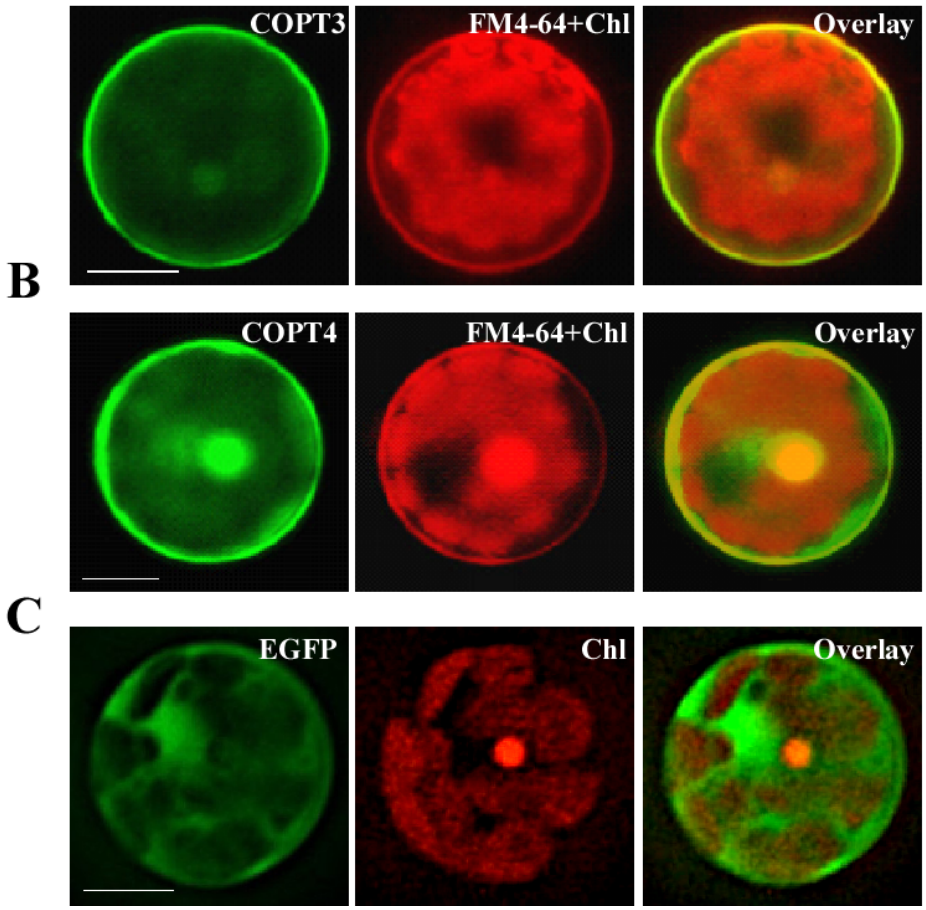

Figure 9. Subcellular localization of BdCOPT3 and BdCOPT4 in brachypodium protoplasts. Protoplasts isolated from leaves of 25-day-old plants were transfected with BdCOPT3-EGFP (**A**) or BdCOPT4-EGFP (**B**) constructs or the empty SAT6-N1-EGFP vector (**C**) and co-stained with the plasma-membrane dye, FM4-64. EGFP-mediated fluorescence derived from BdCOPT3-EGFP (**COPT3**) or BdCOPT4-EGFP**,** (**COPT4**)**,** or from EGFP of the SAT6-N1-EGFP vector (**EGFP**) was detected using the FITC filter set while FM4-64 (**FM4-64**) and chlorophyll autofluorescence (**Chl**) were visualized using the Rhodamine filter set of an Axio Imager M2 microscope equipped with a motorized Z-drive (Zeiss). Images collected from FITC and Rhodamine filter sets were overlaid (**Overlay**) to show the plasma membrane subcellular localization of the Cu transporters. Scale bar = 10 μm.

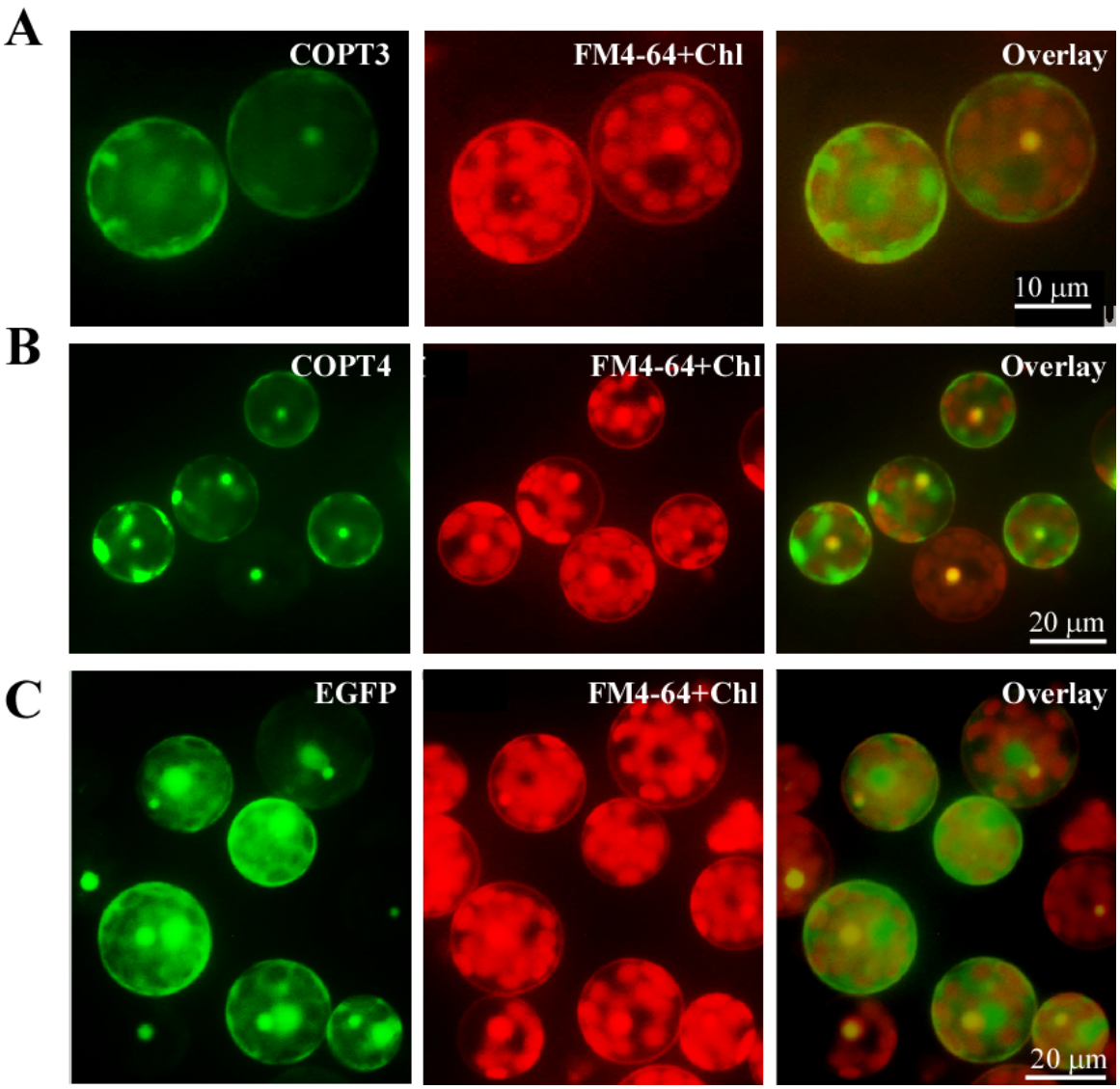

Figure 10. Subcellular localization of BdCOPT3 and BdCOPT4 in brachypodium protoplasts. Protoplasts were transfected with BdCOPT3-EGFP (**A**) or BdCOPT4-EGFP (**B**) constructs or empty SAT6-N1-EGFP vector (**C**) and co-stained with the plasma-membrane dye, FM4-64. EGFP-mediated fluorescence derived from BdCOPT3-EGFP (**COPT3**) or BdCOPT4-EGFP**,** (**COPT4**)**,** or from EGFP of the SAT6-N1-EGFP vector (**EGFP**) was detected using the FITC filter set while FM4-64 (**FM4-64**) and chlorophyll autofluorescence (**Chl**) were visualized using the Rhodamine filter set of an Axio Imager M2 microscope equipped with the motorized Z-drive (Zeiss). Images collected from FITC and Rhodamine filter sets were overlaid (**Overlay**) to show the plasma membrane subcellular localization of the Cu transporters.

BdCOPT proteins interact with each other in yeast-two-hybrid assays

Homo- and heterodimerization of CTR/COPT proteins have been demonstrated in eukaryotes (De Feo et al., 2007, De Feo et al., 2009, Lee et al., 2002, Yuan et al., 2010, Yuan et al., 2011).

Furthermore, although interaction of *A. thaliana* COPT6 with COPT1 is not required for the ability of these proteins to transport Cu (Jung et al*.,* 2012), the activity of *O. sativa* CTR/COPT proteins seem to depend on their interactions with each other (Yuan et al*.,* 2011). Therefore, we tested if the CTR/COPT family members in brachypodium would also interact with either themselves or/and with other family members. For this purpose we used the split-ubiquitin-based membrane yeast-two-hybrid (MYTH) approach (Kittanakom et al*.,* 2009). In this system, a modified ubiquitin protein is split into its C- and N-terminal halves (Cub and NubG, respectively), which are fused to membrane-localized bait or prey proteins, respectively. The C-terminus of ubiquitin is attached to an artificial transcription factor, PLV (**P**roteinA-**L**exA-**V**P16). If bait and prey proteins are oriented in the cytosol and interactions occur, the modified ubiquitin is reconstituted and recognized by ubiquitin-specific proteases, which release PLV from Cub. PLV enters the nucleus to induce expression of *lexA*-controlled reporter genes *ADE2*, *HIS3* and *lacZ* ((Kittanakom et al*.,* 2009), allowing protein interactions to be assessed by adenine and histidine prototrophy and by the β-galactosidase assay.

We fused Cub-PLV and NubG at the C-terminus of BdCOPT1, BdCOPT3, BdCOPT4, and BdCOPT5 since their predicted topology is consistent with a cytosolic orientation of their C-termini. We then co-expressed BdCOPT proteins in different combinations with themselves or with the empty Cub-PLV vector as a negative control (Figure 12). We included *S. cerevisiae* co-expressing AtCOPT6-Cub-PLV and AtCOPT6-NubG in our assays as a positive control since AtCOPT6 interacts with itself in the MYTH assay (Jung et al*.,* 2012). To control for false positives, the empty Cub-PLV vector was co-expressed with BdCOPTs fused to NubG. These studies showed that all of the tested BdCOPT proteins interacted in both homo- and heterodimer combinations, regardless of whether interactions were assayed by growth on selective medium or

with β-galactosidase (Figure 12). Whether these interactions are required for their ability to transport Cu remains to be elucidated.

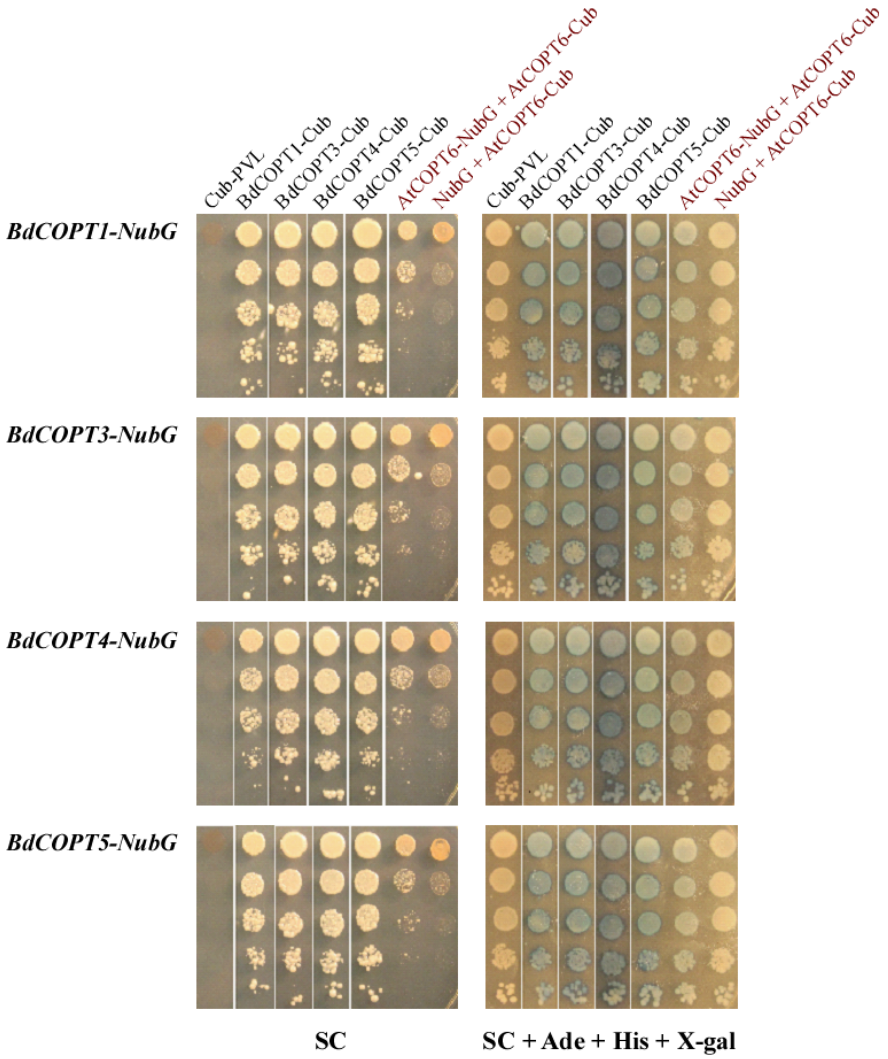

Figure 11. **Analyses of protein-protein interactions of brachypodium CTR/COPT transporters using the split-ubiquitin membrane yeast two-hybrid system (MYTH).** Shown are yeast cells co-expressing NubG constructs fused with *BdCOPT1*, *BdCOPT3*, *BdCOPT4* or *BdCOPT5* cDNA (***BdCOPT1-*, *BdCOPT3-*, *BdCOPT4-*, *BdCOPT5-NubG***) and a Cub-PLV construct lacking a cDNA insert (**Cub-PLV**) or Cub-PLV fused to *BdCOPT1-*, *BdCOPT3-*, *BdCOPT4-*, *BdCOPT5* (***BdCOPT1-*, *BdCOPT3-*, *BdCOPT4-*, *BdCOPT5-Cub***). Interactions were visualized by colony formation on selective media SC medium (**SC**) or as blue colonies in a ß-galactosidase assay (**SC + Ade + His + X-gal**). Growth was monitored for 2 days under conditions indicated below each panel. Interactions of AtCOPT6 with itself (**AtCOPT6-NubG + AtCOPT6-Cub**), or lack of interactions between *AtCOPT6-Cub-PLV* and the empty NubG vector (**NubG + AtCOPT6-Cub**) were used as controls and are indicated in red. Shown are representative results of at least three biological replicates. SC = synthetic complete medium; Ade = adenine; His = histidine; X-gal = bromo-chloro-indolylgalactopyranoside.

Discussion

Biological attributes of brachypodium, such as root architecture, grain structure, and the continued development of molecular and genetic resources prompted us to establish this plant as a preferred model for Cu homeostasis studies in grain cereals (*e.g.* wheat, barley and oat) which are reported to be more sensitive to Cu availability in agricultural soils in comparison to other crops (Shorrocks and Alloway 1988, Solberg et al*.,* 1999). To begin investigations of the underlying molecular basis of this phenomenon, we initiated studies of the brachypodium CTR/COPT Cu transporters since members of this family in *A. thaliana* provide an entry point for Cu into the root and are suggested to contribute to subsequent Cu partitioning in photosynthetic tissues (Burkhead et al*.,* 2009, Merchant 2010, Ravet and Pilon 2013). Towards this goal, we have identified five putative CTR/COPT family members in brachypodium based on amino acid similarity and motifs organization of CTR/COPT proteins in different species and we classified them as BdCOPT1 through 5. Phylogenetic analyses of the predicted CTR/COPT members in brachypodium and their counterparts from a dicot, *A. thaliana,* and a monocot, *O. sativa*, show that, with the exception of BdCOPT4, brachypodium and *O. sativa* CTR/COPT proteins are more closely related to each other than to *A. thaliana* (Figure 1B), reflecting a closer evolutionary relationship of brachypodium to *O.* sativa than to *A. thaliana*. Furthermore, analysis of membrane topology and the motif organization in brachypodium CTR/COPT proteins revealed that while polypeptides of all BdCOPT included the N-terminal Mets motifs, the location of M*XXX*M-X_{12}-G*XXX*G motifs varies within different BdCOPT polypeptides, affecting the location of the positionally conserved Met residue, which is essential for the translocation of Cu across lipid bilayer (Figure 2). For example, M*XXX*M motifs are predicted to be located within TM2 only in BdCOPT3, BdCOPT4, and BdCOPT5, similar to CTR/COPT family

members in other species. In contrast, M*XXX*M motifs are predicted to be located outside of TM2 in BdCOPT1 and BdCOPT2, suggesting that these proteins might not be able to mediate Cu transport due to a shift in the position of the essential Mets motifs. Although the topology predictions have to be validated experimentally, the ability of BdCOPT3, BdCOPT4, and BdCOPT5, but not BdCOPT1, to rescue partially the Cu-deficiency associated respiratory defects of the *S. cerevisiae ctr1ctr2ctr3* mutant (Figure 6) was consistent with this suggestion. We also note that BdCOPT3, BdCOPT4, and BdCOPT5 conferred growth to the yeast mutant only when a low concentration of Cu was added to the growth medium (Figure 6). This result might be interpreted using at least two not mutually exclusive scenarios: 1) BdCOPT3, BdCOPT4, and BdCOPT5 are low affinity Cu transporters, unlike their high-affinity counterparts from *A. thaliana* and/or 2) in order to confer high affinity transport, BdCOPT3, BdCOPT4, and/or BdCOPT5 must interact with other CTR/COPTs and/or other transporters. In this regard it has been shown that most of CTR/COPTs in *O. sativa* form dimers/trimers with other CTR/COPTs or other proteins to function as high-affinity transporters (Yuan et al*.,* 2010, Yuan et al*.,* 2011). In contrast, the plasma membrane-localized CTR/COPT family members from *A. thaliana* are high-affinity transporters by themselves even though can form hetero-complexes (Gayomba et al*.,* 2013, Jung et al*.,* 2012, Nakagawa et al*.,* 2010). We found that brachypodium CTR/COPT transporters homo- and heterooligomerize in the MYTH system (Figure 12); whether these interactions are required for transport capabilities of brachypodium CTR/COPTs has yet to be determined.

We have also examined the subcellular localization of BdCOPTs by analyzing the localization pattern of functional BdCOPT3-EGFP and BdCOPT4-EGFP constructs by heterologous expression in yeast or transient expression in brachypodium protoplasts. Towards

this goal we have established procedures for preparing viable protoplasts from brachypodium mesophyll cells and for protoplast transfection (Figure 8). These studies showed that both, BdCOPT3-EGFP and BdCOPT4-EGFP, localize to the plasma membrane, regardless of whether assays were done in yeast or protoplasts (Figures 7, 9, and10), further suggesting that these two CTR/COPT proteins may function in Cu uptake. Finally, BdCOPT3 and BdCOPT4 genes were highly expressed in roots, and old and young leaves, and their expression was tightly regulated by Cu availability (Figure 5), as was shown for other CTR/COPT proteins from different species, including plants.

To conclude, this manuscript shows that brachypodium can be used for analyses of the molecular mechanisms underlying the increased susceptibility of small grain cereals to Cu deficiency and of Cu homeostasis overall. Analyses of the phylogenetic relationship between CTR/COPT proteins of brachypodium, *O. sativa*, and *A. thaliana*, and the clear divergence of *A. thaliana* CTR/COPT members, suggest differences may exist in characteristics of the CTR/COPT proteins between monocots and dicots. This is further validated by studies of Cu transport capabilities of brachypodium CTR/COPTs. Heterologous expression of brachypodium CTR/COPTs in the *S. cerevisiae* Cu uptake mutant *ctr1ctr2ctr3* suggest that increased sensitivity to Cu deficiency in some grass species may arise from lower efficiency of Cu uptake and, possibly, other properties of components of Cu uptake and tissue partitioning systems. It is also possible that the CTR/COPT family members in brachypodium require homo- or heterooligomerization for high-affinity Cu uptake, unlike corresponding family members in *A. thaliana*, reinforcing the importance of using brachypodium as a model for the comprehensive analyses of Cu homeostasis in cereal crops.

Methods and Materials

Plant material and growth conditions

Seeds of the 21-3 inbred line of brachypodium (Vogel and Hill 2008) were sterilized in 100% ethanol for 1 min and rinsed 3 times with sterile water. The lamella and palea were softened by further incubation in sterile water for 2 h and removed with forceps, taking care not to damage the seed. Prepared seeds were then spread onto rinsed perlite irrigated with a standard hydroponic solution, described below. After stratification at 4°C for 24 h, plants were grown for 7 days at 22^{o}C; 12-h light/12-h dark photoperiod at photosynthetic photon flux density of 150 µmol photons $m^{-2}s^{-1}$ before transferring to a hydroponic solution prepared as described (Arteca and Arteca 2000) except that Cu (as $CuSO_4$) was added at a higher concentration of 0.25 µM. For Cu limitation and sensitivity assays, 7-day old seedlings were transferred from perlite to hydroponic solution supplemented with the indicated concentrations of $CuSO_4$, or without $CuSO_4$ but with the specific Cu chelator, bathocuproine disulfonate (BCS) (Rapisarda et al*.,* 2002). Plants were grown for 18 days before subsequent analyses. For all experiments, the hydroponic solution was changed every 7 days.

RNA extraction

Root and leaf tissues were separated from 25-day-old plants grown under the indicated conditions and flash-frozen in liquid nitrogen. Samples were homogenized in liquid nitrogen using a mortar and a pestle, and total RNA was isolated using the Plant RNA Kit (Omega Bio-Tek), according to the manufacturer's instructions. Genomic DNA in RNA samples was digested with DNAse *I* (Omega Bio-Tek) prior to cDNA synthesis using the iScript cDNA Synthesis kit (BioRad).

Quantitative real-time (qRT)-PCR analysis

Prior to qRT-PCR analysis, primers (Table 4) and cDNA concentrations were optimized to reach a qRT-PCR amplification efficiency of 100 ± 10%. Two microliters of 10-fold diluted cDNA was used as a template in a total reaction volume of 10 µl containing 500 nM of each PCR primer, 50 mM KCl, 20 mM Tris-HCl, pH 8.4, 0.2 mM dNTPs and 1.25 units of iTaq DNA polymerase in iQ SYBR Green Supermix (BioRad), containing 3 mM $MgCl_2$, SYBR Green I, 20 nM fluoresein, and stabilizers. PCR was carried out using the CFX96 Real-Time PCR system (BioRad). The thermal cycling parameters were as follows: denaturation at 95°C for 3 min, followed by 39 cycles of 95°C for 10 s then 55°C for 30 s. Amplicon dissociation curves, *i.e.* melting curves, were recorded after cycle 39 by heating from 60°C to 95°C with 0.5^{o}C increments and an average ramp speed of 3.3°C s^{-1}. Data were analyzed using the CFX Manager Software, version 1.5 (BioRad). A brachypodium gene encoding ACTIN2 was used as a reference for normalizing gene expression. qRT-PCR experiments were conducted using three independent biological samples, each consisting of three technical replicates, unless indicated otherwise. Statistical analysis was performed using the Relative Expression Software Tool (REST, Qiagen [Pfaffl et al*.,* 2002]).

Table 4. Primers used in this study. Sequences in italics indicate *att* sites used for Gateway cloning and * indicate sequences without a stop codon.

Gene	5′ → 3′	Purpose
BdCOPT1-F	atggccatgccgatgccgatg	qPCR
BdCOPT1-R	atgcccatgtccatgtccatccct	qPCR
BdCOPT2-F	ccggagcagcgtaaacttgaca	qPCR
BdCOPT2-R	ggcatcggcatggacatcttgttt	qPCR
BdCOPT3-F	atggacatgggaggagggcatca	qPCR
BdCOPT3-R	aaggtcatgtgcatgtagtgcgtc	qPCR
BdCOPT4-F	tcatgctcgccatcatgtcgtt	qPCR
BdCOPT4-R	ttgtcgaccacgacgagatcct	qPCR
BdCOPT5-F	tatctcgtgatgctggcggtcat	qPCR
BdCOPT5-R	tacggcttggatccgttcgact	qPCR
BdActin-F	tggattggaggatccatcttggca	qPCR
BdActin-R	agcatttcctgtgcacaatggacg	qPCR
BdCOPT1-F	*ggggacaagtttgtacaaaaaagcaggcttc*atggccatgccgatgccgat	Gateway cloning
BdCOPT1-R	*ggggaccactttgtacaagaaagctgggtc*ctaaggtttgggctcagctgcct	Gateway cloning
*BdCOPT1-R**	*ggggaccactttgtacaagaaagctgggtc*aggtttgggctcagctgcct	Gateway cloning
BdCOPT3-F	*ggggacaagtttgtacaaaaaagcaggcttc*atggacatgggaggagggcat	Gateway cloning
BdCOPT3-R	*ggggaccactttgtacaagaaagctgggtc*ctagcagcacgccgcc	Gateway cloning
*BdCOPT3-R**	*ggggaccactttgtacaagaaagctgggtc*gcagcacgccgccggc	Gateway cloning
BdCOPT4-F	*ggggacaagtttgtacaaaaaagcaggcttc*atgatgcacatgaccttctactgg	Gateway cloning
BdCOPT4-R	*ggggaccactttgtacaagaaagctgggtc*ctacgcgcaggcgca	Gateway cloning
*BdCOPT4-R**	*ggggaccactttgtacaagaaagctgggtc*cgcgcaggcgcag	Gateway cloning
BdCOPT5-F	*ggggacaagtttgtacaaaaaagcaggcttc*atggcgccgccgcgg	Gateway cloning
BdCOPT5-R	*ggggaccactttgtacaagaaagctgggtc*ctacggcttggatccgttcgactgc	Gateway cloning
*BdCOPT5-R**	*ggggaccactttgtacaagaaagctgggtc*cggcttggatccgttcgactgc	Gateway cloning

Plasmid construction

Total RNA isolated from brachypodium leaves and oligonucleotides pairs that are indicated in Table 4 were used for RT-PCR amplification of *BdCOPT1*, *BdCOPT3*, *BdCOPT4*, and *BdCOPT5* cDNAs with or without the stop codon. Primers were designed to contain *attB* sites on resulting PCR products for subsequent Gateway cloning (Invitrogen) into the DONR-Zeo entry vector (Invitrogen) and appropriate destination vectors described below.

Functional complementation of the *S. cerevisiae* copper uptake deficient *ctr1ctr2ctr3* mutant strain

S. cerevisiae SEY6210 (*MATa ura3-52 leu2-3,-112 his3Δ200 trp1Δ901 lys2-801 suc2Δ9)* wild-

type and the *ctr1ctr2ctr3* triple mutant (*MATa ura3-52 his3Δ200 trp1-901 ctr1::ura3::Knr ctr2::HIS3 ctr3::TRP1)* used for functional complementation assays were the generous gift of Dr. Dennis Thiele (Duke University). Yeast cells were transformed with YES3-Gate-BdCOPT1, YES3-Gate-BdCOPT3, YES3-Gate-BdCOPT4, YES3-Gate-BdCOPT5 constructs or an empty YES3-Gate vector using the Frozen-EZ yeast Transformation II Kit (Zymo Research). Transformants were selected for uracil prototrophy on YNB medium (YNB-Ura) containing 0.67% (w/v) Yeast Nitrogen Base without amino acids (Difco), 0.077% (w/v) CSM-Ura, 0.05% (w/v) NaCl, 2% dextrose, 2% (w/v) agar. Respiration competence was evaluated by testing the ability of transformants to grow on the non-fermentable carbon sources, glycerol and ethanol (YPEG) as described (Dancis et al*.,* 1994a, Puig et al*.,* 2002). Briefly, transformants were grown in liquid YNB-Ura to an OD_{600nm} = 1.0, serially-10-fold diluted and spotted onto YPEG medium containing 1% (w/v) yeast extract, 2% (w/v) bacto-peptone, 3% (v/v) glycerol 2% (v/v) ethanol and 2% (w/v) agar and the indicated concentration of $CuSO_4$ or onto YNB-Ura for controls. Plates were incubated for 3 days at 30°C.

Isolation of protoplasts from brachypodium leaves

Protoplasts were isolated from leaves of 25-day-old brachypodium grown as described above. The protoplast isolation procedure was based on (Zhai et al*.,* 2009). Briefly, 0.2 g of young leaf tissue was immersed in 15 ml of filter-sterilized TVL solution (Table 5), finely chopped with a fresh razor blade and transferred to a 200 ml beaker containing 20 ml of Enzyme solution (Table 5). The beaker was wrapped in aluminum foil to protect samples from light and samples were vacuum infiltrated for 30 min before incubation at 30°C for 60 min. The mixture was then agitated at 35 rpm at room temperature for 18 to 20 h. Released protoplasts were collected into

50-ml Falcon centrifuge tubes by carefully sieving the mixture through eight layers of cheesecloth, pre-wetted with W5 solution (Table 5). To increase the protoplast yield, the cheesecloth was rinsed with an additional 10 ml of W5 solution. Sieved protoplasts were then carefully overlaid with 5 ml of W5 solution and left at room temperature for 1 h to allow protoplasts to float to the interface of Enzyme solution and W5 solution. Fifteen milliliters of protoplasts were collected from the interface and transferred into a new 50 ml Falcon tube containing 20 ml of W5 solution. Protoplasts were collected by centrifugation for 7 min at 100 × *g*. The residual Enzyme solution was removed by two rounds of rinsing protoplasts with 10 ml W5 solution and centrifuged for 5 min at 60 × *g*. Purified protoplasts were resuspended in 3-5 ml W5 solution and the protoplast yield was evaluated by cell counting using a hemocytometer. Protoplast viability was evaluated using the Plant Cell Viability Assay Kit (Sigma), according to manufacturer's recommendations.

Transfection of protoplasts with plasmid DNA

Protoplasts were transfected using a procedure adopted from (Jung et al*.,* 2011). Briefly, purified protoplasts were incubated on ice for 30 min and centrifuged for 5 min at 60 x *g* and W5 solution was removed. Protoplasts were then re-suspended in MMG solution (Table 5) and 100 µl aliquots were transferred into a 2-ml round-bottom microcentrifuge tube. Plasmid DNA (5 to 10 µg) was added to protoplasts and mixed gently. For controls, DNA was omitted and replaced with equivalent volumes of sterile water (mock transfection). Transfection was initiated by the addition of 110 µl of PEG-calcium solution (Table 5). Protoplasts were gently mixed with PEG-calcium solution by tapping the tube followed by incubation for 7 min at room temperature. Transfection was terminated by diluting the mixture by an addition of 700 µl of W5 solution.

Transfected protoplasts were collected by centrifugation for 2 min at 100 × *g*, and supernatant was removed to leave 50 to 100 µl of protoplast suspension. Each sample was then brought up to a volume of 1 ml with W5 solution and incubated in the dark at room temperature for 18 h.

Table 5. Solutions used in protoplast isolation and transfection. All solutions were filter sterilized before use.

Name	Composition
TVL solution	0.3 M sorbitol, 50 mM $CaCl_2$
Enzyme solution	0.5 M sucrose, 20 mM $CaCl_2$, 40 mM KCl, 1% (w/v) Cellulase, 1% (w/v) Macerozyme 20 mM MES-KOH, pH 5.7
W5 solution	0.037% (w/v) KCl, 0.9% (w/v) NaCl, 1.84% (w/v) $CaCl_2$, 2 mM MES-KOH, pH 5.7
MMG solution	0.4 M mannitol, 15 mM $MgCl_2$, 4 mM MES-KOH, pH 5.7
PEG-Calcium solution	0.2 M mannitol, 100 mM $CaCl_2$, 40% PEG-4000

Subcellular localization and fluorescent microscopy

For studies of the subcellular localization in brachypodium protoplasts, *BdCOPT3* and *BdCOPT4* cDNAs lacking the stop codon were fused at the C-terminus to the enhanced green fluorescent protein (EGFP) of the SAT6-N1-EGFP-Gate vector and expressed under the control of the cauliflower mosaic virus (CaMV) *35S* promoter. The resulting $35S_{pro}$*-BdCOPT-EGFP* constructs or SAT6-N1-EGFP-Gate lacking cDNA inserts were transfected into brachypodium protoplasts as described above. Plasma membranes were stained with 50 μM FM4-64 as described (Ueda et al*.,* 2001).

For studies of subcellular localization in *S. cerevisiae*, entry clones containing *BdCOPT1*, *BdCOPT3*, *BdCOPT4*, or *BdCOPT5* cDNAs without the stop codon were fused at C-terminus with EGFP in the YES3-EGFP-Gate vector (Jung et al*.,* 2012). The resulting constructs and the empty YES3-EGFP-Gate vector were transformed into *S. cerevisiae ctr1ctr2ctr3* triple mutant using the Frozen-EZ yeast Transformation II Kit (Zymo Research) and transformants were

selected on YNB-Ura medium, as described above. Subcellular localization was assessed in cells grown overnight in liquid YNB-Ura.

EGFP- and FM4-64- mediated fluorescence, and chlorophyll autofluorescence were visualized using FITC (for EGFP) or rhodamine (FM4-64 and chlorophyll) filter sets of the Axio Imager M2 microscope equipped with the motorized Z-drive (Zeiss). Z-stack (1.3 μm-thick) images were collected with the high-resolution AxioCam MR Camera and then 3D deconvoluted using an inverse filter algorithm of the Zeiss AxioVision 4.8 software. Images were processed using the Adobe Photoshop software package, version 12.0.

Split-ubiquitin membrane yeast two-hybrid system (MYTH)

Vectors and *S. cerevisiae* strains THY.AP4 (*MATa leu2-3,112 ura3-52 trp1-289 lexA::HIS3 lexA::ADE2 lexA::lacZ)* and THY.AP5 (*MATα URA3 leu2-3,112 trp1-289 his3-Δ1 ade2Δ::loxP)* for MYTH were obtained from the Frommer lab (Stanford University) depository at *Arabidopsis* Biological Resource Center (ABRC) http://www.arabidopsis.org/abrc/index.jsp. AtCOPT6-Cub-PLV and AtCOPT6-NubG fusions were previously described (Jung et al*.,* 2012). Full-length *BdCOPT1, BdCOPT3, BdCOPT4,* and *BdCOPT5* cDNAs without stop codons were introduced into the MetYC-dest and pXN-dest22-3HA destination vectors by Gateway cloning (Invitrogen) to generate bait, BdCOPT-CubPLV, and prey, BdCOPT-NubG, constructs in THY.AP4 and THY.AP5 strains, respectively. In all cases, C- and N terminal fragments of ubiquitin were placed at the C-terminus of the BdCOPT proteins. Protein interactions were selected in diploid cells after 2 days of growth on SC medium lacking adenine and histidine. Interactions were verified using *β*-galactosidase assays, as detailed in (Kittanakom et al*.,* 2009).

Construction of phylogenetic tree

The phylogenetic tree was built using the Neighbor-Joining method (Saitou and Nei 1987). The bootstrap consensus tree inferred from 500 replicates is taken to represent the evolutionary history of the taxa analyzed (Felsenstein 1985). Branches corresponding to partitions reproduced in less than 50% bootstrap replicates are collapsed. The percentage of replicate trees in which the associated taxa clustered together in the bootstrap test (500 replicates) are shown next to the branches (Felsenstein 1985). The tree is drawn to scale, with branch lengths in the same units as those of the evolutionary distances used to infer the phylogenetic tree. The evolutionary distances were computed using the number of differences method (Nei and Kumar 2000) and are in units of the number of amino acid differences per sequence. The analysis involved 22 amino acid sequences. All positions containing gaps and missing data were eliminated. There were a total of 75 positions in the final dataset. Evolutionary analyses were conducted in MEGA5 (Tamura et al*.,* 2011) with *A. thaliana* IRT1 as an outgroup.

Accession Numbers

Accession numbers for genes used in this study were according to nomenclature from ARAMEMNON 7.0 (http://aramemnon.botanik.uni-koeln.de/) and MIPS (http://mips.helmholtz-muenchen.de/plant/brachypodium/): *Bradi1g24180* (*BdCOPT1*), *Bradi1g24190* (*BdCOPT2*), *Bradi2g51210* (*BdCOPT3*), *Bradi4g31330* (*BdCOPT4*), *Bradi5g09580* (*BdCOPT5),* *Bradi1g10630.1* (*BdACTIN*) and *At2g26975* (*AtCOPT6*).

REFERENCES

Andrés-Colás, N., Perea-García, A., Puig, S. and Peñarrubia, L. (2010) Deregulated copper transport affects *Arabidopsis* development especially in the absence of environmental cycles. *Plant Physiol*, **153**, 170-184.

Arteca, R.N. and Arteca, J.M. (2000) A novel method for growing *Arabidopsis thaliana* plants hydroponically. *Physiol Plant*, **108**, 188-193.

Barhoom, S., Kupiec, M., Zhao, X., Xu, J. and Sharon, A. (2008) Functional characterization of CgCTR2, a putative vacuole copper transporter that is involved in germination and pathogenicity in *Colletotrichum gloeosporioides*. *Eukaryot Cell*, **7**, 1098 - 1108.

Bragg, J.N., Wu, J., Gordon, S.P., Guttman, M.E., Thilmony, R., Lazo, G.R., & Vogel, J.P. (2012) Generation and characterization of the Western Regional Research Center Brachypodium T-DNA insertional mutant collection. *PLoS One*, **7**, e41916.

Brkljacic, J., Grotewold, E., Scholl, R., Mockler, T., Garvin, D.F., Vain, P., & Vogel, J.P. (2011) *Brachypodium* as a Model for the Grasses: Today and the Future. *Plant Physiol*, **157**, 3-13.

Burkhead, J., Reynolds, K., Abdel-Ghany, S., Cohu, C. and Pilon, M. (2009) Copper homeostasis. *New Phytol*, **182**, 799 - 816.

Chochois, V., Vogel, J.P. and Watt, M. (2012) Application of *Brachypodium* to the genetic improvement of wheat roots. *J Exp Bot*, **63**, 3467-3474.

Dancis, A., Haile, D., Yuan, D.S. and Klausner, R.D. (1994a) The *Saccharomyces cerevisiae* copper transport protein (Ctr1p). Biochemical characterization, regulation by copper, and physiologic role in copper uptake. *J Biol Chem*, **269**, 25660-25667.

Dancis, A., Yuan, D., Haile, D., Askwith, C., Eide, D., Moehle, C., & Klausner, R. (1994b) Molecular characterization of a copper transport protein in *S. cerevisiae*: an unexpected role for copper in iron transport. *Cell*, **76**, 393 - 402.

De Feo, C., Aller, S. and Unger, V. (2007) A structural perspective on copper uptake in eukaryotes. *Biometals*, **20**, 705 - 716.

De Feo, C.J., Aller, S.G., Siluvai, G.S., Blackburn, N.J. and Unger, V.M. (2009) Three-dimensional structure of the human copper transporter hCTR1. *Proc Natl Acad Sci U S A*, **106**, 4237-4242.

Felsenstein, J. (1985) Confidence limits on phylogenies: An approach using the bootstrap. *Evolution*, **39**, 783-791.

Garcia-Molina, A., Andrés-Colás, N., Perea-García, A., del Valle-Tascón, S., Peñarrubia, L. and Puig, S. (2011) The intracellular *Arabidopsis* COPT5 transport protein is required for photosynthetic electron transport under severe copper deficiency. *Plant J*, **65**, 848-860.

Garcia-Molina, A., Andrés-Colás, N., Perea-García, A., Neumann, U., Dodani, S.C., Huijser, P., & Puig, S. (2013) The *Arabidopsis* COPT6 transport protein functions in copper distribution under copper-deficient conditions. *Plant Cell Physiol*, **54**, 1378-1390.

Gayomba, S.R., Jung, H.I., Yan, J., Danku, J., Rutzke, M.A., Bernal, M., & Vatamaniuk, O.K. (2013) The CTR/COPT-dependent copper uptake and SPL7-dependent copper deficiency responses are required for basal cadmium tolerance in *A. thaliana*. *Metallomics*, **5**, 1262-1275.

Glerum, D.M., Shtanko, A. and Tzagoloff, A. (1996) Characterization of COX17, a yeast gene involved in copper metabolism and assembly of cytochrome oxidase. *J Biol Chem*, **271**, 14504-14509.

Johnson, D.S., Mortazavi, A., Myers, R.M. and Wold, B. (2007) Genome-wide mapping of in

vivo protein-DNA interactions. *Science*, **316**, 1497-1502.
Jung, H.I., Gayomba, S.R., Rutzke, M.A., Craft, E., Kochian, L.V. and Vatamaniuk, O.K. (2012) COPT6 is a plasma membrane transporter that functions in copper homeostasis in *Arabidopsis* and is a novel target of SQUAMOSA Promoter-Binding Protein-like 7. *J Biol Chem*, **287**, 33252-33267.
Jung, H.I., Zhai, Z. and Vatamaniuk, O.K. (2011) Direct transfer of synthetic double-stranded RNA into protoplasts of *Arabidopsis thaliana*. *Methods Mol Biol*, **744**, 109-127.
Kampfenkel, K., Kushnir, S., Babiychuk, E., Inze, D. and Van Montagu, M. (1995) Molecular characterization of a putative *Arabidopsis thaliana* copper transporter and Its yeast homologue. *J Biol Chem*, **270**, 28479-28486.
Kittanakom, S., Chuk, M., Wong, V., Snyder, J., Edmonds, D., Lydakis, A., & Stagljar, I. (2009) Analysis of membrane protein complexes using the split-ubiquitin membrane yeast two-hybrid (MYTH) system. *Methods Mol Biol*, **548**, 247-271.
Klaumann, S., Nickolaus, S.D., Fürst, S.H., Starck, S., Schneider, S., Ekkehard Neuhaus, H. and Trentmann, O. (2011) The tonoplast copper transporter COPT5 acts as an exporter and is required for interorgan allocation of copper in *Arabidopsis thaliana*. *New Phytol*, **192**, 393-404.
Lee, J., Peña, M.M., Nose, Y. and Thiele, D.J. (2002) Biochemical characterization of the human copper transporter Ctr1. *J Biol Chem*, **277**, 4380-4387.
Marschner, H. (1995) *Mineral nutrition of higher plants* London; San Diego: Academic Press.
Mendel, R.R. and Kruse, T. (2012) Cell biology of molybdenum in plants and humans. *Biochim Biophys Acta*, **1823**, 1568-1579.
Merchant, S.S. (2010) The Elements of Plant Micronutrients. *Plant Physiol*, **154**, 512-515.
Mochida, K., Yoshida, T., Sakurai, T., Yamaguchi-Shinozaki, K., Shinozaki, K. and Tran, L.-S.P. (2011) In silico analysis of transcription factor repertoires and prediction of stress-responsive transcription factors from six major gramineae plants. *DNA Res*, **18**, 321-332.
Mur, L.A., Allainguillaume, J., Catalan, P., Hasterok, R., Jenkins, G., Lesniewska, K., & Vogel, J. (2011) Exploiting the *Brachypodium* tool box in cereal and grass research. *New Phytol*, **191**, 334-347.
Nagalakshmi, U., Waern, K. and Snyder, M. (2010) RNA-Seq: a method for comprehensive transcriptome analysis. In *Current Protocols in Molecular Biology*: John Wiley & Sons, Inc.
Nakagawa, Y., Kikuchi, S., Sakamoto, Y. and Yano, A. (2010) Identification and characterization of CcCTR1, a copper uptake transporter-like gene, in *Coprinopsis cinerea*. *Microbiol Res*, **165**, 276 - 287.
Nei, M. and Kumar, S. (2000) *Molecular Evolution and Phylogenetics* New York: Oxford University Press.
Nevitt, T., Öhrvik, H. and Thiele, D.J. (2012) Charting the travels of copper in eukaryotes from yeast to mammals. *Biochim Biophys Acta*, **1823**, 1580-1593.
Peña, M.M., Puig, S. and Thiele, D.J. (2000) Characterization of the *Saccharomyces cerevisiae* high affinity copper transporter Ctr3. *J Biol Chem*, **275**, 33244-33251.
Peñarrubia, L., Andrés-Colás, N., Moreno, J. and Puig, S. (2010) Regulation of copper transport in *Arabidopsis thaliana*: a biochemical oscillator? *J Biol Inorganic Chem*, **15**, 29 - 36.
Perea-García, A., Garcia-Molina, A., Andrés-Colás, N., Vera-Sirera, F., Pérez-Amador, M.A., Puig, S. and Peñarrubia, L. (2013) Arabidopsis copper transport protein COPT2 participates in the cross talk between iron deficiency responses and low-phosphate signaling. *Plant Physiol*, **162**.

Pfaffl, M.W., Horgan, G.W. and Dempfle, L. (2002) Relative expression software tool (REST) for group-wise comparison and statistical analysis of relative expression results in real-time PCR. *Nucleic Acids Res*, **30**, e36.

Puig, S., Lee, J., Lau, M. and Thiele, D. (2002) Biochemical and genetic analysis of yeast and human high affinity copper transporters suggest a conserved mechanism for copper uptake. *J Biol Chem*, **277**, 26021 - 26030.

Rapisarda, V.A., Volentini, S.I., Farias, R.N. and Massa, E.M. (2002) Quenching of bathocuproine disulfonate fluorescence by Cu(I) as a basis for copper quantification. *Anal Biochem*, **307**, 105-109.

Ravet, K. and Pilon, M. (2013) Copper and Iron Homeostasis in Plants: The Challenges of Oxidative Stress. *Antioxid Redox Signal*, **19**, 919-932.

Rees, E.M., Lee, J. and Thiele, D.J. (2004) Mobilization of intracellular copper stores by the Ctr2 vacuolar copper transporter. *J Biol Chem*, **279**, 54221-54229.

Saitou, N. and Nei, M. (1987) The neighbor-joining method: a new method for reconstructing phylogenetic trees. *Mol Biol Evol*, **4**, 406 - 425.

Sancenón, V., Puig, S., Mateu-Andres, I., Dorcey, E., Thiele, D. and Peñarrubia, L. (2004) The *Arabidopsis* copper transporter COPT1 functions in root elongation and pollen development. *J Biol Chem*, **279**, 15348 - 15355.

Schwacke, R., Schneider, A., van der Graaff, E., Fischer, K., Catoni, E., Desimone, M., & Kunze, R. (2003) ARAMEMNON, a novel database for *Arabidopsis* integral membrane proteins. *Plant Physiol*, **131**, 16-26.

Shorrocks, V.M. and Alloway, B.J. (1988) *Copper in plant, animal and human nutrition* Potters Bar, Hertfordshire: Copper Development Association.

Solberg, E., Evans, I. and Penny, D. (1999) Copper deficiency: Diagnosis and correction. Agri-facts. Soil Fertility/Crop Nutrition. Alberta Agriculture, Food and Rural Development, Agdex 532–3, pp. 1–9.

Tamura, K., Peterson, D., Peterson, N., Stecher, G., Nei, M. and Kumar, S. (2011) MEGA5: Molecular Evolutionary Genetics Analysis using maximum likelihood, evolutionary distance, and maximum parsimony methods. *Mol Biol Evol*, **28**, 2731-2739.

Thole, V., Peraldi, A., Worland, B., Nicholson, P., Doonan, J.H. and Vain, P. (2012) T-DNA mutagenesis in *Brachypodium distachyon*. *J Exp Bot*, **63**, 567-576.

Ueda, T., Yamaguchi, M., Uchimiya, H. and Nakano, A. (2001) Ara6, a plant-unique novel type Rab GTPase, functions in the endocytic pathway of *Arabidopsis thaliana*. *EMBO J*, **20**, 4730-4741.

Valko, M., Morris, H. and Cronin, M.T. (2005) Metals, toxicity and oxidative stress. *Curr Med Chem*, **12**, 1161-1208.

Vida, T.A. and Emr, S.D. (1995) A new vital stain for visualizing vacuolar membrane dynamics and endocytosis in yeast. *J Cell Biol*, **128**, 779-792.

Vogel, J. and Hill, T. (2008) High-efficiency *Agrobacterium*-mediated transformation of *Brachypodium distachyon* inbred line Bd21-3. *Plant Cell Rep*, **27**, 471-478.

Wu, X., Sinani, D., Kim, H. and Lee, J. (2009) Copper transport activity of yeast Ctr1 is down-regulated via its C terminus in response to excess copper. *J Biol Chem*, **284**, 4112-4122.

Xiao, Z., Loughlin, F., George, G., Howlett, G. and Wedd, A. (2004) C-terminal domain of the membrane copper transporter Ctr1 from *Saccharomyces cerevisiae* binds four Cu(I) ions as a cuprous-thiolate polynuclear cluster: sub-femtomolar Cu(I) affinity of three proteins involved in copper trafficking. *J Am Chem Soc*, **126**, 3081 - 3090.

Yordem, B.K., Conte, S.S., Ma, J.F., Yokosho, K., Vasques, K.A., Gopalsamy, S.N. and Walker, E.L. (2011) Brachypodium distachyon as a new model system for understanding iron homeostasis in grasses: phylogenetic and expression analysis of Yellow Stripe-Like (YSL) transporters. *Ann Bot*, **108**, 821-833.

Yuan, M., Chu, Z., Li, X., Xu, C. and Wang, S. (2010) The bacterial pathogen *Xanthomonas oryzae* overcomes rice defenses by regulating host copper redistribution. *Plant Cell*, **22**, 3164-3176.

Yuan, M., Li, X., Xiao, J. and Wang, S. (2011) Molecular and functional analyses of COPT/Ctr-type copper transporter-like gene family in rice. *BMC Plant Biol*, **11**, 69.

Zhai, Z., Jung, H.I. and Vatamaniuk, O.K. (2009) Isolation of protoplasts from tissues of 14-day-old seedlings of *Arabidopsis thaliana*. *J Vis Exp*, **30**, 1149.

Zhang, H. and Li, L. (2013) SQUAMOSA promoter binding protein-like7 regulated microRNA408 is required for vegetative development in *Arabidopsis*. *Plant J*, **74**, 98-109.

Zhu, J.-Y., Sun, Y. and Wang, Z.-Y. (2012) Genome-wide identification of transcription factor-binding sites in plants using chromatin immunoprecipitation followed by microarray (ChIP-chip) or sequencing (ChIP-seq). In *Plant Signalling Networks* (Wang, Z.-Y. and Yang, Z. eds): Humana Press, pp. 173-188.

CHAPTER V

OPT3 is a Phloem-Specific Iron Transporter that is Essential for Systemic Iron Signaling and Redistribution of Iron and Cadmium in *Arabidopsis*

Abstract

Iron is essential for both plant growth and human health and nutrition. Knowledge of the signaling mechanisms that communicate iron demand from shoots to roots to regulate iron uptake as well as the transport systems mediating iron partitioning into edible plant tissues is critical for the development of crop biofortification strategies. Here, we report that OPT3, previously classified as an oligopeptide transporter, is a plasma membrane transporter capable of transporting transition ions *in vitro*. Studies in *Arabidopsis thaliana* show that OPT3 loads iron into the phloem, facilitates iron recirculation from the xylem to the phloem, and regulates both shoot-to-root iron signaling and iron redistribution from mature to developing tissues. We also uncovered an aspect of crosstalk between iron homeostasis and cadmium partitioning that is mediated by OPT3. Together, these discoveries provide promising avenues for targeted strategies directed at increasing iron while decreasing cadmium density in the edible portions of crops and improving agricultural productivity in iron deficient soils.

Introduction

Iron (Fe) is essential for plant growth and development and is an important component of the human diet. Cadmium (Cd), on the other hand, is a non-essential and highly toxic element that competes with Fe for uptake and partitioning in plant tissues, thus posing a threat to crop productivity and human health. The ability of Fe to change its oxidation state ($Fe^{3+} \leftrightarrow Fe^{2+}$) highlights its importance in biological processes that involve electron transfer reactions (*e.g.*

respiration and photosynthesis). However, the same property imposes toxicity when Fe is accumulated in cells in excess due to its ability to promote the formation of reactive oxygen species (Valko et al*.,* 2005). Bioavailability of Fe in aerobic soils with neutral to basic pH is below the limits required to sustain plant growth and development because insoluble Fe (III) chelates prevail under these conditions. Consequently, alkaline soils, occupying approximately 30% of the world's arable lands, are considered Fe-limiting for plant growth (Marschner 1995). To increase Fe bioavailability, *Arabidopsis thaliana* and other dicotyledonous and non-graminaceous monocotyledonous plants use a reduction strategy (Hindt and Guerinot 2012, Kobayashi and Nishizawa 2012). In brief, this mechanism includes the acidification of the rhizosphere by the H^+-ATPases of the *Arabidopsis* H^+-ATPase (AHA) family (Santi and Schmidt 2009), the reduction of Fe(III) chelates to soluble Fe(II) by the root surface-localized ferric chelate reductase FRO2 (Robinson et al*.,* 1999) and the subsequent uptake of Fe(II) into root epidermal cells by the high-affinity Fe(II) transporter IRT1 (Eide et al*.,* 1996). The FRO2/IRT1 system constitutes the major pathway for Fe entry into root epidermal cells. Given the essential and toxic nature of Fe, expression of *FRO2* and *IRT1* is under tight local and long-distance regulation (Hindt and Guerinot 2012, Kobayashi and Nishizawa 2012). Interestingly, Fe itself plays a signaling role and is regarded as a positive regulator of local signaling (Vert et al*.,* 2003). In contrast, it is suggested to act as a negative regulator of shoot-to-root signaling *via* the phloem (Hindt and Guerinot 2012, Kobayashi and Nishizawa 2012). However, the latter suggestion has not been substantiated experimentally.

After initial uptake from the soil into root epidermal cells, Fe moves symplastically towards the vasculature and is effluxed into the xylem vessels were it is chelated with citrate to form a tri-Fe(III) tri-citrate complex that undergoes long-distance transport to the shoot (Durrett et al*.,*

2007). Another strong Fe ligand which is responsible for the translocation of Fe in the phloem is a non-proteinogenic amino acid, nicotianamine (NA) (Curie et al., 2009). The molecular machinery contributing to root-to-shoot partitioning of Fe, its redistribution between source and sink tissues, and events involved in shoot-to-root communication of shoot Fe status, are much less understood. The key identified players in *A. thaliana* are the multidrug and toxin efflux family (MATE) member FRD3, the ferroportin (FPN)-like protein FPN1 (*alias* IREG1, iron regulated 1) and members of two distinct clades of the Oligopeptide Transporter family, the Yellow Stripe-like (YSL) proteins and the Oligopeptide Transporters (OPTs), for which the family was named (Green and Rogers 2004, Lubkowitz 2011, Morrissey et al., 2009, Rogers and Guerinot 2002). FRD3 mediates citrate release into the apoplastic space and is essential for xylem-based Fe movement and Fe nutrition in tissues lacking symplastic connections (Green and Rogers 2004, Rogers and Guerinot 2002, Roschzttardtz et al., 2011), FPN1 is proposed to load Fe into the xylem (Morrissey et al., 2009), while YSL2 is suggested to be involved in lateral distribution of Fe-NA complexes from the xylem into neighboring cells (DiDonato et al., 2004, Schaaf et al., 2005).

The phloem-based long-distance transport to sink tissues such as young leaves, developing seeds, and roots involves apoplastic loading of Fe into the companion cells/sieve elements complex (CC/SE) as well as unloading into corresponding sink tissues. Knowledge of transporters contributing to phloem loading/unloading is scarce. The main contributors in this process are At-YSL1, At-YSL3 and Os-YSL2, which mediate Fe-NA transport and facilitate Fe loading into seeds of *A. thaliana* and rice (*Oryza sativa*) (Chu et al., 2010, Ishimaru et al., 2010, Waters et al., 2006). In this regard a member of the OPT family in *A. thaliana*, OPT3, has been under scrutiny for more than a decade since the discovery of its role in Fe homeostasis (Stacey et

al., 2002, Stacey et al., 2006, Stacey et al., 2008). Studies in heterologous systems have implicated *A. thaliana* and *O. sativa* OPT family members, and the closest OPT3 homolog from *Brassica juncea,* Bj-GT1, in transport of synthetic peptides, as well as of the ubiquitous tripeptide glutathione (GSH) (Bogs et al., 2003, Cagnac et al., 2004, Osawa et al., 2006). However, the physiological substrate(s) of OPTs, including OPT3, has not yet been identified. With respect to Fe homeostasis, it was shown that: 1) *OPT3* mRNA is expressed in the vasculature where it is transcriptionally upregulated by Fe deficiency; 2) OPT3 is involved in Fe accumulation in seeds, and loss of this function is suggested to cause embryo lethality in the *opt3-1* null mutant; 3) the *opt3-2* knockdown mutant harboring a T-DNA insertion in the promoter region is viable but accumulates high levels of Fe in both shoots and roots while exhibiting constitutive Fe starvation phenotypes (*e.g.* upregulated expression of *IRT1* and *FRO2*) even when the mutant is grown under Fe-sufficient conditions (Stacey et al., 2002, Stacey et al., 2008). However, the mechanistic basis of the misregulated Fe signaling in the *opt3-2* knockdown mutant and the physiological substrate of OPT3 are unknown.

It is noteworthy that disrupted Fe signaling observed in the *opt3-2* mutant has been also found in several other mutants such as the *frd3* (*man1*) mutant and the quadruple nicotianamine synthase mutant (*nas4x-1*) of *A. thaliana*, the *dgl and brz* iron homeostasis mutants of pea (*Pisum sativum* L.), and the chloronerva, *chln,* mutant of tomato (*Solanum lycopersicon* Mill.), all showing constitutive activation of Fe-acquisition genes even when grown under Fe-sufficient conditions (Grusak and Pezeshgi 1996, Grusak et al., 1990, Kneen et al., 1990, Scholz et al., 1985, Schuler et al., 2012). Importantly, foliar application of Fe blocked the expression of Fe-acquisition genes in the wild-type cultivars and in *frd3-3, brz*, and *chln* mutants, but not in *opt3-2* and *dgl* mutants, reinforcing the previous suggestion of the existence of an Fe-related repressive

signal moving from leaves to roots and pointing to distinct molecular mechanisms of shoot-to-root communication of Fe status in different mutants (Garcia et al., 2013, Maas et al., 1988). Therefore, the identification of the physiological substrate of OPT3 is among the key questions to be addressed with respect to its role in Fe homeostasis and shoot-to-root Fe signaling.

Iron homeostasis is tightly linked with homeostasis of essential elements such as zinc (Zn), manganese (Mn), cobalt (Co), and the non-essential and potentially toxic element cadmium (Cd) due to the low substrate specificity of IRT1 (Baxter et al., 2008, Eide et al., 1996). The crosstalk between essential elements and Cd has been under scrutiny over past decades because Cd is increasingly released into the environment as industrial and consumer waste, and poses a threat to crop productivity, and human health (Jarup 2003). Cadmium causes stunting and chlorosis in plants and affects major biochemical processes including redox balance, photosynthesis, and water status (Hasan et al., 2009). Cadmium is detoxified in the cytosol by forming a bidentate Cd-GS_2 complex with GSH (Li et al., 1997), which then facilitates synthesis of strong Cd ligands, phytochelatins (PC) (Rea 2012). Cd-PC complexes, as well as free Cd ions, are either sequestrated into the vacuole in the root, or bypass the vacuole and instead load into xylem vessels of the root to travel into shoot with the transpiration stream, and are eventually loaded into vacuoles in the shoot (Park et al., 2012, Salt et al., 1995, Wong and Cobbett 2009). With respect to Fe nutrition, it has been shown that Cd competes with Fe(II) for the uptake into root epidermal cells *via* IRT1, and that *IRT1*-overexpressing *A. thaliana* plants accumulate more Cd (Connolly et al., 2002, Eide et al., 1996). Recent finding that co-overexpression of a master regulator of Fe homeostasis, FIT, with its binding partners, the transcription factor bHLH38 or bHLH39, enhances Cd tolerance in *A. thaliana* by increasing Cd sequestration in roots and improving Fe homeostasis of shoots (Wu et al., 2012), further emphasizes important relationship

between Cd resistance and Fe homeostasis.

Here, we report that a member of the oligopeptide transporter family in *A. thaliana*, OPT3, is a phloem-specific transporter that mediates Fe loading into the phloem, which, unlike other members of this family, transports transition metal ions rather than small peptides as the name oligopeptide transporter implies. Our findings also suggest that by loading of Fe into the phloem in leaves, OPT3 regulates both signaling of Fe demand from shoots to roots and Fe transport to developing tissues. We also present data showing an aspect of crosstalk between Fe homeostasis and Cd partitioning that is mediated by OPT3.

Results

OPT3 localizes to the plasma membrane in *A. thaliana* protoplasts

To begin the investigation of the role of OPT3 in the regulation of Fe deficiency responses, its physiological substrate and function in *A. thaliana,* we first determined its subcellular localization. We fused the *OPT3* cDNA with a coding sequence of green fluorescence protein (GFP), and transiently expressed the OPT3-GFP construct under the control of the cauliflower mosaic virus (CaMV) 35S promoter in *A. thaliana* protoplasts. GFP-mediated fluorescence was present in the cytosol and did not overlap with chlorophyll autofluorescence in protoplasts transfected with GFP only (Figure 1).

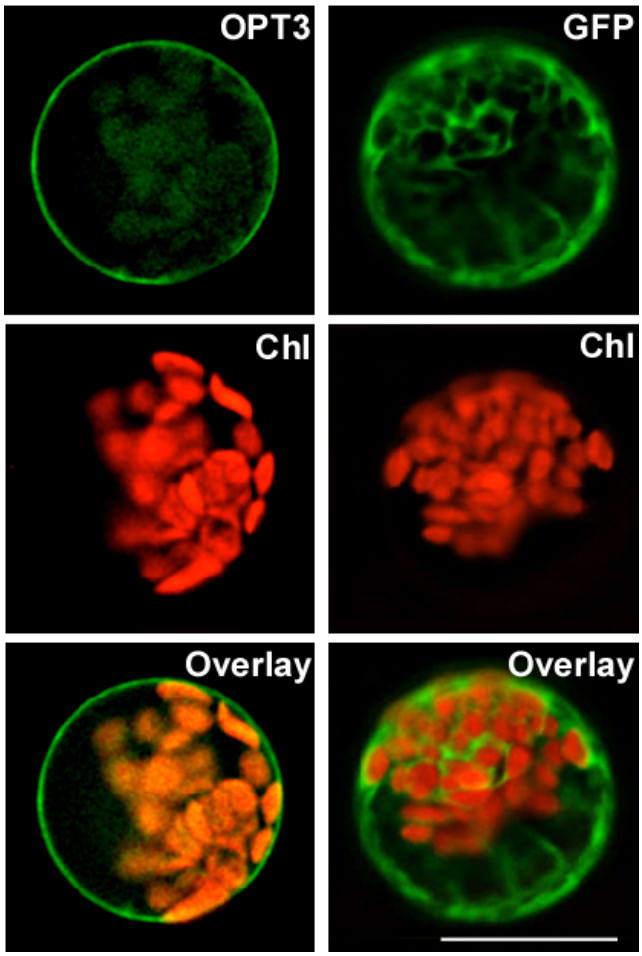

Figure 1. OPT3 localizes to the plasma membrane in *A. thaliana* protoplasts. GFP-mediated fluorescence, derived from the OPT3-GFP (**OPT3**) or empty GFP vector (**GFP**), and chlorophyll autofluorescence (**Chl**) were visualized using FITC or rhodamine filter sets. Superimposed images of chlorophyll autofluorescence and GFP-mediated fluorescence (**Overlay**) were created to demonstrate that green fluorescence was derived from GFP. Bar = 20 μm.

In contrast, OPT3-GFP-mediated fluorescence was present at the periphery of transfected protoplasts, did not overlap with chlorophyll autofluorescence and was absent in the tonoplast (Figure 1). The plasma membrane localization of OPT3 was further confirmed by transient expression of the OPT3-GFP construct in onion (*Allium cepa*) epidermal cells (Figure 2). Therefore, we concluded that OPT3 localizes to the plasma membrane in *A. thaliana* and thus, is involved in movement of substrate(s) into or out of the cell rather than in subcellular (*e.g.*

vacuolar) sequestration.

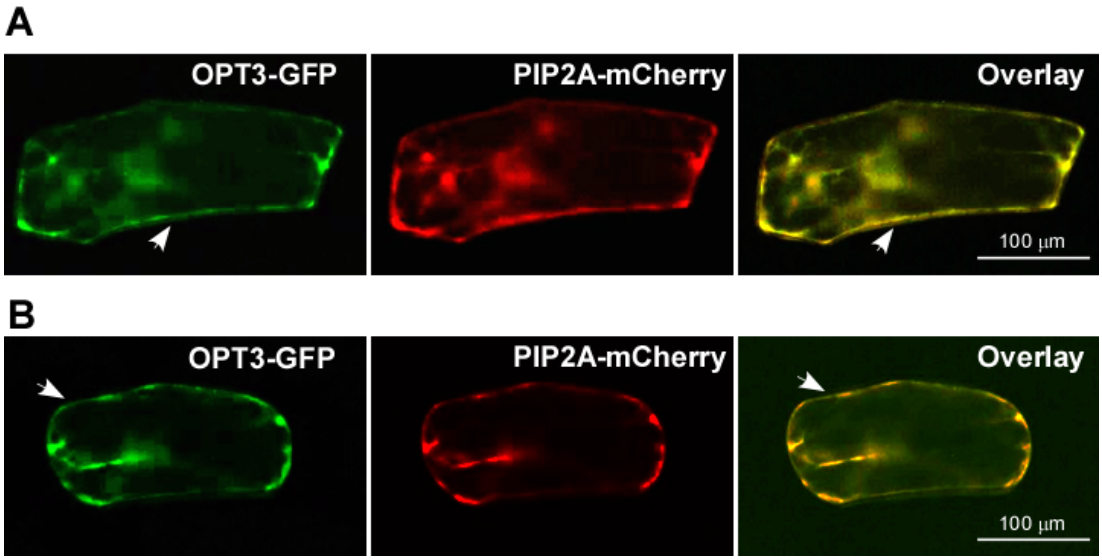

Figure 2. **OPT3-GFP localizes to the plasma membrane in epidermal onion cells.** **A**. Onion cells were co-transformed with OPT3 fused to GFP (**OPT3-GFP**) and a plasma membrane marker, PIP2A, fused to mCherry (**PIP2A-mCherry**). **B**. Onion cells transiently co-expressing OPT3-GFP and PIP2A-mCherry were plasmolyzed in 20% sucrose solution for 10 min before imaging. GFP- and mCherry-mediated fluorescence was visualized using FITC and Rhodamine filter sets respectively. Arrows point to plasma membrane localization of OPT3-GFP. Superimposed images (**Overlay**) of OPT3-GFP- and PIP2A-mCherry-mediated fluorescence were generated to demonstrate the co-localization of OPT3-GFP with PIP2A-mCherry (**A** and **B**).

OPT3 does not complement the GSH uptake deficiency of the *S. cerevisiae* GSH uptake mutant, *opt1*, and does not mediate GSH uptake in yeast

The closest OPT3 homolog from *B. juncea*, Bj-GT1, transports GSH (Bogs et al., 2003). To test whether OPT3 could transport GSH as well, we used functional complementation and *in vitro* transport assays in the *S. cerevisiae* mutant lacking a plasma membrane localized GSH transporter, Opt1p *(alias* Hgt1p) (Bourbouloux et al., 2000). As *opt1* mutant cells do not grow on medium with GSH as the sole source of sulfur, we first tested whether heterologously expressed At-*OPT3* could complement the GSH uptake deficiency of the *opt1* mutant. We transformed

opt1 mutant cells with the vector expressing Sc-*OPT1* or At-*OPT3 (opt1/OPT1* and *opt1/OPT3*, respectively), or with the empty vector (*opt1/EV*), and analyzed the ability of transformants to grow in liquid minimal medium with GSH as the only sulfur source. As a control, we replaced GSH with ammonium sulfate. We found that while the growth of *opt1/OPT3* and *opt1/EV* yeast lines was undistinguishable from *opt1/OPT1* in control medium (Figure 3), only cells transformed with Sc-*OPT1* were able to grow in medium with GSH as the only source of sulfur (Figure 4A).

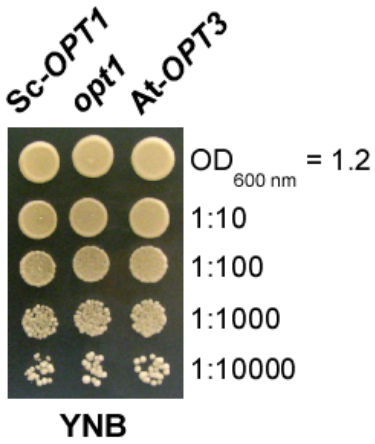

Figure 3. **OPT3 does not alter growth of the *opt1* mutant of *S. cerevisiae* under control conditions.** *S. cerevisiae opt1* mutant cells expressing Sc-*OPT1* cDNA (**Sc-*OPT1***), the empty vector (***opt1***) or the vector with the At-*OPT3* cDNA insert (**At-*OPT3***) were grown in liquid YNB media overnight to an OD 600 nm of 1.2. Cells were then serially 10-fold diluted and spotted onto solid YNB medium. Colonies were visualized after incubating plates for 3 days at 30°C. Dilution series are indicated on the left.

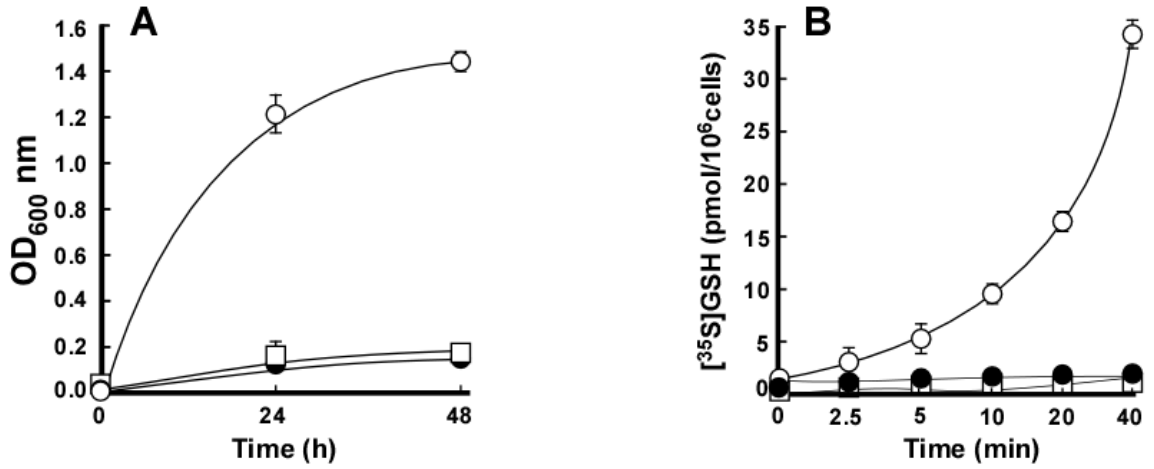

Figure 4. OPT3 does not mediate GSH transport in *S. cerevisiae*. A. *S. cerevisiae opt1* mutant cells expressing Sc-*OPT1*cDNA (open circles), the empty vector (squares) or vector with the At-*OPT3* cDNA insert (filled circles), were grown in SC-S media supplemented without or with 200 µM of GSH. OD values were measured after 24 and 48 h of culturing at 30°C. **B**. Time course of *in vitro* [^{35}S]GSH uptake by *opt1* mutant cells expressing Sc-*OPT1*cDNA (open circles), the empty vector (squares) or vector with the At-*OPT3* cDNA insert (filled circles). Error bars represent S.E. (n=3).

These data indicated that heterologously expressed At-*OPT3* could not complement the GSH uptake defect of the *opt1* mutant. We also performed *in vitro* uptake assays and found that while *opt1/OPT1* cells absorb [^{35}S] GSH, *opt1/OPT3* and *opt1/EV* yeast lines were not able to accumulate [^{35}S] GSH (Figure 4B). These data suggested that, in this heterologous system, At-OPT3 does not mediate GSH transport.

Heterologously expressed *OPT3* partially rescues the iron uptake defect of the *S. cerevisiae fet3fet4* mutant

Because OPT3 has been linked to Fe homeostasis in *A. thaliana* (Stacey et al*.,* 2002, Stacey et al*.,* 2008, Wintz et al*.,* 2003), we next tested whether it would be able to rescue Fe accumulation defects of the *S. cerevisiae fet3fet4* mutant, which lacks both, high and low affinity Fe uptake systems and cannot grow in Fe limited conditions (Dix et al*.,* 1994). DY1457 wild-type and

fet3fet4 mutant yeast cells were transformed with an empty vector, and the *fet3fet4* mutant was transformed with a vector containing At-*OPT3* cDNA or At-*IRT1* cDNA (used here as a positive control). Cell lines were grown on solid medium with or without the Fe chelator, bathophenanthroline disulfonate (BPS). All yeast strains grew well on medium without BPS (Figure 5A). In contrast to wild-type cells expressing the empty vector, the *fet3fet4* mutant expressing the empty vector was not able to grow on medium supplemented with BPS. Consistent with the function of At-IRT1 in high affinity Fe(II) transport (Eide et al*.,* 1996), its heterologous expression rescued the growth defect of the *fet3fet4* mutant on Fe-limited medium. Heterologous expression of At-OPT3 partially rescued the growth defect of *fet3fet4* on Fe-limited medium, suggesting that it might be involved in Fe transport.

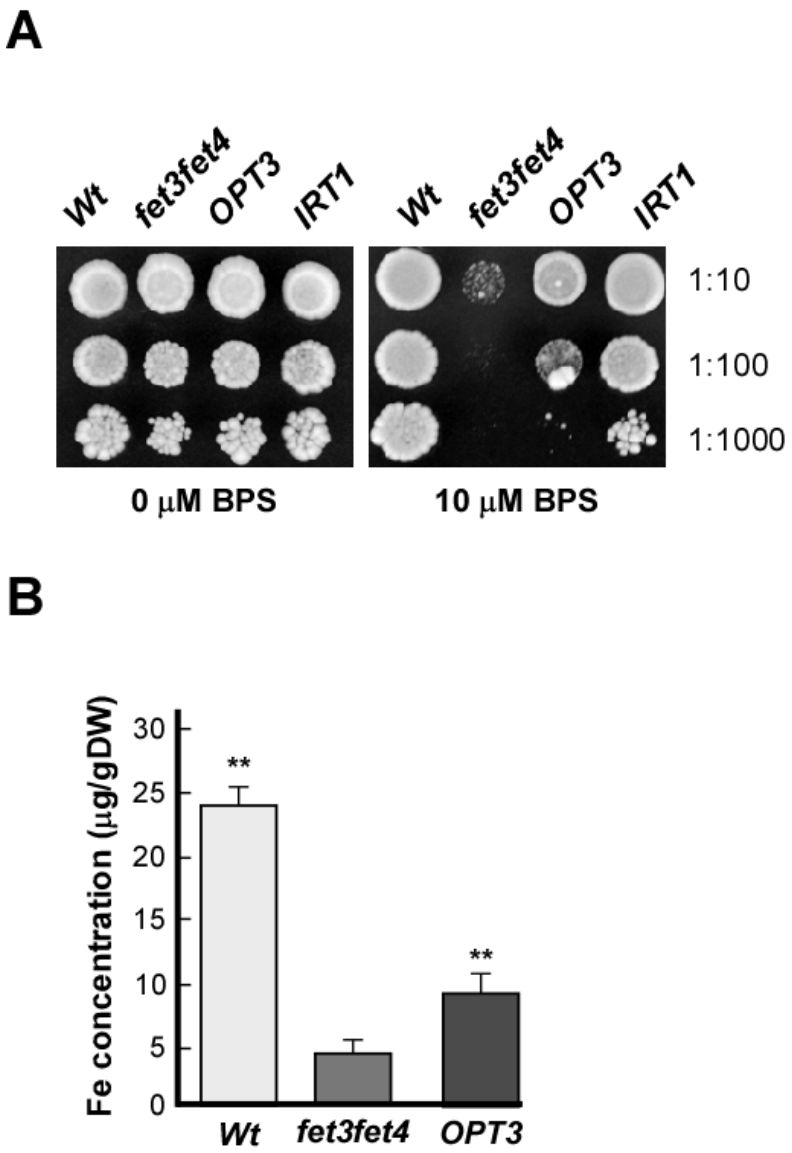

Figure 5. OPT3 partially rescues iron deficiency of the *fet3fet4 S. cerevisiae* mutant. A. Wild-type and the *fet3fet4* mutant, transformed with the empty vector (***Wt*** and ***fet3fet4***, respectively), and the *fet3fet4* mutant transformed with At-*OPT3* or At-*IRT1* cDNAs (***OPT3*** and ***IRT1***) were serially 10-fold diluted and spotted onto solid medium supplemented with the indicated concentrations of the Fe chelator, bathophenanthroline disulfonate (BPS). Colonies were visualized after incubating plates for 6 days at 30°C. Dilution series are indicated on the left. **B**. Iron concentration in different *S. cerevisiae* lines, designated as in **A**. Shown are mean values ± S.E. (n = 5-8); asterisks (**) indicate statistically significant differences ($p \leq 0.001$) from the empty vector-expressing *opt2* or *fet3fet4* mutant cells.

We then compared the Fe concentration of the wild-type cells expressing the empty vector with that of the *fet3fet4* mutant expressing either the empty vector or the vector with At-*OPT3*

cDNA. We found that the Fe concentration was 2-fold higher in At-*OPT3*-expressing cells in comparison with *fet3fet4* cells expressing the empty vector (Figure 5B). We note that in these experiments, cells were grown in medium lacking Fe ligands such as nicotianamine. Therefore, the increased Fe concentration of the At-*OPT3* expressing cells (Figure 5B) could be due to the ability of At-OPT3 to mediate uptake of Fe ions. This suggestion challenges the prevailing view that At-OPT3 is involved in the transport of peptides, as was shown for other OPT family members (Lubkowitz 2011).

OPT3 mediates transition ions transport in *Xenopus laevis* oocytes

Transport properties of OPT3 were examined in *Xenopus laevis* oocytes. On the onset of uptake studies, we examined the localization of OPT3-GFP in oocytes, characterized electrophysiological properties of *OPT3*-expressing oocytes, and determined suitable uptake conditions. We found that OPT3 resided at the plasma membrane in oocytes, as shown by the localization of the OPT3-GFP-mediated fluorescence at the cell periphery (Figure 6).

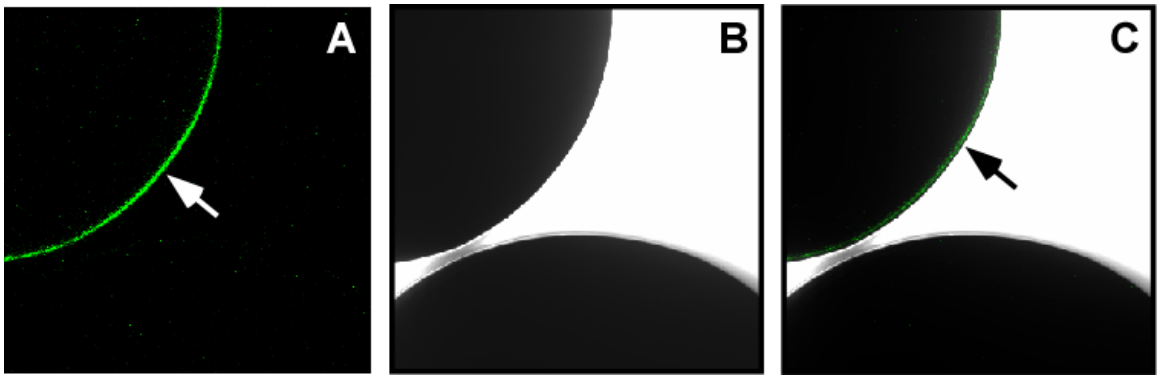

Figure 6. **OPT3 localizes to the plasma membrane in *X. laevis* oocytes.** The fluorescence signal from the OPT3-EGFP chimera expressed in *X. laevis* oocytes (upper cell) was localized to the plasma membrane (arrow) (**A**). Water-injected cells showed no fluorescence background signal (lower cell). Images illustrate fluorescence image (**A**), the corresponding bright field image (**B**), and the overlay of both images (**C**).

When bathed in ND96 recording solution, oocytes injected with *OPT3* cRNA had significantly less negative resting membrane potentials (RMP) than control cells in the same ND96 recording solution (Figure 7A), suggesting that the expression of *OPT3* resulted in an OPT3-mediated electrogenic transport. Further investigations were performed by measuring ion transport under voltage clamp conditions, using the conventional two-electrode voltage-clamp (TEVC) method (Figure 7B).

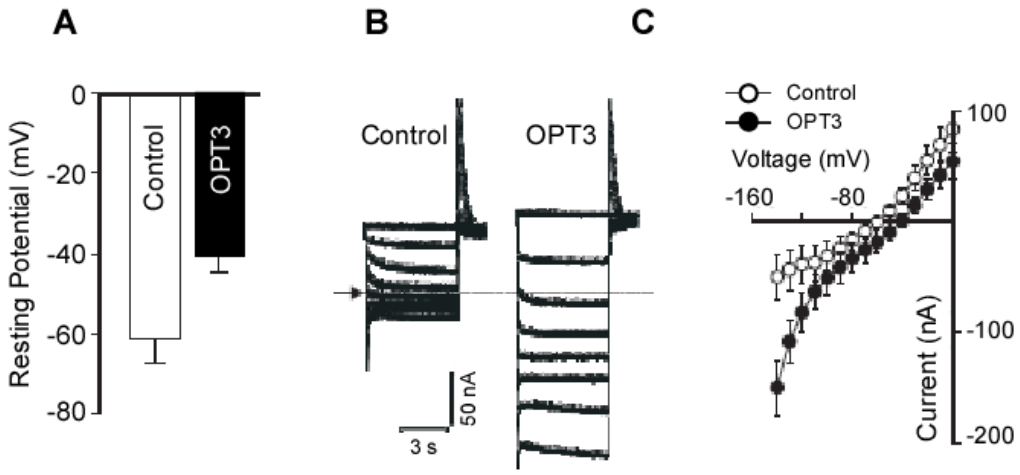

Figure 7. *OPT3* is functional in *X. laevis* oocytes. A. Resting membrane potentials (RMP) of *OPT3*-expressing (**OPT3**) and water-injected (**Control**) cells measured in standard ND96 recording solution. **B**. Example of OPT3-mediated currents (right panel) elicited in response to holding potentials ranging from 0 to -140 to mV (shown only in 20 mV increments for clarity) in standard ND96 recording solution. Endogenous currents recorded in control cells are shown for reference on the left panel. The arrow and dotted line on the left margin indicates the zero current level. **C**. Mean current-voltage (I/V) curves constructed from the steady-state currents recordings such as those shown in (**B**) for holding potentials ranging from 0 to -140 mV in 10 mV steps. Error bars represent S.E. (n=5).

In ND96 recording solution, *OPT3*-expressing cells mediated larger inward (*i.e.* negative) currents relative to those recorded in control cells. Additionally, the *OPT3*-mediated currents

reversed at less negative membrane potentials than those recorded in control cells (about -40 mV in contrast to -60 mV observed for control cells [Figure 7C]). By convention, the recorded inward (*e.g.* negative) currents are the product of net positive charge influx (or net negative charge efflux). Although we propose that OPT3 mediates cation influx, the exact nature of the ion(s) carrying the OPT3-mediated current in this ionic environment remains unknown. However, we speculate that under these conditions, the inward currents and decreased RMP observed in *OPT3*-expressing oocyte cells are the product of a broad substrate specificity of OPT3, which results in OPT3-mediated uptake of the high level of Ca^{2+} present in the ND96-recording solution. Unfortunately, efforts to reduce this large Ca^{2+} background (*e.g.* 1.8 mM $CaCl_2$) present in the ND96 recording solution below 0.9 mM resulted in an increased activity of endogenous inward currents in control cells (Figure 8A).

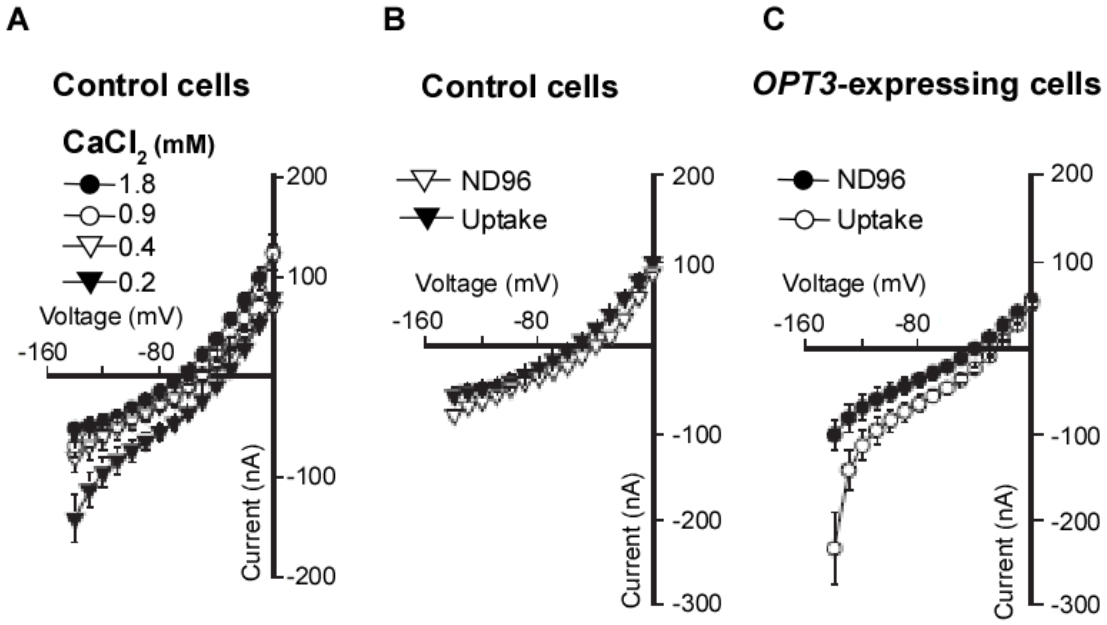

Figure 8. **Electrophysiological properties of *X. laevis* oocytes expressing *OPT3*.** The mean current-voltage (I/V) curves shown were constructed from currents recorded in either water-injected control or OPT3-expressing cells elicited and measured as described in Figure 4. Notice the difference in the Y-axis magnitude between A, B, and C. **A.** Reducing extracellular Ca^{2+} from the ND96 recording solution results in increasingly inward current activity (i.e. negative currents) in control cells. The total $CaCl_2$ concentration present in the modified ND95 recording bath solutions are indicated in the legend. **B**. The electrical activity in control cells (i.e. endogenous currents in cells injected with water) is not altered in basal uptake solution (i.e. pH 6.0 and 0.9 mM $CaCl_2$) relative to that observed in ND96 recording solution. **C**. *OPT3*-expressing cells show an increase in inward current activity (i.e. negative currents) in basal uptake solution control cells relative to that observed in ND96 recording solution. Error bars represent S.E. (n=5).

Furthermore, total removal of $CaCl_2$ from the bath solution resulted in the activation of a large endogenous inward conductance (>1 μA at -140 mV) similar to the reported large Ca^{2+}-inactivated Cl^- conductance (CaIC) (Amasheh and Weber 1999). Therefore, based on these preliminary electrophysiological findings, we modified the ionic conditions of the uptake solution to maximize our chances to characterize metal uptake in *OPT3*-expressing oocytes. We maintained 0.9 mM $CaCl_2$ in the medium used for the cation uptake experiments to minimize the

activity of endogenous transporters. Likewise, as moderate acidification of the basal uptake media (from 7.5 to 6.0) did not alter the basal transport characteristics of control cells (Figure 8B), the pH of the uptake media was adjusted to 6.0. We note that in contrast to control cells, extracellular acidification resulted in a stimulation of the *OPT3*-mediated inward currents, particularly at holding potentials more negative than -100 mV (Figure 8C). This is consistent with the proton-coupled nature of OPT-mediated transport (Osawa et al*.,* 2006). Taken together, our data show that OPT3 is functional at the plasma membrane of oocytes, making this heterologous system suitable for cation uptake experiments.

Having established the uptake conditions that would not lead to changes in the endogenous transport in oocytes, we analyzed Fe^{2+} uptake in OPT3-expressing cells. Significant uptake of Fe^{2+} was observed in oocytes expressing *OPT3* cRNA only after 4-hours of incubation possibly due to the high endogenous levels of Fe^{2+} found in oocytes (about 55 ng/cell) (Figure 9A).

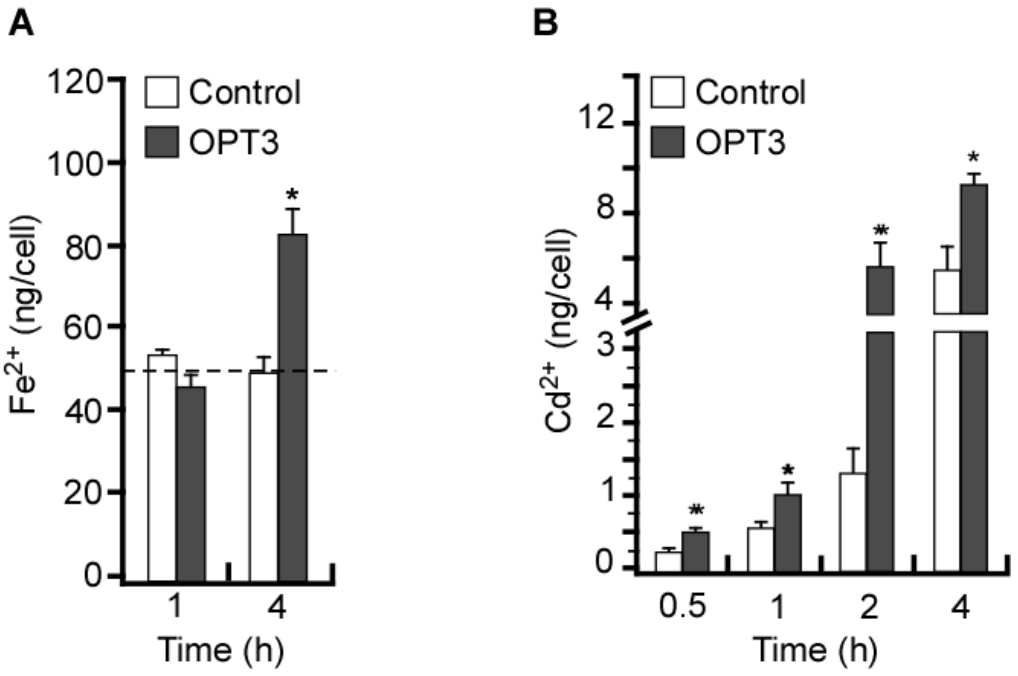

Figure 9. OPT3 mediates cellular cation uptake in *X. laevis* oocytes. Uptake of Fe^{2+} (**A**) and Cd^{2+} (**B**) in *OPT3*-expressing oocytes (**OPT3**) or water-injected cells (**Control**) at different time points. The basal uptake solution supplemented with (**A**) 0.4 mM $FeSO_4$ + 1 mM L-ascorbic acid or (**B**) 0.5 mM $CdCl_2$, yielded free extracellular ionic activities of 35 µM and 150 µM of $\{Cd^{2+}\}_{out}$ and $\{Fe^{2+}\}_{out}$ respectively, as determined by GEOCHEM-EZ (Shaff et al., 2010). The dashed line in panel **A** indicates the basal concentration of endogenous Fe^{2+}. Error bars represent S.E. (n=5). Asterisks (*) indicate statistically significant differences ($p \leq 0.05$).

Since our electrophysiological studies (Figure 7) suggest that OPT3 might have broad substrate specificity and because Fe transporters such as IRT1 can also transport other divalent metals among which is the toxic metal Cd (Eide et al*.,* 1996), we examined the ability of OPT3 to transport Cd^{2+} ions as well. Differences in Cd^{2+} uptake between control and OPT3-expressing cells were detected after 30 minutes of incubation of oocytes in the Cd^{2+}-containing uptake solution (Figure 9B), with the magnitude of OPT3-mediated Cd^{2+} uptake increasing in a time-dependent manner. It is worth noting that although these results indicate that OPT3 is capable of mediating the transport of Fe^{2+} and Cd^{2+}, they do not provide an estimate of the relative affinity of the transporter for these ions (*e.g.* selectivity), which would ultimately determine their role *in*

planta. Nonetheless, these results provide functional proof that OPT3 is a multispecific transporter of transition metal ions unlike other OPT family members that transport peptides.

OPT3 is expressed in the phloem and the majority of its expression is associated with the minor veins of leaves and nodes of stems

We next examined the cell-type specificity of *OPT3* expression since this knowledge is critical for building the predictive models of the physiological function of OPT3 *in planta*. Analysis of the expression pattern of *OPT3* in transgenic plants expressing an $OPT3_{pro}$-*GUS* construct revealed GUS activity predominantly in the vascular tissues of leaves and reproductive organs in *A. thaliana* (Figure 10A-E) and not in roots (Figure 10A), which is consistent with previous findings (Stacey et al*.*, 2006).

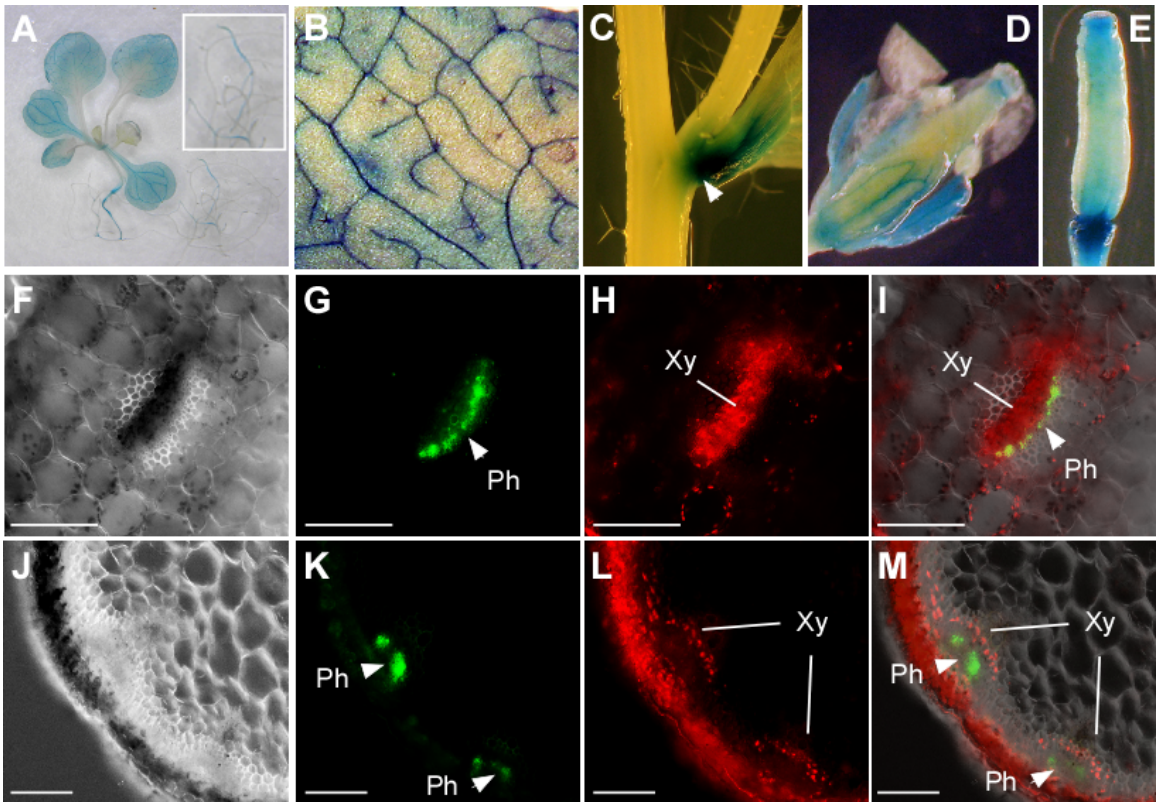

Figure 10. Tissue- and cell-type specificity of *OPT3* expression in *A. thaliana*. A-E. Histochemical analysis of the *OPT3* promoter activity in transgenic plants expressing the $OPT3_{pro}$-*GUS* construct. **A.** Representative expression pattern for *OPT3* in a whole seedling. Note the bulk of OPT3 expression in shoots (main figure) but not in roots (*Inset*). **B.** Close-up of the leaf area to demonstrate *OPT3* expression in minor veins. **C.** Expression of *OPT3* at the node (white arrow). **D** and **E.** Pattern of *OPT3* expression in reproductive organs. **F-M**. Hand-cut cross-sections through the petiole (**F-I**) or inflorescence stem (**J-M**) of 21-day-old transgenic plants expressing the $OPT3_{pro}$-*GFP* construct. **F** and **J** show differential interference contrast images of sections through the petiole and stem at the nodal region, respectively. Overlay images (**I** and **M**) were created to show that GFP-mediated fluorescence (**G** and **K**) does not overlap with phenolics-mediated autofluorescence in xylem vessels and chlorophyll-mediated autofluorescence in parenchyma cells (**H** and **L**). Xy, xylem; Ph, phloem, bar = 100 µm.

We noticed, however, that the majority of GUS activity in leaves was localized to minor veins of the vasculature (Figure 10B). We also found the bulk of *OPT3* expression at the nodes of the stem (Figure 10C). Microscopic analysis of the cell-type specificity of *OPT3* expression was conducted in transgenic plants expressing the $OPT3_{pro}$-*GFP* construct. Transverse cross-sections through petioles (Figure 10F-I) and a nodal section of a stem (Figure 10J-M) showed

that the majority of *OPT3*$_{pro}$-*GFP*-mediated fluorescence is associated with the phloem. Consistent with our data, profiling of the translatome of discrete cell populations identified *OPT3* in companion cells (CC) in leaves (Mustroph et al*.,* 2009). The tissue and cell-type specificity of *OPT3* expression, along with results from subcellular localization and uptake studies (Figures 1, 3 and 5) suggest that OPT3 may function in apoplastic loading of transition ions into the phloem companion cells/sieve element complex (CC/SE) for subsequent long-distance transport. In addition, because xylem-to-phloem transfer is suggested to occur at the nodal regions in the stem as well as in minor veins in leaves (Andriunas et al*.,* 2013, Bouche-Pillon et al*.,* 1994), which are the sites of the preferential expression of *OPT3* (Figure 10B, C), we hypothesized that OPT3 participates in xylem-to-phloem transfer of transition elements.

Characterization of a non-lethal mutant allele of *OPT3*

To further examine the physiological function of OPT3 in Fe and Cd transport in *A. thaliana,* we obtained two T-DNA insertion alleles, SALK_021168C (*alias opt3-2*), possessing a T-DNA insertion 36 bp upstream of the *OPT3* start codon (Stacey et al*.,* 2008) and SALK_058794C, designated *opt3-3,* bearing a T-DNA insertion 41 bp upstream of the *OPT3* start codon (Figure 11A).

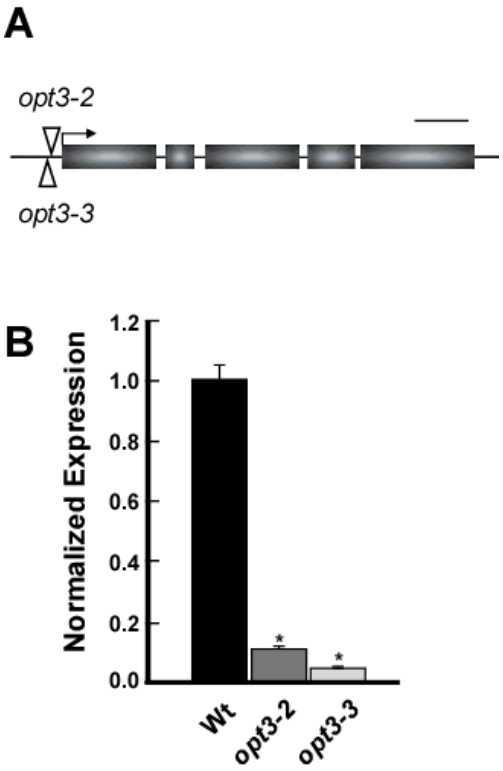

Figure 11. **T-DNA insertions upstream of the *OPT3* start codon reduce the *OPT3* transcript. A**. The exon-intron structure of *OPT3*. Open arrowheads indicate T-DNA insertions located 36 and 41 bp upstream of start codon (black arrow) in *opt3-2* and *opt3-3* alleles, respectively. Bar = 500 bp. **B**. Transcript abundance of *OPT3* in wild-type (**Wt**) and *opt3-2* and *opt3-3* alleles (***opt3-2*** and ***opt3-3***, respectively). Expression of *OPT3* in mutant alleles is shown relative to its expression in wild-type, which was set to 1. Shown are mean values ± S.E.; n = 9; asterisks (*) indicate statistically significant differences ($p < 0.001$) of *OPT3* transcript abundance in *opt3-2* or *opt3-3* vs. Wt.

Quantitative reverse transcriptase (qRT)-PCR studies revealed more than 90% reduction of the *OPT3* transcript in plants carrying either allele in comparison with wild-type (Figure 11B). We then evaluated the effect of the T-DNA insertion using *opt3-3* mutant plants. Consistent with previous findings with the *opt3-2* allele (Stacey et al*.,* 2008), *opt3-3* mutant plants were smaller than wild-type plants (Figure 12A), developed necrotic lesions in cotyledons and older leaves (Figure 12B, C), had significantly higher concentrations of Fe compared to wild-type (Table 1), and exhibited a constitutive Fe-deficiency response that was manifested by increased expression

of *IRT1,* and *FRO2* (Figure 12D).

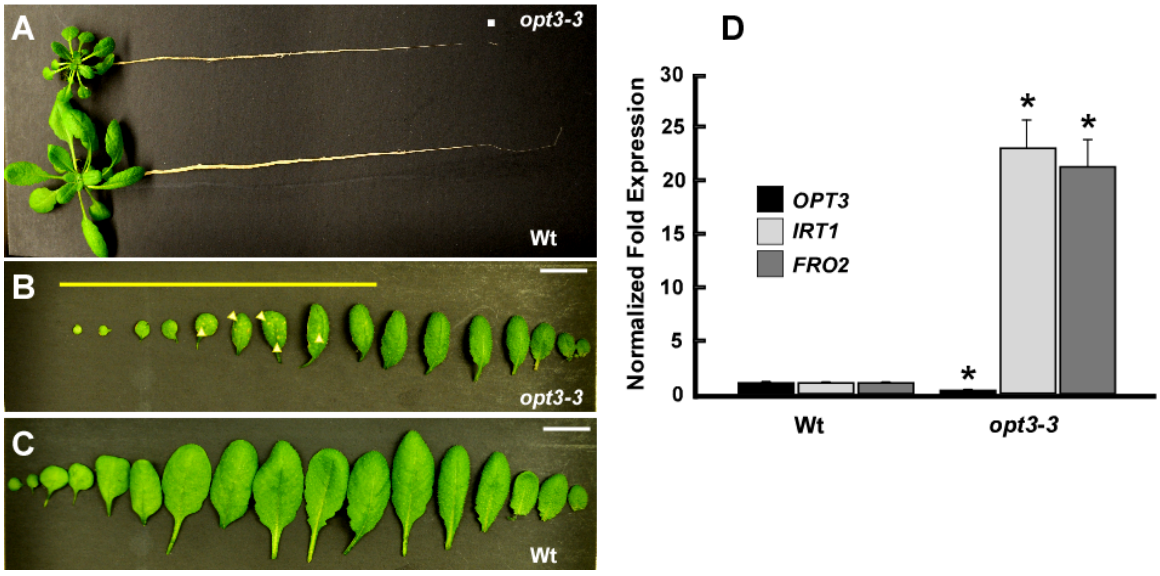

Figure 12. The *opt3-3* knockdown allele (*opt3-3*) exhibits constitutive iron deficiency symptoms. A. Representative images of hydroponically-grown wild-type and *opt3-3* plants are shown. **B**. Individual leaves of the *opt3-3* plant arranged from the oldest (left) to youngest (right) leaf. The yellow line shows older leaves with necrotic lesions (yellow arrows). **C**. Individual leaves of the wild-type plant, from oldest (left) to youngest (right). Bar = 1 cm. **D**. Quantitative real-time (qRT)-PCR analysis of the expression of Fe deficiency-responsive genes, *IRT1* and *FRO2*, in roots of wild-type (**Wt**) and ***opt3-3*** mutant (***opt3-3***) plants. Error bars indicate S.E. (n = 6). Asterisks (* $p < 0.05$) indicate statistically significant differences of transcript abundance of analyzed genes in opt3-3 vs. corresponding genes in wild-type, which were set to 1.

Table 1. Leaf element profile of wild-type (Wt) and the *opt3-3* (*opt3-3*) allele. Data represent the mean of 12 independent plants per genotype ± S.D. Data in bold represent elements with significant differences ($p \leq 0.05$) between *opt3-3* and wild type. The raw elemental concentrations for individual plant samples are available at www.ionomicshub.org in experimental tray1789 (Salk_058794). *ns*, not significant.

Element	Wild-type (μg g^{-1} Dry weight)	*opt3-3* (μg g^{-1} Dry weight)	Percentage Difference from the Wild Type	*P*-Values
Li	10.31±3.24	10.12±3.11	-2	Ns.
B	**97.38±9.37**	**71.25±7.13**	**-27**	**<0.0001**
Na	558.72±93.46	529.11±65.71	-5	ns
Mg	8507.89±589.40	8828.14±581.52	4	ns
P	8959.96±688.65	8778.49±873.51	-2	ns
K	**45192.01±3937.93**	**34799.39±4059.54**	**-23**	**<0.0001**
Ca	33529.96±2438.29	32300.06±3020.20	-4	ns
Mn	**59.08±27.74**	**158.43±48.21**	**168**	**<0.0001**
Co	**0.52±0.11**	**1.77±0.28**	**241**	**<0.0001**
Ni	1.00±0.10	1.12±0.15	12	ns
Cu	**7.92±2.02**	**10.43±2.11**	**32**	**0.0014**
Zn	**115.77±81.87**	**240.83±82.70**	**108**	**0.0006**
As	0.88±0.33	0.80±0.30	-9	ns
S	**11415.58±1525.68**	**9676.14±1129.73**	**-15**	**0.005**
Fe	**101.88±6.83**	**213.53±25.54**	**110**	**<0.0001**
Se	8.64±3.18	8.74±2.36	1	ns
Rb	**83.74±15.43**	**68.79±11.26**	**-18**	**0.008**
Sr	67.03±8.23	66.75±6.08	0	ns
Mo	**28.65±1.86**	**24.97±3.08**	**-13**	**0.0004**
Cd	**0.64±0.089**	**1.10±0.13**	**72**	**<0.0001**

Since *opt3-2* and *opt3-3* mutants exhibited similar phenotypes and fold-decreases in *OPT3* transcript abundance, we used the *opt3-3* mutant for subsequent studies.

OPT3 mediates partitioning of iron, but not cadmium, from source to sink tissues

OPT3 is expressed in the phloem, which delivers nutrients, including mineral elements, from

source to sink tissues. Therefore, to determine the contribution of OPT3 to Fe, and, possibly, Cd partitioning, we examined concentrations of Fe and Cd in old leaves (sources) and young leaves and seeds (sinks) of the *opt3-3* mutant and wild-type plants. We reasoned that if Fe and Cd are physiological substrates of OPT3, then young leaves and seeds of the *opt3-3* mutant would have a lower concentration of Fe and Cd than young leaves and seeds of wild-type plants.

For analyses of ion concentrations in young and old leaves we used plants at the late vegetative stage and performed long-term (for Fe, Figure 13A) and short-term (for Fe and Cd, Figure 13B, C, respectively) uptake and transport assays.

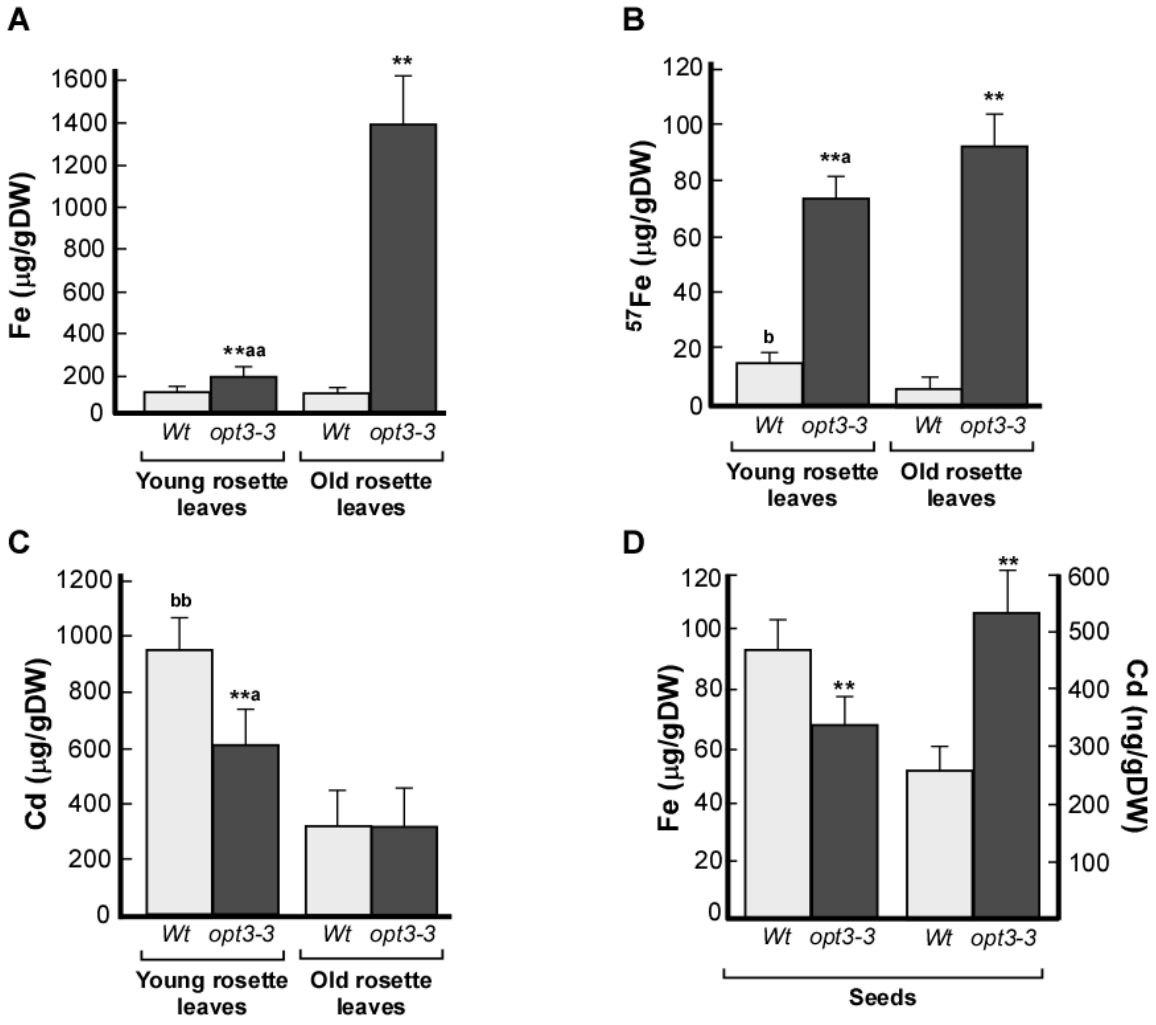

Figure 13. OPT3 mediates iron transport from source to sink tissues. ICP-MS analysis of Fe and Cd concentrations in old and young leaves (**A** to **C**) and seeds (**D**) of wild-type (**Wt**) and *opt3-3 (**opt3-3**)* mutant plants. In **A** to **C**, young and old rosette leaves were harvested at the late vegetative stage from hydroponically-grown plants. In **A,** plants were grown in 10 µM of ^{56}FeHBED (**Fe**) until tissues were collected for the ICP-MS analysis. In **B**, plants were grown in ^{56}Fe until the late vegetative stage and then transferred for 24 h to a fresh hydroponic medium containing 25 µM ^{57}FeHBED (**^{57}Fe)**, while in **C,** plants were grown for additional 24 h with 25 µM $CdCl_2$ before sink and source leaves were harvested and subjected to the ICP-MS analysis. **D**. Iron and Cd concentrations in plants grown in soil with 7.5 nM Cd or 10 µM Fe. Error bars represent S.E. (n=3). Asterisks (**) indicate statistically significant differences from the corresponding leaves in the wild-type ($p \leq 0.001$). Letters (^{a} and ^{aa}) indicate statistically significant differences between old and young rosette leaves of the *opt3-3* mutant (^{a} $p \leq 0.05$ or ^{aa} $p \leq 0.01$). Statistically significant differences between old and young rosette leaves in the wild-type are indicated as ^{bb} ($p \leq 0.001$).

The long-term Fe uptake and accumulation experiment revealed that while there were no significant differences in the concentration of Fe in young and old leaves of wild-type plants, the concentration of Fe was 8-fold higher in old *vs.* young rosette leaves of *opt3-3* mutant plants, and 14-fold higher in old leaves when compared to the corresponding leaves in wild-type plants (Figure 13A). Consistent with these data, we were able to detect Fe using the Perls' staining only in old leaves of the *opt3-3* mutant (Figure 14).

Figure 14. **Iron localizes at minor veins of old rosette leaves in the *opt3-3* mutant.** Iron was localized using Perls' stain in plants grown hydroponically in Fe sufficient conditions until the late vegetative stage. Three old and young leaves were photographed from each plant line. Note the Fe staining in old leaves but not the young leaves of the *opt3-3* mutant (***opt3-3***). The lack of staining in young leaves of the *opt3-3* mutant and in all leaves of the wild-type (**Wt**) is due to low levels of Fe that are below the limit of detection. The inset shows that Fe is associated with minor veins of the *opt3-3* mutant.

It is noticeable that young leaves of the *opt3-3* mutant accumulated 1.6-fold more Fe than

corresponding leaves of the wild-type (Figure 13A). This result was not entirely surprising because the Fe concentration in leaves of the *opt3-3* mutant is significantly higher than in the wild-type (Table 1), which is likely due to increased expression of *IRT1/FRO2* (Figure 12D online and (Stacey et al*.,* 2008)). Consistent with the role of OPT3 in Fe partitioning from source to sink leaves and the fact that young leaves are more susceptible to Fe deficiency (Marschner 1995), young leaves of the *opt3-2* mutant were more sensitive to Fe deficiency than young leaves of the wild-type (Figure 15).

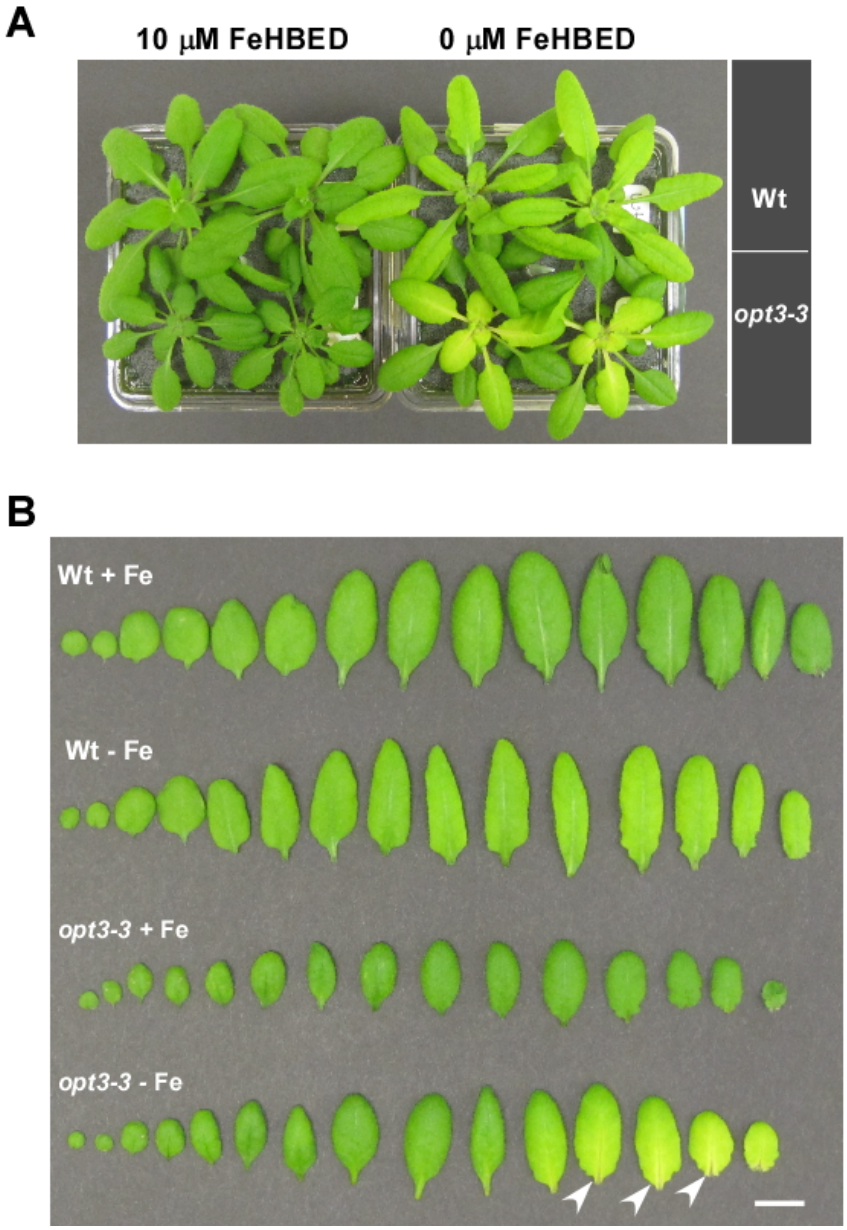

Figure 15. **Young leaves of the *opt3-3* mutant are more sensitive to iron deficiency than corresponding leaves of wild-type plants. A**. Wild-type and *opt3-3* plants were grown hydroponically to the late vegetative stage before transferring to a fresh medium with (10 mM FeHBED) or without (0 mM FeHBED) 10 mM FeHBED. Plants were photographed after 7 days of subsequent growth. **B**. Individual leaves of wild-type grown with or without 10 mM FeHBED (**Wt + Fe** and **Wt - Fe**, respectively) and *opt3-3* mutants grown with or without 10 mM FeHBED (***opt3-3* + Fe** and ***opt3-3* - Fe**, respectively) were arranged from the oldest (left) to youngest (right) leaf. Note that the youngest leaves of the opt3-3 mutant are more chlorotic than the wild-type, especially at the midrib (arrows). Bar = 1 cm.

In short-term Fe and Cd transport and loading experiments, plants were grown

hydroponically until the late vegetative stage and then transferred into a fresh hydroponic medium in which the most common isotope of ^{56}Fe (*alias* Fe) was replaced with the stable isotope, ^{57}Fe (provided as ^{57}FeHBED [25 μM]), or to hydroponic medium, supplemented with 25 μM $CdCl_2$. After 24h, roots and shoots were harvested and analyzed for ^{57}Fe and Cd by ICP-MS. In these experiments, young leaves of wild-type accumulated significantly more ^{57}Fe than old leaves (Figure 13B). In contrast, the concentration of ^{57}Fe in young leaves of the *opt3-3* mutant was still significantly lower than in old leaves of the mutant, further supporting the role of OPT3 in Fe partitioning between source and sink tissues. The concentration of ^{57}Fe in young leaves of the *opt3-3* mutant was significantly higher than in young leaves of the wild-type as well (Figure 13B). In contrast to ^{57}Fe accumulation pattern, the concentration of Cd was similar in young and old leaves of wild-type and *opt3-3* mutant plants (Figure 13C), suggesting that *opt3-3* might not be involved in the phloem-based remobilization of Cd from source to sink tissues.

We then compared Fe and Cd concentrations in seeds of wild-type and the *opt3-3* mutant, grown in soil with 7.4 nM of Cd or 10 μM Fe. Consistent with previous findings (Stacey et al*.,* 2008), the concentration of Fe in seeds of the *opt3-3* mutant was 1.4-fold lower in comparison with the seeds of wild-type plants (Figure 13D). In contrast, the concentration of Cd in seeds of the *opt3-3* mutant was 2.1-fold higher in comparison with seeds of wild-type plants (Figure 13D). Collectively, these results suggest that OPT3 functions in Fe but not Cd remobilization from source to sink tissues *via* the phloem in *A. thaliana* and thus Fe but not Cd is a physiological substrate of OPT3.

The phloem sap of the *opt3* mutant contains less iron, while the xylem sap of the *opt3-3* mutant contains more iron and less cadmium than wild-type

Localization of *OPT3* expression in minor veins of leaves, at the nodal section of stems (Figure 10A, B), and in the phloem throughout the plant (Figure 10F-M), and the inability of the *opt3-3* mutant to remobilize Fe from the sources to sinks (Figure 11) suggested a function of OPT3 in apoplastic Fe phloem loading and, possibly, xylem-to-phloem Fe transfer along the transport pathway. If this hypothesis is correct, then the concentration of Fe in the phloem would be lower in plants lacking functional OPT3 in comparison with the wild-type and accordingly, the Fe concentration in xylem sap would be higher in *opt3* mutant *vs.* wild-type.

Analysis of phloem sap revealed that the Fe concentration in the phloem was 2.3-fold lower in the mutant than in wild-type (Figure 16A).

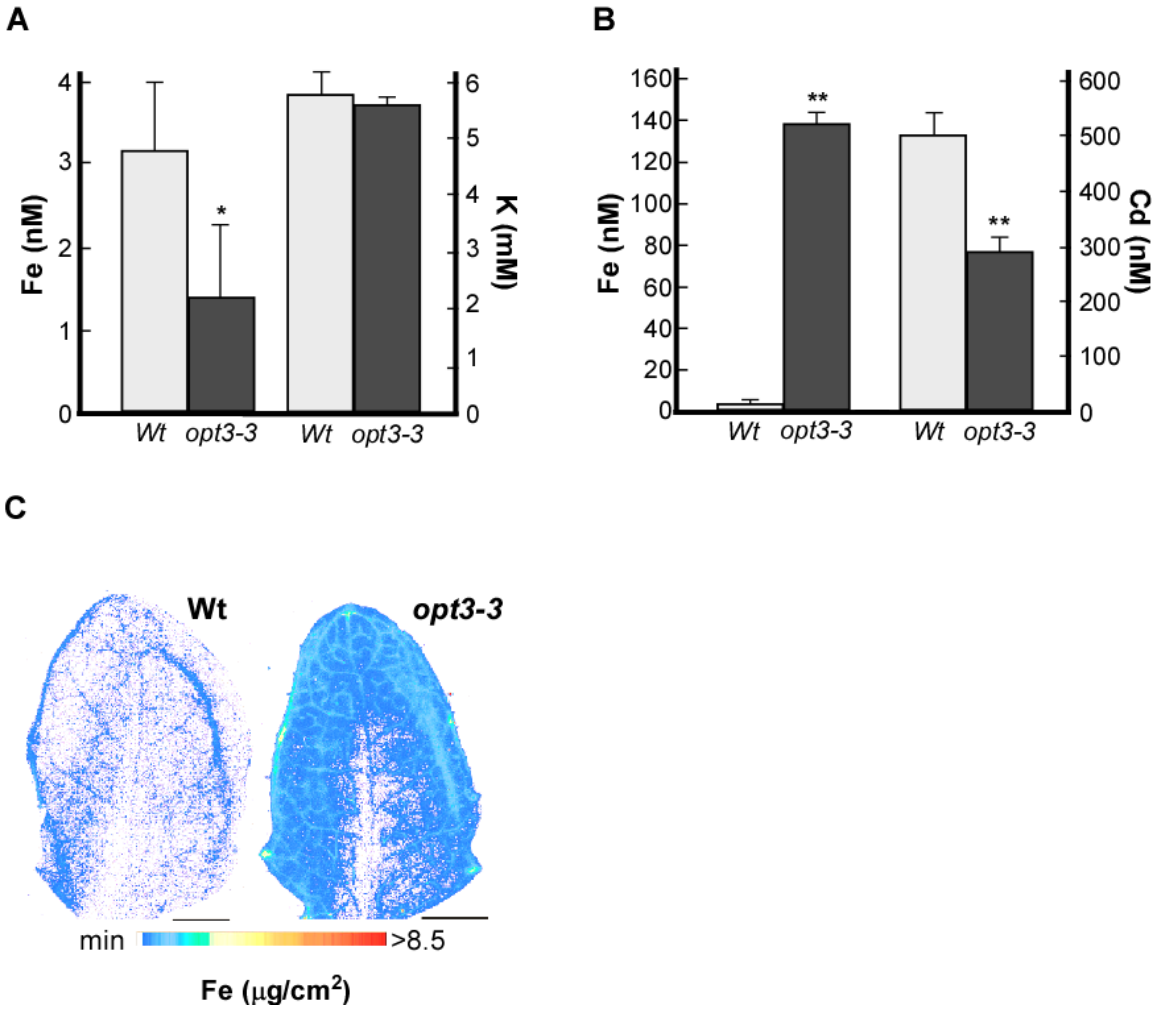

Figure 16. OPT3 mediates xylem-to-phloem iron transfer. The concentration of Fe and K in phloem sap (**A**) or Fe and Cd in xylem sap (**B**), both collected from wild-type (**Wt**) and *opt3-3* mutant (***opt3-3***) plants grown hydroponically under Fe sufficient conditions. **C.** Synchrotron X-ray fluorescence map of Fe distribution in leaves of wild-type (**Wt**) and the *opt3-3* mutant (***opt3-3***) in *A. thaliana*. Note that the line of Fe in the leaf of wild-type is an artifact of the leaf folding. Bar = 1 mm. Error bars represent S.E. (n=3). Asterisks indicate statistically significant differences (* $p \leq 0.05$ and ** $p \leq 0.001$).

To ensure that the lower concentration of Fe in the phloem of the *opt3-3* mutant was due to its inability to load Fe into the CC/SE complex rather than lower amounts of phloem exudates, we also compared the concentration of one of the major osmolytes in the phloem, potassium (K), which plays an important role in maintaining hydraulic pressure and pressure-flow-based translocation of solutes from source leaves to sink tissues such as developing leaves, seeds and

roots (Marschner 1995). Since there was no statistically significant difference between the concentration of K in the phloem of the *opt3-3* mutant and wild-type plants (Figure 16A), we concluded that the decreased Fe concentration in the phloem of the *opt3-3* mutant is due to its inability to load Fe into the CC/SE complex. Due to technical difficulties with phloem sap collection from Cd-treated plants, we were not able to determine the Cd concentration in the phloem.

Analysis of xylem sap revealed that the concentration of Fe in the sap of the *opt3-3* mutant was 42-fold higher in comparison with wild-type (Figure 16B). This result could be explained using the following not mutually exclusive scenarios: it is possible that lack of an Fe sufficiency signal in the phloem causes upregulation of *FRO2* and *IRT1*, driving enhanced Fe uptake and loading into the xylem. Alternatively, the *opt3-3* mutant may lack the ability to remove Fe from the xylem and load it into the phloem. Consistent with the latter suggestion, analysis of the spatial distribution of Fe using synchrotron X-ray fluorescence microscopy (SXRF) revealed that Fe was associated primarily with the minor veins of the *opt3-3* mutant and was located at the hydathodes and towards the leaf-blade periphery, while leaves of the wild-type contained significantly less Fe (Figure 16C). Iron was also associated with minor veins of leaves of the *opt3-3* mutant stained with Perls' stain (Figure 12). Because minor veins and the leaf periphery are the sites of the preferential expression of *OPT3* (Figure 6B) and are the sites of the intensive xylem-to-phloem transfer (Andriunas et al*.,* 2013, Bouche-Pillon et al*.,* 1994, Turgeon and Webb 1973), we propose that OPT3 loads Fe into the phloem by mediating xylem-to-phloem cycling.

In contrast to Fe, the concentration of Cd was 1.7-fold lower in xylem sap of the mutant in comparison with wild-type plants (Figure 16B). This finding further supports the notion that although OPT3 is capable of transporting Cd ions *in vitro*, Cd is not the physiological substrate

of OPT3 *in planta*.

Shoots of Cd-treated the *opt3-3* mutant accumulate less cadmium and are less sensitive to cadmium than shoots of wild-type plants

The decreased concentration of Cd in xylem sap of the *opt3-3* mutant suggests that Cd delivery from roots to shoots might be affected in the mutant, which would result in altered Cd sensitivity. To test this prediction, we grew plants hydroponically to a late vegetative stage and exposed them to Cd for 4 days. We found that roots of the Cd-grown *opt3-3* mutant accumulated significantly more Cd, while leaves accumulated significantly less Cd compared to corresponding organs in wild-type plants (Figure 17A).

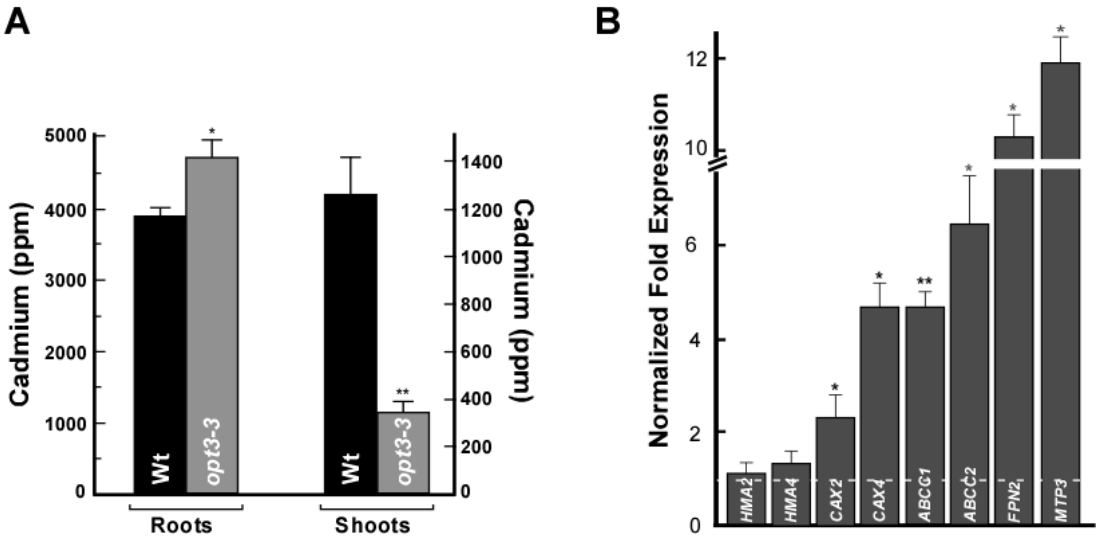

Figure 17. Leaves of *opt3-3* plants accumulate less cadmium than leaves of wild-type plants. **A**. The concentration of Cd in roots **(Roots)** and shoots **(Shoots)** of wild-type **(Wt)** and *opt3-3* mutant plants **(*opt3-3*)** grown for 4 days with 25 μM of $CdCl_2$. Shown are mean values ± S.E.; n = 3. Asterisks indicate statistically significant differences (* $p \leq 0.05$, ** $p \leq 0.001$). **B**. Transcript abundance of the indicated genes was analyzed in roots of wild-type and *opt3-3* plants, both grown hydroponically to the vegetative stage. Results are presented relative to expression of these genes in roots of wild-type plants designated as 1 (dashed line). Error bars indicate S.E. (n = 6). Asterisks indicate statistically significant differences (* $p \leq 0.05$ and ** $p \leq 0.001$, respectively).

As a result of the decreased Cd concentration, leaves of the *opt3-3* mutant were less sensitive to Cd than leaves of wild-type, both grown under the same conditions (Figure 18).

Expression of vacuolar heavy metal transporters is upregulated in roots of the *opt3-3* mutant

Given that the *opt3-3* mutant has altered root-to-shoot signaling of Fe deficiency that is manifested by the constitutive upregulation of the expression of *IRT1* and *FRO2* in roots of *A. thaliana* (Figure 12 and Stacey et al*.,* 2008), we hypothesized that expression of genes encoding transporters implicated in vacuolar sequestration or xylem loading of Cd might be altered in roots of the *opt3-3* mutant as well. To test this hypothesis, we examined the steady state mRNA level for genes encoding HMA2 and HMA4, which are responsible for Cd loading into the xylem in roots (Wong and Cobbett 2009), FPN2 (*alias* IREG2), MTP3, CAX2 and CAX4, which are suggested to play a role in vacuolar heavy metal sequestration (Arrivault et al*.,* 2006, Korenkov et al*.,* 2007, Schaaf et al*.,* 2006), or ABCC1 and ABCC2, which are involved in the vacuolar sequestration of Cd-PC complexes (Park et al*.,* 2012). The qRT-PCR analyses did not reveal statistically significant differences in transcript abundance of *HMA2* and *HMA4* in roots of *opt3-3 vs.* wild-type plants (Figure 17B). In contrast, transcript abundance of *CAX2, CAX4, ABCC1, ABCC2*, *FPN2,* and *MTP3* were significantly higher in roots of the mutant compared to the wild-type. These data suggest that increased abundance of these and, possibly, other vacuolar heavy metal transporters, is among the reasons for Cd retention in roots, decreased Cd loading into the xylem and accumulation in leaves of the *opt3-3* mutant *vs.* wild-type (Figures 8B, 17A), leading to Cd resistance phenotypes in shoots of the *opt3-3* mutant (Figure 18).

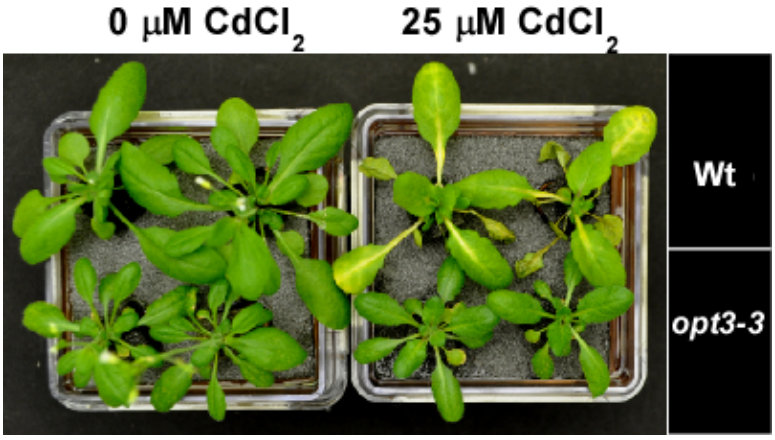

Figure 18. Leaves of *opt3-3* mutant plants are less sensitive to cadmium than leaves of wild-type. Wild-type (**Wt**) and *opt3-3* mutant plants (***opt3-3***) were grown hydroponically till the late vegetative stage and then treated with the indicated concentration of CdCl2. Plants were photographed after 4 days of subsequent growth with Cd. Note that after exposure to 25 μM CdCl2, leaves of wild-type plants wilted and developed chlorosis, while leaves of the *opt3-3* mutant did not show symptoms of Cd toxicity.

Discussion

OPT3 transports transition ions

OPT3 belongs to the oligopeptide transporter family, whose members transport synthetic tetra- and pentapetides when expressed in heterologous systems; however, the physiological substrates and the physiological role of OPTs, including OPT3, in *A. thaliana* are unknown (Lubkowitz 2011). Therefore, after finding that OPT3 localizes to the plasma membrane (Figure 1), we examined if OPT3, similar to is closest homolog from *B. juncea*, Bj-GT1, as well as other OPTs from *A. thaliana,* would transport GSH. We found that heterologously-expressed *OPT3* did not complement the GSH uptake defect of the *S. cerevisiae* GSH uptake mutant, *opt1,* nor did it transport GSH (Figure 3 and 4), suggesting that GSH might not be the physiological substrate of OPT3. In contrast, heterologously expressed *OPT3* partially rescued the growth of the *fet3fet4* mutant in Fe limited conditions (Figure 5A and (Wintz et al*.,* 2003)). Importantly, we showed that the ability of OPT3 to rescue Fe deficiency of the *fet3fet4* mutant is associated with the

OPT3-dependent increase in accumulation of Fe in cells of the mutant, even though yeast were grown in medium that lacked the Fe ligand, NA (Figure 5B). These data suggested that OPT3 might mediate transport of ions rather than peptides or ion-ligand complexes. Consistent with this suggestion, chelation of Fe^{2+} with the addition of NA to the growth medium, abolished the ability of OPT3 to rescue growth of the *fet3fet4* mutant (Wintz et al*.,* 2003).

The nature of OPT3-mediated transport was examined in *X. laevis* oocytes. After establishing that OPT3 resides at the plasma membrane in oocytes as it does in *A. thaliana* (Figure 6)*,* we employed uptake conditions that would minimize activation of endogenous oocyte transporters, and found that OPT3 likely mediates proton-coupled inward currents as was documented for other OPT family members (Osawa et al*.,* 2006) (Figure 8 and 8). Subsequently, we showed that OPT3 indeed mediates uptake of Fe^{2+} *into X. laevis* oocytes in a time-dependent manner in medium lacking metal ligands (Figure 9A). Because several characterized Fe transporters have broad substrate specificity, and IRT1 transports Cd in addition to Fe, we also examined whether OPT3 would be able to transport Cd^{2+} ions as well. We found that in addition to Fe, OPT3 mediated Cd^{2+} uptake in *X. laevis* oocytes in medium lacking metal ligands (Figure 9B).

OPT3 functions in the translocation of iron but not cadmium to sink organs

To begin the investigation of the role of OPT3 in transition ion transport *in planta*, we first determined the cell type specificity of its expression. Using transgenic plants expressing $OPT3_{pro}$*-GUS* or $OPT3_{pro}$*-GFP* fusions, we found that *OPT3* is expressed in minor veins of the vasculature in leaves and nodes of stems and that the bulk of its expression is associated with the phloem (Figure 10B, C and F-M). Further, *OPT3* was found in CC of the phloem (Mustroph et al*.,* 2009). Because OPT3 mediated Fe and Cd influx in *X. laevis* oocytes as well as Fe

accumulation in yeast cells (Figures 5 and 9), we hypothesized that OPT3 is involved in loading of Fe and, possibly, Cd into the CC/SE complex. Because the phloem plays a key role in redistribution of mineral elements from source to sink tissues, we compared Fe and Cd accumulation in older and younger rosette leaves and seeds of the *opt3-3* mutant *vs.* the wild-type. We found that the Fe concentration was 8-fold higher in old *vs.* young rosette leaves of *opt3-3* mutant plants, and 14-fold higher in old leaves when compared to the corresponding leaves in wild-type plants (Figure 13A). This result suggested that OPT3 plays a significant role in the delivery of Fe to sink tissues. Because symptoms of Fe deficiency are more prominent in younger tissues (Marschner 1995), we expected that if OPT3 functions in the phloem-based Fe partitioning then young leaves of the *opt3-3* mutant would be more susceptible to Fe deficiency than young leaves of the wild-type. Consistent with this hypothesis, we observed that young leaves of the *opt3-3* mutant were significantly more chlorotic compared to wild-type grown in the same conditions (Figure 15). Finally, OPT3 was important for the delivery of Fe to developing seeds (Figure 13D and (Stacey et al*.,* 2008)). Based on these results, we concluded that OPT3 functions in the phloem-based delivery of Fe to sink tissues and that Fe is a physiological substrate of OPT3.

In contrast to Fe, Cd content was similar in young and old leaves of wild-type and *opt3-3* mutant plants (Figure 13C), suggesting that *opt3-3* might not be involved in the phloem-based remobilization of Cd from source to sink tissues. This suggestion was substantiated by distinctively different kinetics of ^{57}Fe and Cd accumulation in young and old leaves of plants (Figure 13B, C) and finding that OPT3 is not involved in Cd loading into seeds (Figure 13D). Together, these results support the notion that although OPT3 can mediate transport of Cd *in vitro*, it is not involved in Cd partitioning *in planta* under physiological conditions. It is possible

that increased accumulation of Cd in seeds of the mutant *vs.* wild-type is due to the effect of the *OPT3* knockdown on the function/abundance of transporters, such as YSL1 or YSL3, or other transporters that are responsible for metal loading into seeds (Chu et al*.,* 2010, Waters et al*.,* 2006).

The role of OPT3 in xylem–to-phloem transfer in *A. thaliana*

It is recognized that young leaves, seeds, and other sink organs receive the majority of their mineral nutrients *via* the phloem (Marschner 1995). In addition to symplastic and apoplastic loading of the CC/CE complex, efficient xylem-to-phloem transfer may occur along the long-distance transport pathway with hubs at the nodal regions in the stem and minor veins in the leaf blade (Andriunas et al*.,* 2013, Bouche-Pillon et al*.,* 1994). The companion cells in these places differentiate into transfer cells to enhance membrane transport capacity and phloem loading and re-distribution of resources (Andriunas et al*.,* 2013). We found that: 1) *OPT3* is expressed in the phloem of minor veins in leaves and at the nodal sections of the stem (Figure 10), where it is associated with companion cells (Mustroph et al*.,* 2009). 2) The *opt3-3* mutant accumulates Fe in the vicinity of minor veins at the leaf blade periphery (Figure 14C and 16), which is suggested to have the strongest source strength (Turgeon and Webb 1973). 3) OPT3 mediates uptake of Fe ions in yeast and *X. laevis* oocytes (Figures 5 and 9). 4) The xylem sap of the *opt3-3* mutant hyperaccumulates Fe, while phloem sap contains less Fe compared to xylem and phloem saps of the wild-type (Figure 16A, B). Collectively, these data suggest that OPT3 might contribute to xylem-to-phloem transfer of Fe for subsequent partitioning from source-to-sink tissues.

OPT3 contributes to shoot-to-toot signaling of iron status

Revealing the physiological substrate and function of OPT3 has provided fundamental insights that have implications for the nature and mechanism of systemic Fe signaling in plants (summarized in Figure 20). First, our finding that the concentration of Fe is significantly lower in the phloem sap of the *opt3-3* mutant (Figure 16A), which overexpresses *IRT1* and *FRO2* in the root even under Fe sufficient conditions, provides experimental evidence that is consistent with the hypothesis that Fe availability in the phloem is essential for the regulation of Fe deficiency responses in the root. Second, it has been suggested that OPT3 plays a role in communicating Fe status from shoots to roots (Stacey et al*.,* 2008), and we provide a mechanistic basis for this phenomenon where OPT3 mediates Fe recirculation from the xylem to the phloem (Figure 16). Loss of this ability results in Fe hyperaccumulation in leaves of *opt3* knockdown mutants (Table 1 online and (Stacey et al*.,* 2008)). The mechanistic explanation of foliar Fe hyperaccumulation phenotypes of the *opt3* knockdown mutant provided by our data also rationalize findings by Garcia et al. (Garcia et al*.,* 2013) that foliar application of Fe rescues constitutive Fe acquisition responses manifested in roots of the *A. thaliana frd3*, pea *brz,* and tomato *chln* mutants, but not in the root of the *opt3-2* mutant. We reason that knockdown of *OPT3* results in plants incapable of loading Fe into the phloem for the long distance transport into the root and thus, foliar application of Fe does not rescue its Fe deficiency responses. In contrast, we found that grafting wild-type shoots onto *opt3-3* mutant roots downregulated *FRO2* and *IRT1* expression relative to their expression in control grafts (wild-type shoots onto wild-type roots) (Figure 19A). This finding emphasizes that OPT3-mediated Fe transport function in the shoot is sufficient to regulate the transcriptional Fe deficiency responses in the root. Consistent with the suggestion that OPT3 function is required in shoots, its transcript abundance in shoots was 10-fold higher

than in roots of wild-type plants (Figure 19B). Collectively these data provide molecular evidence that Fe availability in the phloem regulates expression of Fe acquisition genes in the root and identify OPT3 as an important contributor to the systemic signaling of Fe status.

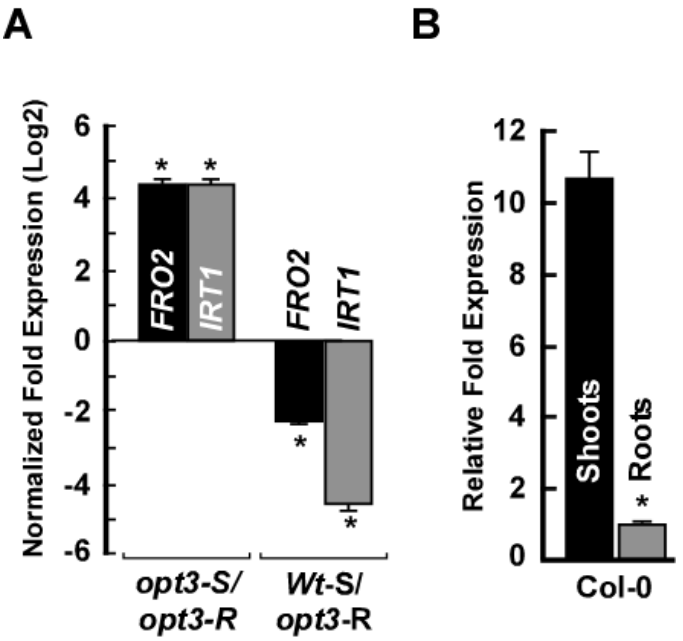

Figure 19. OPT3 functions primarily in shoots in *A. thaliana*. **A**. Transcript abundance of FRO2 and IRT1 in roots of hydroponically grown the self-grafted *opt3*-3 mutant (***opt3*-S/*opt3*-R**) and reciprocally grafted plants with wild-type shoots and opt3-3 roots (**Wt-S/*opt3*-R**). Data were normalized to the steady state level of FRO2 and IRT1 in roots of wild-type plants grown under identical conditions. **B**. The qRT-PCR analysis of the relative expression levels of OPT3 in roots and leaves of wild-type plants. Mean values ± S.E. (n = 3) are shown. Asterisks indicate statistically significant differences (* $p < 0.05$).

Our data also suggest that the decreased Cd concentration in xylem sap and shoots of the *opt3-3* mutant and increased Cd tolerance of leaves of the mutants *vs.* wild-type (Figures 16B, 17A and 18) is a consequence of OPT3 contribution to phloem-based systemic Fe signaling (Figure 20).

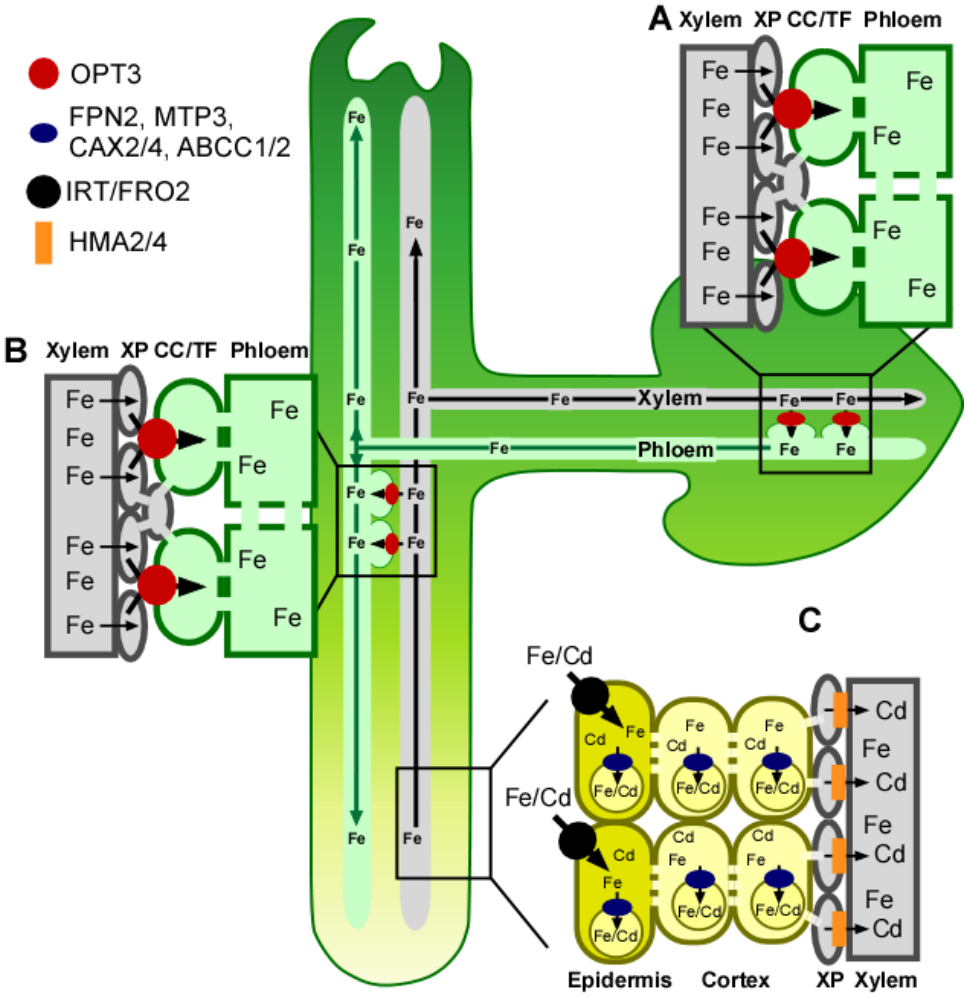

Figure 20. Model of OPT3 function in *A. thaliana*. This figure summarizes the proposed dual roles of OPT3 in the redistribution of Fe from source to sink tissues, in shoot-to-root signaling of shoot Fe status and its contribution to Cd partitioning in *A. thaliana*. **A.** *OPT3* is expressed in companion cells (**CC**) of the phloem that might differentiate into the transfer cells (**TF**) in minor veins of leaves and in nodes of stems. In these sites, OPT3 facilitates Fe loading into the phloem, possibly by direct xylem-to-phloem Fe transport. **B**. At the whole plant level, OPT3 is involved in re-distribution of Fe from sources to sinks and Fe recirculation into roots. Iron recirculation into roots *via* OPT3 plays a signaling role by conveying Fe status of the shoot. **C**. Although OPT3 transports Cd *in vitro*, it is likely that it mediates root-to-shoot partitioning of Cd indirectly by orchestrating shoot-to-root Fe signaling that, in turn, alters expression of genes encoding multispecific transition ion transporters (*e.g.* FPN2, MTP3, CAX2/4, ABCC1/2 and possibly, others). These transporters facilitate vacuolar sequestration of Cd and its retention in the root, which in turn, affects root-to-shoot Cd partitioning and Cd resistance. Abbreviations: XP, xylem parenchyma cells.

Indeed, we found that expression of genes encoding transporters that are implicated in vacuolar sequestration of Cd ions (FPN2, CAX2, CAX4, MTP3) and vacuolar sequestration of Cd-PC complexes (ABCC1 and ABCC2) is significantly upregulated in roots of the *opt3-3* mutant *vs.* wild-type (Figure 17B). We hypothesize that these, and, possibly, other transporters contribute to the retention of Cd in roots of the *opt3-3* mutant, subsequently affecting Cd loading into the xylem, root-to-shoot Cd partitioning, and increasing Cd tolerance of the shoot.

In conclusion, data presented in this manuscript uncovered a central role of OPT3 in Fe loading into the phloem, provided mechanistic explanation of OPT3-mediated shoot-to-root communication of Fe status in *A. thaliana* and highlighted the role of Fe in the phloem-based systemic signaling, a long-debated area in plant Fe homeostasis research. Our results also indicate that OPT3 contributes to Fe recycling from the xylem and acts as a functional link between the xylem and the phloem. We show that OPT3 is a multispecific transition element transporter. This functional activity distinguishes OPT3 from other peptide-transporting OPT family members. Given the acute Fe -deficiency responses of *OPT3* knockdown and knockout mutants, and the indirect effect of OPT3 on Cd partitioning in *A. thaliana*, we propose that Fe, but not Cd, is a physiological substrate of OPT3, although it is capable of transporting both Cd^{2} and Fe^{2+} ions when expressed in *X. laevis* oocytes. Another important implication from this work is finding that loss of *OPT3* function significantly decreases Fe while increases Cd concentration in seeds, suggesting that manipulation of the expression of this transporter can provide promising avenues for targeted biofortification strategies directed at increasing Fe density, while omitting Cd, in the edible portions of crops.

Materials and Methods

Plant material and growth conditions

All plant lines used in the study were in the *Arabidopsis thaliana* Columbia (Col-0) background. Seeds of *opt3-2* (SALK_021168C) and *opt3-3* (SALK_058794C) T-DNA insertion alleles were obtained from the *Arabidopsis* Biological Resource Center (Alonso et al*.,* 2003). *opt3-2* allele is also described in (Stacey et al*.,* 2002, Stacey et al*.,* 2008). *opt3-2* and *opt3-3* homozygous lines were identified by PCR using the left border T-DNA specific and the gene specific primers (Table 4).

For growing plants in hydroponics, 8-day-old seedlings were transferred from ½ MS agar plates to *Arabidopsis* hydroponic solution described in (Arteca and Arteca 2000). The hydroponic solution was changed every 5 days. For Fe deficiency assays, plants were grown hydroponically for three weeks and transferred to medium without FeHBED for the indicated time. In all experiments, the growth conditions were as follows: 12-h-light/12-h-dark photoperiod (at a photosynthetic photon flux density of 120 μmol photons m^{-2} s^{-1}) at 23°/19°C light/dark temperature regime and 75% relative humidity.

Table 4. **List of oligos.** Nucleotide sequences marked in bold indicate *att* sites.

Name	**Sequence**	**Purpose**
LBb1.3	ATTTTGCCGATTTCGGAAC	genotyping
Fopt3-2	CAAAATCCATTCGGACATGTC	genotyping
Ropt3-2	GAGGCTAAAACTCCACCCAAG	genotyping
Fopt3-3	CGGACAACCAATAGAAAGTGC	genotyping
Ropt3-3	GAGAAGTGGTGGGAAGAGTCC	genotyping
Fcad1-3	AATTGCAGACTGGGACTGGT	genotyping
Rcad13dCAP	CTTCCCAAAGAAGTTTAAGAGGGAT	genotyping
FOPT3	**TCGTCGGGGACAACTTTGTACAAAAAAGTTGG**TCAGAA TCTCCAATCCTACTCTCC	complementation in the *opt3-3* mutant
ROPT3	**GGCGGCCGCACAACTTTGTACAAGAAAGTTGGGT**TGAT GCAATTCCAATGGGTAG	complementation in the *opt3-3* mutant
FOPT3pro	**TCGTCGGGGACAACTTTGTACAAAAAAGTTGG**GGTCCA GTAGGCCATTTCACAT	GUS activity
ROPT3pro	**GGCGGCCGCACAACTTTGTACAAGAAAGTTGGGT**CTGG CAGAAAGTGAATGCTGTT	GUS activity
FOPT3-CDS	**TCGTCGGGGACAACTTTGTACAAAAAAGTTGG**GAAAAT GGACGCGGAGAAG	cloning in YES3-Gate and GWB406
ROPT3-CDS*	**GGCGGCCGCACAACTTTGTACAAGAAAGTTGGGT**TTAG AAAACGGGACAGCCTTT	complementation in *opt1*Δ and *opt2*Δ yeast
ROPT3-CDS	**GGCGGCCGCACAACTTTGTACAAGAAAGTTGGGT**GAAA ACGGGACAGCCTTTGG	complementation in *opt1* Δ and *opt2*Δ yeast
FOPT3	CTCTTCATCGTCTTGACCACTC	qRT-PCR
ROPT3	ACTTGTTTTCCTTCTCGTGC	qRT-PCR
FF14F8.90	TTTCGGCTGAGAGGTTCGAGT	qRT-PCR
RF14F8.90	GATTCCAAGACGTAAAGCAGATCAA	qRT-PCR
FFIT	AGAACATGCTCCTGATGCTC	qRT-PCR
RFIT	CACACCAATCTCACATAAAACCC	qRT-PCR
FIRT1	ACCCGTGCGTCAACAAAGCTAAAG	qRT-PCR
RIRT1	TCCCGGAGGCGAAACACTTAATGA	qRT-PCR
FFRO2	TGTGGCTCTTCTTCTCTGGTGCTT	qRT-PCR
RFRO2	TGCCACAAAGATTCGTCATGTGCG	qRT-PCR
FHMA2	TCAGGGTGTTGTGGTGACAAGAGT	qRT-PCR
RHMA2	TCCAGGCCAGATGGCTTGTTATGA	qRT-PCR
FHMA4	GAACCGCAGCCCAAATCAAAGGAT	qRT-PCR
RHMA4	GGCTCTGCTCTTGCAACACAAACT	qRT-PCR
FFPN2	ACGAGTTCTGAACACCTCCAACCA	qRT-PCR
RFPN2	TCATGGCTGGAGTTGCTGCTTCTA	qRT-PCR
FCAX2	AGACGGCGATGCTGTTCATC	qRT-PCR
RCAX2	GTGTACAAAGAAACTGGCAGCTAC	qRT-PCR
FCAX4	GCTTGTTTTGCCTTGTCCATTC	qRT-PCR
RCAX4	GGGTGAGTTAGAGACAAAGAAGC	qRT-PCR
FABCC1	AGAGCGTTGGTGGCCATCTCTTTA	qRT-PCR
RABCC1	GTGTTGCATTCTGTTCCTCGCCAA	qRT-PCR
FABCC2	TCTAGAGAGGGATGGTTGTCA	qRT-PCR
RABCC2	CATTCGGTTCCTTGCCAATC	qRT-PCR
FMTP3	CTTAATCGAGCAAAAGAAGCAGC	qRT-PCR
RMTP3	CCACTCCGGCTTATACCATATG	qRT-PCR
FACT2	GACCTTTAACTCTCCCGCTA	qRT-PCR
RACT2	GGAAGAGAGAAACCCTCGTA	qRT-PCR

Subcellular localization and fluorescent microscopy

The full-length *OPT3* cDNA was isolated by reverse transcription (RT)-PCR using total RNA from wild-type *A. thaliana* leaves and primers sets that would introduce *attB* sites on the resulting PCR product (Table 4). The PCR product was introduced into the *DONR222* entry vector (Invitrogen) before recombination cloning into the GWB406 destination vector (Nakagawa et al*.,* 2007) to fuse GFP in-frame with the N-termini of OPT3 under the control of the CaMV 35S promoter. The resulting $35S_{pro}$*-OPT3-GFP* construct or GWB406, lacking the cDNA insert were transfected into *A. thaliana* protoplasts (Zhai et al*.,* 2009). GFP-mediated fluorescence and chlorophyll autofluorescence were visualized using FITC or rhodamine filter sets, respectively, of an Axio Imager M2 microscope equipped with the motorized Z-drive (Zeiss). Z-stack (1.3 µm-thick) images were collected with the high-resolution AxioCam MR Camera and then 3D deconvoluted using an inverse filter algorithm of the Zeiss AxioVision 4.8 software.

Expression of *OPT3-GFP* in onion epidermal cells

For visualizing OPT3 localization in onion cells, the $35S_{pro}$*-OPT3-GFP* construct in the GWB406 vector and the plasma membrane marker, PIP2A, fused to mCherry in the BIN vector (Nelson et al*.,* 2007) were introduced into onion epidermal cells by biolistic transformation as described (Jung et al*.,* 2012). Briefly, 2 µg of each construct in 10 µl distilled water was mixed with 10 µl of solution containing 50 mg/ml of 1.0 µm gold particles, 10 µl of 2.5 mM $CaCl_2$, and 4 µl of 0.1 M spermidine. The mixture was incubated for 30 min at room temperature. Gold particles coated with plasmid DNA were rinsed with cold ethanol and then gently suspended in

20 µl of ethanol. Onion pieces were placed onto agar plates containing 1× MS medium and bombarded using a double-barreled extension of the Bio-Rad He/1000 particle delivery system (PDS-1000/He [Bio-Rad]) with 1100 p.s.i. rupture discs under a vacuum of 0.04 bar. Onion pieces were left to recover after bombardment in the dark at 25°C for 16 h. Onion skin epidermal layers were peeled from the onion pieces and placed on glass slides for analyses. When indicated, onion epidermal cells were plasmolyzed by incubating in 20% (w/v) sucrose solution for 10 minutes.

Tissue and cell-type specificity of *OPT3* expression in *A. thaliana*

A 3.5 kb genomic fragment including sequence upstream of *OPT3* start codon was amplified by PCR using indicated primer pairs (Table 4). The resulting amplicon was fused to the bacterial *uidA* gene encoding β-glucuronidase (GUS) of the GUS1-Gate vector (Jung et al*.,* 2012) or to GFP of the YXT2 destination vector (Xiao et al*.,* 2010). The resulting $OPT3_{pro}$-*uidA* ($OPT3_{pro}$-*GUS)* or $OPT3_{pro}$-*GFP* constructs were transformed into wild-type *A. thaliana* (Clough and Bent 1998). GUS staining was performed for 16 h with 2 mM X-Gluc (5-bromo-4-chloro-3-indolyl-β-D-glucuronide) as described (Jefferson et al*.,* 1987). Staining patterns were analyzed using Leica S6E stereomicroscope. Hand-cut sections were prepared from stems and petioles of transgenic *Arabidopsis* plants expressing $OPT3_{pro}$-*GFP* using feather double edge razor blade. GFP- and autofluorescence were visualized using FITC (for GFP) or rhodamine (for autofluorescence) filter sets of the Axio Imager M2 microscope equipped with the motorized Z-drive (Zeiss). Images were processed using the Adobe Photoshop software package, version 12.0.

Functional complementation assays in *Saccharomyces cerevisiae*

S. cerevisiae strains used in this study were: BY4741 (*MAT*a*; his3Δ1; leu2Δ0; met15Δ0; ura3Δ0*); *opt1(alias* ABC822) (*MAT*a*; ura3-52; leu2*Δ*1; lys2-801; his3*Δ*200; trp1*Δ*63; ade2-101; hgt1*Δ*::LEU2*); DY1457 (*MAT*a *ade6 can1 his3 leu2 trp1 ura3*); DEY1453 (*MAT*a/*MAT*α *ade2/+ canl/canl his3/his3 leu2/leu2 trpl/trpl ura3/ura3 fet3-2::HIS3/fet3-2::HIS3fet4-1::LEU2/fet4-1::LEU2).* Briefly, the full-length *OPT3* or *IRT1* cDNAs were cloned by recombination into YES3-Gate vector and resulting vectors, *YES3-Gate-OPT3, YES3-Gate-IRT1* and *YES3-Gate*, lacking the cDNA insert, were transformed into different yeast strains using the Frozen-EZ yeast Transformation II Kit (Zymo Research).

To test if OPT3 would rescue GSH uptake deficiency of *opt1* mutant in medium with GSH as the only sulfur (S) source, the *opt1* mutant expressing either *OPT3* or the empty vector were grown in YNB medium with supplements to an OD_{600nm} = 1.2. Cells were then washed in ice-cold water 3 times and inoculated (1:200) into SC-S media supplemented with 200 μM of GSH. SC-S was prepared according to the YNB recipe (Bacto Yeast Nitrogen Base without amino acids and ammonium sulfate, DIFCO Laboratories, Detroit), with the modification that all sulfur containing reagents in macroelements and microelements were substituted with equal amounts of the corresponding chloride salts (Zhang et al*.,* 2004). The medium was supplemented with His, Trp, Ade, and Lys.

For functional complementation assays in the *fet3fet4* Fe uptake-deficient mutant, YES3-Gate-OPT3, YES3-Gate-IRT1 and YES3-Gate lacking cDNA inserts were transformed into the *fet3fet4* mutant or the empty vector was transformed into the wild-type strains DY1457. The transformants were selected on YNB medium (pH 4.0) lacking uracil but supplemented with adenine sulfate (20 mg/L), tryptophan (20 mg/L) and ferric chloride (10 μM). Yeast colonies

were inoculated into the same liquid medium and grown overnight to an OD_{600nm} of 1.0. Yeast cells were washed in sterile water to desorb excess $FeCl_3$ from cell walls and aliquots of cell suspension were serially diluted and spotted onto solid YNB medium (pH 4.0) lacking uracil but supplemented with adenine sulfate (20 mg/L), tryptophan (20 mg/L) and 10 μM BPS. Colonies were visualized after incubating plates for 6 days at 30^0C.

***In vitro* GSH uptake**

S. cerevisiae opt1 mutant cells transformed with YES3-Gate-ScOPT1, YES3-Gate-At-OPT3 or the empty YES3-Gate vector were grown in YNB-URA to OD_{600} = 0.8. Uptake studies were performed using modified procedures of (Pence et al*.,* 2000, Zhang et al*.,* 2004). Briefly, cells were harvested by centrifugation, washed from the culture medium with deionized water and a washing buffer containing 20 mM MES-KOH, 50 μM $CaCl_2$ and 25 μM $MgCl_2$, pH 5.0, before re-suspension in the ice-cold uptake buffer (washing buffer supplemented with 2% [w/v] glucose), all solutions were kept on ice. After warming to room temperature, cells were mixed with equal volumes of radiolabeled [^{35}S] GSH (100 μM, specific activity 30 Ci/mmol) and incubated at room temperature for the indicated time points. [^{35}S] GSH radioactivity was measured in yeast pellets obtained after centrifugation of 100 μl cell suspension aliquots through a silicone oil/dionyl phthalate mixture onto 10 μl of 40% perchloric acid (Pence et al*.,* 2000).

Elemental analysis

Elemental composition was analyzed in *A. thaliana* and *S. cerevisiae*. For studies in *A. thaliana*, plants were grown hydroponically as described above. In long-term experiments of Fe accumulation in old and young leaves, plants were grown until the late vegetative stage. For

short-term Fe and Cd uptake and transport studies, plants were grown in 10 µM of Fe-HBED (in ^{56}Fe as common isotope of Fe, natural abundance 91.7%) until the late vegetative stage and then transferred for an additional 24 h to a fresh hydroponic medium in which ^{56}Fe was replaced with 25 µM ^{57}Fe (*Isoflex USA,* 95% enrichment), or to a fresh hydroponic medium supplemented with 25 µM $CdCl_2$ for 24 h before sink and source leaves were harvested and subjected to the ICP-MS analysis. Roots and leaves were harvested and roots were desorbed of Cd and Fe as well as other elements by washing with 10 mM EDTA followed by washing in a solution with 0.3 mM bathophenanthroline disulphonate and 5.7 mM sodium dithionite and then rinsed with deionized water. Shoots were rinsed with deionized water. In analyses of Fe and Cd accumulation in young and old leaves, 2 bottommost rosette leaves (old) and uppermost rosette leaves > 3mm (young) were collected from 3-to-5 plants. For analyses of Fe and Cd concentration in seeds, plants were grown in soil with 7.4 nM Cd or 10 µM Fe. Elemental analysis was performed using inductively coupled plasma mass spectrometry (ICP-MS) as described (Lahner et al*.,* 2003)**.** The ICP-MS-based analysis of the Fe concentration in yeast cells was performed as described (Gayomba et al*.,* 2013, Jung et al*.,* 2012) except that liquid YNB media used for growing yeast cells was at pH 4.0, was lacking uracil, and was supplemented with adenine sulphate (20 mg/L), tryptophan (20 mg/L) and 10 µM $FeCl_3$.

Expression of *OPT3* in *X. laevis* oocytes and electrophysiological recordings

The coding region of *OPT3* was cloned into the *T7TS* plasmid (Cleaver et al*.,* 1996), at the *EcoRV* unique site flanked by the 3'- and 5' untranslated regions of a *X. laevis β-globin* gene. The construct was fully sequenced and checked for sequence accuracy. Complementary RNA (cRNA) was synthesized from 1 µg *Sma*I-linearized plasmid DNA template using a mMessage *in*

vitro transcription kit (Ambion) according to the manufacturer's recommendations and stored at -80^{o} C. Stage V–VI *X. laevis* oocytes were harvested, defolliculated and cultured in ND96 solution containing 96 mM NaCl, 2 mM KCl, 1.8 mM $CaCl_2$, 1 mM $MgCl_2$, 2.5 mM Na-Pyruvate, 50 µg/mL gentamycin and 0.4 mg/mL BSA and 5 mM 4-(2-hydroxyethyl)-1-piperazineethanesulfonic acid (HEPES)/NaOH to adjust pH to 7.5, as described previously (Pineros et al*.,* 2008). *X. laevis* oocytes were injected with 50 nL water (control) or 50 nL of water containing 50 ng of *OPT3* cRNA, and incubated in ND96 solution at 18^{o}C for 2-4 days prior to the uptake and electrophysiological measurements.

Electrophysiological recordings were done under constant bath perfusion with both GeneClamp 500 and Axoclamp 900A amplifiers (Axon Instruments) using the two-electrode voltage-clamp (TEVC) technique. Recording electrodes were filled with 0.5 M K_2SO_4 and 30 mM KCl, and had resistances between 0.5 and 1.5 MΩ. Cells were bathed under constant perfusion in a ND96-recording solution consisting of (in mM) 96 NaCl, 1 KCl, and 1.8 $CaCl_2$ with the pH adjusted to 7.5 with 5 mM HEPES/NaOH. Given the presence of variable endogenous inward current at hyperpolarizing holding potentials (Amasheh and Weber 1999, Kuruma et al*.,* 2000) currents under voltage clamp conditions were elicited by a 6s voltage pulses (in 10 mV step increments) restricted between 0 and -140 mV, with a 2-s rest at 0 mV between each voltage pulses. The output signal was digitized and analyzed using Digidatas 1320A and 1440A PClamp 10 data acquisition systems (Axon Instruments). The steady-state current–voltage (I/V) relationships were constructed by measuring the current amplitude at the end of the test pulse. All data points represent the mean of at least eight different cells from three to four donor frogs. Error bars denote S.E. and are not shown when they are smaller than the symbol.

Expression of the *OPT3-EGFP* chimera in *X. laevis* oocytes

The T7TS vector was used as the backbone to generate the *OPT3-EGFP* chimera. First, the *EGFP* ORF was amplified using a 5′ end adaptor consisting of an *SpeI* adaptor followed by a short linker sequence (TSGG) immediately upstream of the *EGFP* coding region (initiation codon removed). The 3′ end adaptor consisted of an additional stop codon downstream of the *EGFP* stop codon, followed by a *SpeI* adaptor. The resulting product was cloned into the *SpeI* site of the T7TS plasmid. This backbone plasmid was named T7TS-C-EGFP. The ORF of *OPT3* without a stop codon was amplified using EcoRV adaptors, and cloned into the EcoRV site of the T7TS-C-EGFP vector, resulting in an *OPT3-EGFP* chimera joint by a DITSTSGG linker.

Metal uptake in oocytes

The basal uptake solution consisted of a modified ND96 solution containing 96 mM NaCl, 1 mM KCl, 0.9 mM $CaCl_2$, buffered with 5 mM 2-(N-morpholino) ethanesulfonic acid/NaOH to pH 6.0. The uptake solutions was supplemented with 0.5 mM $CdCl_2$ or 0.4 mM $FeSO_4$ + 1 mM L-ascorbic acid (freshly prepared) to prevent Fe oxidation. Given the strong interaction of Cd with Cl (*e.g.* 80% of the Cd present in the uptake solution is complexed with Cl), the free Cd^{2+} activity in the uptake solution was estimated to be 35 µM Cd^{2+} while Fe^{2+} free activity was 150 µM as determined by GEOCHEM-EZ (Shaff et al*.,* 2010). Each sample contained 6 oocytes, with 5 replicates per time point. At a given time point, the uptake was terminated by washing oocytes through six consecutive ice-cold basal uptake solution. Samples were digested in 100 µL of 70% $HClO_4$, re-suspended in 10 ml of 0.1 M nitric acid, and analyzed using ICP-MS (PerkinElmerSciex). Uptake data are expressed “per oocyte” and are representative of at least five independent experiments.

Collection and analysis of xylem sap

Xylem sap was collected as previously described (Sunarpi Y. et al., 2005). Briefly, wild-type and *opt3-3* mutant plants were cultured on hydroponic media until the late vegetative stage. For analyses of Cd concentration, plants were subjected to 25 μM $CdCl_2$ for 48h. After removal of rosette leaves, the inflorescence stem was cut with a fresh razor blade. Xylem sap exudation was facilitated through a high humidity environment by covering the plants with a plastic dome. The first droplets were excluded to avoid contamination and then xylem sap was collected quantitatively with a micropipette. Cadmium and Fe concentrations in the sap were analyzed by ICP-MS and normalized per volume of the collected sample.

Collection and analysis of phloem sap

Phloem sap was collected from hydroponically grown wild-type and *opt3-3* mutant plants at the late vegetative stage. To prevent entrance of air bubbles into the vasculature, whole rosettes were removed from the root using a razor blade and immersed in de-ionized water before individual leaves were detached at the petiole. Three leaves (leaf numbers 9-10) collected from one plant were pooled together and flushed of xylem sap by placing the petioles in a tube filled with 300 μL of de-ionized water and incubated in an illuminated growth chamber for 15 minutes before further incubation in darkness for 1 hour. The petioles were then re-cut under 5 mM Na_2-EDTA (pH 7.5) under low light before placing the petioles in 250 μL of 5 mM Na_2-EDTA (pH 7.5). The leaves where then incubated in darkness for 1 hour in a high-humidity chamber lined with wet paper towels and sealed with Vaseline. Samples were diluted with 5 mL of 5% HNO_3 for subsequent detection of K or Fe by ICP-MS.

Synchrotron X-ray fluorescence microscopy (SXRF)

Wild-type and *opt3-3* mutant plants were grown on solid ½ MS medium for 23 days. Fully developed leaves (2nd from the bottom) were detached immediately prior analysis using Teflon-coated forceps and placed, adaxial side uppermost, on 35 mm slide mounts across which Kapton™ metal-free tape was stretched. The distribution of Fe in hydrated leaf tissue was imaged *via* SXRF at hard X-ray microprobe X26A of the National Synchrotron Light Source. This is a bending magnet beamline, which uses Kirkpatrick-Baez focusing optics. Photon Flux at 18 keV is approximately 1x10^{9} photons/sec in focused monochromatic mode, which causes no discernible beam damage to hydrated plant samples. The microprobe is equipped with a Canberra 9-element HPGe Array detector, and two Radiant Vortex-EX Silicon Drift Diode (SDD) detectors, providing trace element analyses detection with 1≈ ppm sensitivity. Leaves were raster scanned in 6 μm steps the x and y directions to provide the Fe map. A focused, monochromatic incident X-ray beam of 11 keV, and dimensions of 7 x 10 μm was used for leaf analysis, with dwell times of 0.25 second/pixel. Each leaf sample took approximately 6 hours to image from petiole to hydathode. Quantification of fluorescence counts into μg cm^{-1} used a standards-based approached as described previously (Punshon et al*.,* 2013).

Perls' staining

Ferric iron was visualized in leaves of *A. thaliana* using Perls' staining as described (Green and Rogers 2004). Briefly, wild-type and *opt3-3* mutant plants were grown hydroponically in Fe-replete conditions until the late vegetative stage. Shoots from 5-week old hydroponically grown Wt and *opt3-3* plants were vacuum infiltrated with Perls' stain solution (4% HCl [v/v] and 4% [w/v] potassium ferrocyanide) and allowed to incubate under vacuum for 1 hour. Samples were

then removed from the vacuum chamber and incubated for 1.5 hours. The reaction was stopped by rinsing samples three times with distilled water.

Reciprocal grafting

Five or seven-day-old seedlings were used for grafting experiments, performed as described (Rus et al*.,* 2006). After recovery for 5 days, robust grafts lacking adventitious roots on the scion were transferred to hydroponics and cultured for 2.5 weeks before $CdCl_2$ (25 μM) was added to the hydroponic medium. Grafts were photographed and tissues were collected at the indicated time points. RNA for qRT-PCR analysis was isolated from roots of grafted plants grown to the late vegetative stage.

RNA isolation and qRT-PCR

A. thaliana wild-type and *opt3-3* mutant plants were grown hydroponically till late vegetative stage. Total RNA was isolated from roots and shoots of hydroponically-grown plants using TRIZOL reagent (Invitrogen) according to manufacturer's recommendations. DNAse *I* (Roche) digestion of gDNA prior to first strand cDNA synthesis and qRT-PCR thermocycling procedures were as described (Gayomba et al*.,* 2013, Jung et al*.,* 2012). Data were normalized to the expression of *F14F8.90 (AT5G15710)* and *ACTIN2* (*AT3G18780).* The fold-difference ($2^{-\Delta\Delta Ct}$) or relative quantities were calculated using the CFX Manager Software, version 1.5 (BioRad).

Statistical analysis

Statistical analyses of the majority of experimental data were performed using the ANOVA Single Factor Analysis. Statistical analysis of qRT-PCR data was performed using the Relative

Expression Software Tool (REST, Qiagen [Pfaffl et al., 2002]).

Accession numbers

Sequence data from this article can be found in the GenBank/EMBL libraries under the following accession numbers (accession numbers in parenthesis): At-*OPT3* (AT4G16370), At-*FIT* (AT2G28160), At-*IRT1* (AT4G19690), At-*FRO2* (AT1G01580), At-*HMA2* (AT4G30110), At-*HMA4* (AT2G19110), At-*FPN2* (AT5G03570), At-*ACT2* (AT3G18780), At-*F14F8.90* (AT5G15710), At-*CAX2* (AT3G13320), At-*CAX4* (AT5G01490), At-*ABCC1* (AT1G30400), At-*ABCC2* (AT2G34660), At-*MTP3* (AT3G58810) and Sc-*OPT1* (NM_001181645)

REFERENCES

Alonso, J., Stepanova, A., Leisse, T., Kim, C., Chen, H., Shinn, P., & Ecker, J. R. (2003) Genome-Wide Insertional Mutagenesis of *Arabidopsis thaliana*. *Science*, **301**, 653-657.

Amasheh, S. and Weber, W. (1999) Further characteristics of the Ca^{2+}-inactivated Cl^- channel in *Xenopus laevis* oocytes. *J Membr Biol*, **172**, 169-179.

Andriunas, F., Zhang, H.-M., Xia, X., Patrick, J. W. and Offler, C. E. (2013) Intersection of transfer cells with phloem biology – broad evolutionary trends, function and induction. *Front Plant Sci*, **4**, 221.

Arrivault, S., Senger, T. and Krämer, U. (2006) The *Arabidopsis* metal tolerance protein AtMTP3 maintains metal homeostasis by mediating Zn exclusion from the shoot under Fe deficiency and Zn oversupply. *Plant J*, **46**, 861-879.

Arteca, R. N. and Arteca, J. M. (2000) A novel method for growing *Arabidopsis thaliana* plants hydroponically. *Physiol Plant*, **108**, 188-193.

Baxter, I. R., Vitek, O., Lahner, B., Muthukumar, B., Borghi, M., Morrissey, J. and Salt, D. E. (2008) The leaf ionome as a multivariable system to detect a plant's physiological status. *Proc Natl Acad Sci U S A*, **105**, 12081-12086.

Bogs, J., Bourbouloux, A., Cagnac, O., Wachter, A., Rausch, T. and Delrot, S. (2003) Functional characterization and expression analysis of a glutathione transporter, BjGT1, from *Brassica juncea*: evidence for regulation by heavy metal exposure. *Plant Cell Environ*, **26**, 1703-1711.

Bouche-Pillon, S., Fleurat-Lessard, P., Fromont, J. C., Serrano, R. and Bonnemain, J.L. (1994) Immunolocalization of the plasma membrane H^+-ATPase in minor veins of *Vicia faba* in relation to phloem loading. *Plant Physiol*, **105**, 691-697.

Bourbouloux, A., Shahi, P., Chakladar, A., Delrot, S. and Bachhawat, A.K. (2000) Hgt1p, a high affinity glutathione transporter from the yeast *Saccharomyces cerevisiae*. *J Biol Chem*, **275**, 13259-13265.

Cagnac, O., Bourbouloux, A., Chakrabarty, D., Zhang, M.-Y. and Delrot, S. (2004) AtOPT6 transports glutathione derivatives and is induced by primisulfuron. *Plant Physiol*, **135**, 1378-1387.

Chu, H. H., Chiecko, J., Punshon, T., Lanzirotti, A., Lahner, B., Salt, D. E. and Walker, E. L. (2010) Successful reproduction requires the function of *Arabidopsis* Yellow Stripe-Like1 and Yellow Stripe-Like3 metal-nicotianamine transporters in both vegetative and reproductive structures. *Plant Physiol*, **154**, 197-210.

Cleaver, O. B., Patterson, K. D. and Krieg, P. A. (1996) Overexpression of the tinman-related genes XNkx-2.5 and XNkx-2.3 in *Xenopus* embryos results in myocardial hyperplasia. *Development*, **122**, 3549-3556.

Clough, S. J. and Bent, A. F. (1998) Floral dip: a simplified method for *Agrobacterium*-mediated transformation of *Arabidopsis thaliana*. *Plant J*, **16**, 735-743.

Connolly, E. L., Fett, J. P. and Guerinot, M. L. (2002) Expression of the IRT1 metal transporter is controlled by metals at the levels of transcript and protein accumulation. *Plant Cell*, **14**, 1347-1357.

Curie, C., Cassin, G., Couch, D., Divol, F., Higuchi, K., Le Jean, M., and Mari, S. (2009) Metal movement within the plant: contribution of nicotianamine and yellow stripe 1-like transporters. *Ann Bot*, **103**, 1-11.

DiDonato, R. J., Roberts, L. A., Sanderson, T., Eisley, R. B. and Walker, E. L. (2004) *Arabidopsis* Yellow Stripe-Like2 (YSL2): a metal-regulated gene encoding a plasma

membrane transporter of nicotianamine–metal complexes. *Plant J*, **39**, 403-414.
Dix, D. R., Bridgham, J. T., Broderius, M. A., Byersdorfer, C. A. and Eide, D. J. (1994) The FET4 gene encodes the low affinity Fe(II) transport protein of *Saccharomyces cerevisiae*. *J Biol Chem*, **269**, 26092-26099.
Durrett, T. P., Gassmann, W. and Rogers, E. E. (2007) The FRD3-mediated efflux of citrate into the root vasculature is necessary for efficient iron translocation. *Plant Physiol*, **144**, 197-205.
Eide, D., Broderius, M., Fett, J. and Guerinot, M.L. (1996) A novel iron-regulated metal transporter from plants identified by functional expression in yeast. *Proc Natl Acad Sci U S A*, **93**, 5624-5628.
García, M. J., Romera, F. J., Stacey, M. G., Stacey, G., Villar, E., Alcántara, E. and Pérez-Vicente, R. (2013) Shoot to root communication is necessary to control the expression of iron-acquisition genes in Strategy I plants. *Planta*, **237**, 65-75.
Gayomba, S. R., Jung, H. I., Yan, J., Danku, J., Rutzke, M. A., Bernal, M. and Vatamaniuk, O. K. (2013) The CTR/COPT-dependent copper uptake and SPL7-dependent copper deficiency responses are required for basal cadmium tolerance in *A. thaliana*. *Metallomics*, **5**, 1262-1275.
Green, L. S. and Rogers, E. E. (2004) FRD3 controls iron localization in *Arabidopsis*. *Plant Physiol*, **136**, 2523-2531.
Grusak, M. A. and Pezeshgi, S. (1996) Shoot-to-root signal transmission regulates root Fe(III) reductase activity in the *dgl* mutant of pea. *Plant Physiol*, **110**, 329-334.
Grusak, M. A., Welch, R. M. and Kochian, L. V. (1990) Physiological characterization of a single-gene mutant of *Pisum sativum* exhibiting excess iron accumulation: I. root iron reduction and iron uptake. *Plant Physiol*, **93**, 976-981.
Hasan, S. A., Fariduddin, Q., Ali, B., Hayat, S. and Ahmad, A. (2009) Cadmium: toxicity and tolerance in plants. *J Environ Biol*, **30**, 165-174.
Hindt, M. N. and Guerinot, M. L. (2012) Getting a sense for signals: Regulation of the plant iron deficiency response. *Biochim Biophys Acta*, **1823**, 1521-1530.
Ishimaru, Y., Masuda, H., Bashir, K., Inoue, H., Tsukamoto, T., Takahashi, M., and Nishizawa, N. K. (2010) Rice metal-nicotianamine transporter, OsYSL2, is required for the long-distance transport of iron and manganese. *Plant J*, **62**, 379-390.
Jarup, L. (2003) Hazards of heavy metal contamination. *Br Med Bull*, **68**, 167-182.
Jefferson, R. A., Kavanagh, T. A. and Bevan, M. W. (1987) GUS fusions: beta-glucuronidase as a sensitive and versatile gene fusion marker in higher plants. *EMBO J*, **6**, 3901.
Jung, H. I., Gayomba, S. R., Rutzke, M. A., Craft, E., Kochian, L. V. and Vatamaniuk, O. K. (2012) COPT6 is a plasma membrane transporter that functions in copper homeostasis in *Arabidopsis* and is a novel target of SQUAMOSA Promoter Binding Protein-Like7. *J Biol Chem*, **287**, 33252-33267.
Kneen, B. E., Larue, T. A., Welch, R. M. and Weeden, N. F. (1990) Pleiotropic effects of *brz*: a mutation in *Pisum sativum* (L.) *cv* 'Sparkle' conditioning decreased nodulation and increased iron uptake and leaf necrosis. *Plant Physiol*, **93**, 717-722.
Kobayashi, T. and Nishizawa, N. K. (2012) Iron uptake, translocation, and regulation in higher plants. *Annu Rev Plant Biol*, **63**, 131-152.
Korenkov, V., Hirschi, K., Crutchfield, J. and Wagner, G. (2007) Enhancing tonoplast Cd/H antiport activity increases Cd, Zn, and Mn tolerance, and impacts root/shoot Cd partitioning in *Nicotiana tabacum* L. *Planta*, **226**, 1379-1387.
Kuruma, A., Hirayama, Y. and Hartzell, H. C. (2000) A hyperpolarization- and acid-activated

nonselective cation current in *Xenopus* oocytes. *Am J Physiol Cell Physiol*, **279**, C1401-1413.
Lahner, B., Gong, J., Mahmoudian, M., Smith, E. L., Abid, K. B., Rogers, E. E. and Salt, D. E. (2003) Genomic scale profiling of nutrient and trace elements in *Arabidopsis thaliana*. *Nat Biotechnol*, **21**, 1215-1221.
Li, Z. S., Lu, Y. P., Zhen, R. G., Szczypka, M., Thiele, D. J. and Rea, P. A. (1997) A new pathway for vacuolar cadmium sequestration in *Saccharomyces cerevisiae*: YCF1-catalyzed transport of bis(glutathionato)cadmium. *Proc Natl Acad Sci U S A*, **94**, 42-47.
Lubkowitz, M. (2011) The oligopeptide transporters: a small gene family with a diverse group of substrates and functions? *Mol Plant*, **4**, 407-415.
Maas, F. M., van de Wetering, D. A., van Beusichem, M. L. and Bienfait, H. F. (1988) Characterization of phloem iron and its possible role in the regulation of Fe-efficiency reactions. *Plant Physiol*, **87**, 167-171.
Marschner, H. (1995) *Mineral nutrition of higher plants* London; San Diego: Academic Press.
Morrissey, J., Baxter, I. R., Lee, J., Li, L., Lahner, B., Grotz, N. and Guerinot, M. L. (2009) The ferroportin metal efflux proteins function in iron and cobalt homeostasis in *Arabidopsis*. *Plant Cell*, **21**, 3326-3338.
Mustroph, A., Zanetti, M. E., Jang, Charles J. H., Holtan, Hans E., Repetti, Peter P., Galbraith, D.W., Girke, T. and Bailey-Serres, J. (2009) Profiling translatomes of discrete cell populations resolves altered cellular priorities during hypoxia in *Arabidopsis*. *Proc Natl Acad Sci U S A*, **106**, 18843-18848.
Nakagawa, T., Suzuki, T., Murata, S., Nakamura, S., Hino, T., Maeo, K. and Ishiguro, S. (2007) Improved Gateway binary vectors: high-performance vectors for creation of fusion constructs in transgenic analysis of plants. *Biosci Biotechnol Biochem*, **71**, 2095-2100.
Nelson, B. K., Cai, X. and Nebenführ, A. (2007) A multicolored set of in vivo organelle markers for co-localization studies in *Arabidopsis* and other plants. *Plant J*, **51**, 1126-1136.
Osawa, H., Stacey, G. and Gassmann, W. (2006) ScOPT1 and AtOPT4 function as proton-coupled oligopeptide transporters with broad but distinct substrate specificities. *Biochem J*, **393**, 267-275.
Park, J., Song, W.-Y., Ko, D., Eom, Y., Hansen, T. H., Schiller, M. and Lee, Y. (2012) The phytochelatin transporters AtABCC1 and AtABCC2 mediate tolerance to cadmium and mercury. *Plant J*, **69**, 278-288.
Pence, N. S., Larsen, P. B., Ebbs, S. D., Letham, D. L., Lasat, M. M., Garvin, D. F., Eide, D. and Kochian, L. V. (2000) The molecular physiology of heavy metal transport in the Zn/Cd hyperaccumulator *Thlaspi caerulescens*. *Proc Natl Acad Sci U S A*, **97**, 4956-4960.
Pfaffl, M. W., Horgan, G. W. and Dempfle, L. (2002) Relative expression software tool (REST) for group-wise comparison and statistical analysis of relative expression results in real-time PCR. *Nucleic Acids Res*, **30**, e36.
Piñeros, M. A., Cancado, G. M. and Kochian, L. V. (2008) Novel properties of the wheat aluminum tolerance organic acid transporter (TaALMT1) revealed by electrophysiological characterization in *Xenopus* oocytes: functional and structural implications. *Plant Physiol*, **147**, 2131-2146.
Punshon, T., Ricachenevsky, F. K., Hindt, M. F., Socha, A. and Zuber, H. (2013) Methodological approaches for using Synchrotron X-Ray fluorescence (Sxrf) imaging as a tool in ionomic characterization: examples from whole plant imaging of *Arabidopsis thaliana*. *Metallomics*, **5**, 1133-1145.
Rea, P. A. (2012) Phytochelatin synthase: of a protease a peptide polymerase made. *Physiol*

Plant, **145**, 154-164.
Robinson, N. J., Procter, C. M., Connolly, E. L. and Guerinot, M. L. (1999) A ferric-chelate reductase for iron uptake from soils. *Nature*, **397**, 694-697.
Rogers, E. E. and Guerinot, M. L. (2002) FRD3, a member of the Multidrug and Toxin Efflux family, controls iron deficiency responses in *Arabidopsis*. *Plant Cell* **14**, 1787-1799.
Roschzttardtz, H., Séguéla-Arnaud, M., Briat, J.-F., Vert, G. and Curie, C. (2011) The FRD3 citrate effluxer promotes iron nutrition between symplastically disconnected tissues throughout *Arabidopsis* development. *Plant Cell* **23**, 2725-2737.
Rus, A., Baxter, I., Muthukumar, B., Gustin, J., Lahner, B., Yakubova, E. and Salt, D. E. (2006) Natural variants of AtHKT1 enhance Na+ accumulation in two wild populations of *Arabidopsis*. *PloS Genet*, **2**, 1964-1973.
Salt, D. E., Prince, R. C., Pickering, I. J. and Raskin, I. (1995) Mechanisms of cadmium mobility and accumulation in Indian mustard. *Plant Physiol*, **109**, 1427-1433.
Santi, S. and Schmidt, W. (2009) Dissecting iron deficiency-induced proton extrusion in *Arabidopsis* roots. *New Phytol*, **183**, 1072-1084.
Schaaf, G., Honsbein, A., Meda, A. R., Kirchner, S., Wipf, D. and von Wirén, N. (2006) AtIREG2 encodes a tonoplast transport protein involved in iron-dependent nickel detoxification in *Arabidopsis thaliana* roots. *J Biol Chem*, **281**, 25532-25540.
Schaaf, G., Schikora, A., Haberle, J., Vert, G., Ludewig, U., Briat, J. F., and von Wirén, N. (2005) A putative function for the *Arabidopsis* Fe-Phytosiderophore transporter homolog AtYSL2 in Fe and Zn homeostasis. *Plant Cell Physiol*, **46**, 762-774.
Scholz, G., Schlesier, G. and Seifert, K. (1985) Effect of nicotianamine on iron uptake by the tomato mutant *chloronerva*. *Physiol Plant*, **63**, 99-104.
Schuler, M., Rellán-Álvarez, R., Fink-Straube, C., Abadía, J. and Bauer, P. (2012) Nicotianamine functions in the phloem-based transport of iron to sink organs, in pollen development and pollen tube growth in *Arabidopsis*. *Plant Cell*, **24**, 2380-2400.
Shaff, J. E., Schultz, B. A., Craft, E. J., Clark, R. T. and Kochian, L. V. (2010) GEOCHEM-EZ: a chemical speciation program with greater power and flexibility. *Plant Soil*, **330**, 207-214.
Stacey, M. G., Koh, S., Becker, J. and Stacey, G. (2002) AtOPT3, a member of the Oligopeptide Transporter family, is essential for embryo development in *Arabidopsis*. *Plant Cell*, **14**, 2799-2811.
Stacey, M. G., Osawa, H., Patel, A., Gassmann, W. and Stacey, G. (2006) Expression analyses of *Arabidopsis* oligopeptide transporters during seed germination, vegetative growth and reproduction. *Planta*, **223**, 291-305.
Stacey, M. G., Patel, A., McClain, W. E., Mathieu, M., Remley, M., Rogers, E. E. and Stacey, G. (2008) The *Arabidopsis* AtOPT3 protein functions in metal homeostasis and movement of iron to developing seeds. *Plant Physiol*, **146**, 589-601.
Sunarpi, Horie, T., Motoda, J., Kubo, M., Yang, H., Yoda, K., Horie, R., Chan, W. Y., Leung, H. Y., Hattori, K., Konomi, M., Osumi, M., Yamagami, M., Schroeder, J. I. and Uozumi, N. (2005) Enhanced salt tolerance mediated by AtHKT1 transporter-induced Na^+ unloading from xylem vessels to xylem parenchyma cells. *Plant J*, **44**, 928-938.
Turgeon, R. and Webb, J. A. (1973) Leaf development and phloem transport in *Cucurbita pepo*: Transition from import to export. *Planta*, **113**, 179-191.
Valko, M., Morris, H. and Cronin, M. T. (2005) Metals, toxicity and oxidative stress. *Curr Med Chem*, **12**, 1161-1208.
Vert, G. A., Briat, J.-F. and Curie, C. (2003) Dual regulation of the *Arabidopsis* high-affinity

root iron uptake system by local and long-distance signals. *Plant Physiol*, **132**, 796-804.
Waters, B. M., Chu, H.-H., DiDonato, R. J., Roberts, L. A., Eisley, R. B., Lahner, B. and Walker, E. L. (2006) Mutations in *Arabidopsis* Yellow Stripe-Like1 and Yellow Stripe-Like3 reveal their roles in metal ion homeostasis and loading of metal ions in seeds. *Plant Physiol*, **141**, 1446-1458.
Wintz, H., Fox, T., Wu, Y. Y., Feng, V., Chen, W., Chang, H. S. and Vulpe, C. (2003) Expression profiles of *Arabidopsis thaliana* in mineral deficiencies reveal novel transporters involved in metal homeostasis. *J Biol Chem*, **278**, 47644-47653.
Wong, C. K. and Cobbett, C. S. (2009) HMA P-type ATPases are the major mechanism for root-to-shoot Cd translocation in *Arabidopsis thaliana*. *New Phytol*, **181**, 71-78.
Wu, H., Chen, C., Du, J., Liu, H., Cui, Y., Zhang, Y. and Ling, H.-Q. (2012) Co-overexpression FIT with AtbHLH38 or AtbHLH39 in *Arabidopsis* enhanced cadmium tolerance *via* increased cadmium sequestration in roots and improved iron homeostasis of shoots. *Plant Physiol*, **158**, 790-800.
Xiao, Y. L., Redman, J. C., Monaghan, E. L., Zhuang, J., Underwood, B. A., Moskal, W. A. and Town, C. D. (2010) High throughput generation of promoter reporter (GFP) transgenic lines of low expressing genes in *Arabidopsis* and analysis of their expression patterns. *Plant Methods*, **6**, 18.
Zhai, Z., Sooksa-nguan, T. and Vatamaniuk, O. K. (2009) Establishing RNA interference as a reverse-genetic approach for gene functional analysis in protoplasts. *Plant Physiol*, **149**, 642-652.
Zhang, M.-Y., Bourbouloux, A., Cagnac, O., Srikanth, C. V., Rentsch, D., Bachhawat, A. K. and Delrot, S. (2004) A novel family of transporters mediating the transport of glutathione derivatives in plants. *Plant Physiol*, **134**, 482-491.

CONCLUSIONS

The generation of plants for phytoremediation of soils contaminated with heavy metals, or the generation of "Cd-safe" crops, can be achieved through manipulation of components that maintain essential mineral element homeostasis, but full knowledge of these homeostasis networks is also required. The work described herein has contributed to a better understanding of plant Cu and Fe homeostasis and how these networks are affected by Cd exposure. OPT3, the long-sought after phloem Fe transporter, is a major component in Fe signaling in *A. thaliana*. Function of OPT3 is also required for Fe loading into sink tissues, especially seeds. The role of OPT3 in Fe and Cd partitioning among tissues revealed two important factors: 1) disruption of OPT3 results in greater Cd accumulation, and less Fe accumulation in seeds, and 2) *opt3-3* mutants are Cd tolerant due to enhanced vacuolar sequestration. Although Cd-related phenotypes in *opt3-3* are indirect, this gene is a promising candidate in creating "Cd-safe crops," where mutation of key sites in OPT3 may result in a transporter that enhances Fe loading into seeds, but restricts Cd to root tissue.

Our understanding of Cu homeostasis in *A. thaliana* has also been expanded based on the research presented here on the characterization of *COPT6* and *COPT2* function *in planta*, their expression patterns, and localization. Further, we have reported the first instance of cross-talk between Cd and Cu homeostasis and emphasized the importance of the SPL7 TF to this, in addition to COPT1, COPT2, and COPT6. We have also provided the first characterization studies of an emerging model species, *Brachypodium*. As cereal crops are generally more susceptible to Cu deficiency, a better understanding of the function of BdCOPT's may be of significant importance in agriculture. Future work in discovering other essential components of

Cu and Fe homeostasis, whether the components are transporters, TFs, or metal sensors, will most likely be essential in the ultimate goal of creating plants for phytoremediation and/or "Cd-safe" crops.